

Εθνικό και Καποδιστριακό
Πανεπιστήμιο Αθηνών
Σχολή Θετικών Επιστήμων
Τμήμα Γεωλογίας και
Γεωπεριβάλλοντος
Τομέας Δυναμικής –
Τεκτονικής – Εφ. Γεωλογίας
Πανεπιστημιούπολη
Ζωγράφου, Αθήνα
15784



National and Kapodistrian
University of Athens
School of Sciences
Faculty of Geology and
Geoenvironment
Department of Dynamic –
Tectonic – Applied Geology
Panepistimioupoli
Zographou, Athens 15784
Greece

**ΜΕΤΑΠΤΥΧΙΑΚΗ ΔΙΑΤΡΙΒΗ ΜΕ ΕΙΔΙΚΕΥΣΗ ΣΤΗ
ΔΥΝΑΜΙΚΗ - ΤΕΚΤΟΝΙΚΗ**
MSc THESIS

**Κινηματική και τεκτονική ανάλυση στην περιοχή του Φενεού, Β.
Πελοπόννησος.**

*Kinematic and structural analysis in the Feneos area, N.
Peloponnese.*



ΚΩΝΣΤΑΝΤΙΝΟΣ Α. ΚΥΔΩΝΑΚΗΣ (Α.Μ. 2920)
KONSTANTINOS A. KYDONAKIS (Reg. No. 2920)

Αθήνα, Ιούλιος 2011

Athens, July 2011

ΤΡΙΜΕΛΗΣ ΕΠΙΤΡΟΠΗ:

Καθηγητής κ. Δημήτριος Παπανικολάου
(Επιβλέπων)
Επ. Καθηγητής κ. Στυλιανός Λόζιος
Επ. Καθηγητής κ. Δημήτριος Κωστόπουλος

JURY:

Prof. Dr. Dimitrios Papanikolaou (Thesis
Supervisor)
Ass. Prof. Dr. Stylianos Lozios
Ass. Prof Dr. Dimitrios Kostopoulos

I perfectly understood the answer but,

what was the question?

Jean-Pierre Burg

ACKNOWLEDGEMENTS

The author is indebted to this supervisor, Prof. Dimitrios Papanikolaou, for the numerous fruitful discussions, during which he willingly shared his geological knowledge, and for the field experience in many type-localities of Greece.

Thesis co-supervisors, Ass. Prof. Stylianos Lozios and Ass. Prof. Dimitrios Kostopoulos, are thanked for the plenty helpful discussions and constructive reviews during this study.

Prof. Jean-Pierre Brun (Géosciences Rennes, France) is particularly thanked for his hospitality and the influential discussions we had during my stay in France.

Marc Poujol (Géosciences Rennes, France) is thanked for his efficient assistance during sample preparation as well as for his expertise on the LA-ICPMS. He is cordially thanked for the dating of the zircons involved in this study.

Evangelos Moulas (ETH Zurich, Switzerland) is thanked for his assistance, particularly related to the thermodynamics of Chapter 4.

Finally, this thesis would have been impossible without the moral and financial support of 3 people, my father, mother and sister. In particular, my sister's help for improvement of the English language is much appreciated.

ΠΕΡΙΛΗΨΗ

Οι ζώνες κυανοσχιστολίθων αποτελούν αναπόσπαστο τμήμα αρχαϊκών και πρόσφατων ορογενετικών συστημάτων. Στην Ελλάδα, η εξωτερική κυανοσχιστολιθική ζώνη παραδοσιακά αντιπροσωπεύεται από την ενότητα των Φυλλιτών - Χαλαζιτών (ή ενότητα Άρνας).

Η βορειότερη εμφάνιση της εν λόγω ενότητας μελετήθηκε στην περιοχή του Φενεού, Β. Πελοπόννησος. Η τεκτονική και κινηματική ανάλυση που διεξήχθει στην περιοχή αποκάλυψε μία αρχική συμπίεση στη διεύθυνση ΒΑ-ΝΔ που οδήγησε στη δημιουργία ΒΔ-πτυχών στην ενότητα των Φυλλιτών - Χαλαζιτών και στα υπερκείμενα στρώματα του Τυρού, ταυτόχρονα με τη δημιουργία της επικρατούσας φύλλωσης. Η αρχική συμπίεση ακολουθήθηκε από έντονη προς ΒΑ διάτμηση η οποία καταγράφηκε τόσο διάσπαρτη σε ολόκληρη τη στρωματογραφική στήλη της περιοχής όσο και σε διακριτές ζώνες διάτμησης. Η συγκεκριμένη ύστερη διάτμηση ξεκίνησε σαφώς στο πεδίο της πλαστικής παραμόρφωσης και φαίνεται να συνεχίστηκε και στο πεδίο της θραυσιγενής παραμόρφωσης κάτω από το ίδιο εντατικό πεδίο. Η διεύθυνση ΒΑ-ΝΔ που χαρακτηρίζει τόσο την αρχική συμπίεση όσο και την ύστερη διάτμηση (πιθανόν συνδεόμενη με την εκταφή των πετρωμάτων) δείχνει πως τα πετρώματα όλων των ενοτήτων της περιοχής δεν υπέστησαν εσωτερική η σχετική περιστροφή κατά μέρος της διάρκειας της γεωλογικής τους ιστορίας. Το γεγονός πως η τελευταία διάτμηση που καταγράφεται σε Πελοπόννησο και Κρήτη, για την ενότητα των Φυλλιτών - Χαλαζιτών, είναι αντίστοιχα προς ΒΑ και προς Β δείχνει τη σχετική περιστροφή μεταξύ της Πελοποννήσου και της Κρήτης ως αποτέλεσμα της οπισθοδρόμησης του ελληνικού τόξου (slab rollback).

Η επανεκτίμηση των συνθηκών πίεσης μεταμόρφωσης από ήδη δημοσιευμένα δεδομένα αποκάλυψεν την ύπαρξη σημαντικού μεταμορφικού κενού μεταξύ της ενότητας των Φυλλιτών - Χαλαζιτών και των υπερκείμενων στρωμάτων του Τυρού στην περιοχή μελέτης.

Η χημεία ολικού πετρώματος και η σημειακή χρονολόγηση εκτριψιγενών (detrital) ζιρκονίων από ένα χαλαζίτη (μετα-ψαμμίτη) της ενότητας των Φυλλιτών - Χαλαζιτών αποκάλυψε: (i) την ανακύκλωση ενός αρχικού όξινου πετρώματος κατά τη διάρκεια ύστερων θερμικών/ορογενετικών γεγονότων και (ii) την έλλειψη ζιρκονίων Βαρίσκιας ηλικίας. Το τελευταίο καταγράφεται εδώ για πρώτη φορά σε Άνω Παλαιοζωικά (μετα)ιζήματα της Κρήτης/Πελοποννήσου.

Λέξεις κλειδιά: Φενεός, κυανοσχιστόλιθοι, τεκτονική ανάλυση, ζώνες διάτμησης, διάτμηση, χρονολόγηση ζιρκονίων, προέλευση ιζημάτων.

ABSTRACT

Blueschist belts form an integral part of many ancient and recent orogens. In Greece, the external blueschist belt is traditionally represented by the Phyllite – Quartzite unit (or Arna unit).

The northernmost exposure of this unit is studied in the Feneos area, N. Peloponnese. Structural and kinematic analysis carried out there revealed an early NE-SW compression that resulted in the formation of NW-trending mesoscopic folds in the Phyllite – Quartzite unit and in the overlying Tyros beds, contemporaneous with the formation of the regional foliation. This early compression is followed by strong NE-shearing, both distributed throughout the pile and localized in well-developed shear zones. This late shearing started clearly in the ductile field and continued possibly in the brittle field under the same stress field. The NE-SW direction for both the initial compression and the later shearing (possibly related to the exhumation of the units) suggests no internal or relative rotation of the units throughout much of their geological history. The post-peak metamorphic NE-shearing recorded in the Phyllite – Quartzite unit from Peloponnese compared to the equivalent N-shearing from Crete adds to the point of view of significant relative rotation between Peloponnese and Crete possibly related to the rollback caused by the negative buoyancy of the subducting slab.

New thermodynamic treatment of already published data revealed the existence of significant metamorphic gap between the Phyllite – Quartzite unit and the overlying Tyros beds in the study area.

The whole-rock chemistry and detrital zircon spot dating from a quartzite (meta-sandstone) from the Phyllite – Quartzite unit revealed: (i) the recycling of an initial arc-related acid rock during later thermal/orogenic events and (ii) the lack of any Variscan zircons. The latter is documented here for the first time from Upper Paleozoic (meta)sediments of Crete/Peloponnese.

Key words: *Feneos, blueschists, structural analysis, shear zones, shearing, zircon dating, sediment provenance.*

Εκτεταμένη περίληψη	1
Chapter 1	6
Introduction to the geology of Greece – The Hellenic blueschists	
Chapter 2	10
The External Blueschist Belt: Introduction to the study area	
2.1 The Phyllite-Quartzite Unit from Peloponnese and Crete: Comparison	11
2.2 Exposure of basement rocks - Adria or Apulia?	17
2.3 Geological setting of the Feneos area	21
2.3.1 Phyllite-Quartzite Unit	22
2.3.2 Tripolitsa Unit	23
2.3.3 Pindos Unit	24
2.3.4 Post-alpine sediments	24
2.4 Problems imposed	26
2.4.1 Metamorphism	26
2.4.2 Tectonic contacts	26
2.5 Purpose of this study	27
2.6 Summary	28
Chapter 3	29
Geological mapping – structural and kinematic analysis	
3.1 Rock types	29
3.2 Structural analysis	34
3.2.1 Foliation map	34
3.2.2 Lineation map	36
3.2.3 Folds – fold axes – axial planes	37
3.3 Kinematic analysis	39
3.3.1 Sense of shear	41
3.3.2 Shear zones	42
3.4 Early shearing – late shearing - the ductile-brittle transition	47
3.5 The opening of the Corinth Gulf: Post alpine sediments and recent faulting	48
3.6 Summary	49
Chapter 4	51
Petrology and P-T estimations	
4.1 Published P-T results from the Feneos and the Kastania areas	51
4.2 P-T estimates	52
4.3 Summary	54

Chapter 5	56
Provenance and geotectonic setting of a quartzite (Phyllite – Quartzite unit)	
5.1 <i>Resolving tectonic problems</i>	56
5.2 <i>Samples analyzed – Analytical methods</i>	58
5.2.1 <i>Major and trace elements – Classification of the rock</i>	58
5.2.2 <i>Multi-element diagrams: Source material and geotectonic setting</i>	60
5.2.3 <i>Zircon dating as a provenance tool</i>	63
5.2.3.1 <i>Zircons extracted – Classification based on their typology other characteristics</i>	64
5.2.3.2 <i>Frequency histograms and probability – density plots</i>	67
5.2.3.3 <i>Concordia and Tera-Wasserburg plots</i>	71
5.2.3.4 <i>Age clusters</i>	72
5.3 <i>Summary</i>	74
Chapter 6	76
Discussion and conclusions	
6.1 <i>Discussion</i>	76
6.2 <i>Conclusions</i>	80
Plates	83
References	88
Appendix A	95
Appendix B	98
Maps	101

ΕΚΤΕΤΑΜΕΝΗ ΠΕΡΙΛΗΨΗ

Το ελληνικό ορογενετικό σύστημα (**Σχ. 1.1**) είναι το αποτέλεσμα της μακρόχρονης σύγκλισης μεταξύ της Ευρώπης και του βόρειου παθητικού περιθωρίου της Γκοντβάνα η οποία οδήγησε στην εξαφάνιση ωκεάνιου φλοιού και στην ενσωμάτωση ηπειρωτικών θραυσμάτων κατά τη διάρκεια του Αλπικού κύκλου. Στις εξωτερικές Ελληνίδες, δύο ζώνες πετρωμάτων υψηλής πίεσης μεταμόρφωσης (HP belts) μπορούν να διακριθούν (**Σχ. 1.3**): (i) η εσωτερική (Κυκλαδική) κυανοσχιστολιθική ζώνη που εμφανίζεται κυρίως στις Κυκλαδες (βλ. Philippou et al. [2010] και παραπομπές) και (ii) η εξωτερική κυανοσχιστολιθική ζώνη που εμφανίζεται στην Κρήτη και στην Πελοπόννησο (βλ. Jolivet et al. [2010] και παραπομπές). Η βορειότερη εμφάνιση της εξωτερικής κυανοσχιστολιθικής ζώνης, η οποία αντιπροσωπεύεται από την ενότητα των Φυλλιτών – Χαλαζιτών (ή ενότητα Άρνας), είναι το αντικείμενο της παρούσας εργασίας.

Η ενότητα των Φυλλιτών – Χαλαζιτών αποτελεί μία μετα-ιζηματογενή ακολουθία Άνω? Λιθανθρακοφόρου – Κάτω (ή Μέσο Τριαδικής) ηλικίας απόθεσης (**Εικ. 2**) η οποία μεταμορφώθηκε σε υψηλή πίεση κατά το Τριτογενές. Η ύπαρξη βασικών και υπερβασικών πετρωμάτων, όπως επίσης και ανθρακικών πετρωμάτων στη ενότητα των Φυλλιτών – Χαλαζιτών υποδεικνύει πως η εν λόγω ενότητα είναι σχετικά σύνθετη (Papanikolaou and Skarpelis 1986, Skarpelis 1989, Trotet et al. 2006). Συναντάται κάτω από τα στρώματα του Τυρού (ή ομόλογες ενότητες σε Κρήτη και Πελοπόννησο) και γενικά την ενότητα της Τρίπολης και πάνω από την ενότητα της Μάνης, σε όποιες περιοχές η τελευταία εμφανίζεται (πχ Ταύγετος, Πάρνωνας, Δίκτη) (**Σχ. 2.3, 2.4**). Η πίεση μεταμόρφωσης είναι μεταξύ 10Kbar και 15Kbar για τη δυτική Κρήτη και τη νότια Πελοπόννησο (Papanikolaou and Skarpelis 1986, Theye and Seidel 1991, Theye et al. 1992, Brix et al. 2002) αν και τόσο υψηλότερη όσο και χαμηλότερη πίεση μεταμόρφωσης έχει προταθεί από διάφορους ερευνητές. Οι μέγιστες μεταμορφικές συνθήκες φαίνεται να μειώνονται προς τα ανατολικά στην Κρήτη και προς τα βόρεια στην Πελοπόννησο.

Τα διαθέσιμα στοιχεία ραδιοχρονολόγησης (κυρίως K/Ar και Ar/Ar σε μαρμαρυγίες) από την ενότητα των Φυλλιτών – Χαλαζιτών δείχνουν μία συγκέντρωση ηλικιών μεταξύ 25 εκ. χρ. και 15 εκ. χρ. (Seidel et al. 1982, Jolivet et al. 1996, 2010). Η παραπάνω κατανομή των ηλικιών οδήγησε πολλούς ερευνητές να συσχετίσουν τις ηλικίες αυτές με την άφιξη της ενότητας στο επίπεδο του μέσου φλοιού, πριν από την αποκάλυψή της σε επιφανειακές συνθήκες πριν από 10 εκ. χρ. όπως προέκυψε από μελέτες των ιζηματογενών ακολουθιών στα Τοπόλια της Κρήτης (Seidel et al. 1986). Αντιθέτως, τα ραδιοχρονολογικά στοιχεία από την υπερκείμενη ενότητα της Τρίπολης δείχνουν πως αυτή παρέμεινε στα ανώτερα 4-7 χιλιόμετρα του φλοιού από το Ηώκαινο (Thomson et al. 1998a). Αυτή η παρατήρηση, σε συνάρτηση με τη διαφορά πίεσης μεταξύ της υποκείμενης ενότητας των Φυλλιτών – Χαλαζιτών και των υπερκείμενων ενοτήτων οδήγησε πολλούς ερευνητές να προτείνουν την ύπαρξη μιας κύριας εφελκυστικής επαφής (ρήγμα αποκόλλησης) μεταξύ τους (πχ. Fassoulas et al. 1994, Jolivet et al. 1996, 2010, Papanikolaou and Royden 2007, Papanikolaou and Vassilakis 2010). Η κινηματική της ενότητας των Φυλλιτών – Χαλαζιτών που σχετίζεται με τη δράση της παραπάνω επαφής είναι προς ΒΑ στην Πελοπόννησο (**Σχ. 2.3**) και προς Β στην Κρήτη όπου επιπλέον επικαλύπτει μία προς Ν παλαιότερη κινηματική (**Σχ. 2.5**).

Η περιοχή μελέτης (**Σχ. 3.1**) αποτελεί τη βορειότερη εμφάνιση της εξωτερικής κυανοσχιστολιθικής ζώνης. Το κεντρικό τμήμα της περιοχής αποτελείται από ένα πυρήνα μεταμορφωμένων ιζημάτων και βασικών πετρωμάτων (**Σχ. 3.2**) ο οποίος πλαισιώνεται κυρίως από ανθρακικά πετρώματα. Η ενότητα των Φυλλιτών – Χαλαζιτών εμφανίζεται στον κεντρικό

πυρήνα και αποτελείται κυρίως από μετα-ιζήματα (χαλαζίτες και μεταπηλίτες). Λιθολογίες αντίστοιχες των στρωμάτων του Τυρού (μεταπηλίτες, ασβεστοπηλίτες, βασικά και λίγα ανθρακικά πετρώματα) εμφανίζονται επίσης στον πυρήνα της περιοχής. Τα ανθρακικά πετρώματα της ενότητας της Τρίπολης εμφανίζονται στις πλευρές του κεντρικού πυρήνα.

Η παλαιότερη επιφάνεια που παρατηρήθηκε στην περιοχή είναι η στρώση (**Σχ. 3.2b, 3.2g**). Οι μετρήσεις φύλλωσης έδειξαν μία κύρια και επικρατούσα φύλλωση με επιφάνεις που κλίνουν προς τα ΝΔ (**Σχ. 3.3 ένθετο**) και είναι πάντα παράλληλες με τη στρώση, δείγμα της έντονης κατακόρυφης βράχυνσης. Η κατανομή των επιφανειών φύλλωσης και ο χάρτης των τροχιών φύλλωσης (foliation trajectories) έδειξαν πως η δομή της ενότητας των Φυλλιτών - Χαλαζιτών είναι αντικλινική με άξονα διεύθυνσης ΒΔ-ΝΑ (**Σχ. 3.3**). Οι περισσότερες μετρήσεις εφελκυστικής γράμμωσης που μετρήθηκαν επί των επιπέδων της φύλλωσης προέρχονται από την ενότητα των Φυλλιτών - Χαλαζιτών και έδειξαν μία σταθερή ΒΑ-ΝΔ διεύθυνση, με την επικρατούσα διεύθυνση να είναι μεταξύ B050° και B060° (**Σχ. 3.4**). Η ίδια ΒΑ-ΝΔ διεύθυνση μετρήθηκε και στα υπερκείμενα πετρώματα του Τυρού (**Σχ. 3.4**). Οι λίγες γραμμώσεις από διατομή που μετρήθηκαν έδειξαν μια σταθερή διεύθυνση ΒΔ-ΝΑ (**Σχ. 3.4**) που συμπίπτει με τους άξονες των μεσοσκοπικών πτυχών (βλ. στη συνέχεια). Οι μεσοσκοπικές πτυχές που μετρήθηκαν περιορίστηκαν κυρίως στους μεταπηλίτες. Οι πλειοψηφία αυτών των πτυχών ήταν σχετικά κλειστές έως ισοκλινείς, με σχεδόν οριζόντιους (ή με μικρή κλίση) άξονες και σχεδόν οριζόντια αξονικά επίπεδα (**Σχ. 3.5**). Η σχέση των πτυχών με τη γενική φύλλωση της περιοχής αποκάλυψε δύο είδη πτυχών: τις πτυχές με αξονικό επίπεδο παράλληλο στη φύλλωση (*Type I - Σχ. 3.5a, 3.5c*) και εκείνες των οποίων τα αξονικά επίπεδα τέμνονται με τη φύλλωση και δεν εμφανίζουν καλά ανεπτυγμένες επιφάνειες παράλληλα με τα αξονικά τους επίπεδα (*Type II - Σχ. 3.5d*). Σε κάθε περίπτωση οι πτυχές του πρώτου τύπου είναι εμφανώς περισσότερες από εκείνες του δεύτερου τύπου. Και οι δύο τύποι πτυχών εμφανίζουν την ίδια γεωμετρία στους άξονές τους (ΒΔ-ΝΑ; **Σχ. 3.5e, 3.5g**) υποδεικνύοντας μία αρχική συμπίεση στη διεύθυνση ΒΑ-ΝΔ.

Η πλειοψηφία των πετρωμάτων που μελετήθηκαν ήταν πλούσια σε φυλλοπυριτικά ορυκτά και ευνοούσαν τη δημιουργία κινηματικών δεικτών. Η κινηματική που καταγράφηκε ήταν συνεχώς προς ΒΑ (**Σχ. 3.6**), ακολουθώντας τη διεύθυνση της εφελκυστικής γράμμωσης. Αν και οι περισσότερες από τις μετρήσεις της κινηματικής αφορούσαν την ενότητα των Φυλλιτών - Χαλαζιτών, λίγες μετρήσεις που έγιναν στα στρώματα του Τυρού έδειξαν να έχουν την ίδια γεωμετρία (**Σχ. 3.6**). Τρεις ζώνες διάτμησης, που αναπτύχθηκαν είτε κοντά στην οροφή της ενότητας των Φυλλιτών - Χαλαζιτών (**Σχ. 3.8**) είτε κοντά στην οροφή του Τυρού (**Σχ. 3.7, 3.9**), επιλέχθηκαν για παρουσίαση. Το κοινό τους χαρακτηριστικό ήταν η κίνηση προς ΒΑ η οποία ξεκίνησε σαφώς στο πεδίο της πλαστικής παραμόρφωσης και συνεχίστηκε στο πεδίο της θραυσιγενούς παραμόρφωσης όπως φάνηκε από (i) τις θραυσιγενείς δομές κοντά στην αξονική περιοχή των προς τα ΒΑ ασύμμετρων πτυχών (**Σχ. 3.7e**), (ii) τη διακοπή των μικρών ζωνών διάτμησης από νεότερα συνθετικά ρήγματα με διεύθυνση ΒΔ-ΝΑ (**Σχ. 3.7d**), (iii) την επανενεργοποίηση των ήδη ασθενών επιπέδων όπως τα επίπεδα C' (**Σχ. 3.8c**), (iv) την ύπαρξη έντονης κατάκλασης στις ίδιες τις ζώνες διάτμησης (**Σχ. 3.8a, 3.9**) και (v) τη διακοπή της συνέχειας των αλλεπάλληλων ενοτήτων από ρήγματα διεύθυνσης ΒΔ-ΝΑ όπως αυτή φαίνεται σε κλίμακα χάρτη (**Σχ. 3.1**).

Το μοντέλο που προτείνεται στην παρούσα εργασία περιγράφεται στις επόμενες γραμμές. Η πτύχωση της αρχικής στρώσης (ή μίας άλλης παλαιάς επιφάνειας) οδήγησε στη δημιουργία πτυχών (*Type I και II*) με διεύθυνση ΒΔ-ΝΑ καθώς και της κύριας φύλλωσης κάτω από ένα συμπιεστικό εντατικό πεδίο με διεύθυνση ΒΑ-ΝΔ. Η συγκεκριμένη φάση πιθανόν να σχετίζεται με

κίνηση προς Δ ή προς ΝΔ που καταγράφηκε σε μικροκλίμακα από τους Xypolias and Koukouvelas (2001). Αν και καταγράφηκε πτύχωση νεότερη της γενικής φύλλωσης (Type II πτυχές), φαίνεται να σχηματίστηκε κάτω από το ίδιο εντατικό πεδίο που περιγράφηκε πιο πάνω (συμπίεση στη διεύθυνση BA-ΝΔ). Οι συγκεκριμένου τύπου πτυχές δεν σχετίζονται με καλά ανεπτυγμένες διαμπερείς επιφάνειες παράλληλες με το αξονικό τους επίπεδο. Στη συνέχεια, όλη η μετα-ιζηματογενής ακολουθία της περιοχής υπέστη έντονη προς BA διάτμηση ταυτόχρονα με (i) τη δημιουργία των ζωνών διάτμησης που μελετήθηκαν, (ii) τη δημιουργία πληθώρας από κινηματικούς δείκτες και (iii) τη δημιουργία της προς BA εφελκυστικής γράμμωσης που χαρακτηρίζει τόσο την ενότητα των Φυλλιτών - Χαλαζιτών όσο και τα υπερκείμενα στρώματα του Τυρού. Το ίδιο εντατικό πεδίο φαίνεται να παρέμεινε ενεργό τουλάχιστον κατά ένα μέρος της επακόλουθης θραυσιγενούς παραμόρφωσης των πετρωμάτων όπως προκύπτει από διάφορες κλίμακες παρατήρησης (Σχ. 3.1, 3.7d). Εντούτοις, λίγα χιλιόμετρα προς τα βόρεια ο εφελκυσμός στο πεδίο της θραυσιγενούς παραμόρφωσης είναι καθαρά σε διεύθυνση B-N, όπως έχει επισημανθεί από πολλούς ερευνητές, και σχετίζεται με τη διάνοιξη του Κορινθιακού Κόλπου (Moretti et al. 2003, 2004). Η σχέση μεταξύ της περιοχής μελέτη και της κατάστασης λίγα χιλιόμετρα βοριότερα μένει να διερευνηθεί. Η αντικλινική δομή της περιοχής, όπως προκύπτει από τις τροχιές της φύλλωσης (Σχ. 3.3), μπορεί είτε να αποτελεί μία κληρονομημένη δομή από το αρχικό συμπιεστικό γεγονός καθώς έχει την ίδια γεωμετρία με κληρονομημένες δομές που χωρίζουν Πλειοκαινικές λεκάνες στα βόρεια (Λεκάνες Δερβενίου και Αιγίου; Ghisetti and Vezzani [2004]) και με το ίδιο το μέτωπο συμπίεσης (fold-and-thrust belt) στα ανατολικά, είτε να σχετίζεται με ισοστατική ισορροπία εξαιτίας της ύστερης, έντονης προς BA, διάτμησης. Το μοντέλο που προτείνεται εδώ είναι συμβατό με εκείνο που προτάθηκε από τους Papanikolaou and Royden (2007) οι οποίοι μελέτησαν την εξωτερική κυανοσχιστολιθική ζώνη σε σαφώς μεγαλύτερη κλίμακα.

Όπως έχει ήδη επισημανθεί από τους Katagas et al. (1991) οι οποίοι μελέτησαν τις συνθήκες μεταμόρφωσης στην περιοχή του Φενεού, η ενότητα των Φυλλιτών - Χαλαζιτών είναι μεγαλύτερου μεταμορφικού βαθμού, συγκρινόμενη με τον υπερκείμενο Τυρό, χωρίς ωστόσο να υπάρχει σημαντικό μεταμορφικό κενό. Συγκεκριμένα, πρότειναν ότι η μέγιστη θερμοκρασία μεταμόρφωσης δεν ξεπέρασε ποτέ τους 440°C με την πιθανότερη τιμή να κείται μεταξύ 340°C και 420°C και ότι η μέγιστη πίεση μεταμόρφωσης, αν και δεν είναι σαφώς ορισμένη, δεν πρέπει να ξεπέρασε τα 5Kbar. Για σύγκριση, οι μεταμορφικές συνθήκες του υπερκείμενου Τυρού, όπως αυτές υπολογίστηκαν από βασικά πετρώματα, είναι 290°C - 380°C και 3.5 - 5Kbar (Baltatzis and Katagas 1984). Αντίθετα, στην κοντινή περιοχή της Καστανιάς (λίγα χιλιόμετρα ΝΑ από τον Φενεό) οι συνθήκες μεταμόρφωσης των Φυλλιτών - Χαλαζιτών είναι σχετικά αυξημένες (10Kbar και 450°C; Jolivet et al. [2010]).

Οι συνθήκες πίεσης και θερμοκρασίας της ενότητας των Φυλλιτών - Χαλαζιτών επανεκτιμήθηκαν στην παρούσα μελέτη χρησιμοποιώντας ήδη δημοσιευμένες αναλύσεις πετρωμάτων από άλλους ερευνητές και το πακέτο θερμοδυναμικής ανάλυσης PERPLE_X. Για το σκοπό αυτό επιλέχθηκαν ένας χαλαζίτης από την περιοχή βόρεια της Ζαρούχλας και ένας μεταπηλίτης από την περιοχή της Καστανιάς. Το δείγμα από την περιοχή της Ζαρούχλας δείχνει να έχει ισορροπήσει στα 9-11Kbar αν και η θερμοκρασία δεν μπορεί να προσδιοριστεί με σχετική ακρίβεια (μεγαλύτερη από 230°C) (Σχ. 4.1). Το δείγμα από την περιοχή της Καστανιάς δείχνει να έχει ισορροπήσει σε σχετικά αυξημένη πίεση (13Kbar ή ακόμα και πίεση μεγαλύτερη από 15Kbar) (Σχ. 4.2). Η πίεση μεταμόρφωσης που υπολογίστηκε στην παρούσα εργασία είναι ιδιαίτερα αυξημένη σε σχέση με τις μέχρι τώρα δημοσιευμένες εκτιμήσεις. Αν οι υπολογισμοί είναι σωστοί

τότε υπάρχει πλέον η ανάγκη για (i) διάκριση υποενοτήτων της ενότητας των Φυλλιτών - Χαλαζιτών με διαφορετικά μεταμορφικά χαρακτηριστικά στις περιοχές του Φενεού και της Καστανιάς ή (ii) διάκριση μεταξύ διαφορετικών μηχανισμών, ή έντασης των μηχανισμών, που συμβάλουν στην αποκάλυψη της εν λόγω ενότητας στις δύο περιοχές.

Για την ανίχνευση της προέλευσης των μητρικών πετρωμάτων της ενότητας Φυλλιτών - Χαλαζιτών χρησιμοποιήθηκε ένας χαλαζίτης από την περιοχή του Φενεού ο οποίος και αναλύθηκε γεωχημικά για κύρια στοιχεία και ιχνοστοιχεία. Επί πλέον, από το πέτρωμα αυτό διαχωρίσθηκαν εκτριψιγενή ζιρκόνια (detrital zircons) τα οποία και χρονολογήθηκαν σημειακά με τη μέθοδο U-Pb. Η ηλικία απόθεσης του πετρώματος αυτού είναι Άνω(;) Λιθανθρακοφόρο - Κάτω Τριαδικό. Το δείγμα είναι ένας χαλαζιακός - αρενίτης (**Σχ. 5.1**) και το μητρικό του πέτρωμα μπορεί να είναι κάποιο μαγματικό ή μεταμορφωμένο πέτρωμα, λιγότερο ή περισσότερο διαφοροποιημένο μέσα από γεωλογικές διεργασίες, ή ακόμα και κάποιο παλαιότερο ιζηματογενές πέτρωμα. Από τα γεωχημικά δεδομένα (**Σχ. 5.3**) διαφαίνεται ότι το μητρικό πέτρωμα ήταν ένα παλαιότερο χαλαζιούχο ιζηματογενές πέτρωμα που είχε αποτεθεί πιθανότατα σε περιβάλλον παθητικού περιθωρίου και το οποίο, με τη σειρά του, πιθανόν προήλθε από όξινα μαγματικά πετρώματα περιβάλλοντος ενεργού περιθωρίου (γρανίτες, ρυόλιθοι). Μια μικρή συμβολή πετρωμάτων βασικού-υπερβασικού χαρακτήρα στη λεκάνη απόθεσης του αρενίτη του Φενεού είναι επίσης ορατή (**Σχ. 5.3**).

Οι περισσότεροι από τους 127 κόκκους ζιρκονίων που επιλέχθηκαν για χρονολόγηση (**Σχ. 5.4**) είναι στρογγυλοποιημένοι, με εξαίρεση μερικούς ιδιόμορφους κρυστάλλους, δείχνοντας μακρά μεταφορά πριν την απόθεσή τους. Με βάση τα μορφολογικά χαρακτηριστικά προέκυψαν τρεις ομάδες ζιρκονίων (**Σχ. 5.4**). Η πρώτη ομάδα περιέχει σχετικά μεγάλα, γκρίζα και αδιαφανή ζιρκόνια, η δεύτερη ομάδα περιέχει σχετικά μικρά, διάφανα και επιμήκη ζιρκόνια ενώ η τρίτη ομάδα περιέχει μεσαίου μεγέθους, ροζ, ημιδιάφανα ζιρκόνια. Από την γεωχημική ανάλυση των ζιρκονίων (**Πίνακας 5.4, Σχ. 5.6**) προέκυψε ότι η δεύτερη ομάδα περιέχει κυρίως μαγματικά ζιρκόνια ενώ οι άλλες δύο ομάδες περιέχουν επιπροσθέτως μεταμορφικά ζιρκόνια. Η χρονολόγηση ζιρκονίων (**Appendix B**) αποκάλυψε την ύπαρξη τεσσάρων ομάδων ηλικιών: 500 - 825εκ. χρ. (Νεο-πρωτεροζωικός - Μ. Κάμβριο), 950 - 1075εκ. χρ. (Άνω Μεσο-πρωτεροζωικός - Κάτω Νεο-πρωτεροζωικός), 1750 - 2000εκ. χρ. (Μ. - Αν. Παλαιο-πρωτεροζωικός) και 2400 - 2750εκ. χρ. (Νεο-αρχαϊκός - Κάτω Παλαιο-πρωτεροζωικός) (**Σχ. 5.5**). Μία ακόμα πιθανή ομάδα ηλικιών εμφανίζεται στα 2925 - 2950εκ. χρ. (**Σχ. 5.5**). Σε γενικές γραμμές τα ζιρκόνια με τη μεγαλύτερη αφθονία είναι εκείνα της νεότερης ομάδας ηλικιών. Επίσης τα ζιρκόνια με τον μεταμορφικό χαρακτήρα προέρχονται κυρίως από την πρώτη δέσμη ομάδα ηλικιών και λιγότερο από την τρίτη δέσμη ηλικιών.

Τα κύρια συμπεράσματα που βγαίνουν από την κατανομή των ζιρκονίων στις διάφορες ομάδες ηλικιών είναι: (i) τα νεότερα θερμικά/τεκτονικά γεγονότα που καταγράφονται από τα μητρικά πετρώματα του χαλαζίτη του Φενεού είναι αυτά των ορογενέσεων Grenville και Pan-African, (ii) τα μητρικά πετρώματα δεν δείχνουν ίχνη της Βαρίσκιας ορογένεσης κάτι το οποία τεκμηριώνεται εδώ για πρώτη φορά σε μετα-ιζήματα της Κρήτης/Πελοποννήσου. Σημειώνεται πως είναι αδύνατο ένα τέτοιας ηλικίας μεταμορφωμένο ίζημα, σαν αυτό που μελετήθηκε (με ηλικία απόθεσης νεότερη από ~300εκ. χρ.), να μην έχει ίχνη της Βαρίσκιας ορογένεσης (η οποία είναι γνωστό πως διήρκησε μεταξύ 330 και 280 εκ. χρ.) εκτός εάν το μητρικό πέτρωμα δεν συμμετείχε σε αυτή. Για συγκριτικούς λόγους αναφέρεται πως στην Κρήτη, οι Kock et al. (2007) έδειξαν σε μεταμορφωμένα ιζηματογενή πετρώματα Άνω Λιθανθρακοφόρου - Κάτω Πέρμιας

ηλικίας (~300εκ. χρ.; Στρώματα Γαληνού) που βρίσκονται κάτω από την ενότητα της Μάνης, την ύπαρξη ζιρκονίων της Βαρίσκιας ορογένεσης.

Συμπερασματικά, η παρούσα μελέτη των ζιρκονίων του αρενίτη του Φενεού καταδεικνύει σαφώς την ανακύκλωση όξινου ηπειρωτικού φλοιού που δημιουργήθηκε κατά την Παναφρικανική ορογένεση και τεκμηριώνει, για πρώτη φορά, την προέλευση από το βόρειο παθητικό περιθώριο της Γκοντβάνας (Απουλία) προ-Αλπικών ιζημάτων των εξωτερικών ελληνίδων.

Introduction to the geology of Greece – The Hellenic blueschists

Chapter 1

The Hellenic orogenic system (Fig. 1.1) is the result of the long-lasting convergence between Europe and the North Gondwana passive margin leading to the consumption of oceanic domains and to the accretion of continental blocks. Major oceanic lithospheres disappeared since M.-Up. Jurassic is the Vardar/Axios oceanic domain, to the north, and Pindos oceanic domain to the south. At present, the three continental crusts along with their sedimentary cover i.e. Rhodope massif s.l., Pelagonian and External Hellenides, are separated by two suture zones i.e. Vardar/Axios and Pindos (Fig. 1.2).

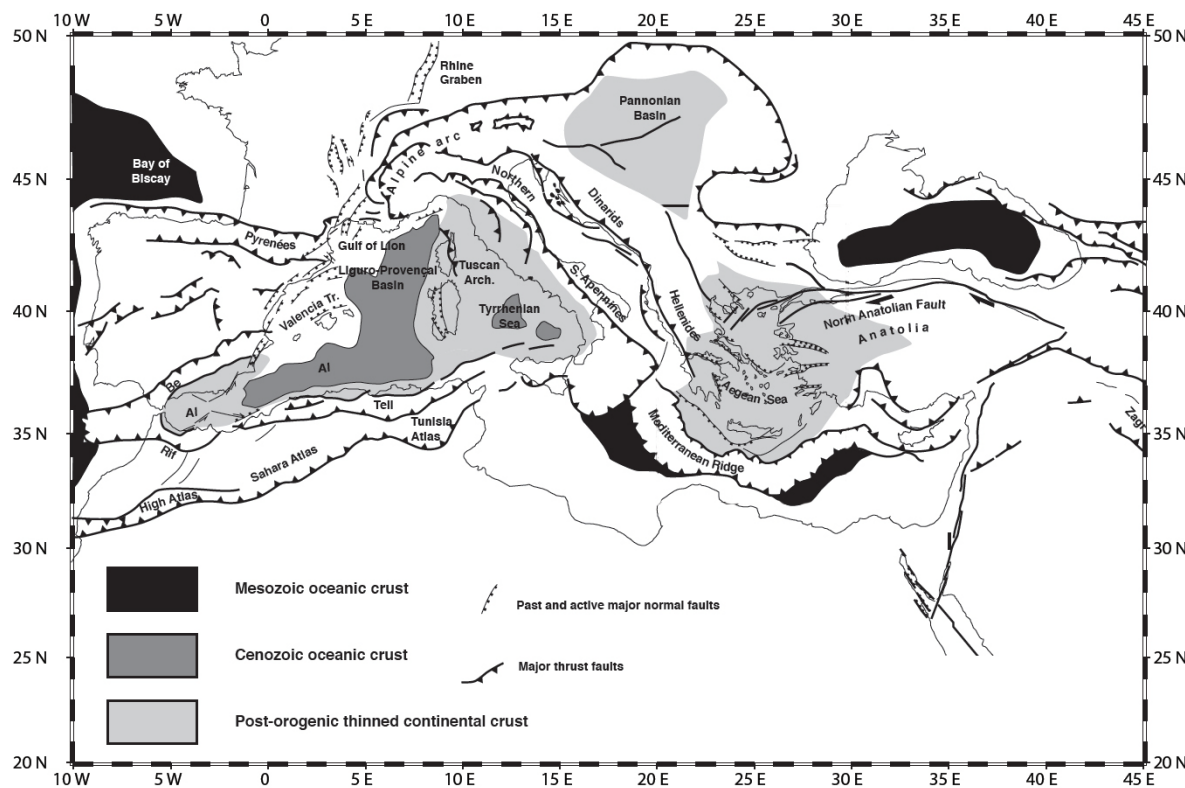


Fig. 1.1. Tectonic map of the Mediterranean region. The main compressional and strike-slip features as well as the extensional basins are highlighted. From Jolivet and Brun (2010).

Σχ. 1.1. Τεκτονικός χάρτης της Μεσογείου. Οι κύριες συμπιεστικές και οριζόντιας ολίσθησης δομές, όπως επίσης και οι εφελκυστικές λεκάνες έχουν τονιστεί. Από Jolivet and Brun (2010).

One of the most well-studied, but still extremely controversial subject, is the *exhumation* of (U)HP rocks. It involves the vertical displacement of previously metamorphosed rock near the surface

through some removal of the overburden (see [Ring et al. 1999](#) for a review). The exact mechanism or the participation of several different mechanisms to the overall exhumation process is still controversial. For example, channel-flow mechanism still has supporters (e.g. [Gerya et al. 2002](#)) despite the fact that low viscosity and/or high erosion rates are required. Buoyancy and/or erosion can account for part of the exhumation assuming the trench moves away from the upper plate i.e. *rollback* ([Dewey 1981](#), [Brun and Faccenna 2008](#)), producing strong extension and thinning of the upper plate. In the Mediterranean realm, sun-convergence exhumation, through a continuous subduction, from depths of 70Km or more has been documented and attributed to the above mechanisms ([Jolivet et al. 1994](#)). On the other hand, post-convergence extension can account for the exhumation of HT rocks within core-complexes, like in the Aegean region ([Lister et al. 1984](#)). Note that, although exhumation is commonly closely related to extension, it may also play a significant role in converging systems (e.g. [Burg et al. 1984](#)).

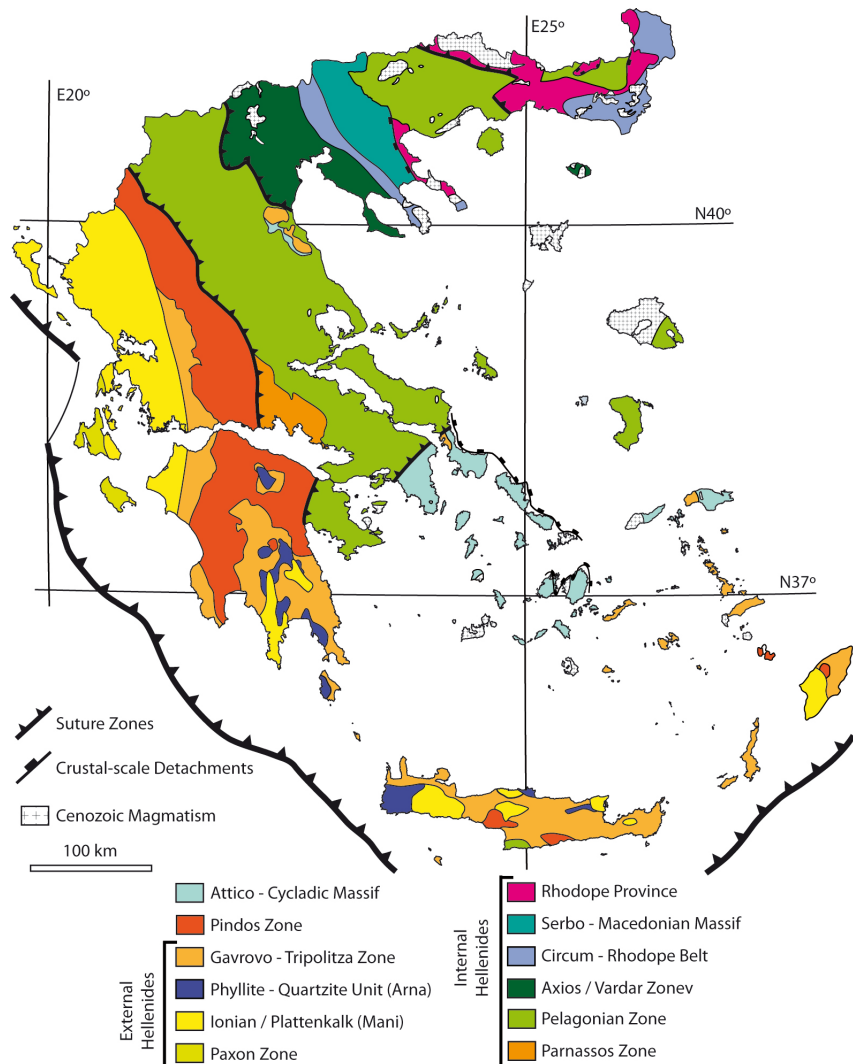


Fig. 1.2. Geotectonic units of the Hellenides based on the work of Papanikolaou (1989), Pe-Piper and Pipper (2002), Papanikolaou et al. (2004), Koglin (2008), Papanikolaou and Vassilakis (2010) and Kostopoulos and Brun (in prep.).

Σχ. 1.2. Γεωτεκτονικές ενότητες των Ελληνίδων με βάση τους Papanikolaou (1989), Pe-Piper and Pipper (2002), Papanikolaou et al. (2004), Koglin (2008), Papanikolaou and Vassilakis (2010) και Kostopoulos and Brun (in prep.).

In Greece, two exhumed HP belts can be distinguished (Fig. 1.3) : (i) the *internal* (or *Cycladic*) *blueschist belt* appearing mainly in Cyclades and (ii) the *external blueschist belt* appearing in Peloponnese and Crete. The Cycladic blueschists (see [Philippon 2010](#) for a review) contain both oceanic and continental material metamorphosed at 15-20Kbar and exhumed between 45Ma and 55Ma (Altherr et al. 1979, Maluski et al. 1987). The external blueschists belt, which is the subject of this study, is mainly represented by the Phyllite Quartzite Unit and composed of continental sediments. The maximum pressure attained is between 10Kbar and 17Kbar ([Trotet et al. 2006](#), [Jolivet et al. 2010](#)) and the exhumation of these rocks to mid-crustal levels is placed between 15Ma and 25Ma ([Jolivet et al. 1996, 2010](#)).

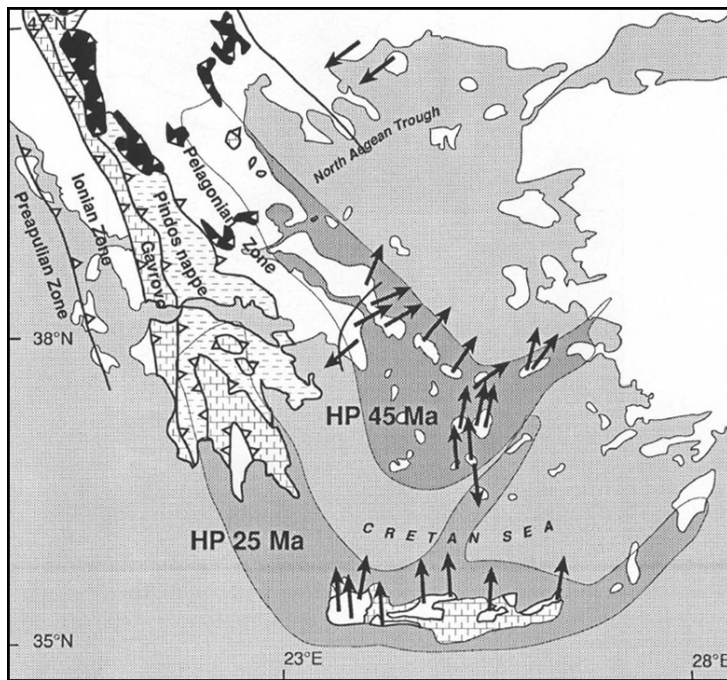


Fig. 1.3. The two main metamorphic belts in the Aegean region. Extensional ductile sense of shear is shown (black arrows). From [Jolivet et al. \(1994\)](#).

Σχ. 1.3. Οι δύο κύριες μεταμορφικές ζώνες της περιοχής του Αιγαίου. Η φορά πλαστικής διάτμησης αποτυπώνεται με τα μαύρα βέλη. Από [Jolivet et al. \(1994\)](#).

In short, the geological history of Greece comprises: (i) initiation of the convergence in Jurassic times with the subduction of the northern Vardar margin and the UHP metamorphic event in Rhodope s.l. ([Reischmann and Kostopoulos 2002](#)), (ii) accretion of the Pelagonian block into the south European margin between Lower Cretaceous and Eocene, (iii) initiation of the subduction of Pindos ocean at Middle Eocene ([Ferrière et al. 2004](#)), development of the South Rhodope Core Complex ([Dinter and Royden 1993](#), [Sokoutis et al. 1993](#), [Brun and Sokoutis 2007](#)) and syn-orogenic exhumation of the Cycladic blueschists ([Jolivet et al. 2003](#)), (iv) accretion of the External Hellenides since Lower Eocene - Oligocene and (v) subduction of the Eastern Mediterranean basin since Middle Miocene ([Le Pichon et al. 2002](#)) contemporaneous with the development of the Cycladic Core Complex ([Lister et al. 1984](#), [Gautier and Brun 1994](#)) and the exhumation of Cretan blueschist belt ([Jolivet et al. 2004](#)). The Hellenic geological

history is marked by the migration of the Hellenic volcanic arc from northern Greece to the current position in south Cyclades (Fytikas et al. 1984, Pe-Piper and Piper 2002, 2006) related to the slab rollback triggered by the subduction of oceanic material (Brun and Faccenna 2008). Slab rollback is responsible for: (i) opening of the Aegean Sea, (ii) the curvature of the trench system from an almost linear geometry in Eocene until today's almost orthogonal geometry (Papanikolaou 1993, Jolivet and Brun 2010), situation similar to what observed in analogue modeling (Funiciello et al. 2003) and in other synchronous Alpine Belts (Rosenbaum et al. 2002) and (iii) clockwise rotation of most of the continental Greece (Kissel et al. 1985, Van Hinsbergen et al. 2005). The puzzle is finished with the westward propagation of the Anatolian block since Upper Miocene (Philippon 2010) and the neotectonic activity mostly accumulated at the Corinth Gulf (Armijo et al. 1996, Rohais et al. 2007) and the North Aegean Trough (Papanikolaou et al. 2006) since Upper Miocene – Lower Pliocene.

The External Blueschist Belt: Introduction to the study area

Chapter 2

Peloponnese covers a significant part of the continental Greece. The main geotectonic units appearing there are, from west to east, *Ionian unit*, *Gavrovo – Tripolitsa unit*, *Pindos unit*, *Phyllite – Quartzite unit*, *Plattenkalk unit* and *Pelagonian platform* (Fig. 2.1). For a summary of the rock-types and ages of the sedimentation of all the units reported here, the reader is referred to **Plate 2**. In the simplified geological map (IGME) (Fig. 2.1) some striking characteristics are: a) Pindos unit is dominant and appears rather flat to the east and relatively deformed to the west as one approaches the fold-and-thrust belt, b) Pindos thrust (on top of Gavrovo – Tripolitsa unit) to the west has a peculiar «S» shape being NW-SE-directed to the north and to the south while between those two segments it appears NE-SW-directed, c) the relatively autochthon, Plattenkalk unit, appears in southern Peloponnese anticlines (Taygetos and Parnon Mt.) where Pindos cover is totally absent, d) Phyllite – Quartzite unit appears mainly in southern Peloponnese on top of the relatively autochthon although in some areas it represents the autochthonous unit (N and SE Peloponnese), e) strong recent extension is either in N-S direction to the north (Gulf of Corinth) or to E-W direction to the south (Messiniakos, Lakonikos and Argolikos Gulfs).

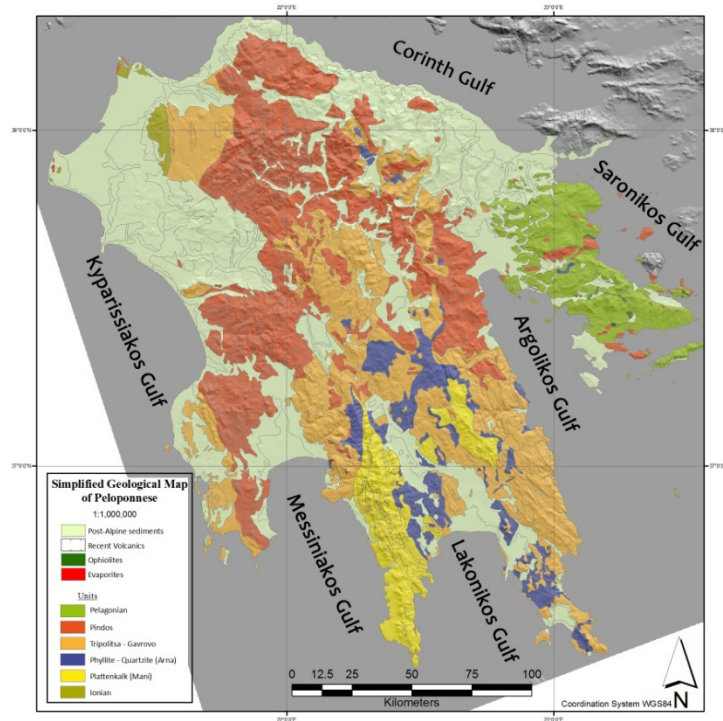


Fig. 2.1. Simplified geological map (1:1,000,000) of Peloponnese. Modified after IGME.
Σχ. 2.1. Απλοποιημένος γεωλογικός χάρτης της Πελοποννήσου (1:1,000,000). Από ΙΓΜΕ, με διορθώσεις.

2.1 The Phyllite-Quartzite Unit from Peloponnese and Crete: A comparison.

Although lots of researchers (e.g. [Seidel et al. 1982](#), [Papanikolaou and Skarpelis 1986](#), [Blumör 1998](#), [Trotet et al. 2006](#), [Jolivet et al. 2010](#)) have been working for decades on the Phyllite – Quartzite unit, many questions still remain unanswered. What is commonly accepted is that the Phyllite - Quartzite unit is lying directly below Tripolitsa or Pindos units and above Plattenkalk unit both in Crete and Peloponnese. In Crete, the *Western Crete* unit is sandwiched between the Phyllite - Quartzite unit and the PkU and is supposed to represent a duplication of the PkU ([Papanikolaou 1988](#)). An ordinary problem in the literature is the discrimination between the lowermost Plattenkalk flysch, the medial intensively deformed metasediments of the Phyllite - Quartzite unit and the uppermost base of the Tripolitsa unit, known as Tyros beds in Peloponnese (or *Ravdoucha* in Crete). The description of the local characteristics of the above units is not easily followed among different authors as already noted by [Papanikolaou and Vassilakis \(2008\)](#). As an example, the Lada sub-unit is either correlated to the Tyros beds ([Papanikolaou and Skarpelis 1986](#) – their fig.6) or to the Phyllite - Quartzite unit ([Jolivet et al. 2010](#)).

The palaeogeographic position of the Phyllite - Quartzite unit is still in debate. Numerous hypotheses have been proposed in the literature according to which, the Phyllite - Quartzite unit could represent: (i) the metamorphic equivalent of the Tyros beds of the basement rocks of the Tyros beds ([Karakitsios 1979](#), [Karakitsios 1986](#), [Bonneau 1982](#)), (ii) a separate palaeogeographic domain of the External Hellenides between the Ionian zone to the west and the Tripolitsa carbonate platform to the east ([Kopp and Ott 1977](#), [Jacobshagen et al. 1978](#)), (iii) an equivalent of the HP units of the Cyclades ([Papanikolaou and Skarpelis 1986](#)).

Peloponnese and Kythira

In Peloponnese, the Phyllite - Quartzite unit can be found in Feneos Valley, in Merkouri and Doliana windows, in Taygetos and in Parnon mountains. In Peloponnese and Kythira, the Phyllite - Quartzite unit represents a metasedimentary sequence which consists mainly of metapelites, metaconglomerates, metapsammites (quartzites) and marble layers ([Papanikolaou and Skarpelis 1986](#), [Trotet et al. 2006](#)) despite that mafic and untramacfic rocks have also been reported ([Papanikolaou and Skarpelis 1986](#), [Skarpelis 1989](#)). Slices of orthogneisses (also referred as *micaschists*) overlying the metasediments have been extensively investigated in Kythira ([Seidel et al. 2006a](#), [Xypolias et al. 2006](#), [Lode et al. 2008](#)) but never reported for Peloponnese even though they do exist in Taygetos (Kostopoulos pers. comm.).

The stratigraphic data available for the Phyllite - Quartzite unit from Peloponnese are extremely poor (**Plate 2**). Phytofossils of Oligocene age have been reported from quartzites, of uncertain geotectonic attribution north of Sparti, near Selasia village ([Lekkas and Ioakim 1980](#)) and also Triassic ostracods in carbonate beds of the Xyli peninsula (SE Lakonia) ([Doert et al 1985](#)). In Lakonia, Brauer et al. (1980) reported Anisian fossils.

Commonly appearing minerals from southern Peloponnese in the metapelites are Fe-Mg carpholite, chloritoid, glaucophane, sudoite and garnet, indicating, at a first approximation medium- to high-pressure metamorphism ([Trotet et al. 2006](#)). The report of lawsonite ([Seidel et al. 1982](#) – Artemisia, Taygetos) indicates again similar metamorphic conditions of possible marl or mafic rock precursor. In

Taygetos Mt. the quartzites appear either as massive rocks (at the road connecting Arna village with Kastania village – South Taygetos) indicating a metapsammitic origin or as boudins in the metapelites possibly related to local dissolution and re-precipitation of Si. Mafic rocks appear tectonically within a metapelitic matrix and they contain glaucophane + epidote + actinolite + albite + sphene (Papanikolaou and Skarpelis 1986) suggesting a HP prograde metamorphism with a strong greenschists-facies overprint. Ultramafic rocks characterized by the assemblage antigorite \pm chlorite \pm magnetite \pm diopside are reported by Skarpelis (1989) in Taygetos (Artemisia), Parnon (Ag. Petros, Vresthena) and Kythira (Ag. Pelagia) and appear as lenticular bodies in metapelitic matrix with the long axis of the lenses following the foliation of the matrix.

In southern Peloponnese, Theye and Siedel (1991), Theye et al. (1992), Seidel and Theye (1993) suggested peak metamorphism at $\sim 17 \pm 4$ Kbar and $\sim 450 \pm 30$ °C. However, other authors suggested lower peak metamorphic condition (i.e. 4-6.5 Kbar / 325-400 °C; Thiebault and Triboulet 1983). The discovery of retrograde carpholite in metapelites from the base of the Phyllite - Quartzite unit in Taygetos allowed the determination of the retrogression path from peak metamorphic conditions of 14 Kbar / 400-450 °C to 3-4 Kbar / 250 °C through a rather continuous cooling during decompression (Trotet et al. 2006). Rather controversial is the incorporation of the *Kastania Phyllites*, outcropping at the core of Taygetos Mt., either to the overlying Phyllite - Quartzite unit (Thiebault and Triboulet 1983, Papanikolaou and Skarpelis 1986) or to the base of the underlying Plattenkalk unit (Psonis 1981, Kowalczyk and Dittmar 1991, Blumör et al. 1994). The peak metamorphic conditions recorded for *Kastania Phyllites* are approximately 7-8.5 Kbar and 310-360 °C (Blumör et al. 1994).

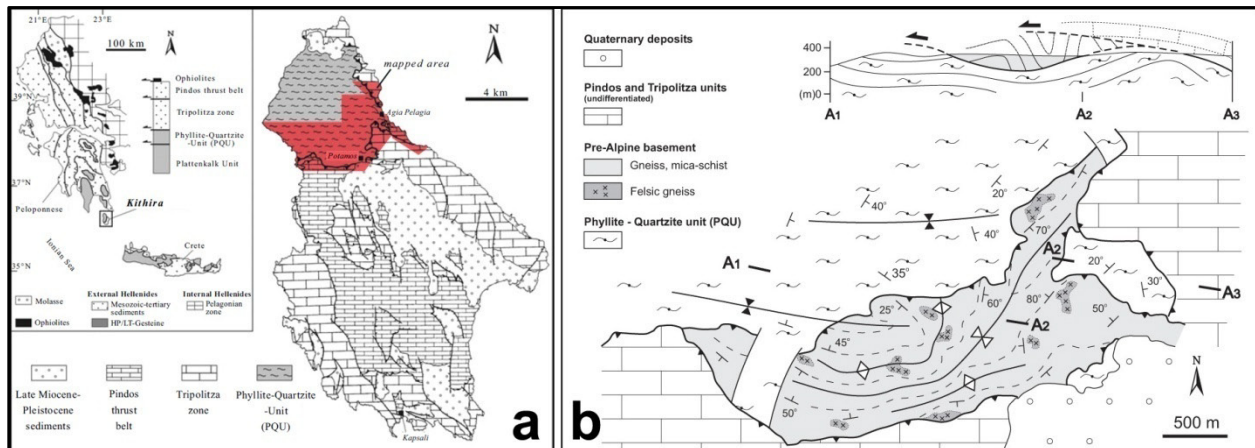


Fig. 2.2. (a) Geographic position and geological map of Kythira island. (b) Geological mapping of the contact between the Phyllite-Quartzite unit and the overlying orthogneisses and mica-schists. From Lode et al. (2008).

Σχ. 2.2. (α) Γεωγραφική θέση και γεωλογικός χάρτης των Κυθήρων. (β) Γεωλογική χαρτογράφηση της επαφής της ενότητας των Φυλλιτών-Χαλαζιών με τους υπερκείμενους ορθογνευσίους και μαρμαρυγιακούς σχιστολίθους. Από Lode et al. (2008).

In southern Peloponnese early studies provided K-Ar ages around 23 Ma for the peak pressure of the Phyllite - Quartzite unit (Seidel et al. 1982), a finding later confirmed by $^{40}\text{Ar}/^{39}\text{Ar}$ dating of the phengites of an orthogneiss from Kythira (~ 19 Ma; Seidel et al. 2006a). Although Seidel et al. (2006a) proposed that the orthogneiss is intercalated within the metasediments of the Phyllite - Quartzite unit, recent mapping supports that the basement rock tectonically overlies the Phyllite - Quartzite unit (Lode et al. 2008; Fig. 2.2). More detailed work ($^{40}\text{Ar}/^{39}\text{Ar}$ spot-fusion on micas) from the Phyllite - Quartzite unit from Jolivet et al. (2010) shows distribution of ages mostly between 26 Ma and 13 Ma for Taygetos

and between 50Ma and 16Ma for Parnon, with the ages obtained becoming younger at the deepest parts of the Phyllite - Quartzite unit. The same authors argued that the ages obtained by $^{40}\text{Ar}/^{39}\text{Ar}$ are cooling ages and the maximum pressure achieved before $\sim 26\text{Ma}$ while the exhumation at mid-crustal levels happened around 13Ma. Zircon fission track (ZFT) ages from Kythira scatter between 9Ma and 13Ma, identical to those of southern Taygetos (Neapoli) while the ages are progressively becoming older, between 13Ma and 21Ma, to the north Taygetos (Marsellos et al. 2010). As noted by the previous authors, only the ZFT scattering between 9Ma and $\sim 14\text{Ma}$ from Kythira and South and North Taygetos are meaningful ages because the older are representing partially reset ZFT ages. Younger apatite fission track (AFT) (5Ma - 8Ma) ages from Kythira and South Taygetos Mt. are in line with the previous ZFT ages and the lower closure temperature of the system (Marsellos et al. 2010). Unfortunately, no data from the surface exposure of the HP rocks are available in Peloponnese.

Stretching lineation and sense-of-shear from Peloponnese is presented by Jolivet et al. (2010). At Taygetos Mt., Parnon Mt. and Feneos the direction of the stretching lineation varies from NE-SW to E-W (Fig. 2.3). The sense of shear is clearly to-the-NE in Feneos (Fig. 2.3b), Central and South Peloponnese (Fig. 2.3a) while in places (western Taygetos) is to-the-SW or-W (Fig. 2.3a).

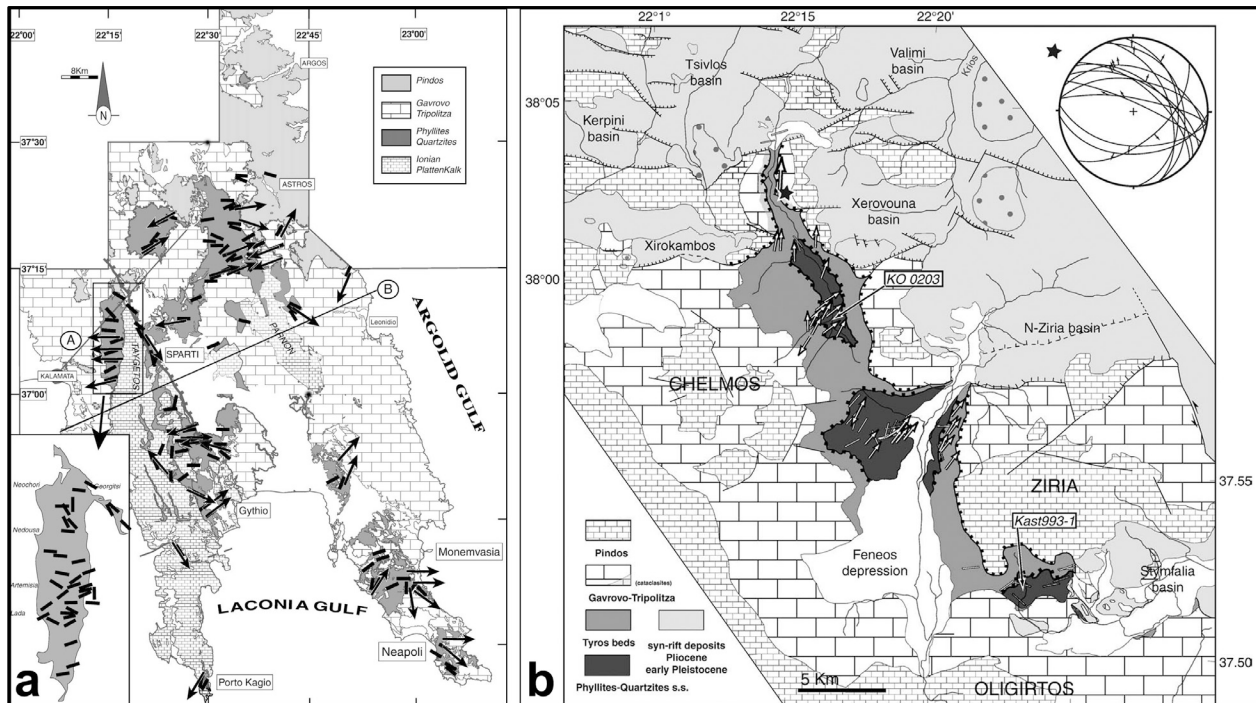


Fig. 2.3. Stretching lineation and sense-of-shear from (a) Southern Peloponnese and (b) Feneos area, Northern Peloponnese. From Jolivet et al. (2010).

Σχ. 2.3. Εφελκυστική γράμμωση και κινηματική από τη (α) Νότια Πελοπόννησο και την (β) Περιοχή του Φενεού, Β.Πελοπόννησο. Από Jolivet et al. (2010).

Crete

As mentioned in the introduction of this paragraph, a major problem, particularly in Crete, is the incorporation of the different lithologies into the different Cretan units. Papanikolaou and Vassilakis (2010) addressing to this problem suggested a revised stratigraphy of Crete (Fig. 2.4). As mentioned in

their work, phyllite-looking rocks can belong to: «(i) the metamorphosed flysch of the Mani unit (Oligocene in age, also known as the Kalavros beds, Fytrolakis [1972]); (ii) the complex unit of Western Crete, comprising a Tyros-type low-grade metamorphosed volcano-sedimentary sequence of Permian to Middle Triassic age, followed by Middle to Late Triassic evaporites and Late Triassic – Early Jurassic crystalline limestones (the latter formation referenced as Madara kalke by Creutzburg [1958] and later as the Trypali unit by Creutzburg et al [1977], Kopp and Ott [1977], Fytrolakis [1980], Krahel et al [1983]). This unit largely corresponds to the unit characterized by Tataris and Christodoulou (1965) as the “Triassic transgressive system of Western Crete” during their geological mapping of the Alikianou sheet (Tataris and Christodoulou 1967); (iii) low to medium grade HP/LT metamorphic rocks of the Phyllite - Quartzite unit. The age of this unit is presumed to be Paleozoic as previously described, but its metamorphism is Tertiary (Seidel et al. 1982, Thomson et al. 1999); and (iv) The Permo-Triassic volcano-sedimentary base of the Tripolitsa carbonate platform, consisting of phyllites, metasandstones, volcanic rocks and some carbonate layers, equivalent to the Tyros beds in Peloponnese (partly known as the Ravidoucha beds – Creutzburg and Seidel 1975)». As an example, rocks which were supposed to represent the Paleozoic basement rocks at the base of the metamorphic succession below the Tripolitsa carbonate platform were dated in Sitia as tertiary (Kalavros beds) by Fytrolakis (1972). Due to the larger extension, compared to Peloponnese, and subsequent shearing across the contacts, the discrimination of the different unit is much more difficult in Crete.

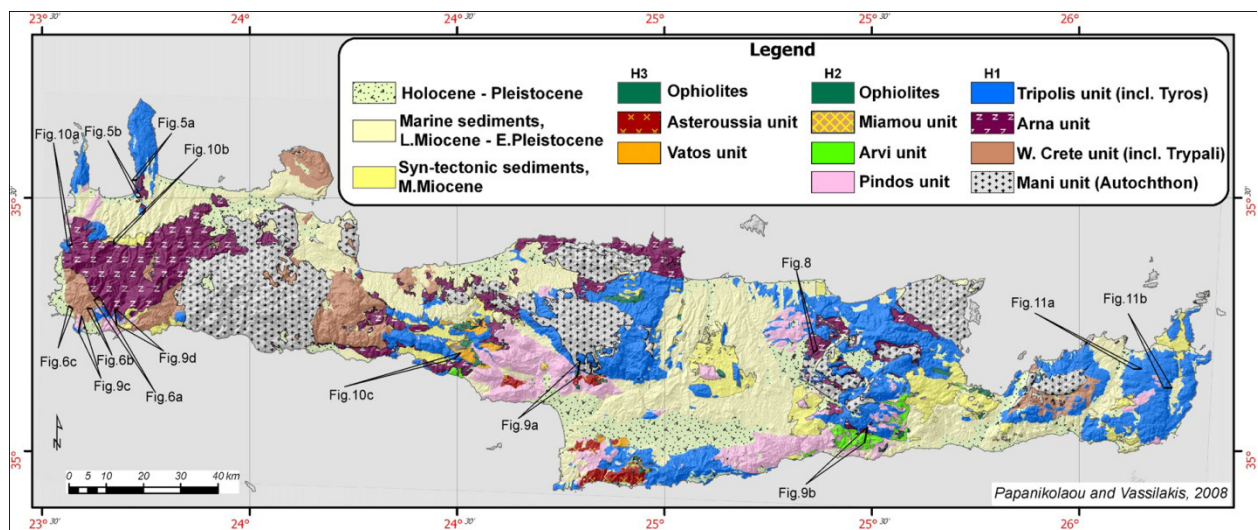


Fig. 2.4. Revised tectono-stratigraphy of Crete. From Papanikolaou and Vassilakis (2010).

Σχ. 2.4. Τεκτονο-στρωματογραφία της Κρήτης. Από Papanikolaou and Vassilakis (2010).

In Crete, the Phyllite - Quartzite unit is outcropping always below Tripolitsa unit (Tyros beds and the overlying carbonates) and above Plattenkalk unit. The thickest section is found in western Crete while is usually missing below the Tripolitsa unit in central Crete. An additional unit named *Western Crete*, comprising the *Trypali* crystalline limestones (Late Triassic–Early Jurassic) on top and a Permian Tyros-type volcano-sedimentary sequence below, is sandwiched between the autochthonous Plattenkalk unit and the uppermost Tripolitsa unit and is traditionally believed to represent either a duplication of the base of the Plattenkalk unit or a separate paleogeographic unit nearby Plattenkalk.

Contrary to Peloponnese, more stratigraphic data are available from Crete. At western Crete, the detailed work of Krahel et al. (1983) revealed unambiguously that lithologies equivalent to the real Phyllite - Quartzite unit (**Plate 5**) (according to the new stratigraphy of Crete proposed by Papanikolaou

and Vassilakis [2010]) maintain fossils (conodonts, ostracods, echinodermata) ranging in age from Carboniferous to Triassic. The following age determinations should be treated carefully due to the fact that the samples collected belong to uncertain stratigraphic positions. At eastern Crete fossils in gypsum reveal an Upper Permian age (Papastamatiou and Reichel 1956), while Lower Triassic ages suggested by Krahl et al. (1986). Lower – Middle Permian ages also suggested by Kozur and Krahl (1987) and Haude (1989). In Central Crete Lower Triassic conodonts has been demonstrated by Epting et al. (1972). Possible Upper Permian – Lower Triassic age has been proposed by Karakitsios (1979). I note again that many of the previous ages reported (e.g. from Haude [1989]) in spite of the fact that they have initially been reported for the Phyllite - Quartzite unit, according to the new stratigraphy proposed by Papanikolaou and Vassilakis (2010) for Crete, they seem to belong to the Tyros beds, the base of Tripolitsa unit. The only exception is the ages proposed from Krahl et al. (1983) for western Crete which clearly shows that the protolith of the Phyllite - Quartzite unit is of Carboniferous to Triassic age.

The Phyllite - Quartzite unit shows similar lithological characteristics like those described in detail for Peloponnese. Metapelites, quartzites and minor marble layer dominate. Typical lithologies of the Phyllite - Quartzite unit like those described from Taygetos Mt. in Peloponnese (Papanikolaou and Skarpelis 1986) can be found in several localities in Crete (Papanikolaou and Vassilakis 2010) like: (i) the metabasalts in Preveli and Agia Pelagia, (ii) the metaconglomerates in Almyros to the east of Agia Pelagia and in Sitia, north of the airport and (iii) the serpentinized peridotites in Malaxa.

The existence of carpholite, chloritoid and phengite in the metapelites as well as glaucophane in the metamorphic rocks indicates at least medium pressure of metamorphism (Seidel et al. 1975). The estimated metamorphic conditions in eastern Crete are about 8-10Kbar and 300-350°C based on paragenesis with carpholite, chloritoid or sudoite while in western Crete the peak metamorphic conditions are 10±3kbar and 400±50°C (Theye and Seidel 1991). Theye et al. (1992) studying aluminous metasediments from the Phyllite - Quartzite unit estimated 8Kbar and ~300°C for eastern Crete, 9Kbar and 350°C for Central Crete and 10Kbar and 400°C for western Crete suggesting slight increase in pressure and temperature from east to west. Identical results produced by Brix et al. (2002). Theye and Seidel (1993) reported aragonitic marbles belonging to the Phyllite - Quartzite unit of southwest Crete but according to the Cretan map proposed by Papanikolaou and Vassilakis (2010) they belong to the Western Crete unit mentioned above. In any of these cases, the non-retrogressed aragonite discovered, implies relatively high pressure of metamorphism, either for the Phyllite - Quartzite unit or for the Western Crete unit, and subsequent relative fast exhumation.

Judging from the above, it is obvious that the peak temperature is higher in western than in eastern Crete. The temperature is a first-order factor for the geochronology/thermochronology, thus the temperature gap observed is responsible for the difference in ZFT ages; 17-22Ma (Brix et al. 2002) in western Crete and 414-145Ma (Brix et al. 2002) or 184±11Ma (Romano et al 2006) in eastern Crete, implying that the peak temperature in eastern Crete was not high enough to fully anneal the fission tracks. The same is reflected to the $^{40}\text{Ar}/^{39}\text{Ar}$ system obtained by Jolivet et al. (1996) where ages as old as 180Ma were suggested for eastern Crete while in western Crete the ages are strictly scattering between 15Ma and 25Ma. The $^{40}\text{Ar}/^{39}\text{Ar}$ ages obtained by Seidel et al. (1982), i.e. 16-24Ma, are in agreement with the previous authors. The youngest ages were obtained by AFT from Thomson et al. (1998a) (~10-15Ma).

Jolivet et al. (1996) summarizing the geological history of Crete, suggested a top-to-the-south early vergence inferred from the asymmetry of folds followed by a constant top-to-the-north post-high-pressure extension recorded by the Phyllite - Quartzite unit of Crete (Fig. 2.5). The pressure gap

observed between the high-pressure Phyllite - Quartzite unit and the relative lower (or null) pressure recorded by the Tripolitsa unit led Fassoulas et al. (1994), Jolivet et al. (1996, 2010) and Papanikolaou and Vassilakis (2010) to suggest the existence of a detachment separating the Phyllite - Quartzite unit from the overlying Tripolitsa (and Pindos) unit.

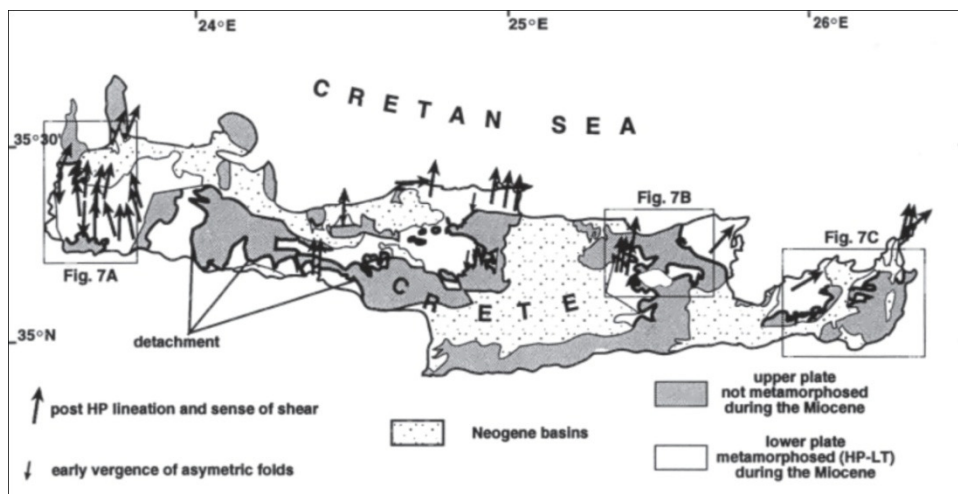


Fig. 2.5. Simplified geological map of Crete showing the direction and sense of post-HP shear observed in Phyllite-Quartzite unit (big black arrows). Early vergence also shown (small black arrows). From Jolivet et al. (1996).

Σχ. 2.5 Απλοποιημένος γεωλογικός χάρτης της Κρήτης με σημειωμένη τη διεύθυνση γράμμωσης και την κινηματική (μεγάλα μαύρα βέλη) των Φυλλιτών – Χαλαζιτών που σχετίζεται με τεκτονικά γεγονότα ύστερα από τη μεταμόρφωση υψηλής πίεσης. Η προηγούμενη τεκτονική παραμόρφωση σημειώνεται με μικρά μαύρα βέλη. Από Jolivet et al. (1996).

Comparison between Peloponnese-Kythira and Crete

Summarizing the above, it is obvious that the Phyllite - Quartzite unit in Peloponnese-Kythira and Crete shows both similarities and dissimilarities. In all places studied, the Phyllite - Quartzite unit represents a metasedimentary sequence (mainly metapelites, metasandstones and metaconglomerates with mafic rocks intercalations) of Upper Paleozoic – Lower Triassic stratigraphic age that is closely related to the locally exposed basement rocks (orthogneisses). The Phyllite - Quartzite unit is always below Tripolitsa or Pindos units and appears either as the autochthon unit or above Plattenkalk unit. Peak-metamorphic conditions decrease eastward in Crete and northward in Peloponnese while exhumation to mid-crustal levels is between 25Ma and 15Ma (based on K/Ar isotopic dating on micas) for both places. To my knowledge, ultramafic rocks have never been reported for Crete, which is not the case for Taygetos. Finally, post-HP shearing in to-the-E or to-the-NE in Peloponnese while in Crete is constantly to-the-N.

2.2 Exposure of basement rocks - Adria or Apulia?

Exposure of basements rocks

In general, the basement rocks consist of orthogneisses with mafic dykes and paragneiss intercalations. A powerful method for constraining old magmatic events is provided by zircon or monazite geochronology (U/Pb) due to their high closure temperature (Cherniak and Watson 2001, Cherniak et al. 2004). K/Ar and $^{40}\text{Ar}/^{39}\text{Ar}$ system have lower closure temperature ($\sim 350^\circ\text{C}$ in white micas or $\sim 500^\circ\text{C}$ in amphiboles) and is likely to date lower temperature thermal/metamorphic events. The existence of the two suture zones of Greece, Vardar/Axios and Pindos, allows the basement rocks to be grouped into three families: (i) basement rocks belonging to the Rhodope s.l. massif, (ii) basement rocks belonging to the Pelagonian continental crust and (iii) basement rocks belonging to the Adria/Apulia continental crust. The first group is located above Vardar/Axios suture zone, the second is between the two suture zones and the third is lying below Pindos suture zone (Fig. 1.2). In general, mostly Paleozoic ages have been documented (Fig. 2.6, Plate 2).

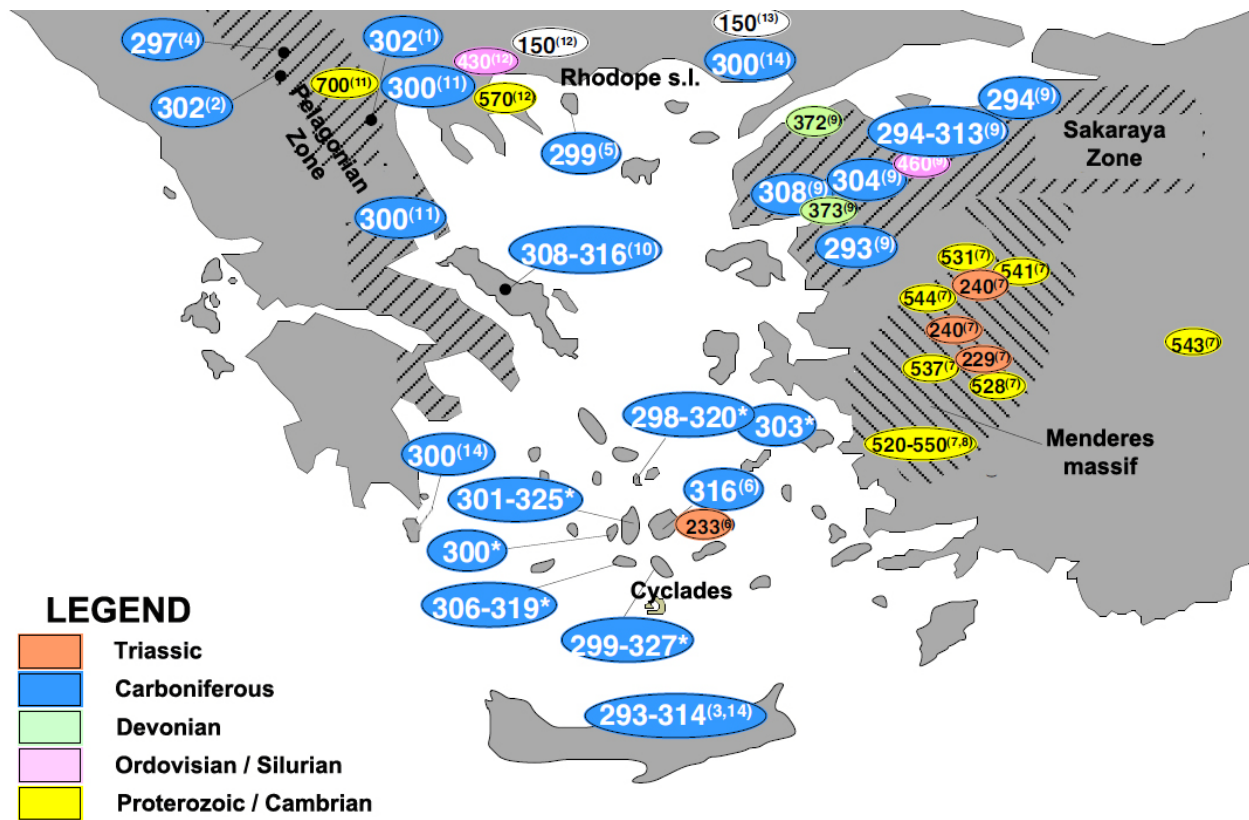


Fig. 2.6. Distribution of known ages corresponding to basement rocks from Greece and Turkey. From Engel (2006). For the references, shown as numbers or asterisks, inside the circles the reader is referenced to Engel (2006).

Σχ. 2.6. Κατανομή ηλικιών ορθογνευσιακών πετρωμάτων από την Ελλάδα και την Τουρκία. Από Engel (2006). Οι αριθμοί και οι αστερίσκοι στους κύκλους αναφέρονται σε βιβλιογραφικές παραπομπές (βλ. Engel 2006).

The dating of the Pelagonian basement rocks reveals the incorporation of Pre-Cambrian terrains ($\sim 700\text{Ma}$) into a Permo-Carboniferous Hercynian ($\sim 280\text{Ma} - 320\text{Ma}$) crust (Anders et al. 2006). In many places at the eastern or western Pelagonian zone, acid intrusions of Permo-Triassic age ($\sim 250\text{Ma}$) are

attributed to the rifting stage (Anders et al. 2007), contemporaneous with the opening of the Pindos ocean to the east and the Vardar/Axios ocean to the west, and are usually closely related to volcano-sedimentary sequences.

It is obvious that the appearance of basement rocks in Peloponnese, Crete, Cyclades and Attica belongs to Adria/Apulia continental crust as they lie below the Pindos suture zone although a long-lasting debate for the terms "Adria" and "Apulia" still exists (see below). The orthogneisses appear as non-molten rocks, usually fine- to medium-grained with a major exception in Naxos and Paros where partially-molten rocks are outcropping. In the case of Kythira and Crete the basement rocks are always in close relationship with the external high-pressure belt (Phyllite - Quartzite unit) even if it is not clear whether they appear above or within the Phyllite - Quartzite unit.

Many studies related to the dating of the Adria/Apulia basement rocks in Greece are published in the literature (Plate 2). In Peloponnese, the basement rocks are outcropping to the south in Taygetos Mt. (Kostopoulos pers. comm.), as well as in Kythira island. For Peloponnese there are no data available from the U/Pb system. However, dating of orthogneisses from Kythira (Agia Pelagia and Potamos) clearly shows a Late Carboniferous age (~320Ma; Xypolias et al. 2006, 300±12Ma; Seidel et al. 2006a). Xypolias et al. (2006) also suggested inherited zircon ages in the range of 2.4 – 2.5Ga. For the same rocks in Kythira the $^{40}\text{Ar}/^{39}\text{Ar}$ system indicates the age of 19.3±0.44Ma related to cooling after the high-pressure event (Seidel et al. 2006a).

In Crete, the basement rocks are outcropping mainly to the east of the island. The basement rocks belong to the upper *Chamezi Crystalline Complex* (CCC) and to the lower *Myrsini Crystalline Complex* (MCC). The structurally lowest part of MCC is also known as *Kalavros* basement rocks (Franz 1992). For the CCC orthogneiss a Late Panafrican age is suggested (511±16Ma; U/Pb zircon upper intercept; Romano et al. 2004, 521±28Ma; U/Pb monazite; Finger et al. 2002). Similar age is suggested for MCC orthogneiss (Exo Mouliana) (514±14Ma; U/Pb zircon upper intercept, Romano et al. 2004) while Finger et al. (2002) has also documented a Carboniferous age (345±18Ma; U/Pb monazite) from the same rocks. Micaschists from MCC yield also a Carboniferous age (335±20Ma; U/Pb monazite; Finger et al. 2002) while at the base of the pile (*Kalavros* basement rocks) a Permo-Triassic age was documented (257±19Ma; U/Pb monazite; Finger et al. 2002). Romano et al. (2006) suggested ages ranging from 380Ma to 260Ma for MCC and from 308Ma to 214Ma for the structurally lowest parts (*Kalavros* basement rocks). Zircon fission track (ZFT) ages, obtained by Romano et al. (2006), suggest cooling below ~350°C at 150±14Ma for MCC. Another orthogneiss from Vai shows lower intercept age of 223±11Ma (U/Pb zircon; Romano et al. 2006) while the ZFT age is 184±11Ma (Romano et al. 2006).

In the Cyclades the basement rocks are well preserved in Delos (Engel and Reischmann 1999), Ios (Henjes-Kunst and Kreuzer 1982), Sikinos (Andriessen et al. 1987) and Syros (Tomaschek et al. 2008) while in Naxos (Keay et al. 2001) and Paros (Engel and Reischmann 1998) appear partially molten. The non-molten orthogneisses have Permo-Carboniferous ages ranging between 290Ma and 330Ma (Engel and Reischmann 1999) while the partially-molten gneisses have identical primary magmatic age. Permo-Triassic ages related to rifting have also been reported from the Cyclades (e.g. Tinos; 240±3Ma; Tomaschek et al. 2001) or Attica (e.g. 240±4Ma; Liati et al. 2009). The melting event in the partially-molten lithologies is dated at ~20Ma (e.g. Keay et al. 2001).

To summarize, in Crete, the basement orthogneisses (CCC and MCC) yields a clear Late Panafrican age (~500Ma) with an important Hercynian magmatic event at ~330Ma. At the base of the basement pile of eastern Crete (*Kalavros*) Permo-Triassic ages reveal the rifting stage before the final

cooling of the rocks below $\sim 350^{\circ}\text{C}$ between 180 and 150 Ma. In Kythira island, south of Peloponnese, the basement rocks are dated as Late Carboniferous (~ 320 Ma) with much younger $^{40}\text{Ar}/^{39}\text{Ar}$ ages (~ 20 Ma) while in Peloponnese dating is missing. In Attico-Cycladic massif the basement rocks are mainly dated as Hercynian with some clear Permo-Triassic ages.

Adria or Apulia ?

Adria and *Apulia* terms are very often used as synonyms in the literature. The classic interpretation of the Hellenic orogen is that of a complex nappe pile between an Apulian microcontinent foreland and a Rhodope hinterland (Aubouin et al. 1970, Jacobshagen 1986) [from Piper Igneous rocks p11]. Accordingly, the term *pre-Apulian* was used extensively since 70's or 80's for the most external part of the nappe pile known also as *Paxon unit* appearing to the western part of Greece.

Although much debated, a more recent terminology implies that the Adria microplate is a continental block that extends NW–SE, and is mainly occupied by the Adriatic basin but also includes the Po Plain, Istria, the Gargano Promontory and the Apulian Peninsula. The microplate is surrounded by several strongly deformed belts originating: (i) from the collision with the Eurasian plate (e.g. the Dinaric–Albanian–Hellenic chain during the Cretaceous – Paleocene; the Southern Alpine chain from Oligocene to the present), (ii) post-collisional rotation of the Sardinia Block (Northern Apennine belt) and (iii) from subduction-related migration towards the SE (Southern Apennine belt) of the Calabrian arc. The Adria microplate, including the Adriatic region, has generally been considered as a single, rigid and nearly aseismic block with seismicity mostly confined to its margins (e.g. [Scisciani and Calamita 2009](#)).

According to the most accepted reconstructions, (e.g. [Stampfli and Borel 2002, 2004, Moix et al. 2008, von Raumer and Stampfli 2008, von Raumer et al. 2009, Spiess et al. 2010](#)) Apulian plate, along with Cimmerian plate, represents a part of the southern (“Gondwanian”) passive margin of the Paleo-Tethys since Late Ordovician – Silurian (**Fig. 2.7a**). During the northward subduction of Paleo-Tethys below the southern European margin in Carboniferous times, magmatic events affected the continental crust below the future Pelagonian and Adria platform (**Fig. 2.7b**). Shortly after, at M. – L. Permian, the northern Gondwanian margin splits for the creation of the Neotethys and the separation of the Cimmerian and the Apulian block (**Fig. 2.7c**). Branches of the Neo-Tethys are both Vardar/Axios and Pindos oceanic domains bordered by Permo -Triassic rift-related magmatism and sedimentation. The continuous northward subduction of the neo-Tethian branches, in the Hellenic realm, resulted in the consumption of these oceanic domains and the accretion of the Pelagonian and Adria continental crust onto the stable southern European margin. The coupling of the Apulia and Adria microplates happened in Late Cretaceous – Paleogene according to [Stampfli and Borel \(2002\)](#).

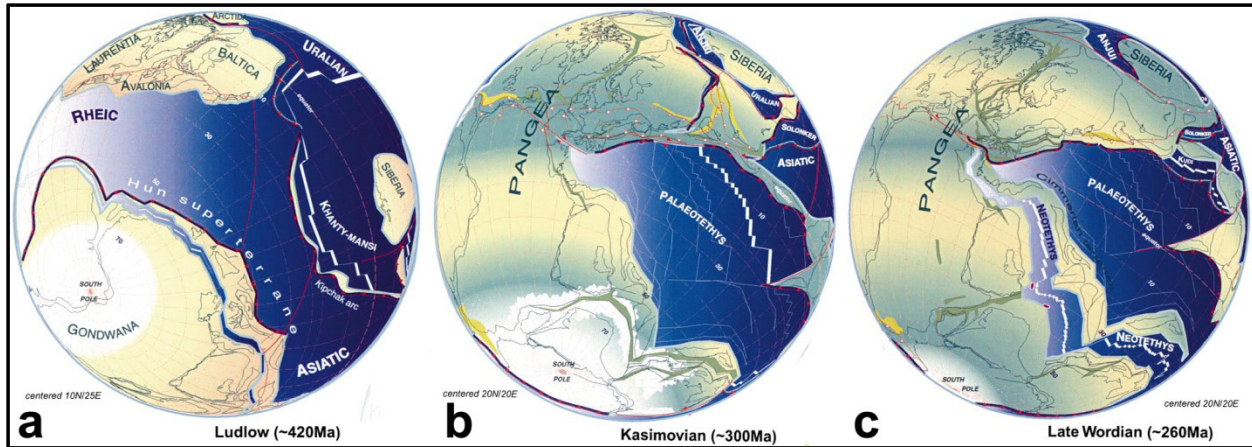


Fig. 2.7. Plate reconstruction model (Stampfli and Borel 2002). (a) Ordovician – Silurian rifting and opening of the Paleo-Tethys is accompanied by the separation of the so-called *Hun Superterrane* (see also von Raumer et al. [2008] for a younger terminology) from the northern Gondwana margin. (b) Continuous northward subduction of the Paleo-Tethys beneath the southern European margin caused the Permo-Carboniferous magmatic event in Pelagonian and Adria continental crust. (c) Rifting near the southern margin of the Paleo-Tethys led to the opening of the Neo-Tethys and the separation of Apulian and Cimmerian blocks (or the so called *Cimmerian Greater Apulian Terrane*).

Σχ. 2.7. Μοντέλο παλαιογεωγραφικής αναπαράστασης (Stampfli and Borel 2002). (a) Η ταφρογένεση του Ορδοβισίου – Σιλουρίου οδήγησε στη διάνοιξη της Παλαιο-Τηθύος συνοδευόμενη από την αποκόλληση του τεκτονοστρωματογραφικού πεδίου *Hun* (βλ. επίσης την εργασία των von Raumer et al. [2008] σχετικά με τη νεότερη ονοματολογία) από το βόρειο περιθώριο της Γκοντβάνα. (b) Η προς βορρά βύθιση της Παλαιο-Τηθύος προκάλεσε εκτεταμένο μαγματικό στο Πέρμιο – Λιθανθρακοφόρο που επιρρέασε τον ηπειρωτικό φλοιό της Πελαγονικής και της Άντριας. (c) Ταφρογένεση κοντά στο νότιο περιθώριο της Παλαιο-Τηθύος οδήγησε στη διάνοιξη της Νεο-Τηθύος και την αποκόλληση των θραυσμάτων της Απούλιας και των Κιμμερίδων.

Judging from the above, it is obvious that European affinity is suitable for the Adria microplate which is characterized by Permo-Carboniferous magmatism while Apulia microplate is totally missing this subduction-related magmatism. The extensive Permo-Carboniferous magmatism reported from Kythira and Crete place the External Hellenides at the southern European margin during the subduction of the Paleo-Tethys during that time. Taking into consideration that the age of the continental crust below Tripolitsa unit is known from Kythira and Crete but below Paxon unit is not known, the latter unit can either represent a southern prolongation of Adria platform or a part of Apulia amalgamated with Adria in Cenozoic as is the case in Italy. In other words, Permo-Carboniferous magmatism is only compatible with Adria microplate.

The present-day relatively small distance between the western part of Greece (Paxon and Ionian units) and the eastern part of Italy (Apulia s.s.) is caused by the rapid roll-back of the Calabrian arc since Upper Miocene (~6Ma; Rosenbaum et al. 2006), contemporaneous with the Hellenic rollback (Jolivet and Brun 2010) and the initiation of Kephalonia transform fault (~5Ma; Royden and Papanikolaou 2011, in press). This means that Paxon unit (and Ionian unit also) doesn't necessarily correlate with the Apulia s.s. platform simply due to their present geographical position.

2.3 Geological setting of the Feneos area

Feneos area is situated at the Northern Peloponnese. The Feneos valley (Fig. 2.8), with an almost triangular N-S directed shape, separates Ziria Mt. to the east from Helmos Mt. (Aroania) to the west. The main geotectonic units found at the northern Peloponnese are, from bottom to top, *Phyllite-Quartzite unit*, *Tyros beds* (or equivalent) and *Tripolitsa carbonates* (also referred as *Tripolitsa unit* in general), *Pindos unit*, *Pelagonian platform* and finally, the uncomfortably overlying post-alpine sediments related to the Corinth Gulf.

The study area (Fig. 2.8, 2.9) occupies the central and northern Helmos Mt. as well as the western flanks of Ziria Mt. and, at a first approximation, is mainly covered by deformed metasediments, mafic volcanics and carbonate rocks. The geotectonic units appearing are the Phyllite - Quartzite unit and the Tripolitsa unit, especially the base of it, known as Tyros beds.

Pioneering work was done in this area by De Wever (1975) according to whom the relative autochthonous was named as "Zarouchla Group". In Parnon and Taygetos, South Peloponnese, the relative autochthon is instead the *Plattenkalk unit*. De Wever (1975) recognized five distinct units based on the different mineralogical composition (Fig. 2.9b): i) The *Feneos formation*, consisting of quartzites, quartz-phyllites and pelitic schists; ii) The *Goura formation*, consisting of irregular alternations of thin limestone beds and sericite schists; iii) The *Ag. Elias formation*, composed mainly of intermediate and basic metavolcanics; iv) The *Ag. Nikolaos formation*, consisting of various metaclastic lithologies (impure quartzites, metaconglomerates and schists) and v) The *Kinigos formation*, with green and violet sandy schists and local intercalations of small calcarenitic lenses.

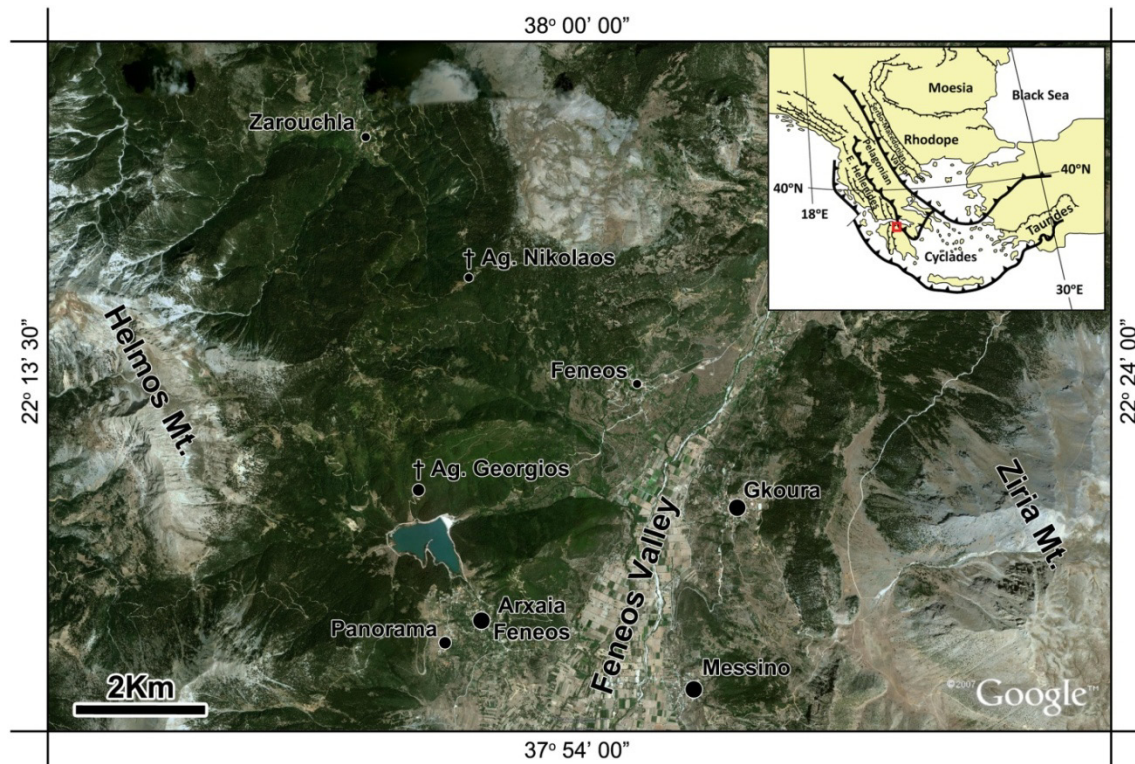


Fig. 2.8. Satellite image (Google Earth) of the study area. Projection system: WGS84.
Σχ. 2.8. Δορυφορική εικόνα (Google Earth) από την περιοχή μελέτης. Προβολικό σύστημα: WGS84.

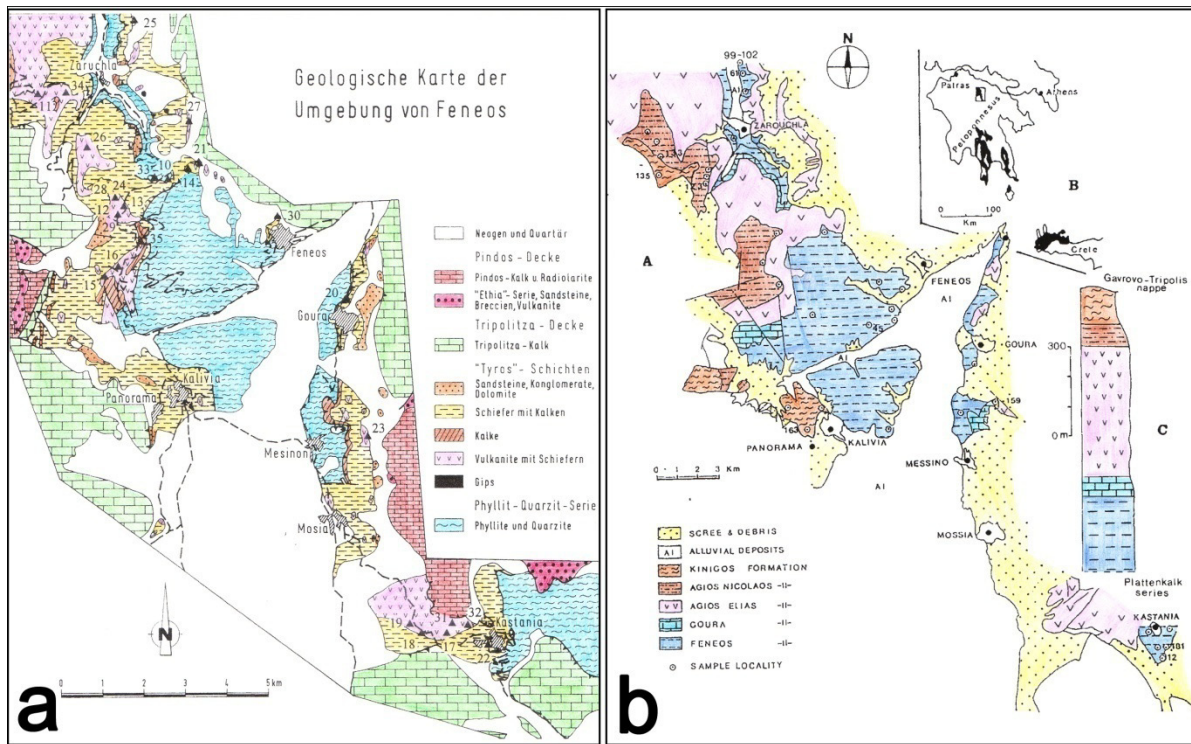


Fig. 2.9. Geological map of the Feneos area after (a) Dornsiepen and Manutsoglu (1996) and (b) De Wever (1975) (from Katagas et al. [1991]).

Σχ. 2.9. Γεωλογικός χάρτης της περιοχής του Φενεού κατά (a) Dornsiepen and Manutsoglu (1996) και (b) De Wever (1975) (από Katagas et al. [1991]).

2.3.1 Phyllite-Quartzite Unit

Lekkas and Papanikolaou (1977) distinguished the five above formations into two piles: the uppermost, consisting of Ag. Elias metavolcanics and Ag. Nikolaos and Kinigos metaclastics, and the lowermost, consisting of Feneos and Goura quartzites and metapelites. The uppermost pile is generally accepted that it represents the Tyros beds in the Feneos area. Despite the fact that Lekkas and Papanikolaou (1977) correlated the lowermost pile with the Plattenkalk unit, numerous authors later on, correlated it with the Phyllite - Quartzite unit (e.g. Xypolias and Doutsos 2000, Xypolias and Koukouvelas 2001, Jolivet et al. 2010).

The Phyllite - Quartzite unit in Feneos (Feneos and Goura formations) is a metasedimentary pile dominated by pure quartzites, micaceous quartzites and metapelites with irregular alterations of thin limestone beds (Katagas et al. 1991). The main assemblage reported by these authors is quartz + phengite + chlorite + albite with rare occurrences of garnet (near Kastania area, SE of Gkoura village) and chloritoid (north of Zarouchla village). Pressure-indicative minerals in this kind of metasediments can be the garnet, the chloritoid or the phengite (3.46 Si p.f.u. reported from Katagas et al. 1991). Chloritoid-bearing metasediments were also reported by Dercourt (1964) south of Ag. Nikolaos church.

Summarizing the work of Katagas et al. (1991) has revealed: a) Judging from illite crystallinity and conventional thermobarometry, the Phyllite - Quartzite unit is of greater metamorphic grade

compared to the overlying Tyros beds without, though, a pronounced metamorphic gap in between, b) the peak temperature never exceeded 440°C with the most possible temperature being between 340°C and 420°C, c) peak pressure is not well constrained but it should have never exceeded 5Kbar. The suggested peak metamorphic conditions are compatible with the low-stability field of Fe-chloritoid in typical metapelites in the system KFASH (Spear and Cheney 1989). Significantly higher temperature of ~500°C, but for the same maximum pressure (~4-5Kbar), was suggested by Jolivet et al. (2010) using Raman spectrometry in carbonaceous material. Few kilometers to the SE of Gkoura village, in Kastania area, Jolivet et al. (2010) suggested even higher pressure (~10Kbar) for the same maximum temperature (~500°C). This is the same area where Katagas et al. (1991) reported the existence of garnet.

2.3.2 Tripolitsa Unit

The Tripolitsa unit can be distinguished in the underlying Tyros beds and the overlying carbonates. In its type locality in southern Peloponnese, the Tyros beds is named after Ktenas (1924). The Tyros complex consists of slates with metapyroclastic rocks and meta-andesites and is locally conformably overlain by Triassic limestones, which are correlated with the lower part of the Tripolitsa carbonates (Thiebault 1982). A rather detailed stratigraphy of the Tyros beds is given by Gerolymatos (1993). As described above, Tyros beds is represented, in the study area, by a thick sedimentary pile with, normally massive, mafic bodies. The metasedimentary sequence corresponds to the De Wever's Ag. Nikolaos and Kinigos formations while the related mafic bodies correspond to the De Wever's Ag. Elias formation.

The mafic bodies contain the peak paragenesis quartz + albite + chlorite + lawsonite ± epidote while pumpellyite, actinolite, muscovite, titanite and iron oxides occurring in variable amounts (Baltatzis and Katagas 1984). The metasediments that belongs to the Tyros beds (Ag. Nikolaos and Kinigos formations), contain the paragenesis quartz + albite + phengite + chlorite (Katagas et al. 1991). Note that no relatively high-P minerals do exist and the Si content of phengite is moderate (3.26 a.p.f.u.; Katagas et al. 1991, Table 2).

Judging from illite crystallinity applied in metasediments, Katagas et al. (1991) claimed that the peak metamorphic conditions of the Tyros beds in Feneos are slightly lower than those of the underlying Phyllite - Quartzite unit without a significant metamorphic gap and the peak metamorphic temperature should be around 300°C. Indicative relative high-P minerals, such as lawsonite, reported from the metabasic rocks (Ag. Elias formation) occurring within the sedimentary pile of the study area (Baltatzis and Katagas 1984). The metamorphic conditions, as calculated from the mafic rocks are 290°C – 380°C and 3.5 – 5Kbar, in good agreement with the peak temperature obtained from the related metasediments (Ag. Nikolaos and Kinigos formations). The geochemistry of the mafic rocks belonging to Tyros of Feneos area, corresponds to subduction-related tholeiites while in the type locality (Tyros area, Eastern Peloponnese) are generally calc-alkaline (Pe-Piper 1983).

The equivalent of Tyros beds in Crete is the so called “Ravdoucha beds” (Randoucha, Selia, Lasithi; Sannemann and Seidel 1976) where a relatively low-grade high-P metamorphic degree (e.g. Creutzburg and Seidel 1975, Seidel et al. 1982) is based on the existence of minerals such as carpholite (Kopp and Ott 1977) or by the illite crystallinity (Feldhoff et al. 1991).

Tripolitsa carbonates are known from Peloponnese and Crete to extend from Upper Triassic to Upper Cretaceous just before the flysch deposition in Lower Cenozoic (e.g. [Fleury 1980](#)). Tripolitsa carbonate rocks are found east and west of Feneos Valley, at the mountains of Ziria and Helmos respectively. According to IGME (Fyllo Kandila; [1982](#)), the Upper Triassic has been documented by the existence of *Megalodon*, the Jurassic by the existence of *Protodiceras* and *Clypeina jurassica* and the Middle - Upper Cretaceous by the existence of rudists.

Although much debated, some studies have shown that Tripolitsa in Crete is slightly metamorphosed ([Karakitsios 1979](#), [Hall et al. 1984](#), [Feldhoff et al. 1991](#), [Klein et al. 2004](#), [Rahl et al. 2005](#)). In any case, the temperature of metamorphism doesn't exceed 260°C ([Rahl et al. 2005](#)). Unfortunately, to my knowledge, no data are available for Peloponnese.

2.3.3 Pindos unit

Pindos unit is well known from both Crete and Peloponnese. It represents a pelagic sequence consisting of radiolarites, pelagic limestones and clastic sediments of Triassic – Upper Cretaceous followed by a Lower Cenozoic flysch (e.g. [Dercourt 1964](#), [Fleury 1980](#)). Pindos unit is commonly accepted to be unmetamorphosed and it covers mainly northern and western Peloponnese, as well as Argolis area. Where Pindos unit is missing, the underlying Tripolitsa and Phyllite - Quartzite units are exposed as domes (Taygetos and Parnon mountains, S.Peloponnesos).

In the study area, Pindos unit appears thrusted on top of Tripolitsa north of Feneos village. Further east, Pindos unit is dismembered by E-W-trending normal fault and covered by Plio-pleistocene sediments. To the west, Pindos appears on the hanging wall of Gardiki fault ([Skourtos and Kranis 2009](#)). Further west, Pindos unit appears as a continuous nappe until the fold-and-thrust belt in Erymanthos Mt..

2.3.4 Post-alpine sediments

Northern Peloponnese is strongly influenced by the opening of the Corinth Gulf which resembles a half graben. It is commonly accepted that the opening of the basin is in N-S direction accommodated by E-W-trending normal faults ([Fig. 2.10](#)). Although many authors (e.g. [Armijo et al. 1996](#), [Ghizetti and Vezzani 2005](#), [Rohais 2007](#)) argue for the initiation of the extension in M. – Up. Pliocene, Papanikolaou et al. ([2009](#)) argued for earlier extension (i.e. Middle Miocene). The uplift rates in N.Peloponnese measured between 1 and 1.5mm/yr using Pleistocene marine terraces ([Armijo et al. 1996](#)).

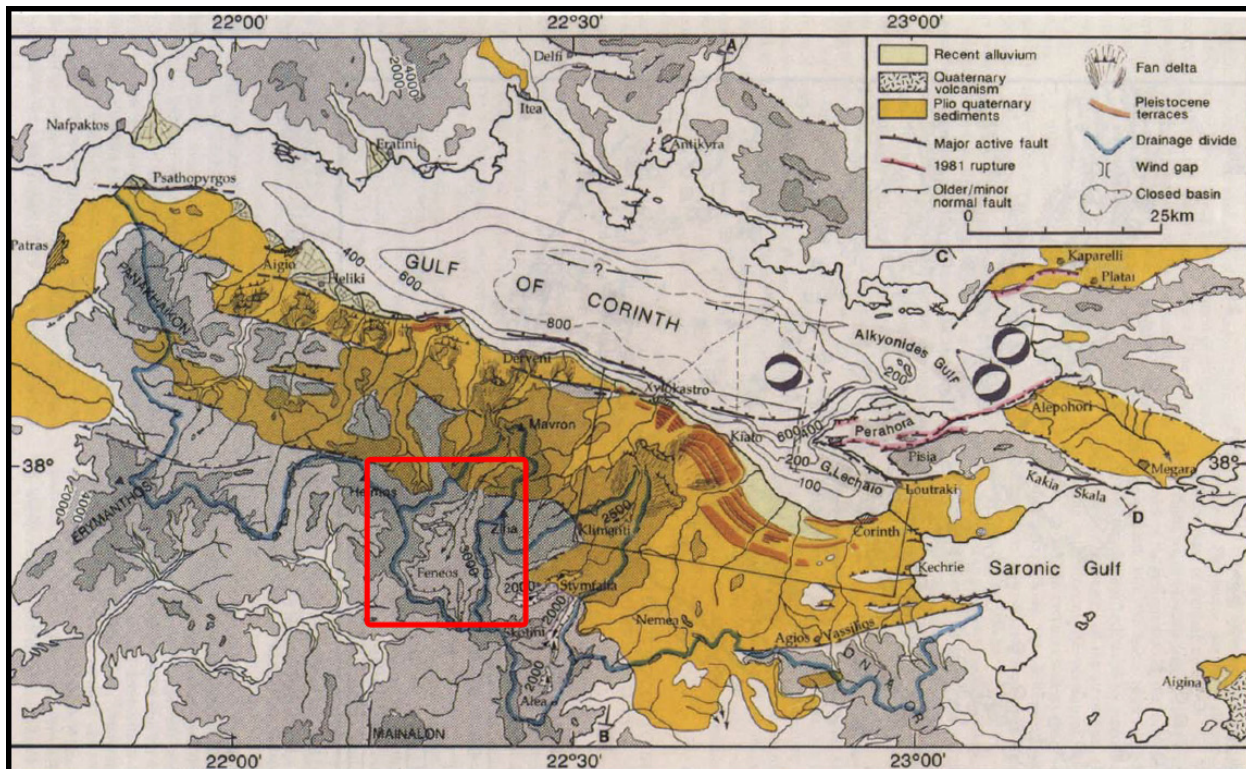


Fig. 2.10. Post-alpine sediments from Northern Peloponnese related to the opening of the Corinth Gulf (Armijo et al. 1996). The study area is marked with a red box.

Σχ. 2.10. Μετα-αλπικά ιζήματα της Β. Πελοποννήσου που σχετίζονται με τον εφελκυσμό του Κορινθιακού Κόλπου (Armijo et al. 1996). Η περιοχή μελέτης σημειώνεται με ένα κόκκινο τετράγωνο.

In the study area, post-alpine sediments related to the Gulf of Corinth can be found to the north, bordered by E-W trending faults (Khelmos and Monodendri fault; Skourtos and Kranis 2009). Sorel (2000) suggested that the opening of the Gulf is related to a north-dipping low angle fault and all the surface-exposed E-W-trending normal faults are branching from this structure. The southern break-away zone of Corinth Gulf is still debated. Although many authors place the southern border of the Gulf just north of Helmos and Ziria mountains, a recent suggestion from Skourtos and Kranis (2009) has placed it further south, to the Northern Mainalon Fault Zone (NMFZ).

2.4 Problems imposed

As far as the Phyllite – Quartzite unit is concerned, its palaeogeographic position, the degree of metamorphism and especially the relationship with the surrounding geological units is a matter of long-lasting debate. In both Peloponnese and Crete, it definitely represents a HP unit underlie by non- or less-metamorphosed units (Tyros beds and Tripolitsa carbonates or Pindos unit) and overlying a possibly equally- or less-metamorphosed unit (Plattenkalk unit).

2.4.1 Metamorphism

The metamorphism of the Phyllite - Quartzite unit itself is a matter of great contradictions. Although it seems that the peak-metamorphic conditions decrease eastward in Crete and northward in Peloponnese, the absolute values of pressure and temperature show great difference between authors. Note that, normally, the metapelites studied from the Phyllite - Quartzite unit are an excellent rock-type to infer metamorphic conditions due to their sensitivity in both pressure and temperature changes.

For example, in southern Peloponnese, the peak-metamorphism took place between 4-6.5Kbar / 325-400°C ([Thiebault and Triboulet 1983](#)) and 17±4Kbar / 450±30°C ([Theye and Seidel 1991](#)). This pressure difference, if real, could correspond to a depth difference of ~20-40Km which is extremely difficult to be believed because of the thickness of the Phyllite - Quartzite unit which is not, at maximum, much more than only 1Km. Possible explanation for this pressure difference, if the conditions suggested by different researchers are correct, is the lack of equilibrium, or the equilibrium at lower metamorphic conditions (during retrogression). In that case, the maximum pressure (~17±4Kbar) obtained could correspond to the real peak-metamorphism which is equal to ~50Km of depth.

In contrast, it is commonly accepted that the overlying Tyros beds (e.g. [Creutzburg and Seidel 1975](#), [Seidel et al. 1982](#), [Baltatzis and Katagas 1991](#), [Feldhoff et al. 1991](#)) and Tripolitsa carbonates (e.g. [Rahl et al. 2005](#)) are slightly metamorphosed and the depth of metamorphism is equal to ~10Km.

2.4.2 Tectonic contacts

From the above, it is obvious that there is a metamorphic gap between the Phyllite - Quartzite unit and the overlying Tyros beds and Tripolitsa carbonates which could be equal to ~20-50Km difference in metamorphic depth. This difference led several authors (e.g. [Fassoulas et al. 1994](#), [Jolivet et al. 1994, 1996, 2010](#), [Papanikolaou and Vassilakis 2010](#)) to suggest the existence of a major extensional tectonic contact (i.e. a detachment) between the Phyllite – Quartzite and the Tripolitsa units for both Crete and Peloponnese. This extensional contact is supposed to have exhumed the Phyllite - Quartzite unit from the depth of ~40-50Km to the mid-crustal level between 25Ma and 15Ma as shown by $^{39}\text{Ar}/^{40}\text{Ar}$ ([Seidel et al. 1982](#), [Jolivet et al. 1996, 2010](#)). Meanwhile, the Tripolitsa unit has rested in the uppermost 4-7Km of the crust since at least 35Ma ([Thomson et al. 1998a](#)) forming the hanging wall of this extensional contact. Although this scenario requires the existence of major (mylonitic) shear zones,

these have never been described from the field. Instead, tectonic breccias of the brittle regime between the two units have been described. The entering in the brittle field (at ~20Ma - 15Ma) and the subsequent erosion of the Phyllite - Quartzite unit is shown in Crete by the Upper Miocene breccias and conglomerates in *Topolia formation* from Crete (Seidel et al. 2006b) where surface exposure of the Phyllite - Quartzite unit must have taken place at ~10Ma or later.

If we accept the concept of the major extensional contact, then the amount of extension is proportional to the metamorphic difference between the overlying Tripolitsa unit and the underlying Phyllite - Quartzite unit. Due to this fact, the extension should be much more pronounced in central – western Crete and southern Peloponnese than elsewhere. The post-HP shearing, related to exhumation of the Phyllite - Quartzite unit is to-the-N in Crete and to-the-NE in Peloponnese.

2.5 Purpose of this study

This study has two major objectives. The first originates from the observation that in places where the extension is intense (e.g. Crete, Taygetos Mt.), the metamorphic gap between the Phyllite - Quartzite unit and the overlying Tyros beds (or Ravidoucha beds in Crete) is large and equals to a depth difference of ~30-40Km. In the study area, the northernmost exposure of PQ blueschists, the metamorphic gap is supposed to be almost null. Moreover, the post-HP shearing recorded in the Phyllite - Quartzite unit is constantly to-the-N in Crete (Fig. 2.5) and to-the-E or to-the-NE in S. Peloponnese (Fig. 2.3). On the contrary, the early pre-HP shearing in the Phyllite - Quartzite unit is to-the-S for Crete (Fig. 2.5; Jolivet et al. 1996) and to-the-W for Peloponnese (Fig. 2.3a). The relationship between shearing (early pre-HP and post-HP), the difference in metamorphic grade (Phyllite - Quartzite unit and Tyros beds) and the transition from ductile to brittle structures are chosen to be studied in the Feneos area.

The second objective of this study is to provide new data on the source material of a quartzite (metasandstone) that belongs to the Phyllite - Quartzite unit. The rock is exposed near Feneos village and the new data obtained will strongly test the accuracy of the reconstruction models proposed for the eastern Mediterranean (e.g. Stampfli and Borel 2002). This work will be based on the available provenance tools (i.e. detrital zircon ages, Sr and Nd isotopes, major- and trace-elements, REE and multi-elements normalized patterns, discrimination diagrams) and is strongly inspired by the work of Meinhold et al. (2010) for the circum-Rhodope belt.

2.6 Summary

Two major blueschist belts appear in the Hellenic orogeny (**Fig. 1.3**): the internal (or Cycladic) blueschists belt appearing mainly in Cyclades and the external blueschists belt appearing in Peloponnese and Crete. The Phyllite - Quartzite unit mainly represents the HP rocks in Peloponnese and Crete. Both the two blueschist belts appear below Pindos suture zone.

The Phyllite - Quartzite unit is a metasedimentary sequence of Upper Permian – Lower Triassic stratigraphic age (**Plate 2**) metamorphosed under blueschist facies. It lies below Tyros beds and Tripolitsa unit and above Plattenkalk unit, wherever exposed (e.g. Taygetos Mt., Parnon Mt., Dikti Mt.) (**Fig. 2.3, 2.4**). The major pressure attained in eastern Crete and southern Peloponnese is between 10Kbar and 15Kbar although both higher and lower pressures have been suggested by different authors. The peak-metamorphic conditions of the Phyllite – Quartzite unit decrease eastward in Crete and northward in Peloponnese.

Exposed continental crust lying below Pindos suture zone is well described from Attica, Kythira, Cyclades and Crete. Those basement rocks (orthogneisses and paragneisses) represent Adria's crustal slices (**Plate 1**) and their magmatic age shows three pronounced peaks (U/Pb in zircons; **Fig. 2.6, Plate 2**): (i) Middle Cambrian ages (~510Ma) representing a late Panafrican event (mainly in Crete), (ii) Permo-Carboniferous ages (290Ma – 330Ma) of the Hercynian event (Kythira, Crete, Cyclades) and (iii) Permo-Triassic rift-related ages (Attica, Tinos).

In the Feneos area, the Phyllite - Quartzite unit and the Tyros beds are dominating (**Fig. 2.9**). Meta-sediments appear in both units while Tyros beds contains also thick massive mafic bodies metamorphosed at lower greenschist facies. The Phyllite - Quartzite unit have, in places, relatively HP-minerals (garnet, chloritoid, phengite) but the metamorphic gap between those two units seems null, in contrast to the situation observed elsewhere. The peak metamorphic conditions should not have exceeded 3-5Kbar and 300-400°C for both units.

The metamorphic gap observed between the Phyllite - Quartzite unit and the overlying Tyros beds from southern Peloponnese and Crete led several authors to suggest the existence of a major extensional tectonic contact (i.e. a detachment) between them. The hanging wall of this contact (Tripolitsa and Pindos units) rested in the 4-7Km of the uppermost crust since Eocene times while the footwall (Phyllite - Quartzite unit) arrived at mid-crustal level between 15Ma and 25Ma (as shown from Ar/Ar dating) and exposed on the surface around 10Ma (as shown by upper Miocene sediments). The post-HP shear direction related to this extensional contact is to-the-NE in Peloponnese (**Fig. 2.3**) and to-the-N in Crete where it also follows an older to-the-S shear direction (**Fig. 2.5**).

Geological mapping – structural and kinematic analysis

Chapter 3

The study area is the northernmost exposure of the external blueschists belt represented by the Phyllite – Quartzite. Xypolias and Doutsos (2000) and Xypolias and Koukouvelas (2001) interpreted the Phyllite – Quartzite unit exposed in the area as a crustal-scale shear zone showing an antiform structure, and concluded that a mixed pure and simple shear model is required to explain the finite strain pattern. In particular, they proposed that within the 1Km thick sedimentary sequence the simple shear mechanism dominates in the lowest structural levels while near the flanks of the exposed antiform the pure shear mechanism is dominant. Top-to-the-W or -SW sense of shear is deduced from the quartz c-axis and the fold asymmetry in mesoscale while top-to-the-E or -NE is only observed to the east and in a distinct thin zone within the exposed dome.

The geological mapping and the structural analysis of the Feneos area (Fig. 2.8) was carried out during the summer of 2010 and the winter of 2011. The geological mapping of this study is widely based on the previous mapping of De Wever (1975) and Dornsiepen and Manutsoglu (1996) while the structural data presented here are mostly deriving from the Phyllite – Quartzite unit and less from the overlying Tyros beds. Among the objectives of this study are: (i) to provide a detailed foliation map, (ii) to provide a detailed lineation map, (iii) to record the extension-related shearing as documented by the various shear sense indicators (S-C structures, porphyroblast rotation, fold asymmetry etc.) and (iv) to study the transition from ductile, to semi-brittle and finally to purely brittle structures. Additionally, a complete provenance analysis of a selected quartzite from the study area was carried out (see Chapter 5).

3.1 Rock types

The study area (Fig. 3.1) is mostly covered by metasediments, mafic rocks and carbonate rocks. Quaternary alluvial deposits obscure the rock structure of the area. The central part of the area studied is covered by an exposed core (dome) of metasediments as well as slightly metamorphosed mafic rocks. The mafic rocks seem to increase towards the north. The exposed core is flanked by carbonate rocks but

chunks of limestones were also found within the core. The post-alpine mostly Pliocene rocks are exposed to the north of the study area on the hanging wall of E-W-trending normal faults.

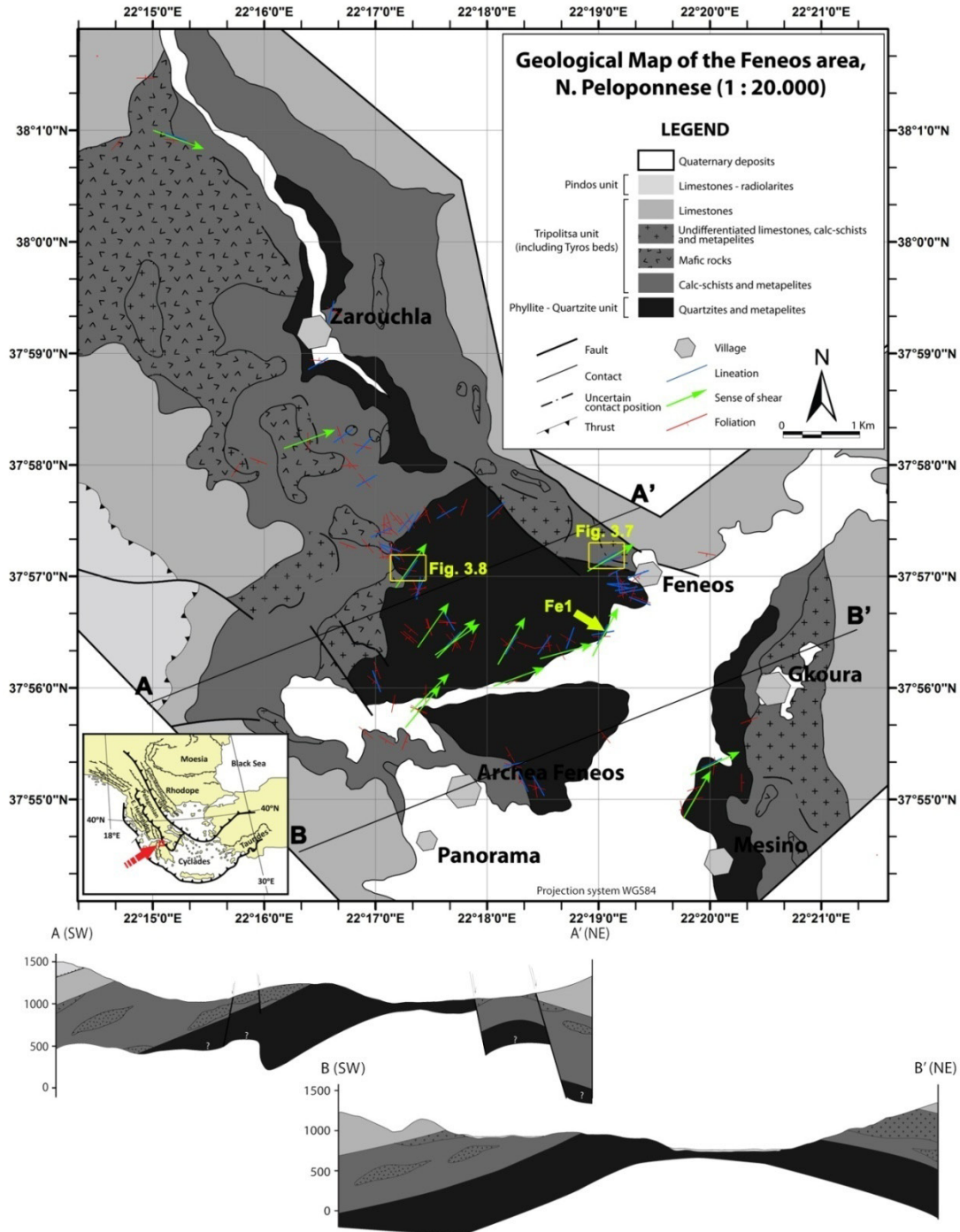


Fig. 3.1. Geological map of the study area corrected after De Wever (1975) and Dornsiepen and Manutsoglu (1996). Lineation (blue lines), sense of shear (green arrows) and foliation measurements (red lines) are superimposed on the geological map. Two selected geological cross-sections are drawn below the map. Sampling locality (Fe1; yellow arrow) and the locality of the outcrops (Fig. 3.7, 3.8; yellow boxes) are also shown. A larger print of the map is presented in the “Map” section (p.99).

Σχ. 3.1. Γεωλογικός χάρτης της περιοχής μελέτης διορθωμένος από τις εργασίες των De Wever (1975) και Dornsiepen and Manutsoglu (1996). Οι μετρήσεις της γράμμωσης (μπλε γραμμές), της κινηματικής (πράσινα βέλη) και της φύλλωσης (κόκκινες γραμμές) είναι σημειωμένες στο γεωλογικό χάρτη. Η θέση δειγματοληψίας (Fe1; κίτρινο βέλος) και οι θέσεις των σχημάτων 3.7 και 3.8 έχουν επίσης σημειωθεί. Δύο επιλεγμένες γεωλογικές τομές έχουν σχεδιαστεί κάτω από το χάρτη. Ο χάρτης παρουσιάζεται σε μεγαλύτερο μέγεθος στο τέλος του συγγράματος (Maps p.99).

The Phyllite – Quartzite unit forms the core of the dome and is represented by meta-sediments (quartzites and metapelites). The other constituent of the dome is the Tyros Beds represented by pure metapelites or metapelites with calcite intercalations (calc-schists) and by mafic rocks. Tripolitsa carbonates appear on both limbs of the exposed dome. Rock types typical of Pindos are observed only to the west where young faulting is responsible for their placement next to Tripolitsa carbonates. Two panoramas near the southern and the northern margin of the study area are shown in **Plate 4**. A brief description of the various rock types found is following.

Quartzites

The most common rock types are fine- to medium-grained quartzites either appearing as massive rocks or as thick-foliated rocks with mm-thick mica-rich layers (**Fig. 3.2a, 3.2b**). Only quartz and white micas are identified in hand specimen. No carbonate intercalations are observed within these rocks except in one place where the calcite is rather connected to secondary processes. The main foliation, wherever observed, is due to the thin mica-rich layers. The stretching lineation (**Fig. 3.2i**) is commonly formed by elongated quartz crystals. This rock-type belongs exclusively to the Phyllite – Quartzite unit. The primary sedimentary bedding is seen mostly as a sharp boundary appearing parallel to the main foliation (**Fig. 3.2b, 3.2g**).

Metapelites

Metapelites appear mostly as fine-grained rocks containing quartz, white mica and chlorite (**Fig. 3.2g, 3.2h**). The foliation is commonly narrow-spaced due to the increased content in sheet silicate minerals and to the intense vertical shortening. In places, S-C structures are formed, helping in the identification of the movement direction. No pressure-indicative minerals such as garnet were found. In one place (north of Feneos village), a quartzite appear as a lense surrounded by these fine-grained metapelites. In outcrop scale two major types of metapelites are observed based on their color rather: (i) the brown ones covering the majority of the area and (ii) the purple ones (possibly rich in chloritoid; not seen in hand specimen) mainly outcropping to the south of the Ag. Nikolaos church and near Arxaia Feneos village. The above discrimination is solely based on the color and not on the mineralogy and other physical characteristics of the rocks studied. This rock-type belongs both in the Phyllite – Quartzite unit and the Tyros beds with the exception of the purple types which belongs clearly to the Phyllite – Quartzite unit.

Calcareous pelites

Calcareous pelites can appear either as fine-grained rocks where the calcite coexists with the surrounding pelitic matrix or as rocks where typical centimeter- to decimeter-thick calcite layers are intercalated with typical pelites (**Fig. 3.2c**) showing low-grade metamorphism. This rock type is rather rare, appearing only to the north, and probably represents mixed biochemical/clastic sedimentation. It belongs exclusively to the Tyros beds.

Mafic rocks

Mafic rocks appear fine- to coarse-grained and commonly massive without (**Fig. 3.2f**) or with no significantly developed foliation (**Fig. 3.2e**). They either appear as huge masses of outcrop scale (**Fig. 3.2f**) or as meter-long boudins surrounded by metapelites (**Fig. 3.2d**). They commonly contain epidote, quartz and amphibole, mineral composition which is totally compatible with that of a metamorphosed mafic rock under lower greenschist facies. In cases of the coarse-grained rock types the amphibole can be up to 5mm long. No significant relict magmatic textures are observed in hand specimen in most of the cases pointing out the dominance of the metamorphic over the magmatic fabrics. In one place, west of Feneos village, an *ex situ* boulder showing relict magmatic textures (vesicles filled by secondary calcite and quartz within a mica-rich fine-grained matrix) was found.

Carbonates

They appear as grey to light-grey thick-bedded limestones or crystalline limestones and they belong either to the Tripolitsa carbonates or appear mixed within the typical Tyros rock-types. No other mineral except calcite is found in hand specimen. Both a stratigraphic succession and a tectonic contact (i.e. a shear zone; **Fig. 3.7, 3.9**) are found between the limestones and the underlying metasediments. In places, the carbonates are intercalated with thin mica-rich layers.

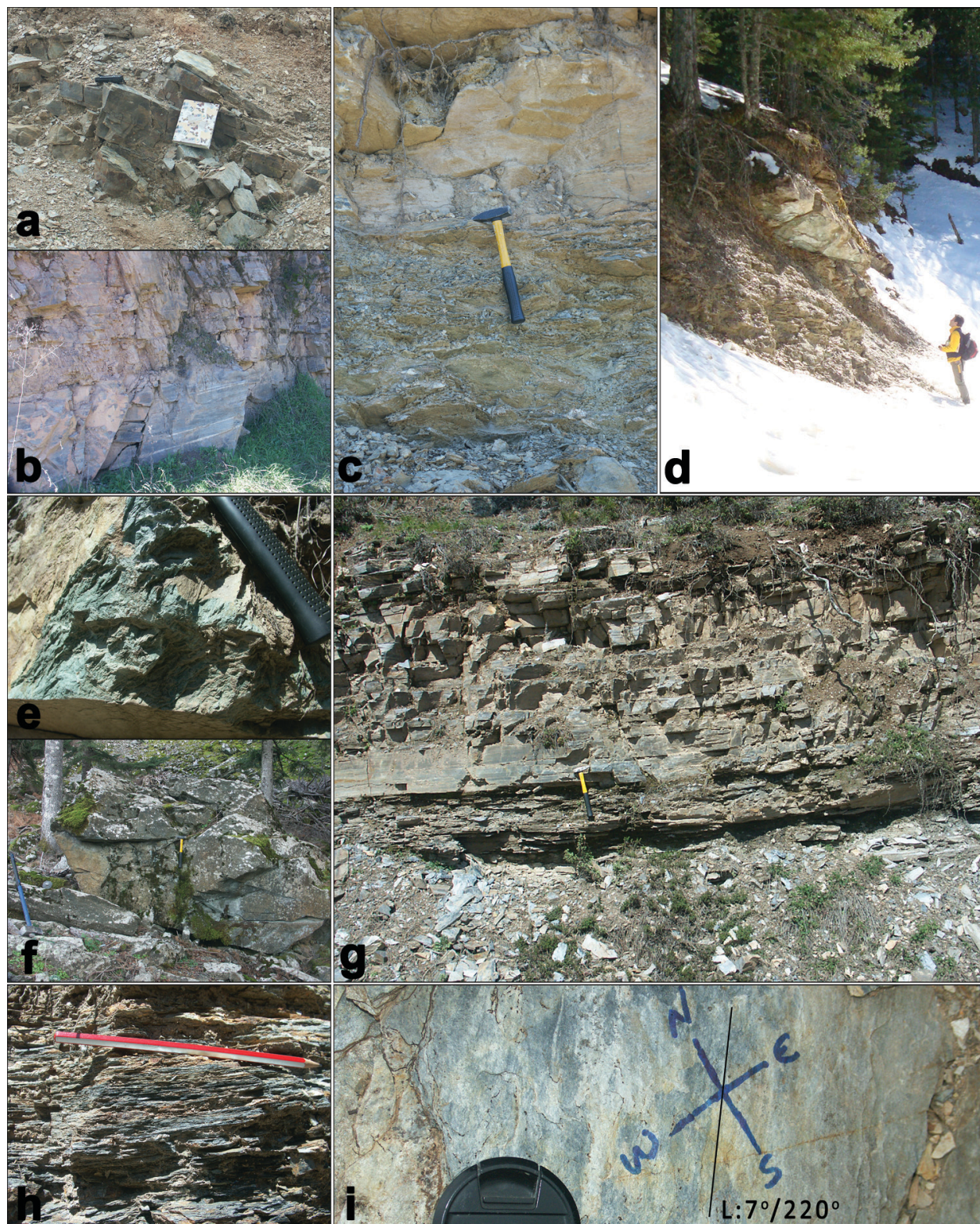


Fig. 3.2. (a) Quartzite with minor thin mica-rich layers forming the foliation of the rock. (b) Massive pure quartzite (below) and bedded impure quartzite with mica-rich layers (above). (c) Thin-bedded calc-schists (below) capped by thick-bedded calcite-dominating calc-schists (above). (d) Mafic rock boudin wrapped by fine-grained metapelites. (e) Fine-grained, epidote-rich mafic rock with minor foliation. (f) Massive mafic rock without significant foliation. (g) Fine-grained metapelites

(below) and quartzites (above). Their contact is a sharp non-tectonic contact possibly reflecting the sedimentary bedding. Note that the foliation is parallel to this sedimentary contact. (h) Typical fine-grained, highly foliated metapelite. It consists of micas, quartz and chlorite. (i) NE-SW-trending stretching lineation developed in thin mica-rich layer intercalated in quartzites. Phyllite – Quartzite unit: (a), (b), (g), (h), (i). Tyros beds: (c), (d), (e), (f).

Σχ. 3.2. (a) Χαλαζίτης με λεπτές ενδιαστρώσεις πλούσιες σε μαρμαρυγίες στις οποίες οφείλεται η σχιστότητα του πετρώματος. (b) Άστρωτος, καθαρός χαλαζίτης που μεταβαίνει σε μη καθαρό χαλαζίτη ενδιαστρωμένο με μαρμαρυγίες. (c) Ασβεστο-πηλίτες με έντονη σχιστότητα που μεταβαίνουν σε ασβεστοπηλίτες στους οποίους επικρατεί το ασβεστιτικό υλικό. (d) Δομή «κομπολογιού» (boudin) ενός βασικού πετρώματος μέσα σε λεπτόκοκκους μεταπηλίτες. (e) Λεπτόκοκκο βασικό πέτρωμα στο οποίο επικρατεί το επίδοτο και το οποίο εμφανίζει ασθενή φύλλωση. (f) Βασικό πέτρωμα χωρίς σημαντική ανάπτυξη της φύλλωσης. (g) Λεπτόκοκκοι μεταπηλίτες που υπόκεινται χαλαζιτών. Η επαφή τους είναι εντελώς οξεία και πιθανότατα αντιπροσωπεύει την πρωτογενή ιζηματογενή στρώση. Η μετέπειτα ανεπτυγμένη φύλλωση είναι παράλληλη με αυτή την επαφή. (h) Τυπικός λεπτόκοκκος μεταπηλίτης με έντονη σχιστότητα. Τα κύρια ορυκτά είναι μαρμαρυγίες, χαλαζίας και χλωρίτης. (i) Γράμμωση έκτασης που αναπτύσσεται σε λεπτά στρωματίδια πλούσια σε μαρμαρυγίες που βρίσκονται ενδιαστρωμένα μέσα σε χαλαζίτες. Ενότητα Φυλλιτών – Χαλαζιτών: (a), (b), (g), (h), (i). Στρώματα Τυρού: (c), (d), (e), (f).

3.2 Structural analysis

In the following paragraphs, the measured foliation, stretching lineation and fold axes will be presented. This will help to understand the geological setting of the study area before discussing the sense of shear and the structural evolution of the area from ductile to brittle deformation. To deduce the sense of movement in the deformed rocks, shear indicators such as those described by Simpson and Schmid (1983) were used.

3.2.1 Foliation map

As described in the previous paragraph, the main foliation is formed by the parallel orientation of fine-grained micas in typical metapelites, calcareous pelites and quartzites. In carbonates and mafic rocks the foliation is usually not well developed. Only a single (dominant) foliation is recorded in the study area without any crosscutting by latter ductile planar surfaces in outcrop scale. The relationship of the foliation with the folds will be discussed in the *Paragraph 3.2.3*. The measured foliation surface is observed to be almost parallel to the initial bedding as marked by the transition between various rocktypes (e.g. metapelites transitioning into quartzites – **Fig. 3.2g**) implying intense vertical shortening. Unfortunately, no HP-indicative minerals, such as garnet, are observed in outcrop and hand-specimen scale being parallel to the foliation, as is the case in the southern Peloponnese. This could reflect the intense retrogression of the rocks forming the study area or the lack of appropriate rock composition. As noted above, the mafic rocks that belong to the Tyros beds act as relatively undeformed and rigid bodies forming map- and outcrop-scale boudins and showing, most of the times, only minor developed foliation (**Fig. 3.1, 3.2e, 3.2f**). The stretching lineation (*Paragraph 3.2.2*) is always measured on the foliation planes (**Fig. 3.2i**).

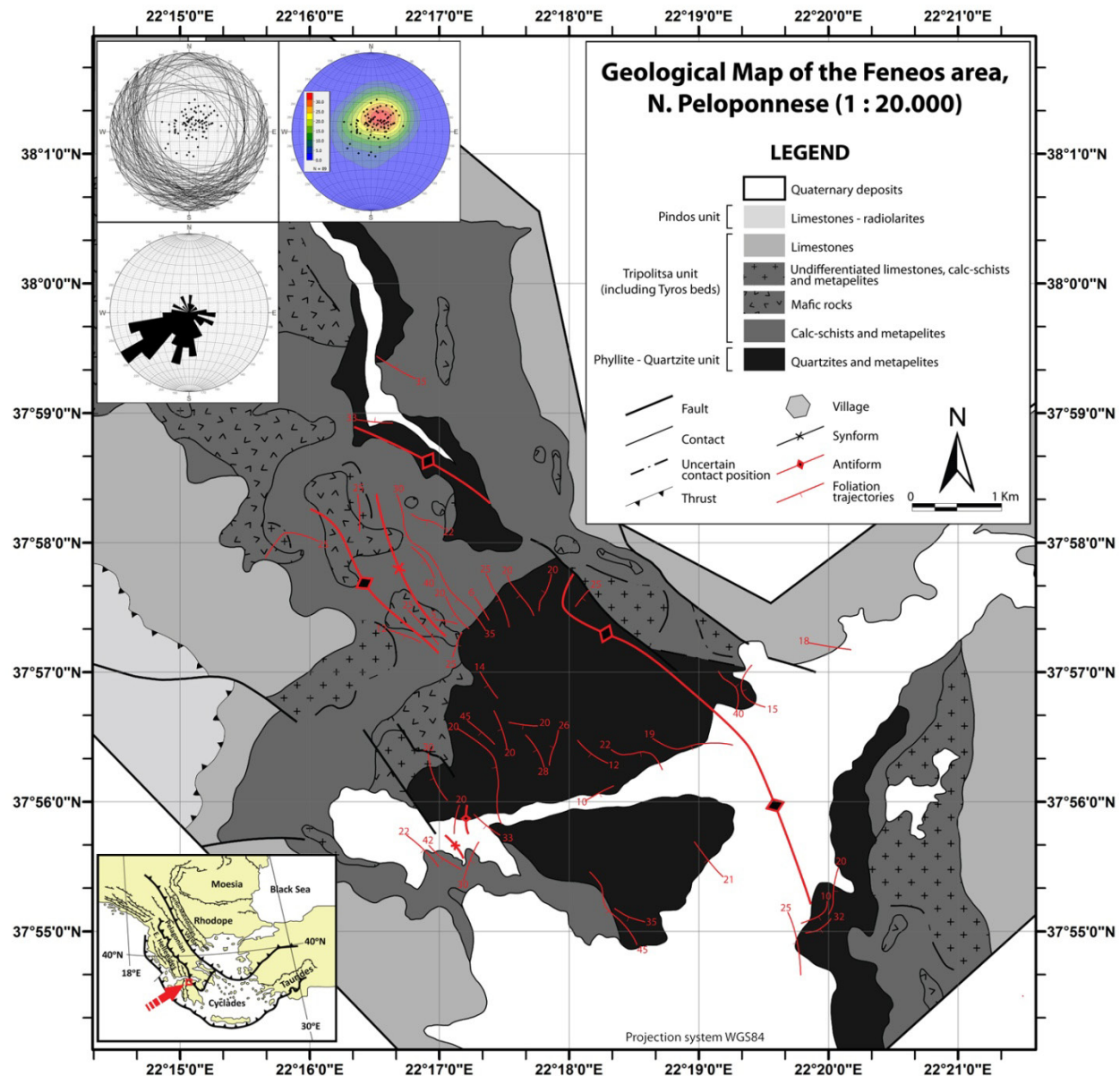


Fig. 3.3. Foliation trajectories map of the study area where the antiform structure of the Phyllite – Quartzite unit is shown. Note the disruption of the antiform due to the NW-SE-trending fault. The axis of the antiform is (sub-)parallel to the fold axes of the mesoscale fold structures. Smaller antiform-synform structure is also shown for the overlying Tyros beds. Small inset: equal area, lower hemisphere projection of the foliations (pole projection as black lozenges), rose diagram and pole density diagram.

Σχ. 3.3. Χάρτης τροχιών φύλλωσης της περιοχής μελέτης όπου φαίνεται η αντικλινική δομή της ενότητας των Φυλλιτών - Χαλαζιτών. Στα ανατολικά φαίνεται η διακοπή της αντικλινικής δομής από ρήγμα διεύθυνσης ΒΔ-ΝΑ. Ο άξονας του αντικλίνου είναι (υπο-)παράλληλος με τις πτυχές μέσης κλίμακας. Μικρότερη αντικλινική-συγκλινική δομή φαίνεται να επιρρεάζει και τα στρώματα του Τυρού. Ένθετο: κυκλογραφική και πολική προβολή των μετρήσεων φύλλωσης, ροδόγραμμα και διάγραμμα πυκνότητας των πόλων της φύλλωσης.

Foliation measurements reveal mostly SW-dipping planes (**Fig. 3.3 inset**), a point crucial for the structural interpretation of the area (see *paragraph 3.4*). The distribution of the foliation planes and the foliation trajectories reveal that the structure of the Phyllite – Quartzite unit is that of an antiform with a roughly NW-SE-directed axis (**Fig. 3.3**). However, a degree of uncertainty during the drawing of the antiform does exist due to the difficulties in approaching and measuring the foliation in more outcrops. The western flank of the antiform is better developed compared to the eastern one which is locally disrupted by NW-SE-trending faults (**Fig. 3.3**). This structure is not considerably different than the structure proposed by Xypolias and Koukouvelas (2001) for the same area, taking into consideration that the detailed mapping during the present study allowed the more careful drawing of the foliation trajectories. The same overall pattern described for the Phyllite – Quartzite unit is true for the overlying Tyros beds where similar NW-trending antiforms and synforms were found (**Fig. 3.3**).

The orientation of the antiform and the synform axes, as shown in map-scale (**Fig. 3.3**), are (sub)parallel to the fold axes measured in outcrop scale both from the Phyllite – Quartzite unit and the overlying Tyros beds (**Fig. 3.5**).

3.2.2 Lineation map

Stretching lineation is mostly measured in metapelites and quartzites on the foliation plane (**Fig. 3.2i**). It is mainly formed by parallel orientation of quartz crystals. The mafic rocks are not likely to show a stretching lineation due to the fact that they behaved as rigid bodies throughout the ductile and brittle deformation without any significant internal deformation.

Most of the stretching lineations measured are from the Phyllite – Quartzite unit and shows a pronounced NE-SW trend (**Fig. 3.4**). The dominant direction of the stretching lineation is between N050° and N060° but minor deviation do exist due to local heterogeneities (**Fig. 3.4 – inset**). Local or regional folding in NW-SE direction causes the lineation to dip either towards the NE or towards the SW. Few intersection lineations measured show a well-defined NW-SE direction and are directly connected to the measured fold axes (see next paragraph). The same NE-SW trend is true for the stretching lineations measured from the overlying Tyros beds (**Fig. 3.4**).

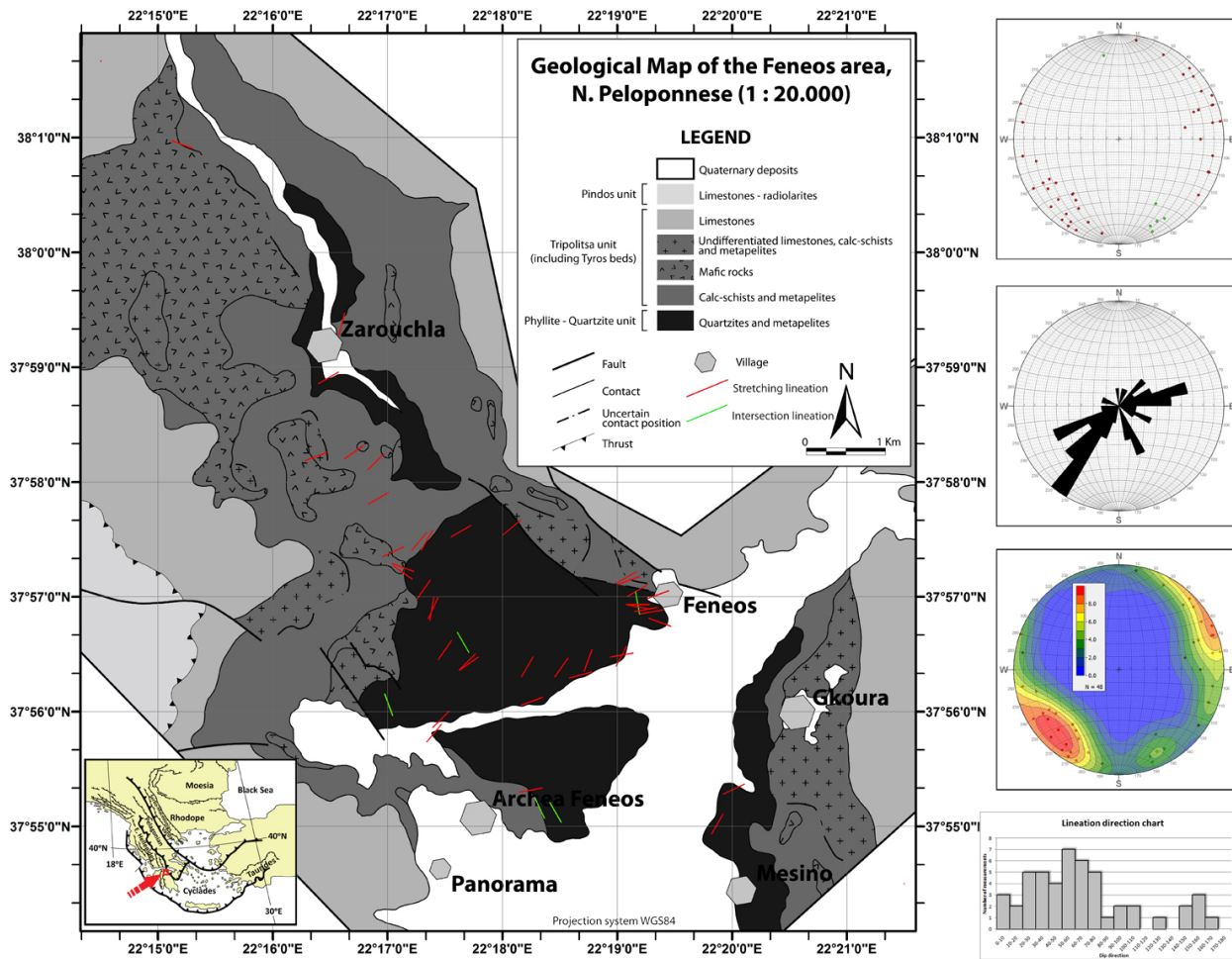


Fig. 3.4. Geological map of the studied area where the stretching (red lines) and intersection (green lines) lineations are superimposed. Inset: Equal area, lower hemisphere projection of the stretching lineation (red dots) and intersection lineation (green dots) along with the related rose diagram and the density plot. The number of measurements vs. dip direction diagram is also shown.

Σχ. 3.4. Γεωλογικός χάρτης της περιοχής μελέτης όπου η εφελκυστική γράμμωση (κόκκινες γραμμές) και η γράμμωση από διατομή (πράσινες γραμμές) έχουν προβληθεί. Στα μικρά σχήματα φαίνονται: η προβολή σε διάγραμμα Schmidt των εφελκυστικών γραμμώσεων (κόκκινες βούλες) και των γραμμώσεων από διατομή (πράσινες βούλες), το σχετικό ροδόγραμμα, το διάγραμμα πυκνότητας και η κατανομή των αριθμού των μετρήσεων σε σχέση με τη διεύθυνση.

3.2.3 Folds – fold axes – axial planes

Folds measured in outcrop scale are mainly restricted to the metasedimentary rocks (in particular to the metapelites) and typically vary from centimeter- to meter-scale (Fig. 3.5). The majority of the folds observed are tight to isoclinal and show gently plunging hinge lines and moderately- to gently-inclined axial planes (Fig. 3.5). Rare folds observed in limestones resembled upright folds with

almost horizontal axis and almost vertical axial plane. Fold asymmetry observed in some cases is used as a shear sense indicator during late shearing (see later). No clues for refolded folds or sheath folds have found.

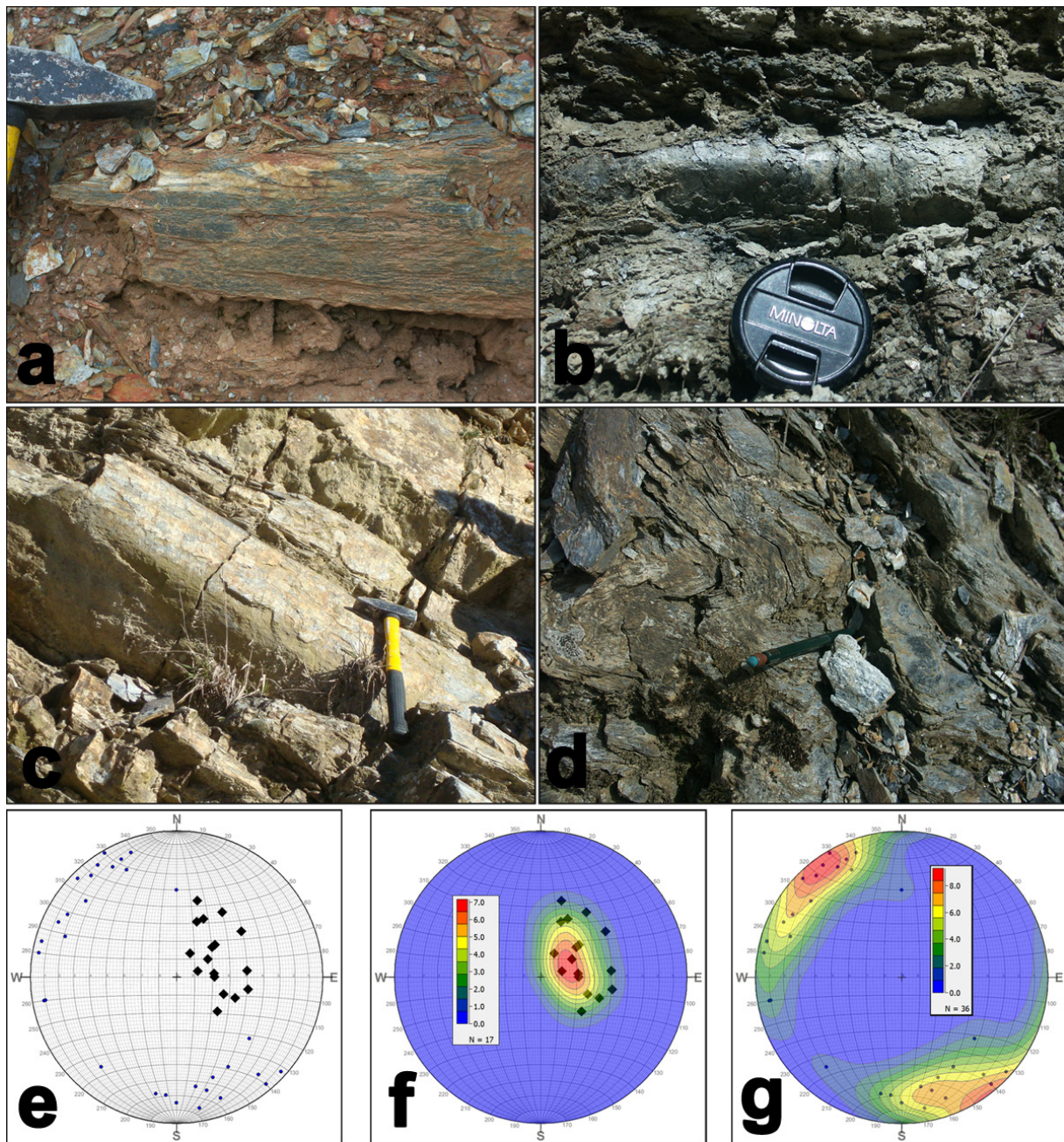


Fig. 3.5. (a) Centimeter-scale isoclinal fold with almost horizontal axial plane in metapelites. (b) Decimeter-scale fold in fine-grained metapelites. (c) Meter-scale fold with W-dipping axial plane in fine-grained metapelites. (d) Decimeter-scale fold with moderately-inclined fold axis and W-dipping axial plane. (e) Projection (equal area, lower hemisphere) of the fold axes (blue circles) and the axial planes (pole projection; black lozenges) measured. (f) Density plot (equal area, lower hemisphere) of the axial planes measured. (g) Density plot (equal area, lower hemisphere) of the fold axes measured.

Σχ. 3.5. (a) Πτυχή σε κλίμακα εκατοστού με σχεδόν οριζόντια αξονικό επίπεδο σε μεταπηλίτες. (b) Πτυχή σε κλίμακα δεκατόμετρου σε λεπτόκοκκους μεταπηλίτες. (c) Πτυχή σε κλίμακα μέτρου με αξονικό επίπεδο που κλίνει προς δυτικά σε λεπτόκοκκους μεταπηλίτες. (d) Πτυχή σε κλίμακα δεκατόμετρου με αξονικό επίπεδο μέτριας κλίσης και αξονικό επίπεδο που κλίνει προς τα δυτικά. (e) Προβολή των αξόνων των πτυχών (μπλε κύκλοι) και των αξονικών επιπέδων (μαύροι ρόμβοι) που μετρήθηκαν στην περιοχή. (f) Διάγραμμα πυκνότητας των αξονικών επιπέδων. (g) Διάγραμμα πυκνότητας των αξόνων των πτυχών.

In most of the cases the axial plane of the folds and the regional foliation are parallel (*Type I folds*). This implies that (a) there is a direct connection between the formation of the folds and the regional ductile foliation (**Fig. 3.5a, 3.5c**) and (b) that the folding of an older surface (e.g. bedding) is responsible for the formation of the folds. However, there are rare cases where the axial plane of the folds is not parallel to the regional foliation (*Type II folds* - **Fig. 3.5d**). In these cases there is no well developed foliation parallel to the axial plane and consequently these structures cannot define a regional-scale separate deformation phase. Instead they can be attributed to local variations of the viscosity/competency between different layers. The same is true for the rare kink folds observed in the area.

The majority of the axes measured coincide with a NW-SE oriented line (**Fig. 3.5e, 3.5g**). This is used to infer an initial compression in NE-SW direction. Note also that the axial planes measured are mainly SW-dipping (**Fig. 3.5f**) coinciding with the dipping of the foliation (**Fig. 3.3 inset**). The orientation of the fold axes is similar to that of the antiform axis defined in map-scale by the foliation trajectories (**Fig. 3.3**) but their time-relationship will be discussed in *Paragraphs 3.4 and 3.6*. Taking into consideration the previous an early NE-SW compression stage can be inferred.

3.3 Kinematic analysis

In the previous paragraphs crucial and basic elements such as foliation, lineation and fold-related elements (fold axis, axial plane) were described. In the following paragraphs the above elements will be used extract the kinematics of the sheared rocks, which will allow adding yet another factor (movement of the rocks) to the problem of analyzing and presenting the overall geometry of the study area.

For this purpose, only outcrops parallel to the shear direction (parallel to the stretching lineation) and perpendicular to the flattening plane (foliation) are used for the extraction of the sense of movement. Among the numerous shear sense indicators, the most commonly used in this study are: S-C fabrics developed mostly in metapelites, the deflection of the foliation along shear planes, asymmetric boudins and porphyroblast rotation.

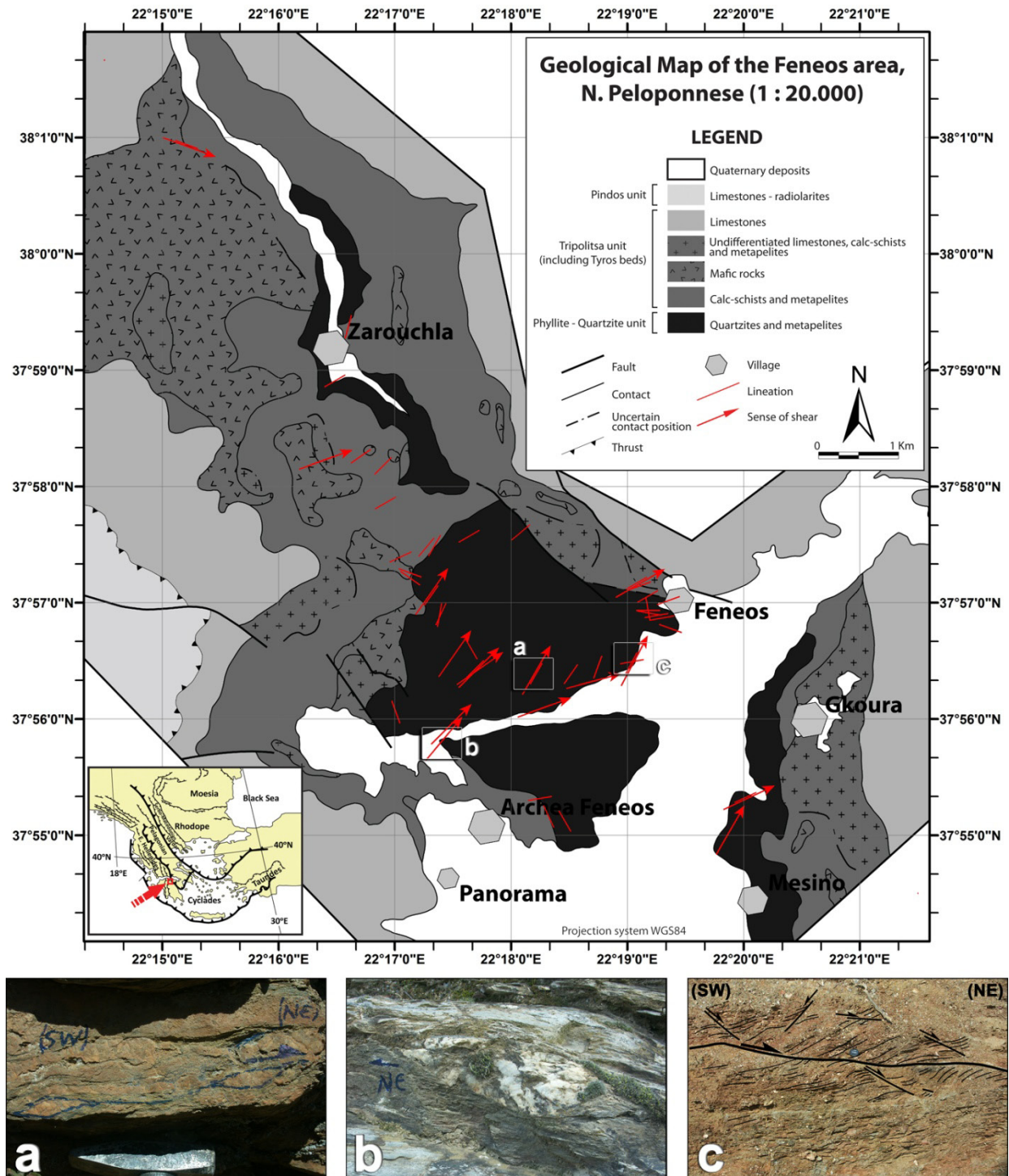


Fig. 3.6. Geological map of the studied area with superposition of the measured lineation (red lines) and the related sense of shear (red arrows). The dominant sense of movement is towards the NE for both the Phyllite – Quartzite unit and the Tyros beds. Small insets shown below the map are characteristic shear indicators. Their position is marked on the map (grey boxes): (a) Centimeter-scale mantled quartz porphyroblast within fine grained quartz-mica matrix. (b) Decimeter-scale sigmoidal quartz polycrystal within fine grained quartz-mica-chlorite matrix (field of view 20cm). (c) Shear zone and synthetic shear band developed within fine-grained mica schists (field of view 2m).

Σχ. 3.6. Γεωλογικός χάρτης της περιοχής μελέτης με επικάλυψη της γράμμωσης (κόκκινες γραμμές) και της κινηματικής (κόκκινα βέλη). Η επικρατούσα κίνηση είναι προς τα ΒΑ για την ενότητα των Φυλλιτών – Χαλαζιτών και τα στρώματα του Τυρού. Οι μικρές εικόνες κάτω από το χάρτη δείχνουν μερικούς χαρακτηριστικούς κινηματικούς δείκτες των ο οποίων η θέση σημειώνεται στο χάρτη (γκρι περιγράμματα). (a) Πορφυροβλάστης χαλαζία κλίμακας εκατοστού μέσα σε μεταπηλιτικό περιβάλλον πέτρωμα. (b) Πολυκρυσταλλικό σύγμοειδές συσσωμάτωμα χαλαζία κλίμακας δεκατόμετρου μέσα σε μεταπηλιτικό περιβάλλον πέτρωμα (εύρος πεδίου 20εκ.). (c) Ζώνη διάτμησης που αναπτύσσεται μέσα σε λεπτόκοκκο μεταπηλίτη (εύρος πεδίου 2μ.).

3.3.1 Sense of shear

Most of the rocks studied are rich in sheet silicates and favor the development of shear indicators. The shearing directions are shown in **Fig. 3.6**. It can be seen that the shearing is constantly towards the NE, following the direction of the stretching lineation (NE-SW; **Fig. 3.4**). Although most of the shearing directions measured are from the Phyllite – Quartzite unit, few measurements from the overlying Tyros beds seems to follow the same pattern. This is also visible from the measured lineation which follows the same pattern for both units (**Fig. 3.4**).

The inferred shearing direction of the present study is somewhat different from the shearing direction suggested from Xypolias and Koukouvelas (2001) for the Phyllite – Quartzite unit. Studying asymmetric mesoscopic folds, oblique grain shape in dynamically recrystallised quartzites and asymmetrical quartz c-axis they concluded that the dominant shearing is towards the W or SW. According to them, top-to-the-NE shearing is recorded only in a relatively narrow zone (~50m thick) several hundred meters below the upper boundary of the Phyllite – Quartzite unit. However, the distribution of NE-directed shearing seen in outcrop scale (**Fig. 3.6**) questions the possibility of the existence of this narrow zone due to the fact that the distribution of top-to-the-NE indicators seems rather homogenous throughout both the Phyllite – Quartzite and the Tyros units. Instead, their SW-directed shearing seen mainly in microscale (quartz c-axis fabrics etc) can be directly correlated to an early progressive shearing contemporaneous with the development of the NW-SE folds.

Consequently, it seems that both Tyros and Phyllite – Quartzite unit has suffered the same continuous NE-directed shearing during their geological history and most possibly during the same time. The distribution of the NE-shearing indicators is rather homogenous throughout the pile (within the mentioned units) and not concentrated in a narrow (~50m thick) zone as suggested by Xypolias and Koukouvelas (2001).

3.3.2 Shear zones

Three well-exposed shear zones were chosen for presentation. Starting from the south, the first shear zone is located near Feneos village (**Fig. 3.7**). The deformation of the underlying mica-rich rocks, probably representing the Tyros Beds, is both ductile (foliation development and folds) and brittle (cataclasis) while that of the overlying Tripolitsa carbonates is mostly cataclastic. It is obvious that the early ductile deformation localized within the mica-rich underlying rocks and the late brittle deformation is disseminated throughout the pile.

The stretching lineation measured in the area is N060° and the shearing recorded by the metasediments is constantly NE-trending as shown by: (i) the rigid clast rotation (**Fig. 3.7b**), (ii) the S-C structures (**Fig. 3.7c**), (iii) the smaller shear zones developed within the underlying rocks (**Fig. 3.7d**) and (iv) the asymmetry of folds (**Fig. 3.7e**). The brittle deformation of these rocks is intense in outcrop or in smaller scale. In outcrop scale the destruction zone can be meter-thick (**Fig. 3.7a**). In smaller scale, the brittle deformation is observed in the disruption of older shear zones by younger synthetic normal faults (**Fig. 3.7d**) or in disharmonic features near the tip of the NE-verging folds (**Fig. 3.7e**).

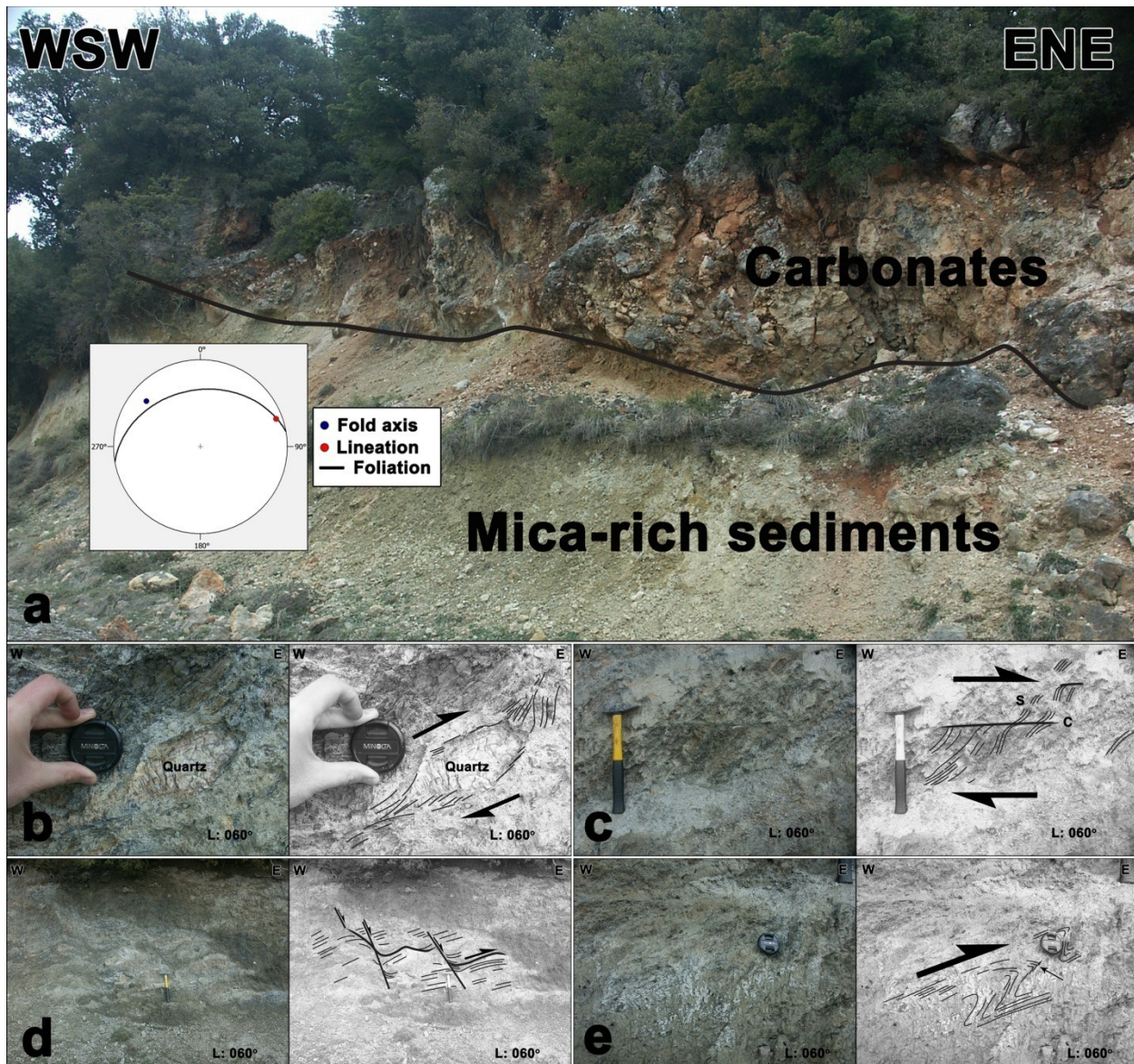


Fig. 3.7. (a) Shear zone near Feneos village (see Fig. 3.1 for the locality) juxtaposing Tripolitsa carbonates against slightly metamorphosed Tyros Beds. Small inset: equal area, lower hemisphere projections of the measured fold axis, lineation and foliation within the Tyros Beds. Field of view towards N340° (parallel to the lineation which measured at N060°). (b), (c), (d) and (e) Shear sense indicators from the Tyros Beds few meters away (in slightly lower stratigraphic position) from the shear zone of the first picture. (b) Quartz aggregate showing dextral shear sense. Note the brecciated material immediately right of the quartz aggregate. (c) S-C structure showing dextral shear sense. (d) Small shear zone disrupted by synthetic normal faults. Note the deflection of the foliation in the central part of the shear zone showing dextral rotation. (e) Right-verging fold. Note the brittle fracture near the hinge of the fold (small black arrow).

Σχ. 3.7. (a) Ζώνη διάτμησης κοντά στο χωριό Φενέός (στο Σχ. 3.1 φαίνεται η τοποθεσία) που φέρνει σε επαφή τα ανθρακικά πετρώματα της Τρίτολης με τα ελαφρώς μεταμορφωμένα ιζήματα του Τυρού. Ένθετο: προβολή των μετρήσεων του αξόνα πτυχής, της γράμμωσης και της σχιστότητας που μετρήθηκε στα μετα-ιζήματα. Η φωτογραφία τραβήχτηκε κοιτώντας προς Β340° (παράλληλα με τη γράμμωση η οποία κλίνει προς Β060°). (b), (c), (d) και (e) Κινηματικοί δείκτες από τα ιζήματα του Τυρού λίγα μέτρα μακριά (σε ελαφρώς χαμηλότερο στρωματογραφικό επίπεδο) από τη ζώνη διάτμησης της πρώτης εικόνας. (b) Συσσωμάτωμα χαλαζία που δείχνει δεξιόστροφη φορά διάτμησης. Ακριβώς δεξιά από το συσσωμάτωμα

φαίνεται η έντονη κατάκλαση του πετρώματος. (c) Δομές S-C που δείχνουν δεξιόστροφη φορά διάτμησης. (d) Μικρή ζώνη διάτμησης που διακόπτεται από νεότερα συνθετικά κανονικά ρήγματα. Στο κεντρικό τμήμα της ζώνης διάτμησης φαίνεται η εκτροπή της σχιστότητας που δείχνει δεξιόστροφη φορά διάτμησης. (e) Ασύμμετρη πτυχή με δεξιόστροφη φορά διάτμησης. Στο επάνω δεξιά άκρο της πτυχής φαίνονται ίχνη θραυσιγενούς παραμόρφωσης (μικρό μαύρο βέλος).

The second shear zone (**Fig. 3.8**) is near the center of the studied area and is found in the uppermost part of the meta-sediments belonging to the Phyllite – Quartzite unit. It is developed within metapelites with thick quartzite layers. A highly brecciated zone with fine grained and rounded rock-fragments separates the relatively non-deformed rock above from the same rock with intense cataclasis below.

The lineation measured is trending towards N035° and the shear zone is compatible with top-to-the-N movement as shown by the foliation deflection (**Fig. 3.8a, 3.8b**). Within the non-deformed rock lying immediately above the shear zone, the rock shows well-developed ductile S-C' structures with the same (top-to-the-N) sense of shear (**Fig. 3.8c**). Some of the C' planes have possibly reactivated in the brittle field and the whole structure may now be interpreted as a north-shearing zone with synthetic smaller-scale shear zones (the ex-C' planes) (**Fig. 3.8c**). In higher magnification, remnant S-C structures show the north-shearing within the ductile field (**Fig. 3.8d**).

The northernmost shear zone chosen for presentation (**Fig. 3.9**) is found almost 10Km north of the Zarouchla village. It is a magnificent, hundred meter long outcrop along the road for Akrata. The Tripolitsa carbonates are forming the hanging wall of the zone showing intense cataclasis and recent E-W-trending normal faults. The footwall of the zone is composed of extremely deformed carbonate rocks (no dolomite is observed) and mica-rich rocks, probably representing a mixture (i.e. a mélange) of the Tripolitsa carbonates and the underlying Tyros Beds. The lineation measured in parts of the exposed carbonates within the shear zone is N010°. The northern and the southern borders of the exposed shear zone are marked by the presence of E-W-trending normal faults along with their destruction zones. The sense of shear in the major shear zone is generally to-the-north as shown by the deflection of the foliation. Another possible smaller shear zone lying in higher stratigraphic levels shows southward sense of shear and resembles the continuation of the south-dipping normal fault.

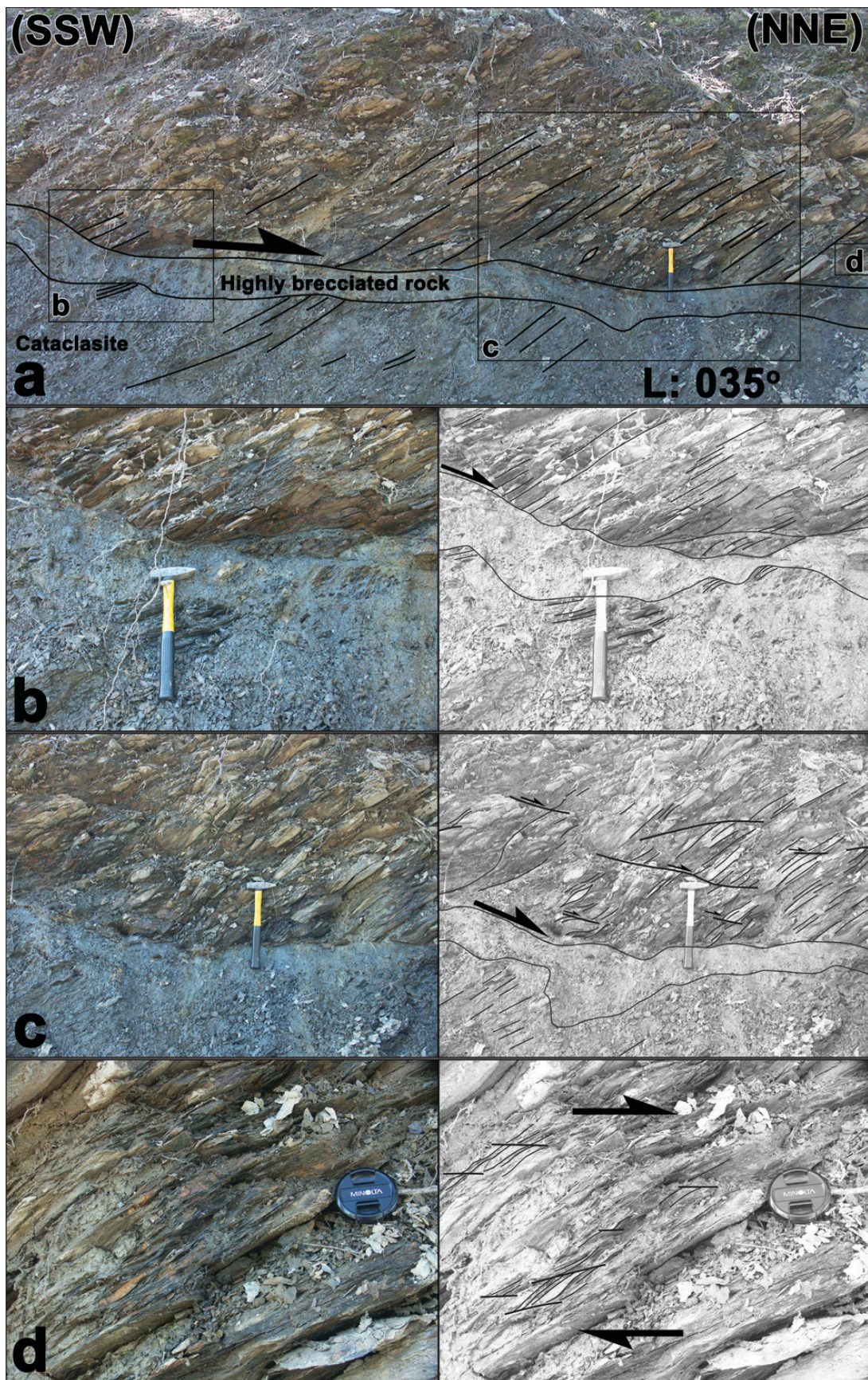


Fig. 3.8. (a) Shear zone (see Fig. 3.1 for the locality) developed within the uppermost parts of the Phyllite – Quartzite unit near Ag. Nikolaos monastery. A highly brecciated zone with fine grained and rounded rock-fragments separates the almost non-deformed rock above from the same rock with intense cataclasis below. The foliation deflection is compatible with northward shearing. The width of view is about 3 meters. (b) Detail of the shear zone where the foliation deflection and the flat-and-ramp structures in the cataclasites are shown. (c) S-C' structures within the relatively non-deformed. Some of the C' surfaces have possibly reactivated in the brittle field and the whole structure can be interpreted as a shear zone with smaller synthetic shear zones. (d) Detail of the relatively non-deformed rock where remnant S-C structures shows northward shearing within the ductile field.

Σχ. 3.8. (a) Ζώνη διάτμησης (στο Σχ. 3.1 φαίνεται η τοποθεσία) στα ανώτερα στρώματα της ενότητας των Φυλλιτών – Χαλαζιτών κοντά στο μοναστήρι του Αγ. Νικολάου. Μια ζώνη έντονης καταπόνησης με μικρά και αποστρογγυλεμένα θραύσματα του πετρώματος χωρίζει το σχετικά απαραμόρφωτο πέτρωμα (πάνω) από το ίδιο πέτρωμα με έντονη κατάκλαση (κάτω). Η εκτροπή της φύλλωσης είναι συμβατή με διάτμηση προς βορρά. Το εύρος πεδίου είναι 3 μέτρα. (b) Λεπτομέρεια της ζώνης διάτμησης όπου φαίνεται η εκτροπή της φύλλωσης και η δομή flat-and-ramp στους κατακλασίτες. (c) Δομές S-C' στο σχετικά απαραμόρφωτο πέτρωμα. Μερικές από τις C' επιφάνειες έχουν επανενεργοποιηθεί στο πεδίο της θραυσιγενούς παραμόρφωσης και η συνολική δομή μοιάζει με μία μεγάλη ζώνη διάτμησης με μικρότερες συνθετικές ζώνες διάτμησης. (d) Λεπτομέρεια του σχετικά απαραμόρφωτου πετρώματος όπου μερικές υπολειμματικές S-C δομές υποδεικνύουν κινηματική προς βορρά στο πεδίο της πλαστικής παραμόρφωσης.

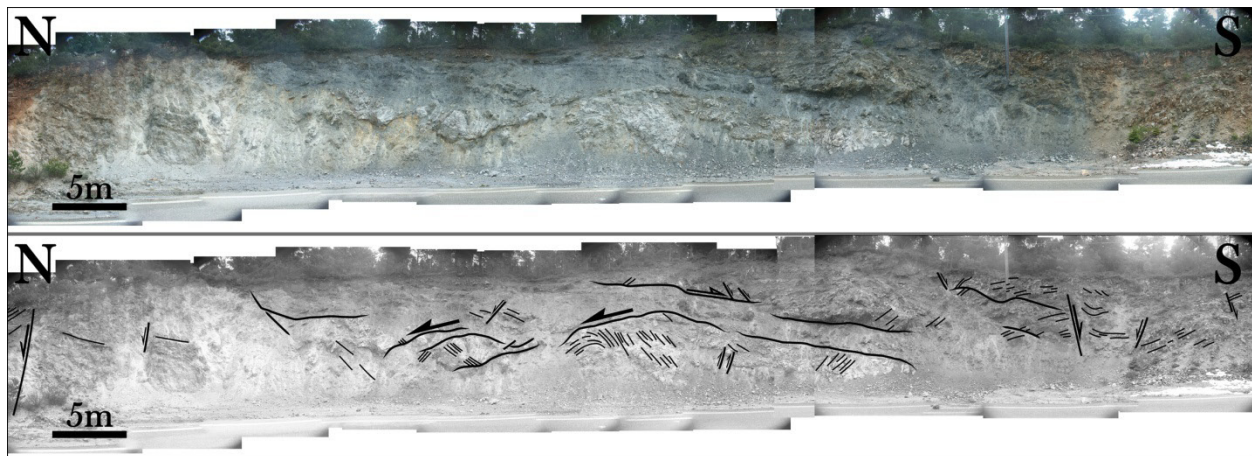


Fig. 3.9. Major shear zone showing northward shear sense. Carbonate rocks belonging to Tripolitsa unit form the hanging wall of the zone while a mixture of deformed carbonate rocks and sediments, probably belonging to the Tyros Beds, form the footwall. The northward sense of shear is mainly gleaned by the foliation deflection shown in the center of the picture. E-W-trending normal faults border the exposed shear zone. Note another smaller possible southward shear zone is observed near the relatively undeformed hanging wall (in higher levels).

Σχ. 3.9. Κύρια ζώνη διάτμησης με κινηματική προς βορρά. Το υπερκείμενο τέμαχος της ζώνης διάτμησης αποτελείται από ανθρακικά πετρώματα της ενότητας της Τρίπολης ενώ το υποκείμενο αποτελείται από ένα μίγμα ανθρακικών πετρωμάτων και ιζημάτων που ανήκουν στην ενότητα της Τρίπολης και τα στρώματα του Τυρού. Η κινηματική εξάγεται κυρίως από την εκτροπή της σχιστότητας στο κεντρικό τμήμα του σχήματος. Η ζώνη διάτμησης οριοθετείται από κανονικά ρήγματα με διεύθυνση Α-Δ. Σημειώνεται μία ακόμα πιθανή μικρότερη ζώνη διάτμησης με κινηματική προς το νότο πλησιέστερα προς το σχετικά απαραμόρφωτο άνω τέμαχος (σε ανώτερους στρωματογραφικούς ορίζοντες).

3.4 Early shearing – late shearing - the ductile-brittle transition

From the above it is clear that the bedding is the oldest planar element observed in the area (**Fig. 3.2b, 3.2g**). Folding of this (or another older) surface resulted in the formation of folds with NW-trending axes (**Fig. 3.5**) contemporaneous with the formation of the regional foliation (**Fig. 3.1, 3.3 inset**) in a NE-SW compressional regime. This early compression can be directly correlated with the top-to-the-W or –SW shearing described by Xypolias and Koukouvelas (2001) who studied micro-scale structures such as quartz c-axis and oblique grain shape in dynamically recrystallised quartzites. Those microscale fabrics survived the younger NE-directed shearing (see below) and most probably, record the subduction-related deformation. The antiform structure of the area seen in map-scale (**Fig. 3.1**), although it definitely correlates in geometry with the mesoscopic folds, it seem to be related to a later isostatic passive folding due to intense shearing.

The compression stage is followed by NE-directed shearing which resulted in the formation of the dominant stretching lineation in NE-SW direction. The sense of movement related to this late shearing is towards the NE as shown by numerous kinematic indicators from both the Phyllite – Quartzite unit and the overlying Tyros beds. This intense shearing affected the older ductile structures and favored the development of shear zones like those described in the previous paragraph. Similar shear zones are observed both near the top of the pile (just below Tripolitsa carbonates) and near its lowest parts (within the Phyllite – Quartzite unit). In outcrop-scale, the older SW-directed shearing ([Xypolias and Koukouvelas 2001](#)) has been almost completely erased and survived only in micro-scale features. Unlike to what Xypolias and Koukouvelas (2001) suggested (concentration of the NE shearing in a narrow ~50m thick zone) the distribution of the various shear-sense indicators (**Fig. 3.6**) points toward a rather distributed NE-directed shearing throughout the metasedimentary pile.

The sense of movement in the shear zones studied is clearly towards the NE. Although the initiation of the shearing happened within the ductile field, as shown by the S-C structures, the small synthetic shear zones and the foliation deflection, it seems probable that the same shearing direction continued in the brittle field with the same geometry. This is demonstrated by: (i) the brittle fractures near the hinge of the NE-verging folds (**Fig. 3.7e**), (ii) the disruption of the small shear zones by younger NW-SE brittle faults showing the same sense of movement (**Fig. 3.7d**), (iii) the reactivation of already existing weak zones like C' planes (**Fig. 3.8c**), (iv) the existence of intense cataclasis within the shear zones (**Fig. 3.8a, 3.9**) and (v) the disruption of the continuity of the pile from NW-SE normal faults in map-scale (**Fig. 3.1**). It is important to note that the same picture seen in outcrop scale with the NW-SE brittle features cutting the NE-directed ductile features (**Fig. 3.7d**) can also be seen in map scale with the NW-SE normal faults disrupting the continuity of the pile (**Fig. 3.1**) and pointing towards NE-directed movement. The whole NE-shearing model is compatible with the SW-dipping foliation planes. In simple words, the foliation planes have rotated counterclockwise above the almost horizontal NE-shearing zones seen both within the Phyllite – Quartzite unit and near the base of the Tripolitsa carbonates. The angular relationship between the foliation planes and the shear zones is used to infer the sense of movement in outcrop scale (**Fig. 3.8a, 3.9**)

Although the ductile lineation measured in the study area is constantly NE-directed (or even E-directed in some places), the only lineation possibly related to a later purely brittle stage, is trending towards N010° (outcrop of the [Fig. 3.9](#)). Of course, many authors (e.g. [Moretti et al. 2003, 2004](#), [Ghisetti and Vezzani 2005](#), [McNeil et al. 2005](#)) have already documented that the brittle deformation related to the opening of the Gulf of Corinth, north of the study area, is accompanied by E-W-trending normal faults (N-S extension). Collectively, looking both my study area and the situation few kilometers to the north, it seems that there is a transition from NE-directed shearing within the ductile field, to NE-directed shearing marking the end of ductile deformation and finally to the purely N-directed extension in the brittle field. The connection of the NE shearing and the N-S extension in the brittle field remains to be defined in terms of time, geometry and geological processes.

3.5 The opening of the Corinth Gulf: Post alpine sediments and recent faulting

The Corinth Gulf, few tens of kilometers to the north of the study area, is one of the fastest extending systems on earth (e.g. [Armijo et al. 1996](#)). It resembles a half-graben having an intensively faulted southern border. It is a well-studied example where the N-S extension is accompanied by the development of E-W-trending normal faults both onshore and offshore (e.g. [Flotté 2003](#), [Moretti et al. 2003, 2004](#), [De Martini et al. 2004](#)).

Plio-pleistocene synsedimentary deposits outcropping at the northern Peloponnese ([Ori 1989](#), [Rohais et al. 2007](#)) mark the initiation of the extension and the opening of the Gulf. A tectonic model proposing the existence of a north-dipping crustal detachment beneath the Corinth gift was proposed by [Sorel \(2000\)](#) and tested by [Chéry \(2001\)](#). However, [Papanikolaou et al. \(2009\)](#) studying the northern border of the Gulf (Itea Gulf), suggested an older NE-directed opening phase acted in Middle Miocene times, as dated by nannofossils, a phase that was later disrupted by younger E-W-trending normal faults.

The NW-SE-trending normal fault studied by [Papanikolaou et al. \(2009\)](#) has the same direction with the normal faults bordering the eastern part of my study area. Taking into consideration the geometrical similarities between the two areas, it seems possible, that the NE-shearing in the ductile crust is accompanied by NE extension in the overlying brittle crust controlling the opening of the Corinth Gulf in a different geometry than the present one. This situation was later almost completely erased by the younger N-S extension described by many authors.

The reason of change in the opening direction could either be the propagation of the North Anatolian Fault as suggested by [Papanikolaou and Royden \(2007\)](#) or the rotation of the western Continental Greece and part of the Peloponnese ([Van Hinsbergen et al. 2005](#)). The later explanation is favoured because it does not involve a change of the stress field but only a rotation of the rocks deforming within that field.

3.6 Summary

The study area (**Fig. 3.1**) is the northernmost exposure of the external blueschists belt represented by the Phyllite – Quartzite unit. The central part of the area studied is covered by an exposed core (dome) of metasediments as well as slightly metamorphosed mafic rocks (**Fig. 3.2**) and is flanked mainly carbonate rocks. The Phyllite – Quartzite unit forms the core of the dome and is represented by meta-sediments (quartzites and metapelites). The other constituent of the dome is the Tyros Beds represented by pure metapelites or metapelites with calcite intercalations (calc-schists) and by mafic rocks. Tripolitsa carbonates appear on both limbs of the exposed dome.

In this chapter, the measured foliation, stretching lineation and fold axes were presented. The oldest planar surface observed is the bedding (**Fig. 3.2b, 3.2g**). Foliation measurements revealed a major regional foliation with dominantly SW-dipping planes (**Fig. 3.3 inset**) always parallel to the initial bedding. This implies that the area suffered intense vertical shortening. The distribution of the foliation planes and the foliation trajectories revealed that the structure of the Phyllite – Quartzite unit is that of an antiform with a roughly NW-SE-directed axis (**Fig. 3.3**). The western flank of the antiform is better developed compared to the eastern one which is locally disrupted by NW-SE-trending faults.

Most of the stretching lineations measured (on the foliation planes) were from the Phyllite – Quartzite unit and showed a pronounced NE-SW trend with the dominant direction being between N050° and N060° (**Fig. 3.4**). Few intersection lineations measured showed a well-defined NW-SE orientation and were directly connected to the measured fold axes. The same NE-SW trend is true for the stretching lineations measured from the overlying Tyros beds (**Fig. 3.4**).

Folds measured in outcrop scale were mainly restricted to the metasedimentary rocks and in particular to the metapelites. The majority of the folds observed was tight to isoclinal and showed gently plunging hinge lines and moderately- to gently-inclined axial planes (**Fig. 3.5**). Their relationship with the regional foliation revealed two types of folds: those with axial planes parallel to the regional foliation (*Type I* – **Fig. 3.5a, 3.5c**) and those whose axial plane crosscut the regional foliation showing no well developed axial plane surfaces (*Type II* – **3.5d**). In any case, the *Type I folds* were the dominant type and both of the fold types showed the same NW-SE-trending axes (**Fig. 3.5e, 3.5g**) suggesting an initial compression in NE-SW direction during their formation.

Most of the rocks studied here were rich in sheet silicates and favored the development of shear indicators. It was shown that the shearing was constantly towards the NE (**Fig. 3.6**), following the direction of the stretching lineation. Although most of the shearing directions measured were from the Phyllite – Quartzite unit, few measurements from the overlying Tyros beds seemed to follow the same pattern (**Fig. 3.6**). Comparing to the work of Xypolias and Koukouvelas (2001) I note that: (i) although that they claimed that the NE-shearing is restricted to a specific (~50m) thick zone within the Phyllite – Quartzite unit, according to my study this NE-shearing seems rather homogenous affecting the whole pile in outcrop scale and (ii) the W- or SW- shearing seen mostly in microscale features (i.e. oblique grain shape in dynamically recrystallised quartzites and asymmetrical quartz c-axis) was never observed in outcrop scale.

Three well-exposed shear zones were chosen for presentation. They were developed either near the top of the Phyllite – Quartzite (**Fig. 3.8**) unit or near the top of the Tyros beds (**Fig. 3.7, 3.9**). Their common feature was the NE-directed shearing that started in the ductile field and continued in the brittle field with the same orientation as shown by (i) the brittle fractures near the hinge of the NE-verging folds (**Fig. 3.7e**), (ii) the disruption of the small shear zones by younger NW-SE brittle faults showing the same sense of movement (**Fig. 3.7d**), (iii) the reactivation of already existing weak zones like C' planes (**Fig. 3.8c**), (iv) the existence of intense cataclasis within the shear zones (**Fig. 3.8a, 3.9**) and (v) the disruption of the continuity of the pile from NW-SE normal faults in map-scale (**Fig. 3.1**).

The model proposed here will be presented in the following lines. Folding of the initial bedding (or another old surface) resulted in the formation of the NW-SE folds (*Type I and II*) and the regional foliation under an early ductile compressional regime with NE-SW orientation. This phase is possibly related to the W- or SW-shearing seen in microscale (e.g. asymmetric quartz c-axis) by Xypolias and Koukouvelas (2001). Although that folds younger than the regional foliation did observed in the area (*Type II* folds), they seem to have formed under the same stress field (NE-SW compression) and before any later event. This type of folds is connected with any well-developed planar element parallel to their axial plane. After the cease of any compressional stresses, the whole pile suffered an intense NE-shearing contemporaneously with (i) the formation of the studied shear zones, (ii) the development of numerous shear indicators within the metasediments and (iii) the NE-oriented stretching lineation that characterizes both the Phyllite – Quartzite unit and the overlying Tyros beds. The same stress field seems to have remained active through part of the brittle deformation, at least in the study area, as seen in outcrop (**Fig. 3.7d**) or in map-scale (**Fig. 3.1**). Few kilometers to the north the brittle extension is definitely to the N-S direction as already noted by several authors and is related to the opening of the Gulf of Corinth (Moretti et al. 2003, 2004). The linkage between the two areas yet remains to be answered. The antiform structure of the area, which correlates in geometry with the mesoscopic folds (NW-SE), could either represent an inherited compressional-related feature like the inherited structures separating young Pliocene basins to the north (Derveni and Aigio basins; Ghisetti and Vezzani [2004]) and the fold-and-thrust belt to the east or it could be related to an isostatic passive flexural folding due to the later intense NE-shearing. The whole model is compatible with the model proposed by Papanikolaou and Royden (2007) studying in much larger scale the external blueschist belt.

Petrology and P-T estimations

Chapter 4

The two northernmost exposures of the Phyllite – Quartzite unit are that of the Feneos and Kastania areas (few kilometers east of the study area). In this chapter, the already published results from the metamorphism of the Phyllite – Quartzite unit exposed in the above-mentioned areas will be summarized. New data will be also presented. This will help to make a direct comparison between the metamorphism of the same HP unit in the two areas.

4.1 Published P-T results from the Feneos and the Kastania areas

The Phyllite – Quartzite unit in the Feneos area is a meta-sedimentary pile composed mainly of pure quartzites, micaceous quartzites and metapelites. The dominance of quartz, chlorite and (phengitic) muscovite does not allow the quantification of pressure and temperature at a first glance. However, Katagas et al. (1991) reported the existence of chloritoid in quartzites near Zarouchla village and metapelites with garnet and phengite (3.46 Si a.p.f.u.) near Kastania village. Based on these reports a re-evaluation of the P-T conditions of metamorphism will be presented here. Chloritoid-bearing metasediments were also reported by Dercourt (1964) south of Ag. Nikolaos chapel and by Xypolias and Koukouvelas (2001) east of Archea Feneos village (their FN8 sample).

The work of Katagas et al. (1991) has revealed that: a) Judging from illite crystallinity and conventional thermobarometry, the Phyllite – Quartzite unit is of greater metamorphic grade compared to the overlying Tyros Beds without, though, a pronounced metamorphic gap in between, b) the peak temperature never exceeded 440°C with the most possible temperature range being between 340°C and 420°C, c) the peak pressure is not well constrained but it should have never exceeded 5Kbar. The suggested peak metamorphic conditions are compatible with the low-T stability field of Fe-chloritoid in typical metapelites in the system KFASH (Spear and Cheney 1989). A significantly higher temperature of ~500°C, but for the same maximum pressure (~4-5Kbar), was suggested by Jolivet et al. (2010) using Raman spectrometry in carbonaceous material from a sample south of Zarouchla village (sample KO 0203, their Fig. 9). For comparison, the metamorphic conditions calculated from the mafic rocks included in the overlying Tyros beds are 290°C – 380°C and 3.5 – 5Kbar (Baltatzis and Katagas 1984).

The situation in nearby Kastania village is different. Pressure indicative minerals, such as lawsonite ([Baltatzis and Katagas 1984](#) – their sample F8L) and garnet ([Katagas et al. 1990](#) – their sample F12, [Jolivet et al. 2010](#) – their sample KAST), have been documented. Jolivet et al. ([2010](#)) suggested peak metamorphic conditions at ~10Kbar and 450°C.

4.2 P-T estimates

Pressure and temperature conditions of metamorphism were calculated using whole-rock major-element chemistry of samples F61 and F12 published by Katagas et al. ([1991](#); **Fig. 2.9b**). Both of the samples belongs to the Phyllite – Quartzite unit. The thermodynamic calculations were made using the free energy minimization method ([Connolly 2005](#)) and the thermodynamic database of Holland and Powell ([1998](#), revised 2002).

Sample Fe61 is a quartzite located 3Km north of Zarouchla village and contains quartz, white mica (3.075 silica a.p.f.u.) and chloritoid. Two pseudosections were produced: one based on the assumption that the total iron is FeO (so the Fe₂O₃ measured is only related to late oxidization of the sample) and one based on the assumption that the measured FeO and Fe₂O₃ contents reflect those during metamorphism (**Fig. 4.1**). The chloritoid-in curves and the silica content of the white mica were used to bracket the possible P-T range of metamorphism. According to the calculations, the pressure of metamorphism most possibly lies between 9 and 13Kbar (or 9 and 10Kbar depending on the pseudosection chosen) (**Fig. 4.1**). The temperature of metamorphism is not so well-constrained i.e. it is higher than ~250°C. The pressure calculated here is significantly higher than that estimated by Katagas et al. ([1991](#)) who proposed that the pressure never exceeded 5Kbar.

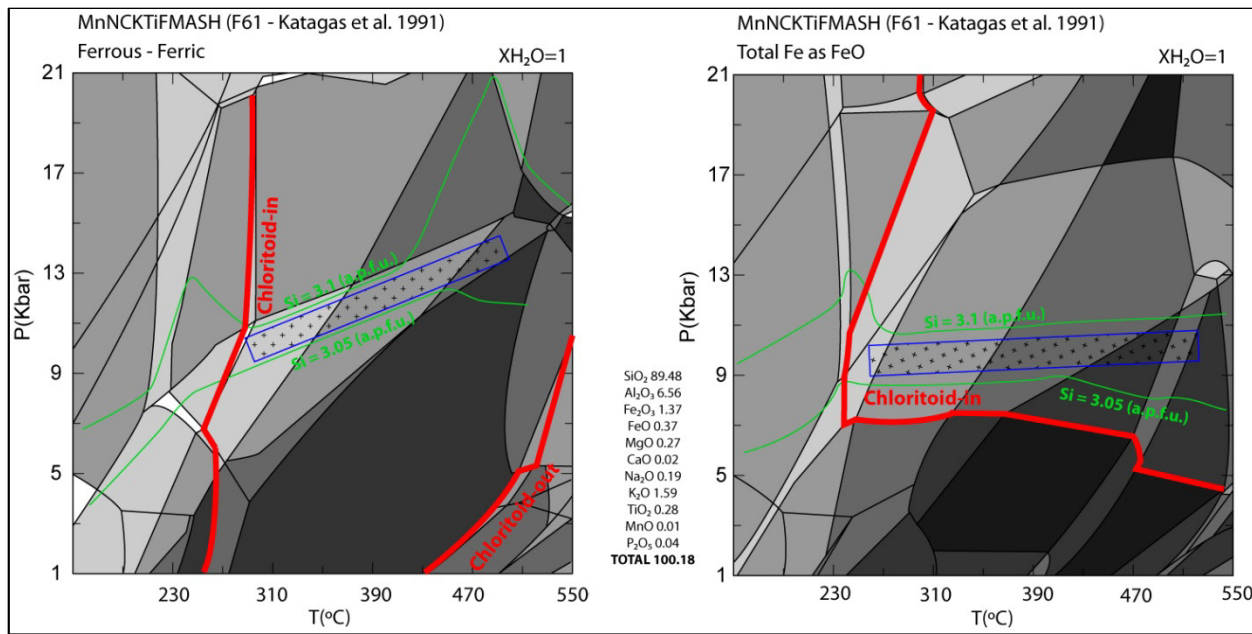


Fig. 4.1. Pseudosections in the system $\text{MnO-Na}_2\text{O-CaO-K}_2\text{O-TiO}_2\text{-FeO-MgO-Al}_2\text{O}_3\text{-SiO}_2\text{-H}_2\text{O}$ for the sample F61 (from Katagas et al. [2001]) made using PERPLE_X (<http://www.perplex.ethz.ch/>) software package. The chloritoid-in and -out curves (red lines), the Si content of the phengite (green lines) and the inferred equilibrium field (blue cross-filled box) are shown. The major-element analysis of the sample is shown in the middle.

Σχ. 4.1. Ψευδοτομές στο σύστημα $\text{MnO-Na}_2\text{O-CaO-K}_2\text{O-TiO}_2\text{-FeO-MgO-Al}_2\text{O}_3\text{-SiO}_2\text{-H}_2\text{O}$ για το δείγμα F61 (από Katagas et al. [2001]) που έγιναν με το λογισμικό PERPLE_X (<http://www.perplex.ethz.ch/>). Στα διαγράμματα φαίνονται οι καμπύλες εισόδου και εξόδου του χλωριτοειδούς (κόκκινες γραμμές), το περιεχόμενο σε πυρίτιο των φεγγιτών (πράσινες γραμμές) και το πεδίο ισορροπίας του δείγματος (μπλε πλαίσιο). Η χημική ανάλυση του δείγματος φαίνεται στο κέντρο.

The second sample (F12) is from the nearby Kastania village, few kilometers east of my study area. It is a metapelite containing quartz, albite, chlorite, phengite (3.46 silica a.p.f.u.) and garnet ($\text{Mg\#}=0.095$). The garnet-in curves and the silica content of the white mica were used to bracket the possible P-T range of metamorphism. Garnet is stable at high pressure (only above $\sim 13\text{Kbar}$) and the measured Mg# suggests garnet formation even above 15Kbar (or 19Kbar depending on the pseudosection chosen) (Fig. 4.2). Phengite (3.46 silica a.p.f.u.) suggests peak conditions above 17Kbar. Assuming a temperature of $\sim 450^\circ\text{C}$ the entrance of garnet at $\sim 17\text{Kbar}$ is in good agreement with the formation of almandine-rich garnet in the petrogenetic grid suggested for metapelites by Spear and Cheney (1989). The pressure of metamorphism is significantly increased compared to the pressure estimated by Jolivet et al. (2010) from metapelites from the same area (10Kbar at 450°C).

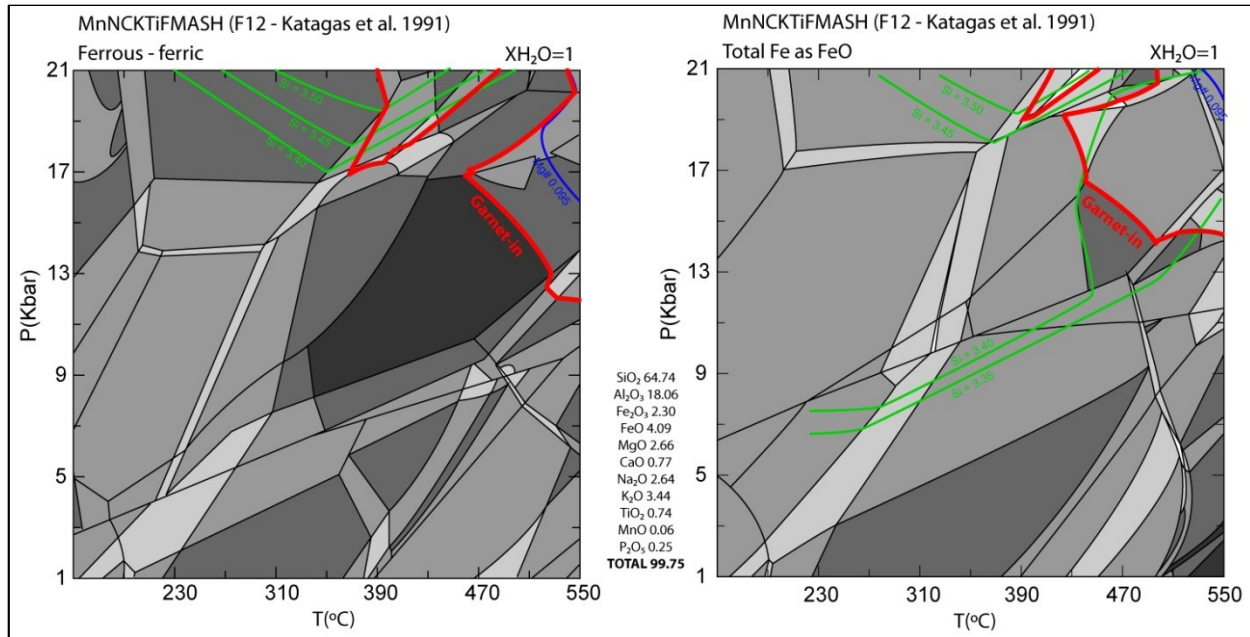


Fig. 4.2. Pseudosections in the system $\text{MnO-Na}_2\text{O-CaO-K}_2\text{O-TiO}_2\text{-FeO-MgO-Al}_2\text{O}_3\text{-SiO}_2\text{-H}_2\text{O}$ for the sample F12 (from Katagas et al. [2001]) made using PERPLE_X (<http://www.perplex.ethz.ch/>) software package. The garnet-in curve (red lines), the Si content of the phengite (green lines) and the Mg# of the garnet (blue line) are shown. The major-element analysis of the sample is shown in the middle.

Σχ. 4.2. Ψευδοτομές στο σύστημα $\text{MnO-Na}_2\text{O-CaO-K}_2\text{O-TiO}_2\text{-FeO-MgO-Al}_2\text{O}_3\text{-SiO}_2\text{-H}_2\text{O}$ για το δείγμα F12 (από Katagas et al. [2001]) που έγιναν με το λογισμικό PERPLE_X (<http://www.perplex.ethz.ch/>). Στα διαγράμματα φαίνονται οι καμπύλες εισόδου του γρανάτη (κόκκινες γραμμές), το περιεχόμενο σε πυρίτο των φεγγιτών (πράσινες γραμμές) και ο αριθμός μαγνησίου του γρανάτη (μπλε γραμμές). Η χημική ανάλυση του δείγματος φαίνεται στο κέντρο.

4.3 Summary

Published P-T estimates for the northernmost exposures of the Phyllite – Quartzite unit in the Feneos and Kastania areas are relatively scarce. For the Feneos area, Katagas et al. (1991) suggested peak metamorphic conditions of <5Kbar and 340-420°C while Jolivet et al. (2010) suggested higher temperature i.e. ~500°C at the same pressure. On the contrary, the peak pressure seems to be higher near Kastania village i.e. 10Kbar at 450°C (Jolivet et al. 2010).

P-T estimates made here allowed the direct comparison between the metamorphism of the two areas mentioned above. From the Feneos area, the sample studied seems to have equilibrated at 9-11Kbar even though that the temperature is not well-constrained (i.e. >230°C) (Fig. 4.1). From the nearby Kastania area, the sample studied equilibrated at significantly higher pressure i.e. >13Kbar (or

even >15Kbar) (**Fig. 4.2**). Overall, the pressure of metamorphism calculated here is considerably increased compared to the already published results from the above-mentioned areas. If the pressure difference between the Feneos and Kastania areas is precise, then this necessitates either (i) the possible discrimination between subunits with different metamorphic histories (all belonging to the Phyllite – Quartzite unit but exposed in the aforementioned areas) or (ii) the discrimination between different mechanisms, or intensity of mechanisms, responsible for the exposure of the specific unit.

Provenance and geotectonic setting of a quartzite (Phyllite – Quartzite unit)

Chapter 5

The term «provenance» in geology applies mainly to the methods used to shed light on the source materials of sedimentary (or metasedimentary) rocks as well as on the related geotectonic settings. It involves simple tools such as mineralogical composition of the rock and single mineral composition or more sophisticated methods such as detrital minerals age distribution (zircon, monazite etc), chondrite- or MORB-normalized incompatible elements diagrams, isotopic composition (Rb/Sr, Sm/Nd, $\delta^{18}\text{O}$, $\delta^{13}\text{C}$, $\delta^{34}\text{S}$), heavy minerals chemistry etc. Identifying ancient source areas and depositional settings is of fundamental importance for palaeogeographical reconstructions.

5.1 Resolving tectonic problems

Zircon geochronology and thermochronology is a particularly powerful approach because zircon occurs in most magmatic, metamorphic and sedimentary rocks and is capable of surviving multiple phases of physical and chemical weathering, erosion and deposition. Due to the continuous improvement of the analytical techniques, U-Pb zircon analyses are becoming more and more accessible by researchers making the application of detrital zircon geochronology extremely useful in resolving provenance- and tectonic-setting-related problems (e.g. [Yamashita et al. 2000](#), [Lahtinen et al. 2002](#), [Meinholt et al. 2009](#)). In addition, the method has become a common approach for determining dispersal patterns and recycling ([Dickinson and Gehrels 2008](#)), timing of tectonic processes such as the onset and kinematic history of mountain building ([White et al. 2002](#), [DeCelles et al. 2004](#)), maximum depositional age of otherwise undatable sedimentary units by using the youngest age component ([Surpless et al. 2006](#), [Fildani et al. 2003](#), [DeCelles et al. 2007](#)), and source-sedimentary basin evolution ([Rahl et al. 2003](#), [Fildani et al. 2009](#)). The major disadvantages of detrital zircon geochronology are: (i) the loss of small zircons in separation; (ii) the lack of contribution from fine-grained volcanic sources; and (iii) the lack of contribution from less felsic sources that may be relatively zircon-poor, thus biasing data toward felsic rock types.

After the pioneering work of Julian Pearce back in the '80s, related to the correlation between the element distribution patterns (e.g. REE, Rb, Ti, Nb, Ta, Y, Sc, Th, Zr, Hf) and the geotectonic setting

(Pearce et al. 1984), numerous authors have contributed to the application or the improvements of this method (McLennan et al. 1993, 1995, Li et al. 2005, Gonzalez-Alvarez et al. 2006, Barovich and Hand 2008). In addition, enrichment or depletion of light REEs relative to heavy REEs and the nature of Eu anomalies can provide additional clues to relate sediments to the bulk compositions of source regions. This method has been proven to be quite powerful because once weathering and sorting processes are accounted for (e.g. Cullers and Podkovyrov 2002, Lopez et al. 2005), the geochemistry of the sediment carries the record of the input of source material, and allows distinction between evolved crustal material and mantle-derived igneous rocks. The effectiveness of this method lies in the fact that even if the content in specific crucial elements may change during transport, metasomatism, metamorphism or weathering, the relative ratios between the parent rock and the newly formed sedimentary rock should remain quite constant.

Sm/Nd and Rb/Sr isotope studies are often combined with REE and trace element geochemistry (Gleason et al. 1995, Tran et al. 2003, Anders et al. 2006). The most important contribution of these heavy elements in geology is the identification of the contribution (or not) of the mantle in the crystallization of the source rock. In general, an initial ratio of $^{87}\text{Sr}/^{86}\text{Sr}$ less than 0,706 implies that the source rock derived from partial melting of the mantle, while values greater than 0,706 indicates that the rock has a significant crustal component. Because Sm/Nd ratios do not readily experience fractionation during diagenesis, chemical weathering, erosion, or sedimentary sorting (Taylor and McLennan 1985, McLennan, 1989), Sm-Nd isotope variations in sedimentary rocks should record their source regions. Furthermore, Sm and Nd are relatively immobile during metamorphism (Green et al. 1969, Jahn 2000) which suggests that Sm-Nd isotope systematics may contribute significantly in solving provenance problems. A positive ϵ_{Nd} value implies that the source rock derived from a depleted mantle source and a negative ϵ_{Nd} value indicates that the rock derived from either an enriched mantle or a crustal source enriched over time.

Additional information on the provenance of sedimentary rocks can be gleaned using Lu/Hf in zircons, Th/U in zircons or other heavy minerals (rutile etc). The Lu/Hf system in zircon is highly refractory (e.g. Corfu and Noble 1992) and its isotopic compositions can be used not only to trace source characteristics, but also to reveal processes involved in the generation of crustal melts and zircon formation mechanisms during partial melting (Flowerdew et al. 2006). It is known (e.g. Hartmann and Santos 2004) that Th/U ratios are high in magmatic zircon (>0.2) and low in metamorphic zircons ($\sim 0.001\text{--}0.1$). The combination of zircon Th/U ratio with zircon typology (Pupin 1980) can reveal the magmatic or metamorphic origin of the zircons analyzed, providing additional information on the source material. Heavy minerals (e.g. cr-spinel, rutile) have been proved very useful in identifying specific characteristics of the source rock (Meinhold et al. 2007, 2008a).

In Greece, such provenance studies are scarce. Only from Circum-Rhodope belt (Meinhold et al 2009, 2010), Chios-Inoussa-Psara (Meinhold et al. 2007, 2008a, 2008b, Meinhold and Frei 2008) and Pindos mid-cretaceous turbidites (Faupl et al. 2006) have been reported until now.

As far as clastic sediments are concerned, several well-established discriminant diagrams exist, based on their petrography, heavy-mineral assemblage (e.g. spinel, rutile) and geochemistry. Thus, a complete provenance analysis of the source of (meta)sedimentary rocks should rely on simple single mineral chemistry or more efficient methods such as datable-mineral (e.g. zircon, monazite, micas) age distribution, major- and trace-element geochemistry, Nd and Sr isotopes. Other heavy minerals (e.g. spinel, rutile) can be used to glean additional information.

5.2 Samples analyzed – Analytical methods

One quartzite (sample *Fe1*; see **Fig. 3.1** for locality) was selected for major- and trace-elements, Nd and Sr isotopes and for dating of the zircons contained. The sample appears as a massive rock with only minor developed foliation. It contains mainly quartz with significant amount of detrital zircons. It belongs to the metamorphosed sediments of the Phyllite – Quartzite unit and it appears in relatively low stratigraphic level within the unit. No alteration is observed in hand-specimen. Although that the exact depositional age is unknown, ages between Upper Carboniferous and Middle Triassic have been reported for rocks of the specific unit from western Crete ([Krahl et al. 1983](#); **Plate 5**) (note that only rock samples belonging to the Phyllite – Quartzite unit, according to the latest stratigraphy of Crete proposed by Papanikolaou and Vassilakis [\[2010\]](#), took into consideration).

Major- and trace- elements

Major- and trace elements analyses were carried out at the University of Nancy¹ using laser ablation inductively coupled plasma mass spectrometry (LA-ICPMS).

Zircons

A classic mineral separation procedure has been applied to concentrate minerals suitable for U-Th-Pb dating using the facilities available at Géosciences Rennes. Rocks were crushed and only the powder fraction with a diameter < 250 µm has been kept. Heavy minerals were successively concentrated by Wilfley table and heavy liquids. Magnetic minerals were then removed with an isodynamic Frantz separator. Zircon grains were carefully handpicked under a binocular microscope and embedded in epoxy mounts. The grains were then hand-grounded and polished to approximately half their original thickness on a lap wheel with a 6 µm and 1 µm diamond suspension successively. Zircons were imaged by cathodoluminescence (CL) using a Reliontron CL system equipped with a digital color camera available in Géosciences Rennes. U-Th-Pb geochronology of zircon was conducted by in-situ laser ablation inductively coupled plasma mass spectrometry (LA-ICPMS) at the Laboratoire Magmas et Volcans in Clermont-Ferrand, France using an ICP-MS Agilent 7500 spectrometer coupled with a fully computer-controlled 193nm Resonetics M-50E laser system equipped with an ATL laser of ultra-short pulse duration (<4ns). Ablation spot diameters of 26 µm with repetition rates of 3 Hz were used for zircon. Data were corrected for U–Pb and Th–Pb fractionation and for the mass bias by standard bracketing with repeated measurements of the GJ-1 zircon standard ([Jackson et al. 2004](#)). Data reduction was carried out with the GLITTER® software package developed by the Macquarie Research Ltd. ([Jackson et al. 2004](#)). Concordia ages and diagrams were generated using Isoplot/Ex ([Ludwig 2001](#)) updated to version 3.6. Binned frequency histograms and probability-density distributions were created using the AgeDisplay excel workbook ([Sircome 2004](#)). All errors given in **Appendix B** are listed at one sigma, but where data are combined for regression analysis or to calculate weighted means, the final results are provided at two sigma.

5.2.1 Major and trace elements – Classification of the rock

The major and trace elements of the sample under investigation are presented in **Table 5.1**. The quartzite has much increased Si content with less amount of Al. Fe, K and Ti exist in minor quantity while Mn, Mg, Na is negligible. Ca and P are below detection limit. The extremely increased Si content, together with field observations, suggests that the sample represents a metasediment rather than an igneous rock. Based on Herron's ([1988](#)) chemical classification of shales and sands the sample represents a quartz-arenite (**Fig. 5.1**).

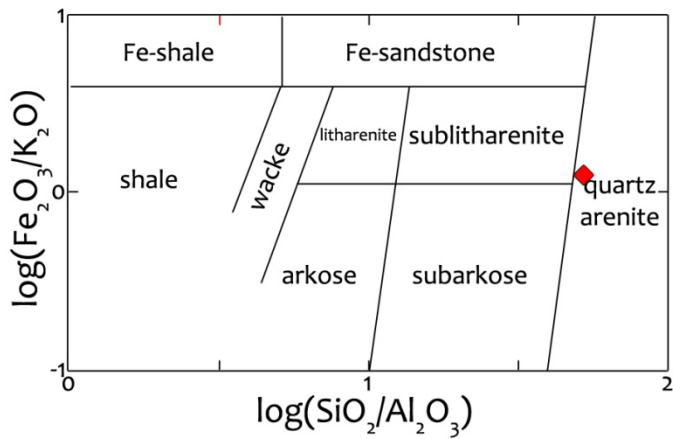


Fig. 5.1. Chemical classification of terrigenous shales and sands (Herron 1988) and projection of the Fe1 sample (red lozenge). The third axis (not shown here) classifies the sample (Fe1) into the noncalcareous (Ca<4%) sediments field.

Σχ. 5.1. Χημική ταξινόμηση για ιλυόλιθους και άμμους ηπειρωτικής προέλευσης (Herron 1988) και προβολή του δείγματος Fe1 (κόκκινος ρόμβος). Ο τρίτος άξονας ο οποίος δεν φαίνεται εδώ ταξινομεί το δείγμα (Fe1) ως μη-ασβεστούχο (Ca<4%) πετρώματα.

Table 5.1. Major and trace elements analysis for the sample Fe1 (quartzite).
Πίνακας 5.1. Κύρια στοιχεία και ιχνοστοιχεία του δείγματος Fe1 (χαλαζίτης).

Trace Elements					Major Elements		
As	1,390	Ge	0,868	Sn	0,743	SiO ₂	96,64
Ba	38,240	Hf	9,064	Sr	6,036	Al ₂ O ₃	1,87
Be	< L.D.	Ho	0,212	Ta	0,413	Fe ₂ O ₃	0,51
Bi	< L.D.	In	< L.D.	Tb	0,141	MnO	0,01
Cd	0,228	La	4,416	Th	4,790	MgO	0,06
Ce	7,480	Lu	0,136	Tm	0,108	CaO	< L.D.
Co	1,593	Mo	< L.D.	U	1,072	Na ₂ O	0,12
Cr	45,210	Nb	4,597	V	9,917	K ₂ O	0,39
Cs	0,231	Nd	4,388	W	0,575	TiO ₂	0,29
Cu	< L.D.	Ni	4,669	Y	6,482	P ₂ O ₅	< L.D.
Dy	0,941	Pb	1,999	Yb	0,824	PF	0,54
Er	0,643	Pr	1,203	Zn	< L.D.	Total	100,41
Eu	0,158	Rb	9,119	Zr	386,500		
Ga	2,152	Sb	0,110				
Gd	0,757	Sm	0,855				

Trace elements in ppm

Major elements in weight per cent

Total iron measured as Fe₂O₃

L.D. below detection limit

All the trace elements, except from Ba, Cr and Zr, are below 10ppm. The increased Cr content (~45ppm) indicates a possible ultramafic source (see paragraph 5.2.2). The extremely high Zr content indicates the presence of detrital zircons possibly coming from an acid igneous or reworked sedimentary source (see paragraph 5.2.2 and 5.2.4.1). Possible input from basalts is not supported, at least at first glance, as the Nb/Ta ratio of the sample is ~11, almost two thirds of the ratio expected in most basalts (~17).

5.2.2 Multi-element diagrams – Source material and geotectonic setting

Chondrite- or MORB-normalized trace element diagrams have been extensively used by numerous authors to enlighten the particular characteristics of the rock under investigation (e.g. [Pearce et al 1984](#), [Kostopoulos 1988](#) etc). It is known that partial melting mobilizes the incompatible elements resulting in the depletion of the source and the enrichment of the newly-formed rock. The main advantage of these diagrams is the possibility of recognizing the relative enrichment (or depletion) in incompatible elements (REE, LIL and HFS) comparing to a non-evolved source (chondrite; chondrite-normalization) or to a mafic rock standard (MORB; MORB normalization).

In sedimentary rocks, the importance of using normalized diagrams lies in the fact that under most of situations, trace elements can be immobile during processes such as erosion, weathering, sedimentary sorting, metamorphism etc (e.g. [Taylor and McLennan 1985](#)). In this case, the trace-elements content can reveal characteristics of the source rock (igneous or metamorphic rock etc). Further, trace elements (REE, LIL, HFS) can give valuable information relative to the geotectonic setting of the source rock. The use of normalized and trace-element classification diagrams can be extremely useful especially when palaeogeographic reconstruction are accounted for.

The source rock of the quartzite can be an igneous or metamorphic rock, more or less evolved, or even an older sedimentary rock. The total REE content is extremely low (Σ REE=22.26ppm) probably due to the quartz dilution. Compared to the chondrite's REE content the quartzite analyzed is enriched both in LREE and HREE, showing a pronounced negative trend with $(La/Lu)_N=3.37$ (**Fig. 5.2a**). This negative trend can be either the result of the partial melting during the formation of a hypothetical igneous source rock or the result of the fractional crystallization during the evolution of this rock. In case that the source rock was of metamorphic origin, this negative trend characterizes the differential mobility of elements during metamorphic-fluids mobility. There is a negative trend in LREE ($La-Sm$; $(La/Sm)_N=3.25$) and a positive one in HREE ($Gd/Lu)_N=0.69$. In particular, the HREE are initially rather flat ($Gd-Er$; $(Gd/Er)_N=0.95$) and increase the slope at the last elements ($Er-Lu$; $(Er/Lu)_N=0.72$). The europium anomaly has a medium negative value ($Eu/Eu^*=0.6$).

The elements in the crust-normalized diagrams (**Fig. 5.2b**) are placed with increasing incompatibility from Sr to Ba and from Yb to Th. Compared to the crust values used (CC, UCC and MCC; [Ludnick and Gao 2003](#)), the sample is relatively depleted both in LIL (Sr-Ba) and HFS (Th-Yb) elements

with the exception of Zr and Hf. The high detrital zircons content is responsible for the increased Zr value (386 ppm; **Table 5.1**) and the increased Hf content relatively to the crust's content as Hf is known to strongly fractionate into the zircon (e.g. [Corfu and Noble 1992](#)). Magmas formed above subduction zones commonly show negative Nb and Ti anomalies. The sample analyzed may show such characteristics only for Ti. On the other hand, a prominent negative anomaly is observed for Sr, Ba and P (P is even below detection limit; **Table 5.1**). Sr and Ba strongly incorporate into plagioclase, revealing that the source of the quartzite suffered fractionation of plagioclase, something which is supported by the negative Eu anomaly. In the same way, P negative anomaly probably shows that apatite played a major role in parent-rock formation.

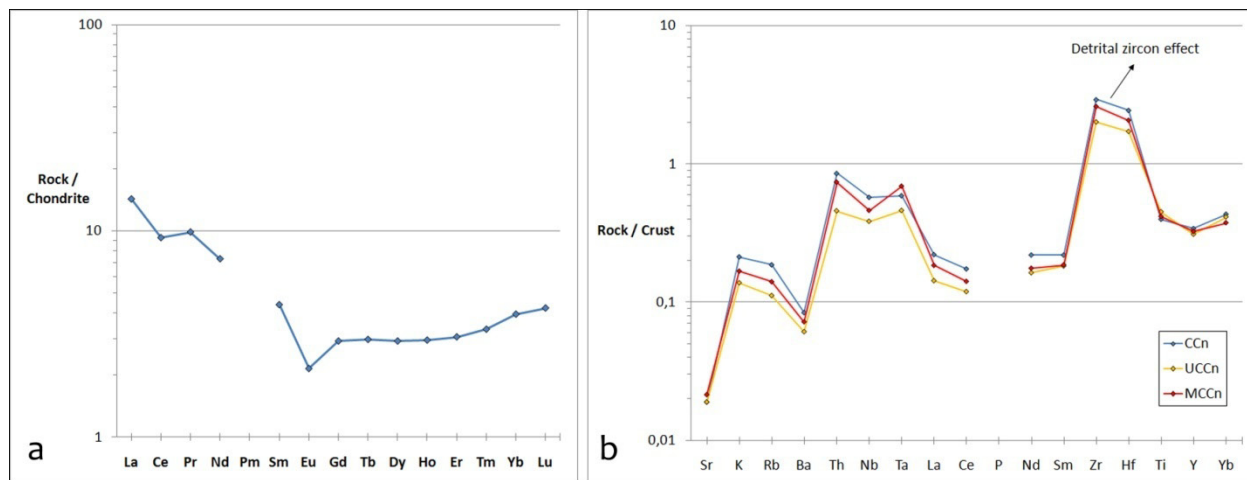


Fig. 5.2. Normalized diagrams for the sample Fe1 (quartzite). (a) Chondrite-normalized REE pattern. Chondrite values from Taylor and McLennan (1985). (b) Crust-normalized LIL/HFS diagrams. CCn: Continental Crust Normalization, UCCn: Upper Continental Crust Normalization, MCCn: Middle Continental Crust Normalization. Average crust values from Rudnick and Gao (2003).

Σχ. 5.2. Ανηγμένα διαγράμμα για το δείγμα Fe1 (χαλαζίτης). (a) Ανηγμένο μοτίβο σπανίων γαλιών (REE) με βάση χονδριτική σύσταση (τιμές από Taylor and McLennan [1985]). (b) Ανηγμένο μοτίβο των στοιχείων υψηλής ιοντικής ακτίνας (LIL) και των στοιχείων υψηλού ιοντικού δυναμικού (HFS) με βάση τη σύσταση του ηπειρωτικού φλοιού. CCn: αναγωγή με βάση το μέσο ηπειρωτικό φλοιό, UCCn: αναγωγή με βάση τον άνω ηπειρωτικό φλοιό, MCCn: αναγωγή με βάση τον μέσο ηπειρωτικό φλοιό. Τιμές στοιχείων του ηπειρωτικού φλοιού από (Rudnick and Gao 2003).

Two provenance diagrams were used. The diagram from Roser and Korsch (1988) suggests a quartz-rich sedimentary source rock for the sample analyzed (**Fig. 5.3a**). The diagram from Floyd and Leveridge (1987) suggests that there is a significant sedimentary component (**Fig. 5.3b**). Collectively, it seems that the sample represents an intermediate between an acidic igneous source and a sedimentary source. This trend is clearly seen in the zircon populations where (i) most of the Th/U ratios are plotted in the stability field of "magmatic zircons" (**Fig. 5.6**) and (ii) the aspect ratios of the zircon analyzed are between 1.668 and 2.262 (**Table 5.3**) showing significant rounding due to sedimentary transport.

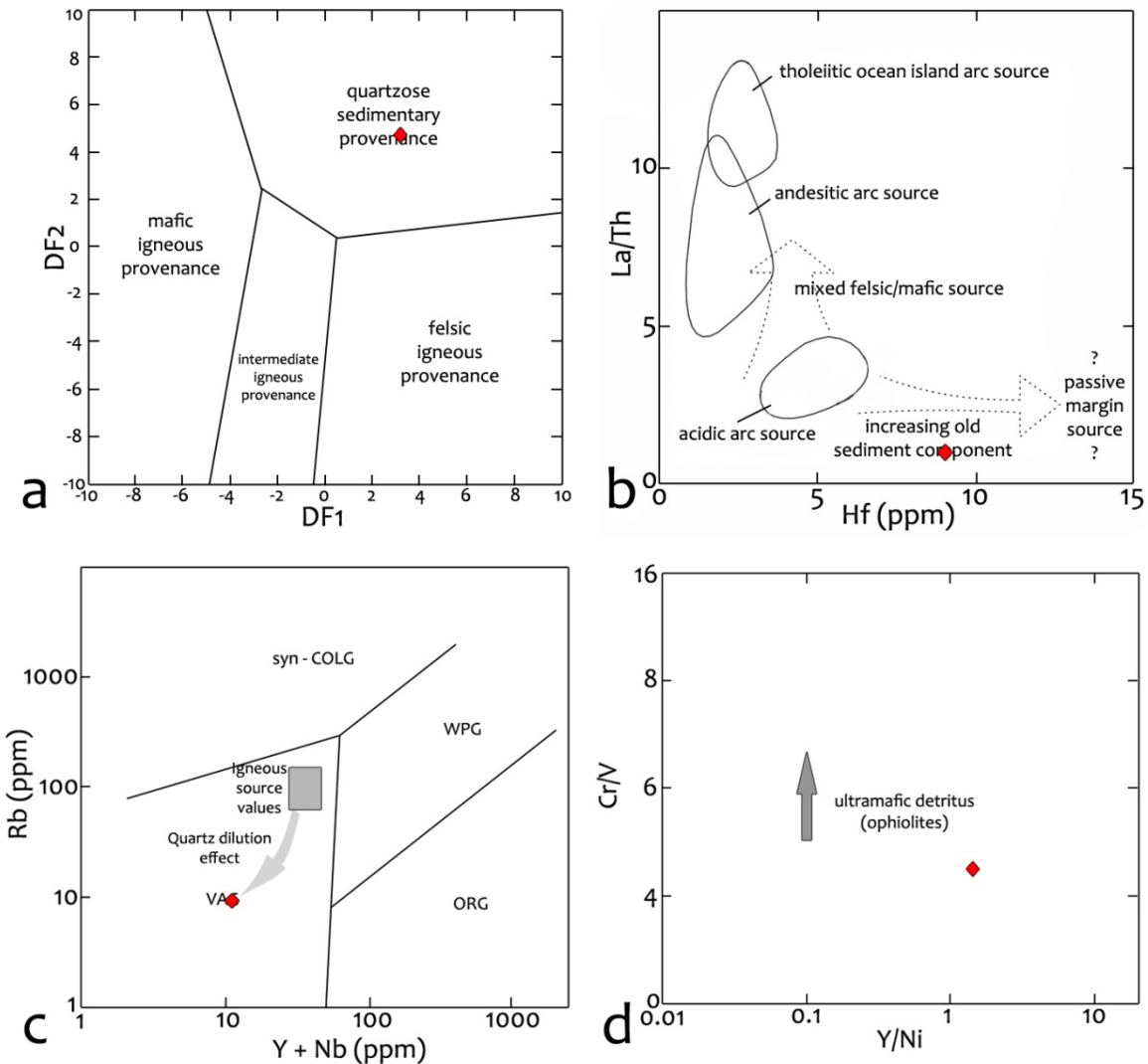


Fig. 5.3. Projections of the sample (Fe1). (a) Provenance diagram based on major oxides ratios (Roser and Korsch 1988). **(b)** Provenance diagram based on La/Th vs. Hf concentration (Floyd and Leveridge 1987). **(c)** Tectonic setting diagram for granitic rocks based on Rb-(Y+Nb) content (Pearce et al. 1984). The red lozenge represents the elemental content measured for sample Fe1 and the grey box represents the elemental values of the igneous source. Details in the text. Syn-COLG: Syn-collisional Granites, WPG: Within Plate Granites, VAG: Volcanic Arc Granites, ORG: Ocean Ridge Granites. **(d)** Cr/V vs. Y/Ni plot (McLennan et al. 1993).

Σχ. 5.3. Προβολές του δείγματος Fe1. (a) Διάγραμμα προέλευσης (provenance) ιζημάτων με βάση τους λόγους των κυρίων οξειδίων (Roser and Korsch 1988). **(b)** Διάγραμμα προέλευσης ιζημάτων με βάση το λόγο La/Th και τη συγκέντρωση σε Hf (Floyd and Leveridge 1987). **(c)** Διάγραμμα διάκρισης του γεωτεκτονικού περιβάλλοντος για γρανιτικά πετρώματα με βάση το περιεχόμενο σε Rb και (Y+Nb) (Pearce et al. 1984). Ο κόκκινος ρόμβος αναπαριστά τη στοιχειακή σύσταση του δείγματος Fe1 και το γκρι τετράγωνο τη σύσταση του πιθανού αρχικού μαγματικού πρωτόλιθου. Λεπτομέρειες στο κείμενο. Syn-COLG: Συν-τεκτονικοί γρανίτες, WPG: Γρανίτες εσωτερικού πλακών, VAG: Γρανίτες ηφαιστειακού τόξου, ORG: Γρανίτες μεσοωκεάνιας ράχης. **(d)** Προβολή με βάση του λόγους Cr/V και Y/Ni (McLennan et al. 1993).

Assuming that the Rb, Y and Nb content is mainly reflecting a granitic source input, then, based on the work of Pearce et al. (1984) it should reflect a typical volcanic-arc granite with low concentration of Rb and Y+Nb (Fig. 5.3c). However, due to the quartz dilution there must be a pronounced shift of the initial igneous source values towards lower Rb and Y+Nb values. In order to make a rough estimation of the Rb and Y+Nb “initial” values that correspond to the igneous source, non-altered sandstones from SW Hungary were chosen for comparison (Varga et al. 2007; Appendix A). The method used is described in the Appendix A. The estimation of the “initial” Rb and Y+Nb (grey box), as well as the measured elementary content (red lozenge), are shown in Fig. 5.3c. As noted by Forster et al. (1997) significant overlapping may exist in this diagram particularly near the borders between two neighbor fields. Consequently, the igneous source is of volcanic-arc origin with a possible within plate affinity.

Cr and Ni can be good indicators of an ultramafic/mafic source. Cr and Ni in shales can be in the form of either detrital particles or absorbed ions while in sandstones Cr concentrates only in detrital minerals (e.g. spinels). Consequently, all the available Cr and Ni coming from a possible ultramafic source can concentrate in shales, resulting in a Cr/Ni ratio analogue to that of the ultramafic source (~1.3-1.5), while in sandstones Cr/Ni ratio tends to be higher with relatively lower absolute values (Garver et al. 1996). In other words, shales can fully accommodate Cr and Ni which is not the case in sandstones where the Cr and Ni contents are strongly influenced by the detrital mineral effect. According to the work of the previous authors for shales, values of Cr>150ppm and Ni>100ppm, Cr/Ni between 1.3 and 1.5 and a high correlation coefficient between Cr and Ni are diagnostic of ultramafic rocks in the source area, whereas higher Cr/Ni ratios (higher than 2) typify an input of mafic volcanic detritus. In case that the Cr and Ni are really coming from a mafic source, then Cr should be highly correlated with V and Ti with high values of V/Cr and V/Ni (Garver and Scott 1995). The sample analyzed is the metamorphic equivalent of sandstone and has low Cr-content (~45ppm), low Ni-content (~4,7ppm), low V/Cr ratio (~0.22), low V/Ni ratio (~2.12) and high Cr/Ni ratio (9.68). According to the above, low V/Cr and V/Ni ratios deny the existence of a mafic source and the increased Cr/Ni ratio reflects the accumulation of few grains of Cr-bearing minerals coming from an ultramafic source. The ultramafic detritus can probably be seen in the Cr/V vs. Y/Ni plot (Fig. 5.3d).

5.2.3 Zircon dating as a provenance tool

U-Pb dating of detrital zircons has become a popular method in provenance studies. The method is used to identify provenance components in a (meta-) sedimentary unit (e.g. Haas et al. 1999, Meinhold et al. 2008b, 2009, 2010), to correlate between sequences (e.g. Bingen et al. 2001), to determine a maximum limit for the age of deposition (e.g. Knudsen et al. 1997, Williams 2001, Bingen et al. 2001) and to study crustal evolution processes on a continent-wide scale (e.g. Davis 2002, Goode et al. 2002, Barr et al. 2003, van Wyck and Williams 2002, Griffin et al. 2004). The most common approach used, is the visualization of U-Pb Concordia plots or probability density diagrams (Sirccombe 2000) of the zircons dated.

The work of identifying the different provenance components (terrains) of (meta-) sediments can suffer some pitfalls. In provenance studies, the most important question still remains the following: “How many grains are needed to identify all the possible contributors?”. Assuming that the separation of

zircons from their host rock and the selection of grains for analysis is strictly a random process, the answer is directly related to the contribution of each terrain, measured in percentage, in the sediment under investigation. Statistical manipulation of the previous problem has revealed that *the smallest number of grains in a sample that must be dated to achieve a required level of statistical adequacy* is 117 (Vermeesch 2004). The 120 spots analyzed in this study equals to less than 1% of detection limit (=percent of abundance in the original sediment) based on the work of Andersen (2005). This means that a possible source which contributes to the zircon population with less than 1%, can be identified using 120 spots and the possibility of not identifying such a terrain is null. Taking into consideration only the spots within the concordance limit (63 out of 120 spots at 95-105% concordance) then, the detection limit is around 5% and there is a 25% chance of not recognizing a source that contributes 2% at the total zircon population.

5.2.3.1 Zircons extracted – Classification based on their typology and other characteristics

A total of 127 grains from the quartzite Fe1 were mounted and allocated into three groups (Fig. 5.4). 102 out of 127 grains were chosen for dating resulting in 120 spot analyses (Table 5.2). 63 out of 120 measurements are within 95-105% concordance limit and 89 out of 120 are within the 90-100% concordance limit. The complete isotopic dataset is presented in Appendix B and the summary of the geometrical characteristics of the different groups is presented in Table 5.3. Most of the grains extracted are rounded and show intense sedimentary transport nullifying in this way the possibility of applying the genetic classification of Pupin (1980).

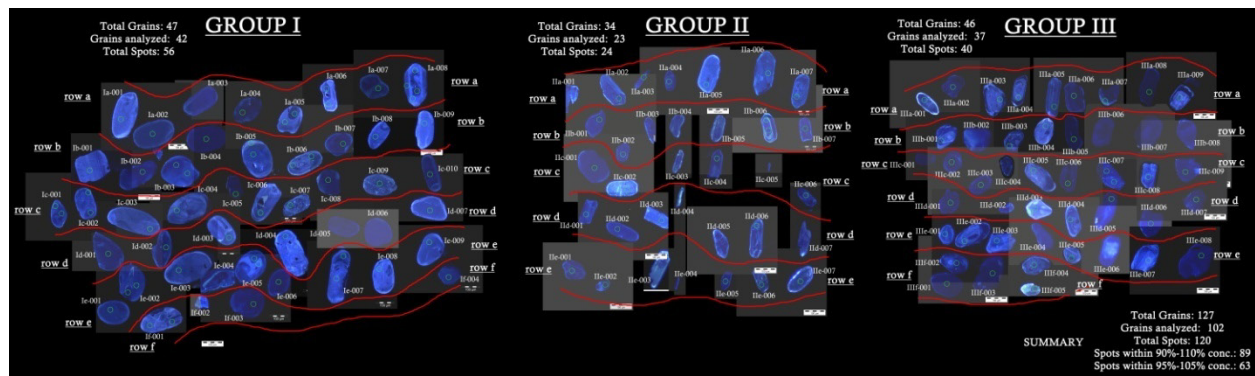


Fig. 5.4. CL images of the 127 zircon grains separated from the quartzite Fe1. The zircons are distributed into three groups based on their typology and the geometrical characteristics (see text for details). Letter–number code next to each zircon: group-row-grain.

Σχ. 5.4. Εικόνες καθοδοφωταύγειας από τους 127 κόκκους ζιρκονίων του χαλαζίτη Fe1. Τα ζιρκόνια έχουν κατανεμηθεί σε τρεις ομάδες με βάση την τυπολογία και τα γεωμετρικά τους χαρακτηριστικά (βλ. κείμενο για λεπτομέρειες). Ο γραμματικός-αριθμητικός κώδικας που αναφέρεται δίπλα σε κάθε κόκκο ζιρκονίου είναι: ομάδα-γραμμή-κόκκος.

Group I

It consists of 47 relatively big, gray, cloudy and mostly rounded zircons with their long axis being between ~ 125 and $\sim 280\mu\text{m}$ (**Table 5.3**). The weighted mean of the length/width (L/W) aspect ratio is 1.7 (**Table 5.3**). A total of 56 spots (42 grains) were measured. Homogenous grains and inherited cores account for 58.9% (33 spots) of the total spots obtained and the overgrowths and rims account for the rest 41.1% (23 spots) (**Table 5.2**). The minimum and maximum ages reported for the Group I are 516 ± 31 Ma ($^{206}\text{Pb}/^{207}\text{Pb}$) and 2746 ± 19 Ma ($^{206}\text{Pb}/^{207}\text{Pb}$) respectively (**Table 5.2, 5.3**). The absence of euhedral zircons along with the rounded shape (relatively low aspect ratio) indicates long-distance sedimentary transport. The Group I has in average the lowest Pb, U and Th content (**Table 5.4**). Only 4 out of 56 dated spots have U content higher than 400ppm (**Appendix B**).

Group II

It consists of 34 relatively small, transparent and elongated zircons with their long axis being between ~ 80 and $\sim 250\mu\text{m}$ (**Table 5.3**). The weighted mean of the length/width (L/W) aspect ratio is 2.262, fairly higher than that of the other groups (**Table 5.3**). Mainly euhedral but also rounded zircons appear in this group with the euhedral ones being cracked either due to sedimentary transport or due to the extraction procedure. A total of 24 spots (23 grains) were measured. Homogenous grains and inherited cores account for 50% (12 spots) of the total spots obtained and the overgrowths and rims account for the rest 50% (12 spots) (**Table 5.2**). The minimum and maximum ages reported for the Group II is 590 ± 11 Ma ($^{206}\text{Pb}/^{238}\text{U}$) and 2669 ± 18 Ma ($^{206}\text{Pb}/^{207}\text{Pb}$) respectively (**Table 5.2, 5.3**). Some of the grains i.e. IIb-006 and IId-006 (**Fig. 5.4**) show quite good euhedral shape and according to the classification of Pupin (1980) they belong to the main group S (S20) or to the subgroup U (U24). For the S20 type, the (100) prism dominates over the (110) prism, as does the (101) pyramid over the (211) pyramid and is compatible with crystallization of sub-alkaline acid magma at $T\sim 800^\circ\text{C}$ indicating in this way the magmatic input. The Group II has in average moderate values of Pb, U and Th content compared to the other groups (**Table 5.4**). Only 4 out of 24 dated spots have U content higher than 400ppm (**Appendix B**).

Group III

It consists of 46 relatively medium-sized, pink, semi-transparent, mainly rounded zircons with their long axis being between ~ 100 and $\sim 225\mu\text{m}$ (**Table 5.3**). The weighted mean of the length/width (L/W) aspect ratio is 1.668, quite identical to that of the first group (**Table 5.3**). A total of 40 spots (37 grains) were measured. Homogenous grains and inherited cores account for 57.5% (23 spots) of the total spots obtained and the overgrowths and rims account for the rest 42.5% (17 spots) (**Table 5.2**). The minimum and maximum ages reported for the Group III is 533 ± 30 Ma ($^{206}\text{Pb}/^{207}\text{Pb}$) and 2992 ± 48 Ma ($^{206}\text{Pb}/^{238}\text{U}$) respectively (**Table 5.2, 5.3**). The euhedral grain IIIa-004 (**Fig. 5.4**) resembles the main type G1 of Pupin (1980) showing dominant (110) prism and (101) pyramid. According to Pupin and Turco (1972) this typology indicates crystallization from an alkaline and relatively cool medium. The Group III has in average the highest values of Pb, U and Th content (**Table 5.4**) and almost half of the dated spots (19 out of 40) show U content higher than 400ppm (**Appendix B**).

Table 5.2. Statistical analysis of the zircons analyzed from the quartzite Fe1.
Πίνακας 5.2. Στατιστική ανάλυση των ζιρκονίων που αναλύθηκαν από τον χαλαζίτη Fe1.

	Total grains	Grains analyzed	Spots measured	Spots within concordance limit*	%	Minimum Age** (Ma)	Maximum Age** (Ma)	Average Age*** (Ma)	Homogenous grains and inherited cores	%	Overgrowths and rims	%
Group I	47	42	56	51	91,1%	516	2746	1149	33	58,9%	23	41,1%
Group II	34	23	24	13	54,2%	590	2669	1112	12	50,0%	12	50,0%
Group III	46	37	40	25	62,5%	533	2992	1337	23	57,5%	17	42,5%
Total	127	102	120	89	74,2%	-	-	-	68	56,7%	52	43,3%

* Concordance limit is set at 90-110%

** Only spots within concordance limit are concerned

*** Arithmetic average of 206Pb/207Pb, 206Pb/238U, 207Pb/235U only for spots within concordance limit

Table 5.3. Geometrical characteristics of the different group of zircons from the quartzite Fe1.
Πίνακας 5.3. Σύνοψη των γεωμετρικών χαρακτηριστικών των τριών ομάδων ζιρκονίων του χαλαζίτη Fe1.

	Group I	Group II	Group III
Min. L (μm)	125	80	100
Max. L (μm)	280	250	225
Min. W (μm)	80	25	65
Max. W (μm)	160	125	150
Arithmetic mean (L/W)	1,692	2,274	1,676
Min L/W	1,000	1,300	1,000
Max L/W	2,750	5,000	2,733
Weighted mean (L/W)	1,700	2,262	1,668

"L" refers to the long axis of the selected zircons and

"W" refers to the length in the perpendicular direction

Table 5.4. Pb, U, Th contents and Th/U ratio of the zircons analyzed. The complete isotopic dataset is given in Appendix B.
Πίνακας 5.4. Το περιεχόμενο σε Pb, U και Th καθώς και ο λόγος Th/U των ζιρκονίων που αναλύθηκαν. Το σύνολο των ισοτοπικών δεδομένων φαίνεται στο Παράρτημα Β.

	Group I	Group II	Group III
Pb content	Minimum	2	8
	Maximum	168	204
	Average	39	61
U content	Minimum	10	78
	Maximum	1717	990
	Average	219	306
Th content	Minimum	0	5
	Maximum	527	347
	Average	96	122
Th/U ratio	Minimum	0.002	0.005
	Maximum	1.823	0.962
	Average	0.604	0.463

5.2.3.2 Frequency histograms and probability – density plots

In provenance studies involving relatively large dataset, the most optimum method to visualize the results is the binned frequency histogram and probability density distribution (e.g. [Morton et al. 1996](#), [Sircombe 2000](#), [Meinhold et al. 2008b](#)). The $^{207}\text{Pb}/^{206}\text{Pb}$ ages (95% concordance) ([Appendix B](#)) yielded 4 prominent age clusters of 500-825 Ma (Neo-proterozoic – M. Cambrian), 950-1075 Ma (Upper Meso-proterozoic – Lower Neo-proterozoic), 1750-2000 Ma (M.-Upper Paleo-proterozoic) and 2400-2750 Ma (Neoarchean – Lower Paleo-proterozoic) ([Fig. 5.5](#)). Based on the $^{206}\text{Pb}/^{238}\text{U}$ and $^{207}\text{Pb}/^{235}\text{U}$ ages (not shown here) the last group can be split into two other clusters i.e. 2400-2500 Ma and 2600-2750 Ma. Another possible age cluster appears at 2925-2950 Ma ([Fig. 5.5](#)). Taking into consideration both the concordant and the discordant zircons, one can claim that the third cluster (1750-2000 Ma) extends up to ~ 1600 Ma (light grey; [Fig. 5.5a, d](#)). This last cluster is also visible using the $^{206}\text{Pb}/^{238}\text{U}$ and $^{207}\text{Pb}/^{235}\text{U}$ ages (not shown here). In general, the most abundant zircon input is coming from the youngest Neo-proterozoic – M. Cambrian age cluster.

The contribution of each group of zircons to the above age clusters is different. The Group I contributes to every age cluster but its contribution to the youngest clusters is more significant. In most cases, its width is equal to the width of the cluster (especially for the ages $< 1.1\text{ Ga}$) ([Fig. 5.5b](#)). Group II appears mainly in the youngest clusters (i.e. $< 1.1\text{ Ga}$) and it is scarce in the rest ([Fig. 5.5c](#)). Note, however, that the concordant zircons of this group are only 7 out of 24 total spots ([Table 5.4](#)). Group III contributes equally to the four age clusters mentioned above, in line with its high-U content ([Table 5.4](#)), and has the most significant contribution to the Late Paleo-proterozoic cluster (1750-2000 Ma). In addition, it probably defines another cluster (the oldest one) at 2925-2950 Ma ([Fig. 5.5d](#)).

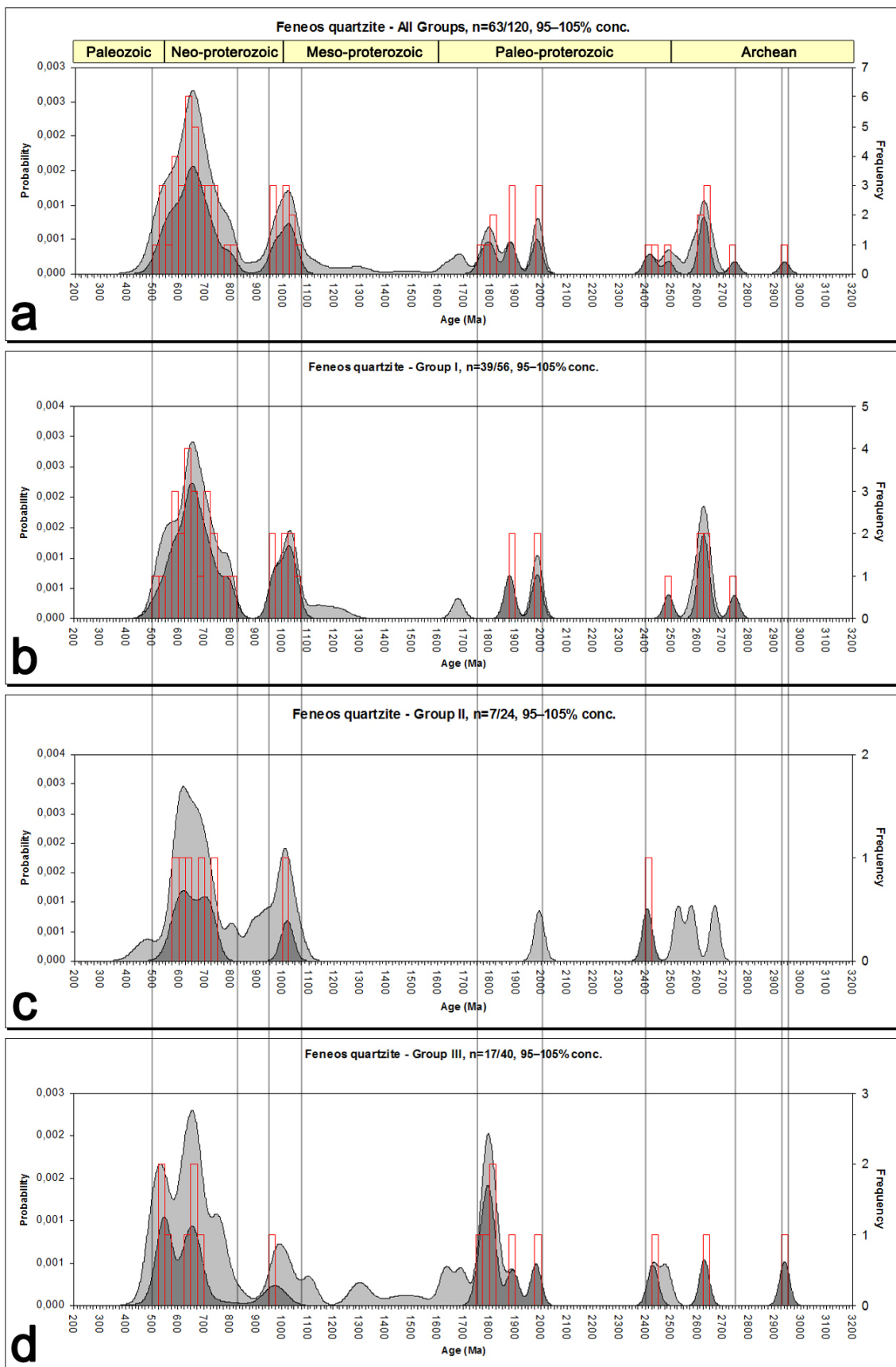


Fig. 5.5. Binned frequency histogram coupled with probability density distribution for the zircons of the sample Fe1 using (a) the full dataset, (b) the ages obtained from Group I, (c) the ages obtained from Group II and (d) the ages obtained from Group III. The $^{206}\text{Pb}/^{207}\text{Pb}$ ages (95% concordance) were chosen for display. The light grey areas represent the complete dataset of each group (or of the total) and the dark grey areas represent the zircon ages within concordance limit. Four prominent age clusters are visible i.e. 500-825 Ma, 950-1075 Ma, 1750-2000 Ma, 2400-2750 Ma (or split into 2400-2500 Ma and 2600-2750 Ma). Another ambiguous age clusters can be spotted at 2925-2950 Ma. See text for details.

Σχ. 5.5. Ιστογράμματα συχνότητας-πιθανότητας των ζιρκονίων του δείγματος Fe1 από (a) το σύνολο των μετρήσεων, (b) τις ηλικίες της Ομάδας I, (c) τις ηλικίες της Ομάδας II και (d) τις ηλικίες της Ομάδας III. Οι ηλικίες του ισοτοπικού συστήματος $^{206}\text{Pb}/^{207}\text{Pb}$ (95% συμφωνία) επιλέχθηκαν για απεικόνηση. Οι περιοχές απαλού γκρι χρώματος αναπαριστούν το σύνολο των μετρήσεων της κάθε ομάδας (ή όλων των ομάδων μαζί) και οι περιοχές σκούρου γκρι χρώματος αναπαριστούν εκείνες τις ηλικίες που συμβαδίζουν με το όριο συμφωνίας. Τέσσερεις διακρίτες δέσμες ηλικιών ξεχωρίζονται: 500-825 εκ. χρ., 950-1075 εκ. χρ., 1750-2000 εκ. χρ., 2400-2750 εκ. χρ. (μπορεί να διακριθεί επιμέρους σε 2400-2500 εκ. χρ. και 2600-2750 εκ. χρ.). Μία ακόμα πιθανή δέσμη ηλικιών μπορεί να εντοπιστεί στα 2925-2950 εκ. χρ.

It is known that the Th/U ratio can be a useful indicator of the magmatic or metamorphic nature of the zircon under investigation (e.g. [Teipel et al. 2004](#)). Values of Th/U>0.3 are generally accepted as the lower limit of magmatic values ([Rubatto et al. 2001](#), [Schaltegger et al. 1999](#), [Vavra et al. 1999](#)) while Th/U ratios <0.1 (or even <0.01) are characteristic of metamorphic zircons ([Rubatto et al. 1999](#), [Schaltegger et al. 1999](#), [Williams et al. 1996](#)).

Measuring the absolute abundance of Th content (as well as the U and Pb content) of zircon using laser ablation inductively coupled plasma mass spectrometry (LA-ICPMS) is not possible. Instead, comparing with the average known Th content of the standard GJ-1, which is not homogeneous throughout the grain, and comparing the corresponding absolute counts with that of the zircon under investigation can give a rough idea of the real content. The Th/U ratios ([Appendix B](#)) obtained by this method can deviate $\pm 10\%$ from the real ratio but they can still be used as a tool.

Two Th vs. U plots are drawn: one based on the three different groups of zircons (**Fig. 5.6a**) and one based on the age clusters mentioned above (**Fig. 5.6b**). The major conclusions coming out of the **Fig. 5.6** are: (i) Group II has dominantly magmatic zircons while the two other groups contain some zircons with metamorphic signature, (ii) Zircons with metamorphic signature originate mainly from the first age cluster (500-825 Ma; Neo-proterozoic – M. Cambrian) and less from the third age cluster (1750-2000 Ma; M.-Upper Paleo-proterozoic). One additional Th/U vs. age plot (**Fig 5.6c**) verifies that most of the metamorphic zircons belong to the youngest age cluster (500-825 Ma).

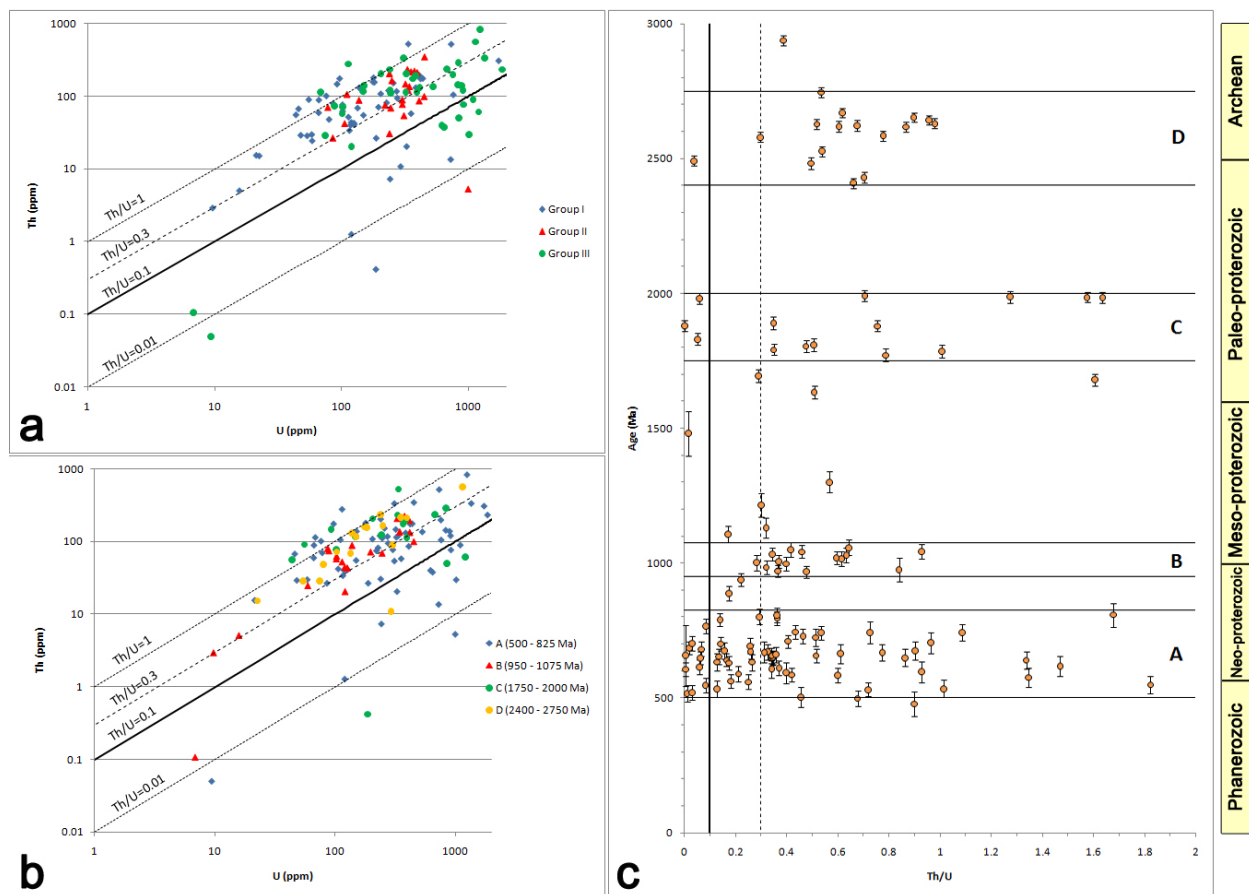


Fig. 5.6. Th vs. U concentrations of the zircons analyzed based (a) on the three different groups of zircons (Groups I, II and III; see text) and (b) on the four age clusters (A, B, C and D) identified in the binned frequency diagram (Fig. 5.5). Most metamorphic zircons ($\text{Th}/\text{U} < 0.1$) originate from the Group II and have M.-Upper Paleo-proterozoic (group C) or Neo-proterozoic – M. Cambrian (group A) ages. (c) Th/U vs. age plotting. The vertical lines correspond to Th/U ratios of 0.1 (left) and 0.3 (right). Horizontal lines correspond to the edges of each age cluster as these are defined in Fig. 5.5. Error bars are considered as 1-sigma. Note that (i) the complete zircon dataset is used in these plots and (ii) zircons outside concordance limit (95-105%) are plotting both inside and outside the age clusters in (c) but they were not took into account in the recognition of the age clusters.

Σχ. 5.6. Διαγράμματα με βάση την περιεκτικότητα σε Th και U των ζιρκονίων που αναλύθηκαν. Οι προβολές έγιναν (a) με βάση τις τρεις ομάδες ζιρκονίων (Ομάδα I, II και III; βλ. κείμενο) και (b) με βάση τις τέσσερεις δέσμες ηλικιών (age clusters; A, B, C και D) που προέκυψαν από τα ιστογράμματα συχνότητας-πιθανότητας (Σχ. 5.5). Τα περισσότερα μεταμορφικά ζιρκόνια ($\text{Th}/\text{U} < 0.1$) προέρχονται από την Ομάδα II των ζιρκονίων και έχουν ηλικία M.-Av. Παλαιο-πρωτεροζωικό (ομάδα C) ή Νεο-πρωτεροζωικό – M. Κάμβριο (ομάδα C). (c) Διάγραμμα Th/U – ηλικίας των ζιρκονίων. Οι κάθετες γραμμές αντιστοιχούν σε λόγους Th/U ίσους με 0.1 (αριστερά) και 0.3 (δεξιά). Οι οριζόντιες γραμμές αντιστοιχούν στα όρια των δεσμίδων ηλικιών (age clusters) όπως αυτές ορίστηκαν στο Σχ. 5.5. Τα σφάλματα ορίζονται ως 1σ. Σημειώνεται πως (i) το σύνολο των δεδομένων χρησιμοποιήθηκε στα παραπάνω διαγράμματα και (ii) τα ζιρκόνια εκτός ορίου συμφωνίας (concordance limit; 95-105%) προβάλλονται τόσο εντός όσο και εκτός των ορίων των δεσμίδων ηλικιών στο (c) αλλά δεν λήφθηκαν απόψη κατά προσδιορισμό τους.

5.2.3.3 Concordia and Tera-Wasserburg plots

“Normal” (or “conventional” or “Wetherill”) concordia diagrams are the most commonly used diagrams for plotting radiogenic U-Pb data (Fig. 5.7). This is because isochron diagrams utilizing only one decay scheme (^{238}U , ^{235}U , ^{232}Th) cannot indicate if the ages are concordant with respect to one of the other two decay schemes. Usually the concordance is defined as the $^{206}\text{Pb}/^{238}\text{U}$ value divided by the $^{207}\text{Pb}/^{206}\text{Pb}$ value and a typical constraint may be between 95% and 105% or as said between 95% concordance and 5% reverse discordance.

In many instances dates calculated for minerals containing U and Th are not concordant (different ages depending on the decay scheme used). The effect of Pb loss on U-Pb dates can be minimised by calculating a date based on the $^{207}\text{Pb}/^{206}\text{Pb}$ ratio, as introduced by the work of Tera and Wasserburg (1972), because this ratio is insensitive to recent Pb loss. The plot based on the $^{207}\text{Pb}/^{206}\text{Pb}$ ratio is known as “inverse concordia” or “Tera-Wasserburg” plot (Fig. 5.8).

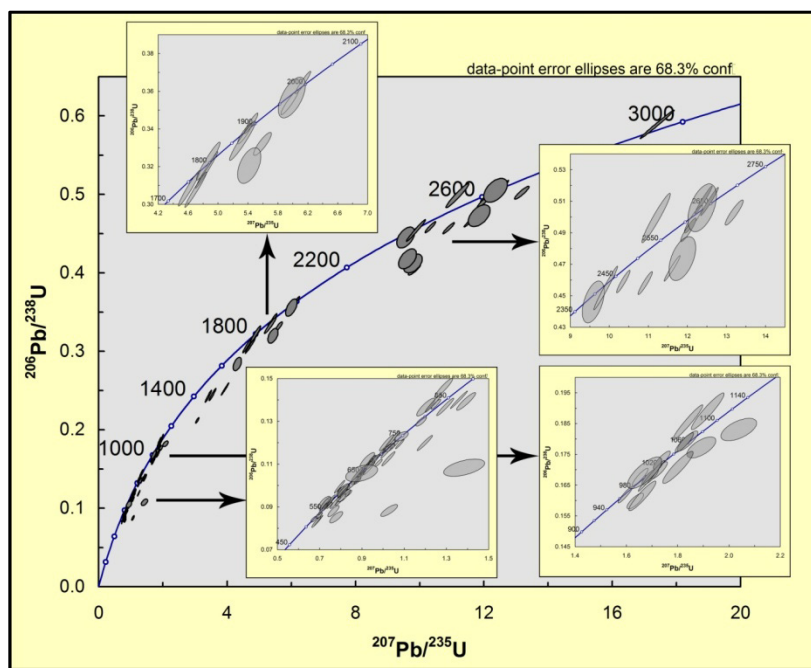


Fig. 5.7. Normal (or Wetherill) concordia plots of the 120 spots analyzed from the sample Fe1. Error ellipses are drawn at 1-sigma level. The complete isotopic dataset is given in Appendix B. The four insets refer to the age clusters defined in Fig. 5.5.

Σχ. 5.7. Προβολές «concordia» των 120 αναλύσεων του δείγματος Fe1. Τα σφάλματα παρουσιάζονται ως 1σ. Το σύνολο των ισοτοπικών δεδομένων παρουσιάζεται στο Παράρτημα B. Οι τέσσερις μικρότερες αναλυτικές προβολές αντιστοιχούν στις δέσμες ηλικιών όπως αυτές ορίστηκαν στο Σχ. 5.5.

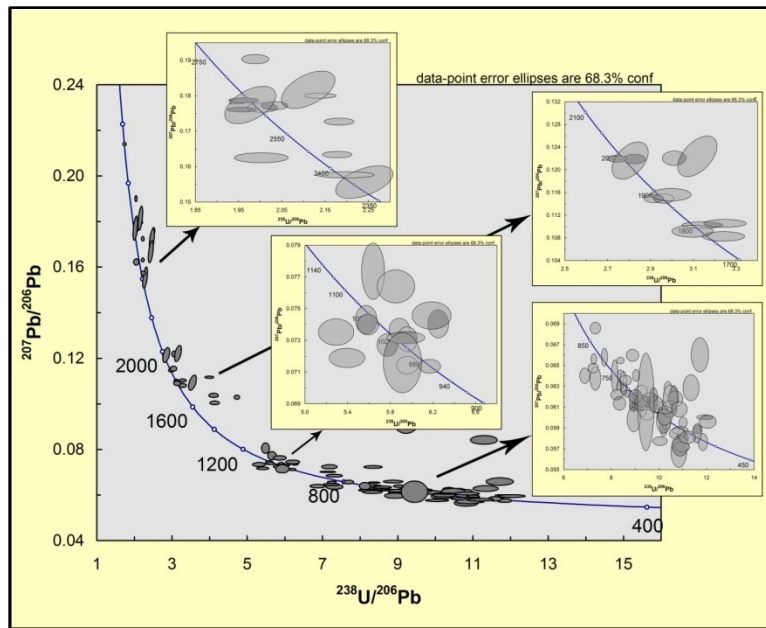


Fig. 5.8. Inverse (or Tera-Wasserburg) concordia plots of the 120 spots analyzed from the sample Fe1. Error ellipses are drawn at 1-sigma level. The complete isotopic dataset is shown in Appendix B. The four insets refer to the age clusters defined in Fig. 5.5.

Σχ. 5.8. Προβολές «Tera-Wasserburg» των 120 αναλύσεων του δείγματος Fe1. Τα σφάλματα παρουσιάζονται ως 1σ . Το σύνολο των ισοτοπικών δεδομένων παρουσιάζεται στο Παράρτημα B. Οι τέσσερεις μικρότερες αναλυτικές προβολές αντιστοιχούν στις δέσμες ηλικιών όπως αυτές ορίστηκαν στο Σχ. 5.5.

5.2.4.4 Age clusters

As mentioned in the previous paragraph, the $^{207}\text{Pb}/^{206}\text{Pb}$ ages (95% concordance) (Appendix B) yielded 4 prominent age clusters of 500-825 Ma (Neo-proterozoic – M. Cambrian; *Cluster A*), 950-1075 Ma (Upper Meso-proterozoic – Lower Neo-proterozoic; *Cluster B*), 1750-2000 Ma (M.-Upper Paleoproterozoic; *Cluster C*) and 2400-2750 Ma (Neoarchean – Lower Paleo-proterozoic; *Cluster D*) (Fig. 5.5).

Age Cluster A (500Ma – 825 Ma)

This dominant age cluster contains mainly Group I and Group III zircons (see Paragraph 5.2.3.1) showing two pronounced peaks at ~ 650 Ma (represented by Group I and III; Fig. 5.5b, 5.5d) and ~ 550 Ma (represented mainly by Group III; Fig. 5.5c). Its zircons show both a magmatic and a metamorphic signature (Fig. 5.6) and no correlation can be made between magmatic/metamorphic character and zircon age.

This age cluster is typical of the Pan-African orogenic event which lasted between ~ 870 and ~ 550 Ma. In fact, the term Pan-African is now used to describe tectonic, magmatic, and metamorphic

activity of Neoproterozoic to earliest Palaeozoic age, especially for crust that was once part of Gondwana (Kröner and Stern 2004). Because of its tremendous geographical and temporal extent, the Pan-African cannot be a single orogeny but must be a protracted orogenic cycle reflecting the opening and closing of large oceanic realms as well as accretion and collision of buoyant crustal blocks. Pan-African events culminated in the formation of the Late Neoproterozoic supercontinent Gondwana. The Pan-African orogenic cycle is time equivalent with the Cadomian Orogeny in western and central Europe and the Baikalian in Asia; in fact, these parts of Europe and Asia were probably part of Gondwana in pre-Palaeozoic times as were small Neoproterozoic crustal fragments identified in Turkey, Iran and Pakistan.

A typical example of late Neo-Proterozoic – early Paleozoic magmatic event is that recorded in the Menderes Massif (~570Ma – 520Ma; Loos and Reischmann [1999]). From Greece, ages from the same orogeny (~550Ma – 590Ma; from paragneisses and orthogneisses) have been reported from the Pirgadikia unit, a unit that borders the western part of the Serbo-Macedonian Massif in northern Greece (Himmerkus et al. 2006). Zircon upper intercept ages (~510Ma) have also been reported for orthogneisses from eastern Crete (Romano et al. 2004) confirming the age obtained (~520Ma) by monazite dating in orthogneisses from the same area (Finger et al. 2002).

The lack of any younger zircon age cluster in the quartzite under investigation suggests that its source material did not participate in any thermal event younger than the Pan-African event (~500Ma). The gap between the age of the source material (pre-Upper Cambrian) and the deposition age of the quartzite (Upper Carboniferous – Middle Triassic; Krahl et al. [1983]; **Plate 5**) can be attributed (i) to the delayed exposure of the source rocks or (ii) to the reworking of already deposited material and its redeposition after Upper Carboniferous. From the above it is clear that the deposition of the precursor (sandstone) of the quartzite happened away from any active margin of the Paleotethys. Instead the deposition must have happened near the southern passive margin of the Paleotethys (on the Apulian s.s. basement), assuming a northward Paleotethys subduction during that time.

Age Cluster B (950Ma – 1075Ma)

This age cluster seems rather homogenous without any pronounced peaks (**Fig. 5.5**) and contains exclusively magmatic zircons (**Fig. 5.6**) from the Group I (see Paragraph 5.2.3.1).

Ages around 1Ga are generally restricted to the Grenvillian – Kibaran orogenic belts that resulted from the amalgamation of the Rodinia supercontinent (e.g. Dalziel 1997). The Grenvillian orogenic belt can be traced from SW Baltica and eastern Greenland over to western Amazonia and the southern part of North America during the Neoproterozoic (Dalziel 1992). However, in the West African Craton and the “Saharan Metacraton” ages around 1.1-0.9Ga has not been reported until now. On the contrary, such ages have been reported from numerous peri-Gondwanan terranes of Europe (Moldanubia; Gebauer et al. 1989, *Mid-German Crystalline Rise*; Zeh et al. 2001, *Iberia*; Fernández-Suárez et al. 2000). In the Mediterranean, such ages have been reported: (i) for Cambrian - Ordovician sandstones from Israel and Jordan (Avigad et al. 2003, Kolodner et al. 2006), (ii) for the leucosome (inherited zircon cores) of a migmatitic paragneiss of Ordovician - early Carboniferous depositional age from the Sredna Gora Zone in Bulgaria (Carrigan et al. 2006), (iii) for metasedimentary rocks of late

Precambrian – early Paleozoic age from the Menderes – Taurus block (Kröner and Sengör 1990), (iv) for Paleozoic metasedimentary rocks of the Cyclades (Keay and Lister 2002), (v) from Crete (Romano et al. 2005), (vi) for Permian – Triassic sandstones from Chios (Meinhold et al. 2008b), (vii) for Cretaceous sedimentary rocks from the Western Circum-Rhodope Belt (Meinhold et al. 2009).

Generally, it seems that Grenvillian – Kibaran zircons have accumulated in post-Cadomian (Paleozoic) cover sequences at the northern margin of Gondwana (Fernández-Suárez et al. 2000, 2002 Avigad et al. 2003, Gutiérrez-Alonso et al. 2005, Kolodner et al. 2006) before being reworked during younger orogenic processes. The huge dispersion of the Grenvillian – Kibaran zircons is still a matter of discussion (see Zeh et al. 2001).

Age Cluster C (1750Ma – 2000Ma)

This age cluster contains mostly magmatic and few metamorphic zircons from Group III and purely magmatic zircons from Group I (Fig. 5.5, 5.6; Paragraph 5.2.3.1). It shows three relatively well-defined peaks at 1800Ma, 1900Ma and 2000Ma.

Age Cluster D (950Ma – 1075Ma)

This age cluster contains only magmatic zircons from Group I and II (Fig. 5.5, 5.6; Paragraph 5.2.3.1). Although this cluster has more than one peak, the most easily-defined is that at ~2625Ma.

5.3 Summary

The term «provenance» in geology applies mainly to the methods used to shed light on the source materials of sedimentary (or metasedimentary) rocks as well as on the related geotectonic settings.

In this study two tools were used as provenance indicators: major- and trace-elements and the powerful tool of detrital zircon dating. Major- and trace-elements can provide insight on the special characteristics of the source material and decipher between various geotectonic settings through projection in the appropriate diagrams. On the other hand, zircon isotopic ratios (Th/U), zircon geochronology and the distribution of the corresponding ages can reveal the age of the source material (terrains), allowing to check the consistency of already published paleogeographic global reconstructions.

For this purpose, one quartzite of possible Upper Carboniferous – Lower Triassic age from Feneos (Fe1) was chosen. The sample is a quartz-arenite based on chemical classification (Fig. 5.1) and its source can be an igneous or metamorphic rock, more or less evolved, or even an older sedimentary rock. Its chemical composition (Table 5.1) revealed increased Ba, Cr and Zr indicating a possible ultramafic input as well as significant accumulation of detrital zircons. Magmas formed above subduction zones commonly shows negative Nb and Ti anomalies which may be the case in the study rock (Fig. 5.2). The prominent negative anomaly which is observed for Eu, Sr, Ba and P (P is even below

detection limit; **Fig. 5.2**) suggests that the plagioclase played an important role in the creation of the source rock. The projection into the appropriate geotectonic setting discrimination diagrams (**Fig. 5.3**) revealed that the sample shows a trend between an acidic arc and a passive margin source.

U-Pb dating of detrital zircons has become a popular method in provenance studies. A total of 127 grains from the quartzite under investigation were mounted and allocated into three groups (**Fig. 5.4**). 102 out of 127 grains were chosen for dating resulting in 120 spot analyses (**Table 5.2**). Most of the grains are rounded (aspect ratios between 1.668 and 2.262), with the exception of few euhedral grains, suggesting rather long sedimentary transport. The first group of zircons (Group I) contains relatively big, gray and cloudy zircons, the second group (Group II) contains relatively small, transparent and elongated zircons and the third group (Group III) contains medium-sized, pink and semi-transparent zircons. Significant differences as far as their geometrical characteristics (**Table 5.3**) and the element content (**Table 5.4**) are observed.

In provenance studies involving relatively large dataset, the most optimum method to visualize the results is the binned frequency histogram and probability density distribution. The $^{207}\text{Pb}/^{206}\text{Pb}$ ages (95% concordance) (**Appendix B**) yielded 4 prominent age clusters of 500-825 Ma (Neo-proterozoic – M. Cambrian), 950-1075 Ma (Upper Meso-proterozoic – Lower Neo-proterozoic), 1750-2000 Ma (M.-Upper Paleo-proterozoic) and 2400-2750 Ma (Neoarchean – Lower Paleo-proterozoic) (**Fig. 5.5**). Another possible age cluster appears at 2925-2950 Ma (**Fig. 5.5**). In general, the most abundant zircon input is coming from the youngest Neo-proterozoic – M. Cambrian age cluster. More differences between the aforementioned groups of zircons can be spotted on the fact that they contribute differently to the age clusters (**Fig. 5.5**).

It is known that the Th/U ratio can be a useful indicator of the magmatic or metamorphic nature of the zircon under investigation. The Th vs. U and the Th/U vs. Age plots (**Fig. 5.6**) clarifies that the second group of zircons (Group II) has dominantly magmatic zircons while the two other groups contain some zircons with metamorphic signature and that zircons with metamorphic signature originate mainly from the first age cluster (500-825 Ma; Neo-proterozoic – M. Cambrian) and less from the third age cluster (1750-2000 Ma; M.-Upper Paleo-proterozoic).

The major conclusions based on the discussion about the different age clusters (**Paragraph 5.2.4.4**) can be summarized as: (i) the youngest thermal events to which the sources of the quartzite participated is that of the Grenvillian – Kibaran and the Pan-African orogenies, (ii) the sources show no signature of the Variscan orogeny and the sample analyzed here is the first reported from Crete/Peloponnese with such a characteristic. Note that, in case that the source rock has participated in the Variscan orogeny, which is known to have lasted between \sim 330Ma and \sim 280Ma, it would be impossible for a quartzite of such an age (post-Upper Carboniferous) to show no Variscan zircons. For comparison, in Crete, Kock et al. (2007) demonstrated metamorphosed sedimentary rocks of Upper Carboniferous – Lower Permian age (\sim 300Ma; Galinos Beds), lying below Plattenkalk Unit and clearly showing accumulation of Variscan zircons. Consequently, the importance of the present study is that it documented for the first time non-Variscan signature in the pre-Triassic sedimentation of the external Hellenides.

Discussion and conclusions

Chapter 6

In this final chapter, all the published and new data presented in the previous chapters will be summarized. The reader is encouraged to read any specific paragraphs of his interest for a more detailed presentation.

6.1 Discussion

The Hellenic orogenic system (**Fig. 1.1**) is the result of the long-lasting convergence between Europe and the North Gondwana passive margin leading to the consumption of oceanic domains and to the accretion of continental blocks during the Alpine orogeny. In the Hellenides, two exhumed HP belts can be distinguished (**Fig. 1.3**): (i) the *internal* (or *Cycladic*) *blueschist belt* appearing mainly in Cyclades (see Philippon et al. [2010] and references therein) and (ii) the *external blueschist belt* appearing in Peloponnese and Crete (see Jolivet et al. [2010] for a review). The northern part of the external blueschist belt, which is traditionally represented by the *Phyllite – Quartzite Unit* (or *Arna Unit*), is objective of the present study.

The Phyllite – Quartzite unit is a meta-sedimentary sequence of Upper? Carboniferous – Lower (or even Middle) Triassic depositional age** (**Plate 2**) metamorphosed under blueschist facies possibly during the tertiary. Mafic and ultramafic rocks, as well as carbonates have also been documented suggesting that the aforementioned unit is a rather complex one (Papanikolaou and Skarpelis 1986, Skarpelis 1989, Trotet et al. 2006). It lies below Tyros Beds and Tripolitsa unit and above Plattenkalk unit, wherever exposed (e.g. Taygetos Mt., Parnon Mt., Dikti Mt.) (**Fig. 2.3, 2.4**). The metamorphic pressure attained in western Crete and southern Peloponnese is between 10Kbar and 15Kbar (Papanikolaou and Skarpelis 1986, Theye and Seidel 1991, Theye et al. 1992, Brix et al. 2002). However, both higher and lower pressures have been suggested by different authors. The peak-metamorphic conditions of the Phyllite – Quartzite unit seems to decrease eastward in Crete and northward in Peloponnese.

** This particular depositional age is based on the detailed work of Krahl et al. (1983) who dated conodonts, and microfauna (ostracoid and echinoderms) from western Crete (**Plate 5**). Note that only samples belonging to the Phyllite – Quartzite unit, according to the revised stratigraphy of Crete proposed by Papanikolaou and Vassilakis (2010), took into consideration.

Available radiometric data (mostly K/Ar or Ar/Ar on micas) from the Phyllite – Quartzite unit shows concentration between 25Ma and 15Ma (Seidel et al. 1982, Jolivet et al. 1996, 2010), leading several authors to relate this age pattern with the arrival of the unit in mid-crustal levels, just before its exposure on the surface around ~10Ma as demonstrated by Seidel et al. (2006b) for the *Topolia formation* of Crete. On the contrary, radiometric data from the overlying Tripolitsa unit shows that it rested in the 4-7Km of the uppermost crust since Eocene times (Thomson et al. 1998a). This, along with the pressure gap observed between the Phyllite – Quartzite and the overlying units, lead several authors to propose the existence of a major extensional contact (i.e. a detachment) separating the previous units (e.g. Fassoulas et al. 1994, Jolivet et al. 1996, 2010, Papanikolaou and Royden 2007, Papanikolaou and Vassilakis 2010). The post-HP shear direction related to this extensional contact is to-the-NE in Peloponnese (Fig. 2.3) and to-the-N in Crete where it also follows an older to-the-S shear direction (Fig. 2.5).

The study area (Fig. 3.1) is the northernmost exposure of the external blueschists belt represented by the Phyllite – Quartzite. The central part of the area studied is covered by an exposed core of metasediments as well as slightly metamorphosed mafic rocks (Fig. 3.2) and is flanked mainly by carbonate rocks. The Phyllite – Quartzite unit appears in the core and is represented by meta-sediments (quartzites and metapelites). The other constituent of the core is the Tyros Beds represented by pure metapelites or metapelites with calcite intercalations (calc-schists), by mafic rocks and minor carbonates. Tripolitsa carbonates appear on both limbs of the exposed core.

The oldest planar surface observed in the study area is the bedding (Fig. 3.2b, 3.2g). Foliation measurements revealed a major regional foliation with dominantly SW-dipping planes (Fig. 3.3 inset) always parallel to the initial bedding. The distribution of the foliation planes and the foliation trajectories revealed that the structure of the Phyllite – Quartzite unit is that of an antiform with a roughly NW-SE-directed axis (Fig. 3.3). Most of the stretching lineations measured (on the foliation planes) were from the Phyllite – Quartzite unit and showed a pronounced NE-SW trend with the dominant direction being between N050° and N060° (Fig. 3.4). The same NE-SW trend is true for the stretching lineations measured from the overlying Tyros beds (Fig. 3.4). Few intersection lineations measured showed a well-defined NW-SE orientation and were directly connected to the measured fold axes (see below). Folds measured in outcrop scale were mainly restricted to the metasedimentary rocks and in particular to the metapelites. The majority of the folds observed was tight to isoclinal and showed gently plunging hinge lines and moderately- to gently-inclined axial planes (Fig. 3.5). Their relationship with the regional foliation revealed two types of folds: those with axial planes parallel to the regional foliation (*Type I* – Fig. 3.5a, 3.5c) and those whose axial plane crosscut the regional foliation showing no well developed axial plane surfaces (*Type II* – Fig. 3.5d). In any case, the *Type I folds* were the dominant type and both of the fold types showed the same NW-SE-trending axes (Fig. 3.5e, 3.5g) suggesting an initial compression in NE-SW direction during their formation.

Most of the rocks studied were rich in sheet silicates and favored the development of shear indicators. It was shown that the shearing was constantly towards the NE (Fig. 3.6), following the direction of the stretching lineation. Although most of the shearing directions measured were from the Phyllite – Quartzite unit, few measurements from the overlying Tyros beds seemed to follow the same

pattern (**Fig. 3.6**). Three well-exposed zones were chosen for presentation. They were developed either near the top of the Phyllite – Quartzite (**Fig. 3.8**) unit or near the top of the Tyros beds (**Fig. 3.7, 3.9**). Their common feature was the NE-directed shearing that started in the ductile field and continued in the brittle field with the same orientation as shown by (i) the brittle fractures near the hinge of the NE-verging folds (**Fig. 3.7e**), (ii) the disruption of the small shear zones by younger NW-SE brittle faults showing the same sense of movement (**Fig. 3.7d**), (iii) the reactivation of already existing weak zones like C' planes (**Fig. 3.8c**), (iv) the existence of intense cataclasis within the shear zones (**Fig. 3.8a, 3.9**) and (v) the disruption of the continuity of the pile from NW-SE normal faults in map-scale (**Fig. 3.1**).

The model proposed here will be presented in the following lines. Folding of the initial bedding (or another old surface) resulted in the formation of the NW-SE folds (*Type I and II*) and the regional foliation under an early ductile compressional regime with NE-SW orientation. This phase is possibly related to the W- or SW-shearing seen in microscale (e.g. asymmetric quartz c-axis) by Xypolias and Koukouvelas (2001). Although that folds younger than the regional foliation did observed in the area (*Type II* folds), they seem to have formed under the same stress field (NE-SW compression) and before any later event. This type of folds is connected with any well-developed planar element parallel to their axial plane. After the cease of any compressional stresses, the whole pile suffered an intense NE-shearing contemporaneously with (i) the formation of the studied shear zones, (ii) the development of numerous shear indicators within the metasediments and (iii) the NE-oriented stretching lineation that characterizes both the Phyllite – Quartzite unit and the overlying Tyros beds. The same stress field seems to have remained active through part of the brittle deformation, at least in the study area, as seen in outcrop (**Fig. 3.7d**) or in map-scale (**Fig. 3.1**). Few kilometers to the north the brittle extension is definitely to the N-S direction as already noted by several authors and is related to the opening of the Gulf of Corinth (Moretti et al. 2003, 2004). The linkage between the two areas yet remains to be answered. The antiform structure of the area, which correlates in geometry with the mesoscopic folds (NW-SE), could either represent an inherited compressional-related feature like the inherited structures separating young Pliocene basins to the north (Derveni and Aigio basins; Ghisetti and Vezzani [2004]) and the fold-and-thrust belt to the east or it could be related to an isostatic passive flexural folding due to the later intense NE-shearing. The whole model is compatible with the model proposed by Papanikolaou and Royden (2007) studying in much larger scale the external blueschist belt.

As already noted by Katagas et al. (1991) who studied the metamorphism of the Feneos area, the Phyllite – Quartzite unit is of greater metamorphic grade, compared to the overlying Tyros Beds, but without, though, a pronounced metamorphic gap. In specific, they claimed that the peak temperature never exceeded 440°C with the most possible temperature being between 340°C and 420°C and the peak pressure, although not well constrained, it should have never exceeded 5Kbar. For comparison, the metamorphic conditions calculated from the mafic rocks included in the overlying Tyros beds are 290°C – 380°C and 3.5 – 5Kbar (Baltatzis and Katagas 1984). On the contrary, the peak pressure from the Phyllite – Quartzite unit seems to be higher in the nearby Kastania village (few kilometers SE of the Feneos village) i.e. 10Kbar at 450°C (Jolivet et al. 2010).

In order to test the consistency of the above results, P-T estimation was conducted using the free energy minimization method (Connolly 2005) and the thermodynamic database of Holland and

Powell (1998, revised 2002). For this purpose, two samples from north of Zarouchla (quartzite - F61) and from Kastania (metapelites - F12) villages were chosen (from Katagas et al. 1991). From the Feneos area, the sample studied seems to have equilibrated at 9-11Kbar even though that the temperature is not well-constrained (i.e. $>230^{\circ}\text{C}$) (Fig. 4.1). From the nearby Kastania area, the sample studied have equilibrated at significantly higher pressure i.e. $>13\text{Kbar}$ (or even $>15\text{Kbar}$) (Fig. 4.2). The pressure of metamorphism estimated here is increased compared to the already published results from the above-mentioned areas. If the pressure difference between the Feneos and Kastania areas is precise, then this necessitates either (i) the possible discrimination between subunits with different metamorphic histories (all belonging to the Phyllite – Quartzite unit but exposed in the aforementioned areas) or (ii) the discrimination between different mechanisms, or intensity of mechanisms, responsible for the exposure of the specific unit.

The term «provenance» in geology applies mainly to the methods used to shed light on the source materials of sedimentary (or metasedimentary) rocks as well as on the related geotectonic settings.

In this study two tools were used as provenance indicators: major- and trace-elements and the powerful tool of detrital zircon dating. For this purpose, one quartzite of possible Upper Carboniferous – Lower Triassic age from Feneos (Fe1) was chosen. The sample is a quartz-arenite based on chemical classification (Fig. 5.1) and its source can be an igneous or metamorphic rock, more or less evolved, or even an older sedimentary rock. Its chemical composition (Table 5.1) revealed increased Ba, Cr and Zr indicating a possible ultramafic input as well as significant accumulation of detrital zircons. Magmas formed above subduction zones commonly shows negative Nb and Ti anomalies which may be the case in the study rock (Fig. 5.2). The prominent negative anomaly which is observed for Eu, Sr, Ba and P (P is even below detection limit; Fig. 5.2) suggests that the plagioclase played an important role in the creation of the source rock. The projection into the appropriate geotectonic setting discrimination diagrams (Fig. 5.3) revealed that the sample shows a trend between an acidic arc and a passive margin source.

U-Pb dating of detrital zircons has become a popular method in provenance studies. A total of 127 grains from the quartzite under investigation were mounted and allocated into three groups (Fig. 5.4). 102 out of 127 grains were chosen for dating resulting in 120 spot analyses (Table 5.2). Most of the grains are rounded (aspect ratios between 1.668 and 2.262), with the exception of few euhedral grains, suggesting rather long sedimentary transport. The first group of zircons (Group I) contains relatively big, gray and cloudy zircons, the second group (Group II) contains relatively small, transparent and elongated zircons and the third group (Group III) contains medium-sized, pink and semi-transparent zircons. Significant differences as far as their geometrical characteristics (Table 5.3) and the element content (Table 5.4) are observed. It is known that the Th/U ratio can be a useful indicator of the magmatic or metamorphic nature of the zircon under investigation. The Th vs. U and the Th/U vs. Age plots (Fig. 5.6) clarifies that (i) the second group of zircons (Group II) has dominantly magmatic zircons while the two other groups contain some zircons with metamorphic signature and (ii) that zircons with metamorphic signature originate mainly from the first age cluster (500-825 Ma; Neo-proterozoic – M. Cambrian) and less from the third age cluster (1750-2000 Ma; M.-Upper Paleo-proterozoic) (see below).

In provenance studies involving relatively large dataset, the most optimum method to visualize the results is the binned frequency histogram and probability density distribution. The $^{207}\text{Pb}/^{206}\text{Pb}$ ages (95% concordance; **Appendix B**) yielded 4 prominent age clusters of 500-825 Ma (Neo-proterozoic – M. Cambrian), 950-1075 Ma (Upper Meso-proterozoic – Lower Neo-proterozoic), 1750-2000 Ma (M.-Upper Paleo-proterozoic) and 2400-2750 Ma (Neoarchean – Lower Paleo-proterozoic) (**Fig. 5.5**). Another possible age cluster appears at 2925-2950 Ma (**Fig. 5.5**). In general, the most abundant zircon input is coming from the youngest Neo-proterozoic – M. Cambrian age cluster.

The major conclusions based on the discussion about the different age clusters (**Paragraph 5.2.4.4**) can be summarized as: (i) the youngest thermal events to which the sources of the quartzite participated is that of the Grenvillian – Kibaran and the Pan-African orogenies, (ii) the sources show no signature of the Variscan orogeny and the sample analyzed here is the first reported from Crete/Peloponnese with such a characteristic. Note that, in case that the source rock has participated in the Variscan orogeny, which is known to have lasted between $\sim 330\text{Ma}$ and $\sim 280\text{Ma}$, it would be impossible for a quartzite of such an age (post-Upper Carboniferous) to show no Variscan zircons. For comparison, in Crete, Kock et al. (2007) demonstrated metamorphosed sedimentary rocks of Upper Carboniferous – Lower Permian age ($\sim 300\text{Ma}$; Galinos Beds), lying below Plattenkalk Unit and clearly showing accumulation of Variscan zircons. Consequently, the importance of the present study is that it documented for the first time non-Variscan signature in the pre-Triassic sedimentation of the external Hellenides.

6.2 Conclusions

The major outlines from the present study are summarized below:

- The Feneos area is mostly occupied by metamorphosed sediments (metapelites, quartzites etc), metamorphosed mafic rocks and carbonates, mainly represented by the Phyllite – Quartzite unit and the overlying Tyros beds (with the carbonates belonging to the Tripolitsa unit). An antiform structure with NW-SE trending axis is inferred from the measured foliation planes.
- An early compression, resulting in NW-trending mesoscopic folds (*Type I* folds) and NW-trending intersection lineation, is true for both the Phyllite – Quartzite unit and the overlying Tyros beds. This deformation phase is contemporaneous with the formation of the regional foliation in the area. No sense of movement is related to this stage in mesoscopic scale. On the contrary, Xypolias and Koukouvelas (2001) studying microscale features (i.e. oblique grain shape in dynamically recrystallised quartzites and asymmetrical quartz c-axis) recorded top-to-the-W or -SW sense of movement that may be possibly related to this early stage. Folds younger than the regional foliation (*Type II* folds) did observed but they are not connected to any well-developed axial planes.

Consequently they are attributed to the same early compressional phase as a result of the progressive deformation during subduction.

- Late shearing in the ductile field resulted in widespread top-to-the-NE sense of movement affecting the whole metasedimentary pile and recorded by many shear indicators. It is contemporaneous with the development of shear zones both near the top of the Phyllite – Quartzite unit and the Tyros beds and the formation of the NE-directed stretching lineation. Although Xypolias and Koukouvelas (2001) claimed that the NE shearing is restricted to a narrow, ~50m thick zone, in this study the NE shearing was shown to be distributed rather homogenously throughout the metamorphosed sediments.
- The NE-shearing possibly continued in the brittle field resulting in the overprinting of previous ductile structures by younger brittle ones with characteristic loss of cohesion of the rocks involved.
- Folding in the area should be connected to the subduction of the rocks under NE-SW compressional regime. Assuming that the late NE-shearing is connected with the post-peak metamorphic stage and the exhumation of the rocks (Phyllite – Quartzite unit and Tyros beds) then the initial compression and late shearing maintained the same direction (NE-SW). This possibly suggests that subduction and exhumation happened without any internal (or relative) rotation of the aforementioned units. The same is true for Crete where the early top-to-the-S shearing is followed by a top-to-the-N post-peak metamorphic shearing.
- The stretching lineation recorded from the Phyllite – Quartzite unit of Peloponnese (towards NE; Jolivet et al. [2010], this study) and Crete (towards N; Jolivet et al. [1996]) suggests that a relative rotation between Peloponnese and Crete must have happened during or after this late post-HP (Miocene?) shearing. This adds to the generally accepted point of view of an almost linear geometry of the Hellenic arc during the Oligocene (Walcott and White 1998, Schellart and Lister 2004) or even during the Eocene (Brun and Faccenna 2008) which was later resulted in the present arc-shaped Hellenic as a result of the slab rollback (Schellart and Lister 2004, Brun and Faccenna 2008).
- The relationship between the well-studied N-S extension in the Gulf of Corinth, few kilometers to the north of the study area, and the Feneos area remains to be answered.
- Although early workers (Katagas et al. [1991]) noted that the pressure of metamorphism of the Phyllite – Quartzite unit in the Feneos area is not more than 5Kbar it was shown here that it may be as high as 9-13Kbar. The conclusion of the previous authors relatively to the lack of a pronounced metamorphic gap between the Phyllite – Quartzite unit and the overlying Tyros beds should at least be re-examined.
- Further, the pronounced pressure gap (Phyllite – Quartzite unit) between Feneos (>13 or 17Kbar; this study) and Kastania areas (~10Kbar; Jolivet et al. 2010) could be attributed to the different bulk chemistry of the protolith or to the intensity of the deformation mechanisms and possibly necessitates the discrimination between subunits with different tectono-metamorphic history in the above-mentioned areas.
- One quartzite of possible Upper Carboniferous – Middle? Triassic age was chosen for geochemistry and for in-situ dating of its detrital zircons. It documented the reworking of an initial acid arc-related rock, formed near an active continental margin, during later thermal/orogenic events. The quartzite

recorded also minor input from an ultramafic material. The youngest thermal events revealed by the detrital zircon dating are that of the Grenville (late Meso-Proterozoic) and Pan-African (late Paleozoic) orogenies. The lack of any Variscan zircons, recorded here for the first time in (meta)sedimentary sequences of Upper Paleozoic deposition age of the External Hellenides, suggests deposition of the protolith far away from any Variscan-related source, possibly near the southern passive margin of the Paleotethys. For comparison, sedimentary sequences of Upper Carboniferous – Lower Permian age (Galinos beds) clearly influenced by a Variscan source ([Kock et al. 2007](#)).

Plate 1

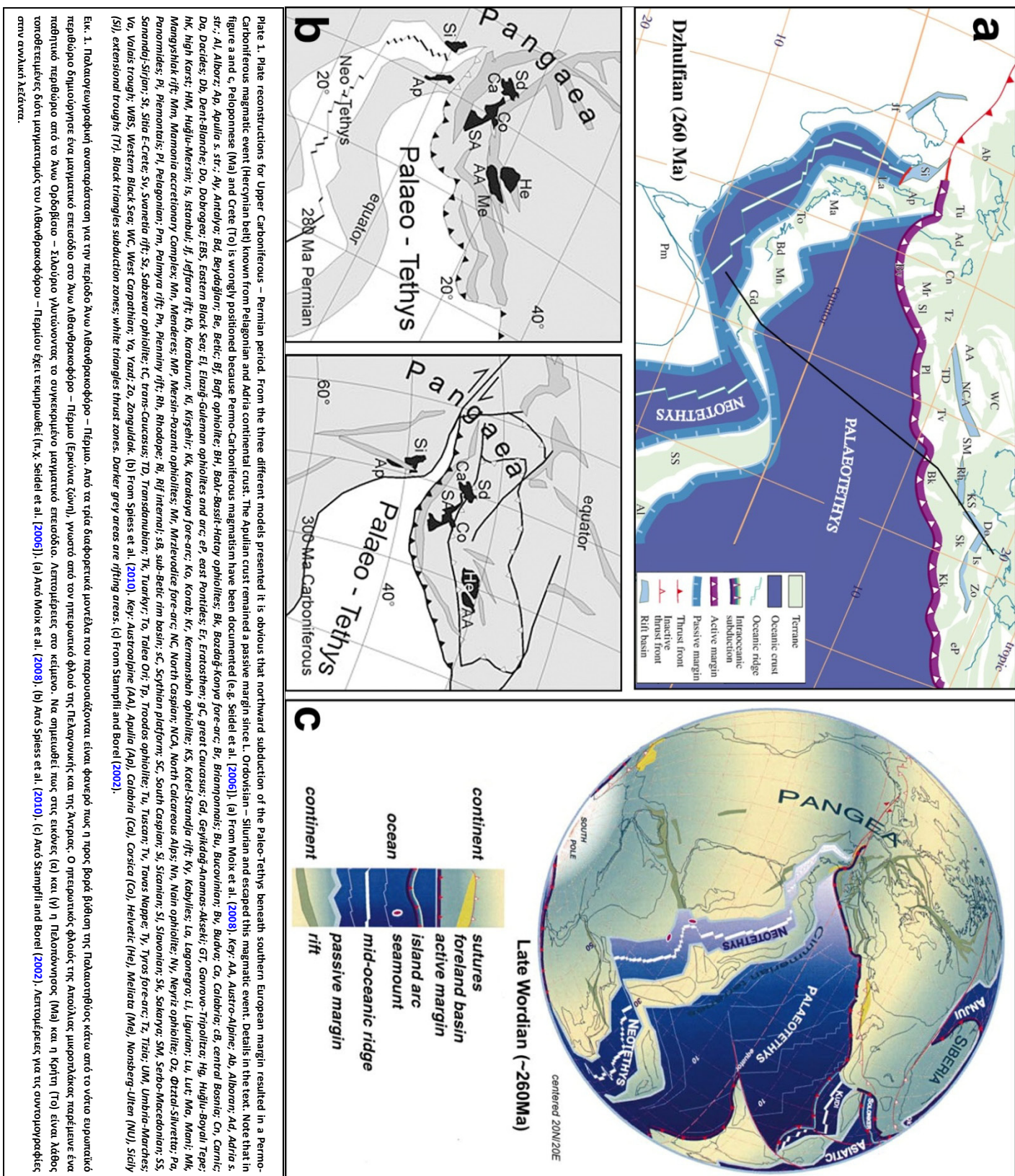


Plate 1. Plate reconstructions for Upper Carboniferous – Permian period. From the three different models presented it is obvious that northward subduction of the Paleo-Tethys beneath southern European margin resulted in a Permo-

Fig. 1. Πλακαγευαραφική αναταράσσων για την περίοδο Ανώ Λιθανθρακούφορο – Πέριο. Αρό τα τρία διαφορετικά μοντέλα που παρουσιάζονται είναι, φανερό πως η προς βορρά βράχιον της Πλακαγευαράς κάτω από το νότιο ευρωπαϊκό περιβόριο δημιούργησε ένα μαργαριτικό επεισόδιο στη Ανώ Λιθανθρακούφορο – Πέριο (Εργασία ζώνης), γνωστό από τον πεντροπικό φάσο της Πελεκονικής και της Αντρας. Ο πεντροπικός φάσος της Απογούσας μιαροτάκας παρέμεινε ένα ποδοθηκιανό περιβόριο από τη Ανώ Λιθανθρακούφορο – Σιδηρόπευρο – Λιγνούνος το συγκεκριμένο μαργαριτικό επεισόδιο. Λεπτομέρειες στο κείμενο. Να σημειωθεί πως στις εικόνες (a) και (b) η Πλακαγευαρά (Ma) και η Κρήτη (Te) είναι λάθος οποιασδήποτε διοίγημα μεταπορίδης του Λιθανθρακούφορου – Περιού έχει τεκμηριωθεί (π.χ. Seidel et al. [2006]). (a) Αρό Moik et al. (2008). (b) Αρό Spiess et al. (2010). (c) Αρό Stampfli and Borel (2002). Λεπτομέρειες για τις ανωμορφώσεις στην ανωτάτη λείαντα.

Plate 2

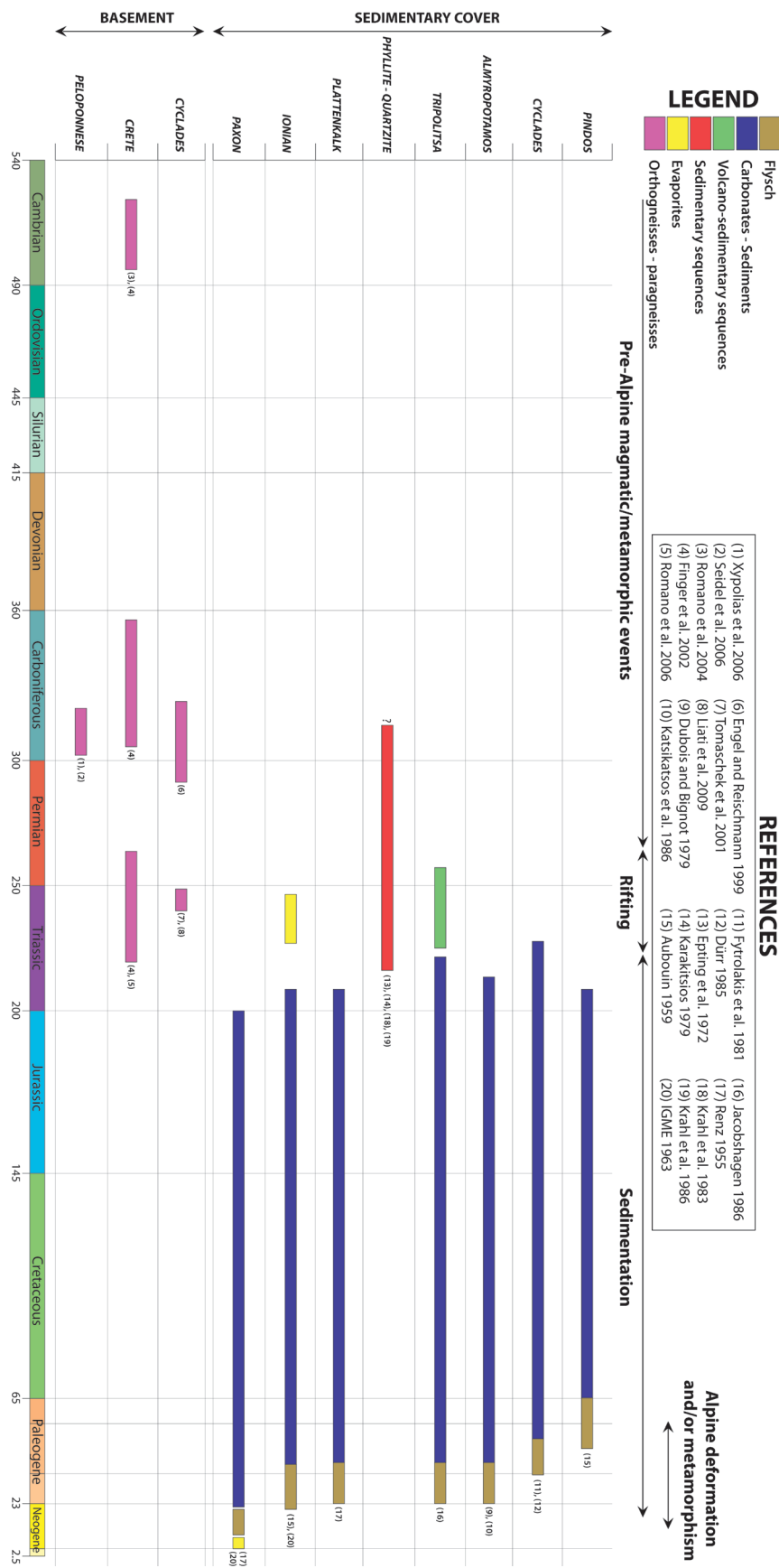


Plate 2. Cumulative table showing the age distribution of the sedimentary cover (i.e. Pindos, Almyropotamos, Tripolitsa, Phyllite-Quartzite, Plattenkalk and Paxon units) and of the basement rocks exposed in Cyclades, Crete and Peloponnes (including Kythira). Note that the ages reported for the sedimentary cover of Cyclades are coming from the most complete sedimentary sequence available in Amorgos island.

Εικ. 2. Συγκεντρωτικό πίνακας με τις ηλικίες των ιδιαίτερων καλυμμάτων (ευόπητες Πίνδου, Αλμυροποτάμου, Τρίπολης, Φυλλιτών – Καλαζτών, Μάνης, Παξών) και των πετρωμάτων υποβάθρου από τις Κυκλαδες, την Κρήτη και την Πελοποννησο (συμπεριλαμβανομένων των Κυθήρων). Σημειώνεται πως η ηλικίες που παρουσιάζονται για το ιδιαίτερο κάλυμμα των Κυκλαδών προέρχονται από την πιο στρωματογραφική στήλη στην Αμοργό.

Plate 3

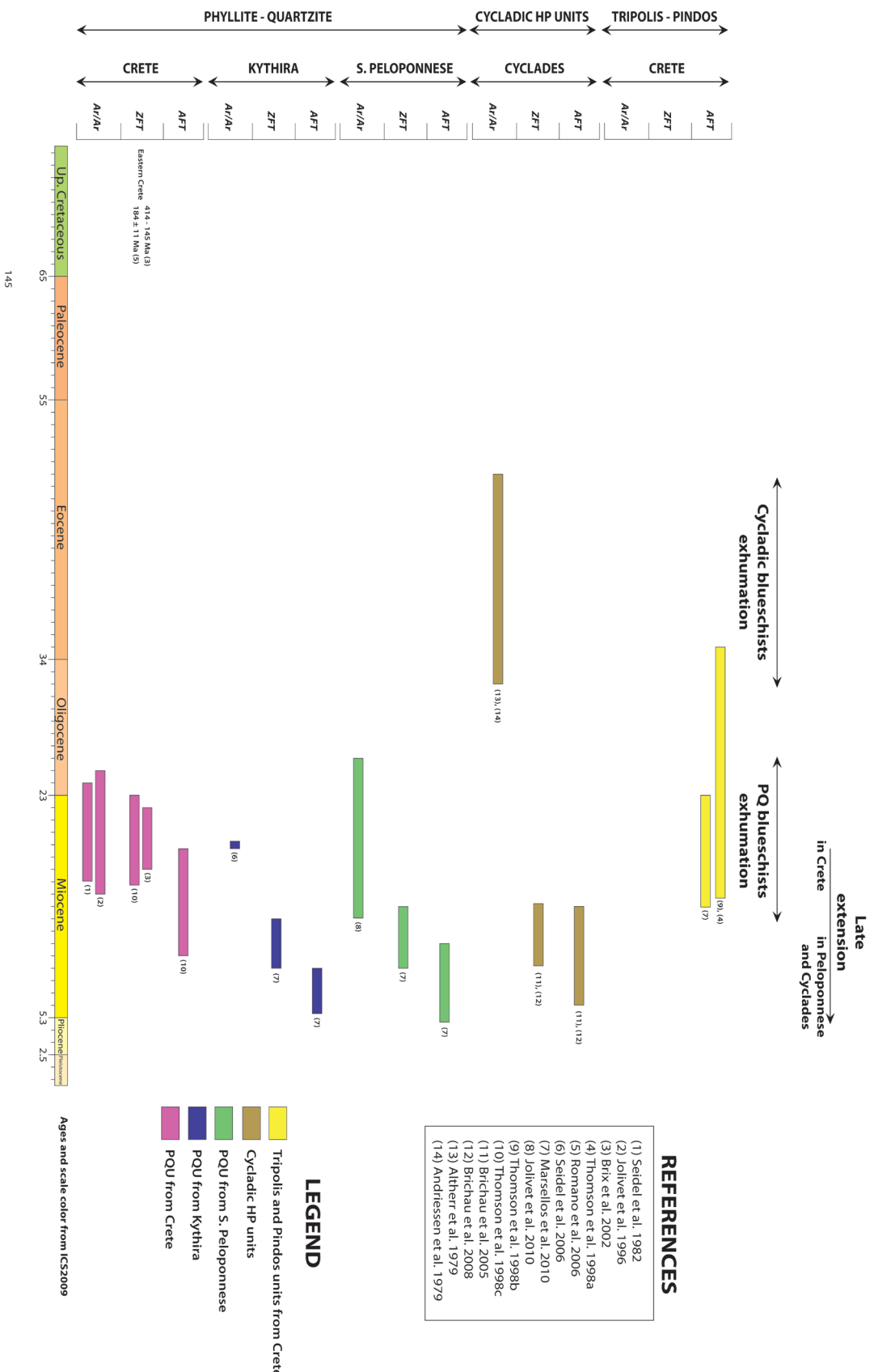


Plate 3. Isotopic ages obtained from the external (Phyllite – Quartzite Unit) and the internal (Cycladic) blueschists belt. Three isotopic systems are presented: i) Ar/Ar (mainly on micas), apatite fission tracks (AFT) and zircon fission tracks (ZFT) from samples coming from Crete, Kythira, S. Peloponnese and Cyclades. Note that: i) Ar/Ar ages mark the exhumation to mid-crustal levels or roughly the brittle/ductile transition, ii) the upper limit of the partial annealing zone in ZFT is around 350°C – 400°C and iii) AFT ages mark the exhumation to the depth that coincides with temperature of $\sim 120^{\circ}\text{C}$. Some additional ages from Tripolitsa and Pindos units are presented. Based on Ar/Ar isotopic system two distinct exhumation events can be recognized: one in Eocene (Cycladic blueschists) and one in Miocene (Quartzite unit). Late extension (M. – Upper Miocene) is marked by young AFT ages as already noted for Syros by Philippou (2010). Late extension in Cyclades, S. Peloponnese and Kythira seems contemporaneous, while in Crete it seems to start a bit earlier as documented by AFT ages.

Εικ. 3. Ισοτοπικές ηλικίες από την ενυπέριη (ενυπέρια Φυλλάτων - Χαλαζίαν) και την ευστρεμπή (Χαλαζίας) κανανομοτολιθική ζώνη. Τρία ισοτοπικά συστήματα παρουσιάσουν: Ar/Ar (κυρίως σε λαρυγγαργές), ληγκ οργανικής σε απαρτίτη (ΑΕΤ) και ληγκ οργάνων σε λιπαρόνια (ΖΕΤ) από διάφορα της Κρήτης, κυρίως, Ν. Πελοποννήσου και Κυκλαδών. Να σημειωθεί πως: i) οι ηλικίες που προκύπτουν από το Ar/Ar δείχνουν την ηλικία εκτιφής στον μέσο φάση ή λισσόνησμα τη μετάβαση από την πιλαστική στη θραυστική πορειαρόφων, ii) τα δύο όρια της μερικής διάδοσης των ωνόν σχέσης στο λιπαρόνιο (ΖΕΤ) είναι περίπου στους 350°C - 400°C και iii) οι ηλικίες που προκύπτουν από τα ληγκ οργάνων σε απαρτίτες (ΑΕΤ) αντιστοιχούν εκτιφήι σωματιδίων πετρωμάτων σε βάθος που αντιστοιχεύει σε θερμοκρασία περίπου 120°C. Παρουσιάζονται επίσης προβετής ηλικίες από την ενυπέριη τριπολής και πιδίων. Διό λεγχηριαστικά σπειρούδια εκτιφήι κανανομοτολιθικών μηρούντων λα διακρίθησαν από το θρεπτικό νεότερης ηλικίας που προκύπτουν από τα ληγκ οργανικής σε απαρτίτες διών έτη ήδη τουςχεί για την Σύρο (Philippon 2010). Όπως προκύπτει από τα δημητρικά σε απαρτίτη, ο συγκεκριμένος νεότερος εφελκυσμός φαίνεται να είναι σύγχρονος σε Κυκλαδες, Ν. Πελοπόννησο και Κύθηρα εών φαίνεται να είναι ξεκυριστέλλει λίγο

Plate 4

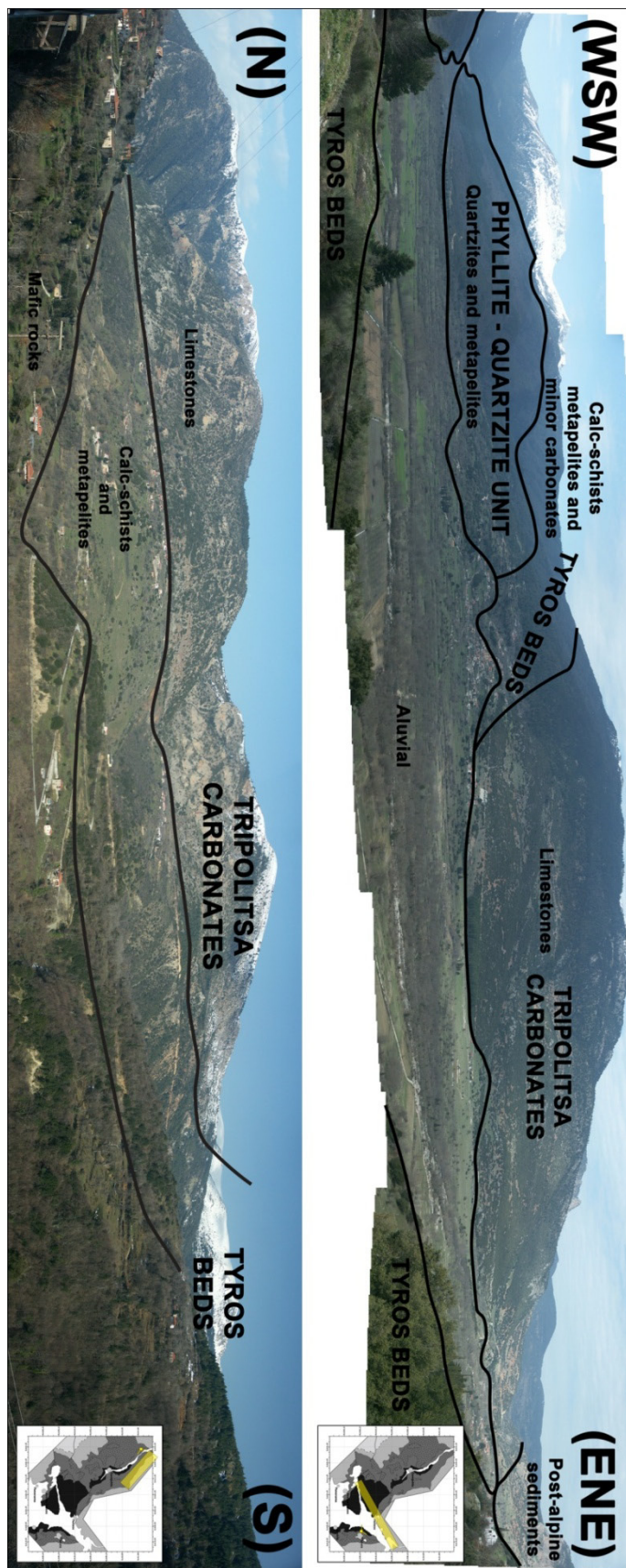


Plate 4. Panoramas of the rocks exposed near Feneos (above) and Zarouchia villages (below). Rock units are marked in upper case and rocktypes are marked in lower case letters. The position of the panorama and the field of view are marked in the small inset.

Εικ. 4. Πανοράματα κοντά στο χωρό Φενεός (πάνω) και Ζαρούχλα (κάτω). Οι γεωλογικές ενότητες σημειώνονται με κεφαλαία γράμματα και οι διάφοροι τύποι πετρωμάτων με μικρά γράμματα. Η θέση φωτογράφησης και το εύρος πεδίου σημειώνονται στα μικρά ένθετα.

Plate 5

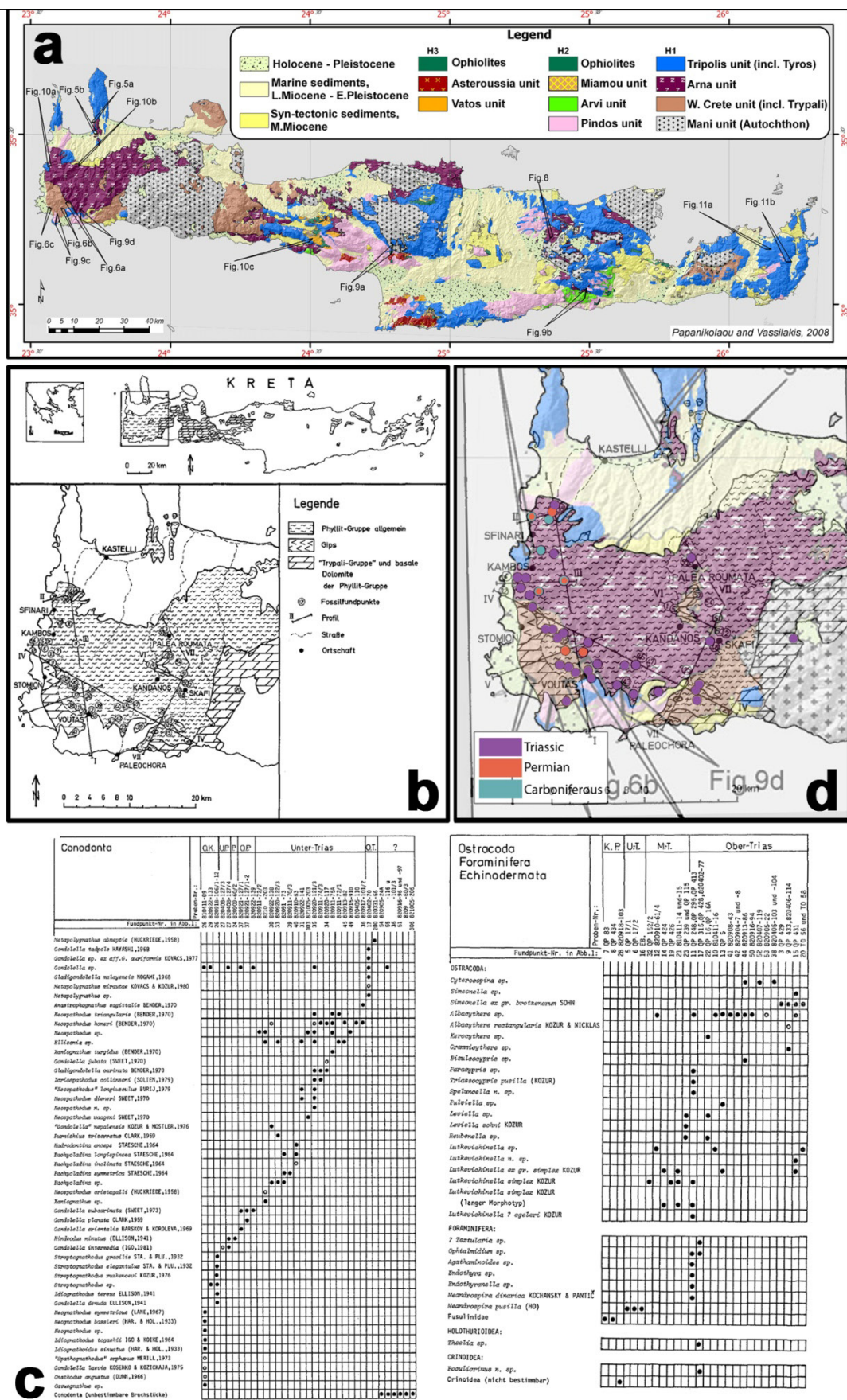


Plate 5. Data relatively to the age of the protolith of the Phyllite – Quartzite unit. (a) Revised stratigraphy of Crete (from Papanikolaou and Vassilakis [2010]). (b) Geological map and sampling places of western Crete (from Krah et al. [1983]). (c) Datablales with ages (conodonts and microfauna) corresponding to the sampling location of the figure “b” (from Krah et al. [1983]). (d) Overlay of the figures “a” and “b” where the age of the protolith of rocks corresponding to the Phyllite – Quartzite unit is shown to be between Upper? Carboniferous and Middle Triassic. Note that according to figure “b” the Phyllite – Quartzite unit includes sedimentary series that latter included in the “Western Crete” unit.

Εικ. 5. Δεδομένα σημεικά με την θητεία του πρωτόλιθους της ενότητας των Φυλλιών - Χαλαζίων. (a) Η αναθεωρημένη στρωματογραφία της Κρήτης (από Papapetrou and Vassilakis [2010]). (b) Γεωλογικός χάρτης και σημεία δενιματοληψίας από τη δυτική Κρήτη (από Krahel et al. [1983]). (c) Πινακες ηλικιών (από κονοδοντά και μικροπολιθώματα) για τα σημεία δενιματοληψίας της εικόνας "η" (από Krahel et al. [1983]). (d) Επικάλυψη των εικόνων "α" και "η" όπου φαίνεται η ηλικία απόθεσης του πρωτόλιθου της ενότητας των Φυλλιών - Χαλαζίων να είναι μεταξύ Ανώτερου, Λιθανθρακοφόρου και Μέσου Τρισδικού. Σημειώνεται πως η ενότητα των Φυλλιών - Χαλαζίων, σύμφωνα με την εικόνα "η", περιλαμβάνει δημιατοληψείς ακολουθίες που αριστερά ευάλωθικαν στη βάση της ενότητας της "Δυτικής Κρήτης".

REFERENCES (#246)

Altherr, R., Schliestedt, M., Okrusch, M., Seidel, E., Kreuzer, H., Harre, W., Lenz, H., Wendt, I., Wagner, G.A., 1979. Geochronology of high-pressure rocks on Sifnos (Cyclades, Greece). *Contrib Mineral Petrol* 70, 245–255.

Anders, B., Reischmann, T., Kostopoulos, D., Poller, U., 2006. The oldest rocks of Greece: first evidence for a Precambrian terrane within the Pelagonian Zone. *Geological Magazine* 143, 41–58.

Anders, B., Reischmann, T., Kostopoulos, D., 2007. Zircon geochronology of basement rocks from the Pelagonian Zone, Greece: constraints on the pre-Alpine evolution of the westernmost Internal Hellenides. *International Journal of Earth Sciences (Geol Rundsch)* 96, 639–661.

Andersen, T., 2005. Detrital zircons as tracers of sedimentary provenance: limiting conditions from statistics and numerical simulation. *Chemical Geology* 216, 249–270.

Andriessen, P., Boelrijk, N., Hebeba, E., Priem, N., Verdurnen, E., Verschure, R., 1979. Dating the events of metamorphism and granitic magmatism in the alpine orogen of Naxos (Cyclades, Greece). *Contribution to Mineralogy and Petrology* 69, 215–225.

Andriessen, P.A.M., Banga, G., Hebeda, E.H., 1987. Isotopic age study of pre-Alpine rocks in the basal units on Naxos, Sikinos and Ios, Greek Cyclades. *Geologie en Mijnbouw*, 66, 3–14.

Armijo, R., Meyer, B., King, G. C. P., Rigo, A., Papanastassiou, D., 1996. Quaternary evolution of the Corinth Rift and its implications for the Late Cenozoic evolution of the Aegean. *Geophys. J. Int.* (1996) 126, 11–53.

Aubouin, J., 1959. Contribution a l'étude géologique de la Grèce septentrionale: Les confins de l'Epire et de la Thessalie. *Annales Géologiques des Pays Helléniques* 10, 1–483.

Avigad, D., Kolodner, K., McWilliams, M., Persing, H., Weissbrod, T., 2003. Origin of northern Gondwana Cambrian sandstone revealed by detrital zircon SHRIMP dating. *Geology* 31, 227–230.

Baltatzis, E.G., Katagas, C.G., 1984. The pumpellyite-actinolite and contiguous facies in part of the Phyllite-Quartzite Series, central Northern Peloponnesus, Greece. *J. Metamorphic Geol.* 2, 349–363.

Barovich, K., Hand, M., 2008. Tectonic setting and provenance of the Paleoproterozoic Willyama Supergroup, Curnamona Province, Australia: Geochemical and Nd isotopic constraints on contrasting source terrain components. *Precambrian Research* 166, 318–337.

Barr, S.M., Davis, D.W., Kamo, S., White, C.E., 2003. Significance of U–Pb detrital zircon ages in quartzite from peri Gondwanan terranes, New Brunswick and Nova Scotia, Canada. *Precambrian Res.* 126, 123–145.

Bingen, B., Birkeland, A., Nordgulen, a., Sigmond, E.M.O., 2001. Correlation of supracrustal sequences and origin of terranes in the Sveconorwegian orogen of SW Scandinavia: SIMS data on zircon in clastic metasediments. *Precambrian Res.* 108, 293–318.

Blumör, T., 1998. Die Phyllit-Quarzit-Serie SE-Lakoniens (Peloponnes, Griechenland): Hochdruckmetamorphe in einem orogenen Keil: Frankfurter geowiss. Arb. Serie A, v. Bd. 17: Frankfurter, 187 p.

Blumör, T., Dollinger, J., Knobel, M., Mutter, A., Zarda, S., Kowalczyk, G., 1994. Plattenkalk series and Kastania Phyllites of the Taygetos Mts, new results on structure and succession. *Bull. Geol. Soc. Greece* XXX (2), 83–92.

Bonneau, M., 1982. Evolution géodynamique de l'arc égéen depuis le Jurassique supérieur jusqu'au Miocène. *Bull. Soc. géol. France.* (7), t. XXIV, no2, 229–242.

Brauer, R., Ittner, R., Kowalczyk, G., 1980. Ergebnisse aus der "Phyllit-Serie" SE-Lakoniens. *N. Jb. Geol. Palaont. Mh.* 3, 129–144.

Brichau, S., Ring, U., Ketcham, R.A., Carter, A., Stockli, D., Brunel, M., 2005. Constraining the long-term evolution of the slip rate for a major extensional fault system in the central Aegean, Greece, using thermochronology. *Earth and Planetary Science Letters* 241, 293–306.

Brichau, S., Ring, U., Carter, A., Bolhar, R., Monie, P., Stockli, D., Brunel, M., 2008. Timing, slip rate, displacement and cooling history of the Mykonos detachment footwall, Cyclades, Greece, and implications for the opening of the Aegean Sea basin. *Geol Soc Lond* 165, 263–277. doi:10.1144/0016-76492006-145.

Brix, M., Stockhert, B., Seidel, E., Theye, T., Thomson, S., Kuster, M., 2002. Thermobarometric data from a fossil zircon partial annealing zone in high pressure–low temperature rocks of eastern and central Crete, Greece. *Tectonophysics* 349, 309–326.

Brun, J.-P., Sokoutis, D., 2007. Kinematics of Southern Rhodope core complex (North Greece). *International Journal of Earth Sciences (Geol. Rundsch.)* 96, 1079–1099.

Brun, J.-P., Faccenna, C., 2008. Exhumation of high-pressure rocks driven by slab rollback. *Earth and Planetary Science Letters* 272, 1–7.

Burg, J.-P., Brunel, M., Gapais, D., Chen, G., Liu, G.H., 1984. Deformation of leucogranites of the crystalline Main Central Sheet in southern Tibet (China). *J. Struct. Geol.* 6, 535–542.

Carrigan, C.W., Mukasa, S.B., Haydoutov, I., Kolcheva, K., 2006. Neoproterozoic magmatism and Carboniferous high-grade metamorphism in the Sredna Gora Zone, Bulgaria: an extension of the Gondwana-derived Avalonian–Cadmian belt? *Precambrian Research* 147, 404–416.

Cherniak, D.J., and Watson, E.B., 2001. Pb diffusion in zircon: Chemical Geology, v.172, p. 5-24.

Cherniak, D.J., Watson, E.B., Grove, M., and Harrison, T.M., 2004. Pb diffusion in monazite: A combined RBS/SIMS study: *Geochimica et Cosmochimica Acta*, v. 68, p. 829–840.

Chéry, J., 2001. Core complex mechanics: from the Gulf of Corinth to the Snake Range. *Geology* 29 (5), 439–442.

Connolly, J.A.D., 2005. Computation of phase equilibria by linear programming: a tool for geodynamic modeling and its application to subduction zone decarbonation. *Earth Planet. Sci. Lett.* 236, 524–541.

Corfu, F., Noble, S.R., 1992. Genesis of the southern Abitibi greenstone belt, Superior Province, Canada: evidence from zircon Hf isotope analysis using a single filament technique. *Geochim Cosmochim Acta* 56, 2081–2097.

Creutzburg, N., 1958. Probleme des Gebirgsbaues und der Morphogenese auf der Insel Kreta. *Freib. Univ. N. F. H.* 26, 5–47.

Creutzburg, N., Seidel, E., 1975. Zum stand ber Geologie des Praneogens auf Kreta. *N. Palaont. Abh.* 149, 363–383.

Creutzburg, N. et al., 1977. General geological map of Crete (scale 1:200,000). I.G.M.E., Athens.

Cullers, R.L., Podkovyrov, V.N., 2002. The source and origin of terrigenous sedimentary rocks in the Mesoproterozoic Ural group, southeastern Russia. *Precamb. Res.* 117, 157–183.

Dalziel, I.W.D., 1992. On the organization of American plates in the Neoproterozoic and the breakout of Laurentia. *GSA Today* 2, 237–241.

Dalziel, I.W.D., 1997. Neoproterozoic–Paleozoic geography and tectonics: review, hypothesis, environmental speculation. *Geological Society of America Bulletin* 109, 16–42.

Danamos, G.D., 1991. The presence of the "Tyros beds" formation at Kythira Island. – *Bull. Geol. Soc. Greece*, 25/1, 399–404.

Davis, D.W., 2002. U–Pb geochronology of Archaean metasedimentary rocks in the Pontiac and Abitibi subprovinces, Quebec, constraints on timing, provenance and regional tectonics. *Precambrian Res.* 115, 97–117.

De Martini, P.M., Pantosti, D., Palyvos, N., Lemeille, F., McNeill, L., Collier, R., 2004. Slip rates of the Aigion and Eliki Faults from uplifted marine terraces, Corinth Gulf, Greece. *C. R. Geoscience* 336, 325–334.

De Wever, P., 1975. Etude géologique de séries apparaissant en fenêtre sous l'allochthon pindique (série de Tripolitsa, série épimetamorphique de Zaroukla) Péloponnèse septentrional, Grèce. These 3ème cycle: 318p Lille.

DeCelles, P.G., Gehrels, G.E., Najman, Y., Martin, A.J., Carter, A., Garzanti, E., 2004. Detrital geochronology and geochemistry of Cretaceous - Early Miocene strata of Nepal: Implications for timing and diachroneity of initial Himalayan orogenesis: Earth and Planetary Science Letters, 227, 313–330, doi: 10.1016/j.epsl.2004.08.019.

DeCelles, G.D., Carrapa, B., Gehrels, G., 2007. Detrital zircon U-Pb ages provide provenance and chronostratigraphic information from Eocene syn-orogenic deposits in northwestern Argentina: Geology, 35, 323–326, doi: 10.1130/G23322A.1.

Dercourt, J., 1964. Contribution à l'étude géologique d'un secteur du Péloponnèse septentrional. Annal. Geol. Pays Hell. 1^{er} série T. XV-1964.

Dewey, J.F., 1981. Episodicity, sequence and style at convergent plate boundaries. The Continental Crust and Its Mineral Deposits. Special Paper, vol. 20. Geological Association of Canada, pp. 553–572.

Dickinson, W.R., Gehrels, G.E., 2008. Sediment delivery to the Cordilleran foreland basin: Insights from U-Pb ages of detrital zircons in Upper Jurassic and Cretaceous strata of the Colorado Plateau: American Journal of Science 308, 1041–1082, doi: 10.2475/10.2008.01.

Dinter, D.A., Royden, L., 1993. Late Cenozoic extension in northeastern Greece: Strymon Valley detachment system and Rhodope metamorphic core complex. Geology 21, 45–48.

Doert, U., Kowalczyk, G., Kauffmann, G., Krahl, J., 1985. Zur stratigraphischen Einstufung der "Phyllit-Serie" von Krokee und der Halbinsel Xyli (Lakonien, Peloponnes). Erlanger geol. Abh., 112, 1–10.

Dornsiepen, U.F., Manutsoglu, M., 1996. Die Vulkanite der Tyros-Schichten Kretas und des Peloponnes - orogene Andesite oder anorogene Trapp-Basalte? Z. dt. geol. Ges. 147/1, 101–123.

Dubois, R., Bignot, T., 1979. Presence d'un "hardground" nummulitique au de la série crétacée d'Almyropotamos (Eubée méridionale, Grèce). Paris, Académie des Sciences Comptes Rendus 289, 993 – 995.

Dürr, St., 1985. Geological Map of Greece, 1:50 000. Amorgos-Donoussa Sheet. IGME, Athens.

Engel, M., Reischmann, T., 1999. Geochronology of the pre-alpine basement of the central Cyclades, Greece. J. Conf. Abs. 4, 805.

Engel, M., 2006. Geochemie, geochronologie und isotopie der grundgebirgsgneise und ausgewählter marmore der zentralen Kykladen, Griechenland. PhD thesis, Johannes Gutenberg-Universität, Mainz.

Epting, H., Kudrass, H.R., Leppig, U., Schafer, A., 1972. Geologie de Talea Ori Kreta. Neues Jb. Geol. Palaontol. Abh. 141, 259 – 285.

Fassoulas, C., Kilias, A., Mountrakis, D., 1994. Postnappe stacking extension and exhumation of HP/LT rocks in the island of Crete, Greece. Tectonics 13 (1), 127–138.

Faupl, P., Pavlopoulos, A., Klötzli, U., Petrakakis, K., 2006. On the provenance of mid-Cretaceous turbidites of the Pindos zone (Greece): implications from heavy mineral distribution, detrital zircon ages and chrome spinel chemistry. Geol. Mag. 143, 329–342.

Feldhoff, R.A., Löcke, A., Richter, D.K., 1991. Über die Diagenese-/Metamorphosebedingungen der Pindos- und Tripolitsa-Serie auf der Insel Kreta (Griechenland). Zbl. Geol. Palaont., Teil I, 1990 (11): 1611–1622, Stuttgart (Schweizerbart).

Fernández-Suárez, J., Gutiérrez-Alonso, G., Jenner, G.A., Tubrett, M.N., 2000. New ideas on the Proterozoic–early Paleozoic evolution of NW Iberia: insights from U–Pb detrital zircon ages. Precambrian Research 102, 185–206.

Fernández-Suárez, J., Gutiérrez Alonso, G., Cox, R., Jenner, G.A., 2002. Assembly of the Armorican microplate: a strike-slip terrane delivery? Evidence from U–Pb ages of detrital zircons. Journal of Geology 110, 619–626.

Frérière, J., Reynaud, J.Y., Pavlopoulos, A., Bonneau, M., Migiros, G., Chanier, 2004. Evolution géologique et contrôle géodynamiques d'un bassin intramontagneux cénozoïque: le bassin méso-hellénique, Grèce. Bull. Soc. Géol. Fr. 175:361–382. doi:10.2113/175.4.361

Finger, F., Krenn, E., Riegler, G., Romano, S., Zulauf, G., 2002. Resolving Cambrian, Carboniferous, Permian and Alpine monazite generations in the polymetamorphic basement of eastern Crete (Greece) by the electron microprobe. Terra Nova, 14, 233–240.

Fildani, A., Weislogel, A., McHargue, T., Tankard, A., Wooden, J., Hodgson, D., Flint, S., 2009. U-Pb zircon ages from the southwestern Karoo Basin, South Africa—Implications for the Permian-Triassic boundary: Geology, 37, 719–722, doi: 10.1130/G25685A.1.

Fleury, J.-J., 1980. Les zones de Gavrovo-Tripolitza et du Pinde-Olonos (Grèce continentale et Péloponnèse du Nord). Evolution d'une plate-forme et d'un bassin dans leur cadre alpin. Société Géologique du Nord. Publication N° 4.

Flotté, N., 2003. Caractérisation structurale et cinématique d'un rift sur détachement: Le rift de Corinthe- Patras, Grèce. Unpublished PhD thesis, 197 pp., Univ. Paris-Sud XI, Paris.

Flowerdew, M.J., Millar, I.L., Vaughan, A.P.M., Horstwood, M.S.A., Fanning, C.M., 2006. The source of granitic gneisses and migmatites in the Antarctic Peninsula: a combined U-Pb SHRIMP and laser ablation Hf isotope study of complex zircons. Contrib. Mineral. Petrol. 151, 751–768.

Floyd, P.A., Leveridge, B.E., 1987. Tectonic environment of the Devonian Gramscatho basin, south Cornwall: framework mode and geochemical evidence from turbiditic sandstones. Journal of the Geological Society, Londo 144, 531 – 542.

Förster, H.-J., Tischendorf, G., Trumbull, R.B., 1997. An evaluation of the Rb vs. (Y+Nb) discrimination diagram to infer tectonic setting of silicic igneous rocks. Lithos 40, 261 – 293.

Franz, L., 1992. Die polymetamorphe Entwicklung des Altkristallins auf Kreta und im Dodekanes (Griechenland): 389 p., Stuttgart (Enke).

Funiciello, F., Faccenna, C., Giardini, D., Regenauer-Lieb, K., 2003. Dynamics of retreating slabs: 2. Insights from three-dimensional laboratory experiments. Journal Geoph. Res. 108, B4, 2207, doi:10.1029/2001JB000896.

Fytikas, M., Innocenti, F., Manetti, P., Mazzuoli, R., Peccerillo, A., Villari, L., 1984. Tertiary to Quaternary evolution of volcanism in the Aegean region. In: Dixon EJ, Robertson AHF (eds) The geological evolution of the Eastern Mediterranean. Geol. Soc. Spec. Pb., vol 17. Geological Society, London, pp 687–699.

Fytrolakis, N., 1972. Die einwirkung gewisser orogener Bewegungen und die Gipsbildung in Osterkreta (prov. Sitia). Bull. Geol. Soc. Greece 9, 81–100.

Fytrolakis, N., 1980. The geological structure of Crete. Problems, Observations and Conclusions, NTUA, Athens, 146 pp.

Fytrolakis, N., Papanikolaou, D., Panagopoulos, A., 1981. Stratigraphy and structure of Amorgos Island, Aegean Sea. Annales Géologiques des Pays Helléniques 30, 455 – 472.

Garver, J.I., Scott, T.J., 1995. Trace elements in shale as indicators of crustal provenance and terrane accretion in the southern Canadian Cordillera. GSA Bulletin 107, 440 – 453.

Garver, J.I., Royce, P.R., Smick, T.A., 1996. Chromium and nickel in shale of the Taconic foreland: A case study for the provenance of fine-grained sediments with an ultramafic source. Journal of Sedimentary Research 66, 100 – 106.

Gautier, P., Brun, J.-P., 1994. Crustal-scale geometry and kinematics of late-orogenic extension in the central Aegean (Cyclades and Evvia Islands). Tectonophysics 238, 399–424.

Gebauer, D., Williams, I.S., Compston, W., Grünenfelder, M., 1989. The development of the Central European continental crust since the Early

Archean based on conventional and ion-microprobe dating of up to 3.84 b.y. old detrital zircons. *Tectonophysics* 157, 81–96.

Gerolymatos, I. 1993. Metamorphose und Tektonik der Phyllit-Quarzit-Serie und der Tyros-Schichten auf dem Peloponnes und Kythira, Freien Universität Berlin.

Gerya, T.V., Stöckert, B., Perchuk, A.L., 2002. Exhumation of high-pressure metamorphic rocks in a subduction channel: a numerical simulation. *Tectonics* 21, 1056, doi:10.1029/2002TC001406.

Ghisetti, F., Vezzani, L., 2004. Plio-Pleistocene sedimentation and fault segmentation in the Gulf of Corinth (Greece) controlled by inherited structural fabric. *C. R. Geoscience* 336, 243–249.

Ghizetti, F., Vezzani, L., 2005. Inherited structural controls on normal fault architecture in the Gulf of Corinth (Greece). *Tectonics*, vol.24, TC4016. doi:10.1029/2004TC001696.

Gleason, J.D., Patchett, P.J., Dickinson, W.R., Ruiz, J., 1995. Nd isotopic constraints on sediment sources of the Ouachita-Marathon fold belt: *Geological Society of America Bulletin* 107, 1192–1210.

Gonzalez-Alvarez, I., Kisiak, M.A., Kerrich, R., 2006. A trace element and chemical Th-U total Pb dating study in the lower Belt-Purcell Supergroup, Western North America: Provenance and diagenetic implications. *Chem. Geol.* 230, 140–160.

Goodge, J.W., Myrow, P., Williams, I.S., Bowring, S.A., 2002. Age and provenance of the Beardmore Group, Antarctica: constraints on Rodinia supercontinent breakup. *J. Geol.* 110, 393–406.

Green, T.H., Brunfelt, A.P., Heier, K.S., 1969. Rare earth element distribution in anorthosites and associated high grade metamorphic rocks, Lofoten Vesteraalen, Norway: *Earth and Planetary Science Letters* 7, 93–98.

Griffin, W.L., Belousova, E.A., Shee, S.R., Pearson, N.J., O'Reilly, S.Y., 2004. Archaean crustal evolution in the northern Yilgarn Craton: UPb and Hf-isotope evidence from detrital zircons. *Precambrian Res.* 131, 231–282.

Gutiérrez-Alonso, G., Fernández-Suárez, J., Collins, A.S., Abad, I., Nieto, F., 2005. Amazonian Mesoproterozoic basement in the core of the Ibero-Armorian Arc: 40Ar/39Ar detrital mica ages complement the zircon's tale. *Geology* 33, 637–640.

Haas, G.J.L.M., Andersen, T., Vestin, J., 1999. Detrital zircon geochronology: new evidence for an old model for accretion of the Southwest Baltic Shield. *J. Geol.* 107, 569–586.

Hall, R., Audley-Charles, M.G., Carter, D.J., 1984. The significance of Crete for the evolution of the Eastern Mediterranean. – In: Dixon, J.E. & Robertson, A.H.F.: The geological evolution of the Eastern Mediterranean. – *Geol. Soc. London, Spec. Publ.*, 17, 499–516, London (Geol. Soc. London).

Hartmann, L.A., Santos, J.O.S., 2004. Predominance of high Th/U, magmatic zircon in Brazilian Shield sandstones. *Geology* 32, 73–76.

Haude, G. 1989. Geologie der Phyllit-Einheit im Gebiet um Paleastro (Nordost-Kreta, Griechenland). – Ph.D. thesis Techn. Univ. Munich: 131 p., Munich.

Henjes-Kunst, F., Kreuzer, H., 1982. Isotopic dating of pre-Alpine rocks from the island of Ios (Cyclades, Greece). *Contributions to Mineralogy and Petrology*, 80, 245–253.

Herron, M.M., 1988. Geochemical classification of terrigenous sands and shales from core or log data. *Journal of sedimentary petrology* 58, 820 – 829.

Himmerkus, F., Reischmann, T., Kostopoulos, D., 2006a. Late Proterozoic and Silurian basement units within the Serbo Macedonian Massif, northern Greece: the significance of terrane accretion in the Hellenides. In: Robertson, A.H.F., Mountrakis, D. (Eds.), *Tectonic Development of the Eastern Mediterranean Region*. Spec. Geological Society, London, Special Publications, vol. 260, pp. 35–50.

Holland, T.J.B., Powell, R., 1998. An internally consistent thermodynamic data set for phases of petrological interest. *J. metamorph Geol* 16, 309–343.

IGME 1963. Geological Map of Greece, 1:50 000. Lefkas Sheet. Mapping by I. Bornovas.

IGME 1982. Geological Map of Greece, 1:50 000. Kandila Sheet. Mapping by P. De Wever and J. Dercourt.

Jackson, S.E., Pearson, N.J., Griffin, W.L., 2004. The application of laser ablation-inductively coupled plasma-mass spectrometry to in situ U-Pb zircon geochronology. *Chem. Geol.* 211, 47–69.

Jacobshagen V., Richter D., Makris J., 1978. Alpidic development of the Peloponnesus, in Closs, H., Roeder, D. and Schmidt, H., eds., *Alps, Appennines, Hellenides*: Stuttgart, E. Schweizerbart'sche Verlagsbuchhandlung, p. 415–423.

Jacobshagen, V., 1986. *Geologie von Griechenland*. Berlin, Gebruder Borntraeger.

Jahn, B.M., 2000. Sm-Nd isotope tracer study of UHP metamorphic rocks: Implications for continental subduction and collisional tectonics, in Ernst, W.G., and Liou, J.G., eds., *Ultra-High Pressure Metamorphism and Geodynamics in Collision-Type Orogenic Belts; Final Report of the Task Group III-6 of the International Lithosphere Project*: Columbia, Bellwether Publishing, p. 245–271.

Jolivet, L., Daniel, J.M., Truffert, C., Goffe, B., 1994. Exhumation of deep crustal metamorphic rocks and crustal extension in arc and back-arc regions. *Lithos* 33, 3–30.

Jolivet, L., Goffe, B., Monie, P., Truffert-Luxey, C., Patriat, M., Bonneau, M., 1996. Miocene detachment in Crete and exhumation P-T-t paths of high-pressure metamorphic rocks. *Tectonics* 15, 1129 – 1153.

Jolivet, L., Faccenna, C., Goffé, B., Burov, E., Agard, P., 2003. Subduction tectonics and exhumation of high-pressure metamorphic rocks in the Mediterranean orogens. *Am J Sci* 303, 353–409.

Jolivet, L., Rimmelé, G., Oberhansli, R., Goffé, B., Candan, O., 2004. Correlation of syn-orogenic tectonic and metamorphic events in the Cyclades, the Lycian Nappes and the Menderes massif, geodynamic implications. *Bull Soc Geol Fr* 175, 217–238.

Jolivet, L., Brun, J.-P., 2010. Cenozoic geodynamic evolution of the Aegean. *Int J Earth Sci (Geol Rundsch)* 99, 109–138.

Jolivet, L., Trotet, F., Monie, P., Vidal, O., Goffe, B., Labrousse, L., Agard, P., Ghorbal, Bad'r, 2010. Along-strike variations of P-T conditions in accretionary wedges and syn-orogenic extension, the HP-LT Phyllite-Quartzite Nappe in Crete and the Peloponnes. *Tectonophysics* 480, 133–148.

Karakitsios, V., 1979. Contribution a l'étude géologique des Hellenides: Étude de la région de Selvia (Crète moyenne-occidentale, Grèce). Les relations lithostratigraphiques et structurales entre la série des Phyllades et la série de Tripolitza: These, 3ème cycle thesis, University Pierre et Marie Curie, Paris.

Karakitsios, V., 1986. Les relations lithostratigraphiques, métamorphiques et structurales entre les phyllades et la série carbonatée de Tripolitza (Crète moyenne – occidentale, Grèce). *Bull. Geol. Soc. Greece*, XXIII, 31–58.

Katagas, C., Tsolis-Katagas, P., Baltatzis, E., 1991. Chemical mineralogy and illite crystallinity in low grade metasediments, Zarouchla Group, Northern Peloponnesus, Greece. *Mineralogy and Petrology* 44, 57 – 71.

Katsikatos, G., Migiros, G., Trianaphyllidis, M., Mettos, A., 1986. Geological structure of internal Hellenides (E. Thessaly-SW. Macedonia, Euboë-Attica-Northern Cyclades islands and Lesvos). *IGME Geological & Geographical Research*, special issue, 191–212.

Keay, S., Lister, G. & Buick, I., 2001. The timing of partial melting, Barrovian metamorphism and granite intrusion in the Naxos metamorphic core complex, Cyclades, Aegean Sea, Greece. *Tectonophysics*, 342, 275–312.

Keay, S., Lister, G., 2002. African provenance for the metasediments and metagneous rocks of the Cyclades, Aegean Sea, Greece. *Geology* 30, 235–238.

Kissel, C., Laj, C., Mialler, C., 1985. Tertiary geodynamical evolution of northwestern Greece: paleomagnetic results. *Earth and Planetary Science Letters* 72, 190-204.

Klein, T., Zulauf, G., Craddock, J. & Heidelbach, F., 2004. Metamorphic Tripolitsa rocks on top of non-metamorphic sediments: consequences for the geological evolution of Crete. – Abstr. 10th Congress Geol. Soc. Greece: 451 p.

Knudsen, T.-L., Andersen, T., Whitehouse, M.J., Vestin, J., 1997. Detrital zircon ages from southern Norway—implications for the Proterozoic evolution of the southwestern part of the Baltic Shield. *Contrib. Mineral. Petrol.* 130, 47-58.

Kock, S., Martini, R., Reischmann, T., Stampfli, G.M., 2007. Detrital zircon and micropalaeontological ages as new constraints for the lowermost tectonic unit (Talea Ori unit) of Crete, Greece. *Palaeogeography, Palaeoclimatology, Palaeoecology* 243, 307-321.

Koglin, N., 2008. Geochemistry, petrogenesis and tectonic setting of ophiolites and mafic-ultramafic complexes in the Northeastern Aegean Region: New trace-element, isotopic and age constraints. PhD thesis. Johannes Gutenberg-Universität, Mainz.

Kolodner, K., Avigad, D., McWilliams, M., Wooden, J.L., Weissbrod, T., Feinstein, S., 2006. Provenance of north Gondwana Cambrian-Ordovician sandstone: U-Pb SHRIMP dating of detrital zircons from Israel and Jordan. *Geological Magazine* 143, 367-391.

Kopp, K., Ott, E., 1977. Spezialkartierungen im Umkreis neuer Fossilfunde in Tripali und Tripolitzakalken Westkretas. *N. Jb. Geol. Palaont. Mh.* 4, 217-238.

Kostopoulos, D., 1988. Geochemistry, petrogenesis and tectonic setting of the Pindos ophiolite, NW Greece. PhD theis, Newcastle University, England.

Kostopoulos, D., Brun, J.-P., 2011. Exhuming Rhodopean diamonds. To be submitted to *Geology*.

Kowalczyk, G., Dittmar, U., 1991. The metamorphic underlying the Plattenkalk carbonates in the Taygetos Mts (Southern Peloponnese). *Bull. Geol. Soc. Greece* XXV(1), 455-467.

Kozur, H., Krahl, J. 1987, Erster Nachweis von Radiolarien im tethyalen Perm Europas. – *N. Jb. Geol. Paläont. Abh.*, 174: 357-372, Stuttgart (Schweizerbart).

Krahl, J., Kauffmann, G., Kozur, H., Richter, D., Förster, O., Heinrich, F., 1983. Neue Daten zur Biostratigraphie und zur tektonischen Lagerung der Phyllit-Gruppe und der Trypali-Gruppe auf der Insel Kreta (Griechenland). *Geol. Rund.*, 72(3), 1147-1166.

Krahl, J., Kauffmann, G., Richter, D., Kozur, H., Möller, I., Förster, O., Heinrich, F., Dornspiepen, U., 1986. Neue Fossilfunde in der Phyllit-Gruppe Ostkretas (Griechenland). – *Z. dt. geol. Ges.*, 137: 523-536, Hannover (Dt. Geol. Ges.).

Kröner, A., Şengör, A.M.C., 1990. Archean and Proterozoic ancestry in late Precambrian and early Paleozoic crustal elements in southern Turkey as revealed by singlezircon dating. *Geology* 18, 1186-1190.

Kröner, A., Stern, R.J., 2004. Pan-African orogeny. *Encyclopedia of Geology*, Vol.1, Elsevier, Amsterdam.

Ktenas, C., 1924. Formations primaires semimetamorphiques au Peloponnes central. – *CR Sommaire, Soc. Geol. France* 24, 1-63.

Le Pichon, X., Lallemand, S., Chamot-Rooke, N., Lemeur, D., Pascal, G., 2002. The Mediterranean Ridge backstop and the Hellenic nappes. In: Westbrook, G.K., Reston, T.J. (Eds.), *The Accretionary Complex of the Mediterranean Ridge; Tectonics, Fluid Flow, and the Formation of Brine Lakes*. *Marine Geology* 186, 111-125.

Lekkas, S., Ioakim, C., 1980. Donnees nouvelles sur l'age des phyllades en Peloponnes (Greece). *Prakt. Acad. Athens*, 55, 350-361.

Lekkas, S., Papanikolaou, D., 1977. On the phyllite problem in Peloponnesus. *Ann Geol Pays Hellen* 29, 395-410.

Lati, A., Skarpelis, N., Pe-Piper, G., 2009. Deciphering the time of igneous activity in the Lavrion ore province, Attica, Greece: Manifestation of Late Miocene and Triassic magmatism. *Geol. Mag.* 146 (5), 2009, pp. 732-742.

Lahtinen, R., Huhma, H., Kouse, J., 2002. Contrasting source components of the Paleoproterozoic Svecofennian metasediments: detrital zircon U-Pb, Sm Nd and geochemical data. *Precamb. Res.* 116, 81-109.

Li, Q., Shuwen, L., Baofu, H., Zhang, J., Zhuyin, C., 2005. Geochemistry of metasedimentary rocks of the Proterozoic Xingxingxia Complex; implications for provenance and tectonic setting of the eastern segment of the central Tianshan tectonic zone, northwestern China. *Can. J. Earth Sci.* 42, 287-306.

Lister, G.S., Banga, G., Feenstra, A., 1984. Metamorphic core complexes of Cordilleran type in the Cyclades, Aegean Sea, Greece. *Geology* 12, 221-225.

Lode, S., Romer, T., Vols, S., Xypolias, P., Zulauf, G., 2008. The pre-Alpine basement rocks of Kythira (Greece). *Z. dt. Ges. Geowiss.*, 159/3, p. 457-468.

Loos, S., Reischmann, T., 1999. The evolution of the southern Menderes Massif in SW Turkey as revealed by zircon dating. *Journal of the Geological Society (London)* 156, 1021-1030.

Lopez, J.M.G., Bauluz, B., Fernandez-Neiot, C., Oliete, A.Y., 2005. Factors controlling the trace-element distribution in fine-grained rocks: the Albian kaolinite rich deposits of the Oliete Basin (NE Spain). *Chem. Geol.* 214, 1-19.

Ludwig, K.R., 2001. Isoplot v. 2.2—a geochronological toolkit for Microsoft Excel. Berkeley Geochronology Center, Special Publication No. 1a, 53 pp.

Marsellos, A.E., Kidd, W.S.F., Garver, J.I., 2010. Extension and exhumation of the HP/LT rocks in the Hellenic forearc ridge. *American Journal of Science*, Vol. 310, 1-36.

McLennan, S.M., 1989. Rare earth elements in sedimentary rocks: Influence of provenance and sedimentary processes, in Lipin, B.R., and McKay, G.A., eds., *Geochemistry and mineralogy of the rare earth elements: Mineralogical Society of America Reviews in Mineralogy*, v. 21, p. 169-200.

McLennan, S.M., Hemming, S., McDaniel, D.K., Hanson, G.N., 1993. Geochemical approaches to sedimentation, provenance, and tectonics. *Geol. Soc. Am. Spec. Paper* 283, 21-39.

McLennan, S.M., Hemming, S.R., Taylor, S.R., Eriksson, K.A., 1995. Early Proterozoic crustal evolution—geochemical and Nd-Pb isotopic evidence from metasedimentary rocks, southwestern North America. *Geochim. Cosmochim. Acta* 59, 1153-1177.

McNeil, L.C., Cotterill, C.J., Henstock, T.J., Bull, J.M., Stefatos, A., Collier, R.E., Papatheodorou, G., Ferentinos, G., Hicks, S.E., 2005. Active faulting within the offshore western Gulf of Corinth, Greece: Implications for models of continental rift deformation. *Geology*, v. 33, no. 4, p. 241-244.

Meinhold, G., Kostopoulos, D., Reischmann, T., 2007. Geochemical constraints on the provenance and depositional setting of sedimentary rocks from the islands of Chios, Inousses and Psara, Aegean Sea, Greece: implications for the evolution of Palaeotethys. *Journal of the Geological Society of London* 164, 1145-1163.

Meinhold, G., Anders, B., Kostopoulos, D., Reischmann, T., 2008a. Rutile chemistry and thermometry as provenance indicator: an example from Chios Island, Greece. *Sedimentary Geology* 203, 98-111.

Meinhold, G., Reischmann, T., Kostopoulos, D., Lehnert, O., Matukov, D., Sergeev, S., 2008b. Provenance of sediments during subduction of Palaeotethys: detrital zircon ages and olistolith analysis in Palaeozoic sediments from Chios Island, Greece. *Palaeogeography, Palaeoclimatology, Palaeoecology* 263, 71-91.

Meinhold, G., Frei, D., 2008. Detrital zircon ages from the islands of Inousses and Psara, Aegean Sea, Greece: constraints on depositional age and provenance. *Geological Magazine* 145, 886-891.

Meinhold, G., Kostopoulos, D., Reischmann, T., Frei, D. BouDagher-Fadel, M.K., 2009. Geochemistry, provenance and stratigraphic age of metasedimentary rocks from the eastern Vardar suture zone, northern Greece. *Palaeogeography, Palaeoclimatology, Palaeoecology* 277, 199–225.

Meinhold, G., Reischmann, T., Kostopoulos, D., Frei, D., Larionov, A.N., 2010. Mineral chemical and geochronological constraints on the age and provenance of the eastern Circum-Rhodope Belt low-grade metasedimentary rocks, NE Greece. *Sedimentary Geology* 229, 207–223.

Moix, P., Beccaletto, L., Kozur, H.W., Hochard, C., Rosselet, F., Stampfli, G.M., 2008. A new classification of the Turkish terranes and sutures and its implication for the paleotectonic history of the region. *Tectonophysics* 451, 7–39.

Moretti, I., Sakellariou, D., Lykousis, V., Micarelli, L., 2003. The Gulf of Corinth: An active half graben? *J. Geodyn.* 36, 323–340.

Moretti, I., Lykousis, V., Sakellariou, D., Reynaud, J.-Y., Benziane, B., Prinzhofer, A., 2004. Sedimentation and subsidence rate in the Gulf of Corinth: what we learn from the Marion Dufresne's long-piston coring. *C. R. Geoscience* 336, 291–299.

Morton, A.C., Claoué-Long, J.C., Berge, C., 1996. SHRIMP constraints on sediment provenance and transport history in the Mesozoic Statfjord Formation, North Sea. *Journal of the Geological Society, London* 153, 915–929.

Ori, G.G., 1989. Geologic history of the extensional basin of the Gulf of Corinth (Miocene-Pleistocene), Greece. *Geology* 1, 918–921.

Papanikolaou, D., Skarvelis, N., 1986. The blueschists in the external metamorphic belt of the Hellenides: composition, structure and geotectonic significance of the Arna Unit. *Ann. Geol. Pays Hell.*, 33/2, 47–68.

Papanikolaou, D., 1988. Introduction to the geology of Crete. IGCP No 276, 1st Field Meeting 1988, Chania, Fieldguide Book, 36 pp.

Papanikolaou, D., 1989. Are the Medial Crystalline Massifs of the Eastern Mediterranean drifted Gondwanan fragments? *Geol. Soc. Greece, Spec. Publ.*, 1, 63–90.

Papanikolaou, D., 1993. Geodynamic evolution of the Aegean. *Bull. Geol. Soc. Greece*, XXVIII, 1, 33–48.

Papanikolaou, D., Bargathi, H., Dabovski, C., Dimitriou, R., El-Hawat, A., Ioane, D., Kranis, H., Obeidi, A., Oaie, G., Seghedi, A., and Zagorchev, I., 2004. Transect VII: East European Craton-Scythian Platform-Dobrogea Balcanides-Rhodope Massif-Hellenides-East Mediterranean-Cyrenaica. In: The TRANSMED atlas: The Mediterranean region from crust to mantle: Geological and geophysical framework of the Mediterranean and the surrounding areas: 32nd International congress, Florence, August 2004. Springer.

Papanikolaou, D., Alexandri, M., Nomikou, P., 2006. Active faulting in the North Aegean basin. In: Dilek, Y., Pavlides, S., (Eds.), Postcollisional Tectonics and Magmatism in the Mediterranean Region and Asia. Geological Society of America Special Paper 409, pp. 189–209, Doi:10.1130/2006.2409 (11).

Papanikolaou, D., Royden, L., 2007. Disruption of the Hellenic arc: Late Miocene extensional detachment faults and steep Pliocene-Quaternary normal faults—Or what happened at Corinth?. *Tectonics* 26, TC5003, doi:10.1029/2006TC002007.

Papanikolaou, D., Vassilakis, E., 2008. Middle Miocene E-W tectonic horst structure of Crete through extensional detachment faults. Donald D Harrington Symposium on the Geology of the Aegean. IOP Conf. Series: Earth and Environmental Science 2 (2008) 012003 doi:10.1088/1755-1307/2/1/012003.

Papanikolaou, D., Vassilakis, E., 2010. Thrust faults and extensional detachment faults in Cretan tectono-stratigraphy: Implications for Middle Miocene extension. *Tectonophysics* 488, 233–247.

Papanikolaou, D., 2009. Timing of tectonic emplacement of the ophiolites and terrane paleogeography in the Hellenides. *Lithos*, 108, 262–280.

Papanikolaou, D., Gouliotis, L., Trianaphyllou, M., 2009. The Itea-Amfissa detachment: a pre-Corinth rift Miocene extensional structure in central Greece. *Geological Society, London, Special Publications*, 311, 293 – 310.

Papastamatiou, J., Reichel, M., 1956. Sur l' age des phyllades de l' île de Crète. *Ecl. Geol. Helv.* 49, 147.

Pe-Piper, 1983. The Triassic Volcanic Rocks of Tyros, Zarouhla, Kalamae, and Epidavros, Peloponnese, Greece. *Schweiz. Mineral. Petrogr. Mitt.* 63, 249 – 266.

Pe-Piper, G., Piper, D.J.W., 2002. The igneous rocks of Greece. The anatomy of an orogen. Berlin/Stuttgart: Gebrüder Borntraeger, 573pp.

Pe-Piper, G., Piper, D.J.W., 2006. Unique features of the Cenozoic igneous rocks of Greece. In: Dilek Y., Pavlides S. (eds) Postcollisional tectonics and magmatism in the Mediterranean region and Asia, doi:210.1130/2006.2409(1114), Geological Society of America, pp 259–282.

Pearce, A.J., Harris, N.B., Tindle, A.G., 1984. Trace Element Discrimination Diagrams for the Tectonic Interpretation of Granitic Rocks. *Journal of Petrology* 25, 956–983.

Philippon, M., 2010. Déformation des unités métamorphiques de haute pression de la subduction à l'exhumation. PhD thesis. Université de Rennes1.

Psionis K.Th., 1981. About the presence of Permian (?) – Lower Triassic beds as a basement of the Plattenkalk series in the Taygetos Mt. Description of a continuous section. *Ann. Geol. Pays. Hell.*, 30, 578–587.

Pupin, J.P., Turco, G., 1972. Le zircon accessoire en géothermométrie. *C R Acad Sci Paris* 274 [D]:2121–2124.

Pupin, J.P., 1980. Zircon and Granite Petrology. *Contrib. Mineral. Petrol.* 73, 207 – 220.

Rahl, J.M., Reiners, P.W., Campbell, I.H., Niculescu, S., Allen, C.M., 2003. Combined single-grain (U-Th)/He and U/Pb dating of detrital zircons from the Navajo Sandstone, Utah: *Geology*, 31, 761–764, doi: 10.1130/G19653.1.

Rahl, J.M., Anderson, K.M., Brandon, M.T., Fassoulas, C., 2005. Raman spectroscopic carbonaceous material thermometry of low-grade metamorphic rocks: calibration and application to tectonic exhumation in Crete, Greece. – *Earth Planetary Sci. Lett.*, 240, 339–354.

Reischmann, T., Kostopoulos, D., 2002. Timing of UHPM in metasediments from the Rhodope Massif, N. Greece. *Geochim. Cosmochim. Acta* 66 Suppl. 1, A633.

Renz, C., 1955. Die vorneogene Stratigraphic der normal sedimentären Formationen Griechenlands. *IGSR* 637 p. Athen.

Ring, U., Brandon, M.T., Willett, S.D., Lister, G.S., 1999. Exhumation processes: normal faulting, ductile flow and erosion. In: Ring, U., Brandon, M.T., Willett, S.D., Lister, G.S. (Eds.), *The Geological Society of London, Special Publication*, vol. 154, pp. 1–27.

Rohais, S., Joannin, S., Colin, J.P., Suc, J.P., Guillocheau, F., Eschard, R., 2007. Age and environmental evolution of the syn-rift fill of the southern coast of the Gulf of Corinth (Akrata-Derveni region, Greece). *Bull Soc Geol Fr* 178, 231–243.

Romano, S.S., Dörr, W., Zulauf, G., 2004. Cambrian granitoids in pre-Alpine basement of Crete (Greece), evidence from U–Pb dating of zircon. *Int. J. Earth Sci. (Geol. Rundsch.)* 93, 844–859.

Romano, S.S., Brix, M., Dörr, W., Krenn, E., Zulauf, G., 2005. The evolution of the Cretan pre-Alpine basement. In: Freiwald, A., Röhling, H.-G., Löffler, S.-B. (Eds.), *GeoErlangen 2005. System Erde – Biosphäre Coupling. Regional Geology of Central Europe. Program and Abstracts. Schriftenreihe der Deutschen Gesellschaft für Geowissenschaften*, vol. 39, p. 317.

Romano, S.S., Brix, M., Dörr, W., Fiala, J., Krenn, E., Zulauf, G., 2006. The Carboniferous to Jurassic evolution of the pre-Alpine basement of Crete: constraints from radiometric dating of orthogneiss, fission-track

dating of zircon and structural/petrological data. *J. Geol. Soc. London, Spec. Publ.*, 260, 69–90.

Rosenbaum, G., Lister, G.S., Duboz, C., 2002. Reconstruction of the tectonic evolution of the western Mediterranean since the Oligocene. *Journal of the Virtual Explorer*, 8, 107–130.

Roser, B.P., Korsch, R.J., 1988. Provenance signatures of sandstone-mudstone suites determined using discriminant function analysis of major-element data. *Chemical Geology* 67, 119 – 139.

Royden, L.H., Papapetrou, D.J., 2011. Slab segmentation and late Cenozoic disruption of the Hellenic arc. *Geochem. Geophys. Geosyst.*, 12, Q03010, doi:10.1029/2010GC003280.

Rubatto, D., Gebauer, D., Compagnoni, R., 1999. Dating of eclogite facies zircons: the age of Alpine metamorphism in the Sesia–Lanzo Zone (Western Alps). *Earth Planet Sci Lett* 167, 141–158.

Rubatto, D., Williams, I.S., Buick, I.S., 2001. Zircon and monazite response to prograde metamorphism in the Reynolds Range, central Australia. *Contrib Mineral Petrol* 140, 458–468.

Rudnick, R.L., Gao, S., 2003. Composition of the continental crust. In: *Treatise on geochemistry*, 2003, Elsevier.

Sannemann, W., Seidel, E., 1976. Die Trias-Schichten von Rawducha/NW-Kreta. Ihre Stellung im kretischen Deckenbau. *N. Jb. Geol. Paläont. Mh.* 4, 221–228.

Schaltegger, U., Fanning, C.M., Gnther, D., Maurin, J.C., Schulmann, K., Gebauer, D., 1999. Growth, annealing and recrystallization of zircon and preservation of monazite in high-grade metamorphism: conventional and in-situ U-Pb isotope, cathodoluminescence and microchemical evidence. *Contrib Mineral Petrol* 134, 186–201.

Schellart, W.P., Lister, G.S., 2004. Tectonic model for the formation of arc-shaped convergent zones and backarc basins. *Geological Society of America, special paper* 383, 237 – 258.

Scisciani, V., Calamita, F., 2009. Active intraplate deformation within Adria: Examples from the Adriatic region. *Tectonophysics* 476, 57–72.

Seidel, E., Okrusch, M., Schubert, W., 1975. Chloritoid-bearing metapelites associated with glaucophane rocks in Western Crete, Greece. *Contrib. Mineral. Petrol.* 49, 105–115.

Seidel, E., 1978. Zur Petrologie der Phyllit-Quarzit-Serie Kretas. *Habilitationsschrift*, TU Braunschweig: 145 p., Braunschweig.

Seidel, E., Kreuzer, H., and Harre, W., 1982, A late Oligocene/early Miocene high pressure belt in the External Hellenides: *Geologisches Jahrbuch*, v. E23, p. 165–206.

Seidel, E., Theye, T., 1993. High-pressure/Low- temperature metamorphism in the External Hellenides (Crete, Peloponnese). *Bull. Geol. Soc. Greece*, XXVIII/1, 49–55.

Seidel, M., Zacher, W., Schwarz, W.H., Jaeckel, P., Reischmann, T., 2006a. A Late Carboniferous age of the gneiss of Potamos (Kythira island, Greece) and new considerations on geodynamic interpretations of the western Hellenides. *N. Jb. Geol. Paläont. Abh.* 241 (3), 325–344.

Seidel, M., Seidel, E., Stöckert, B., 2006b. Tectono-sedimentary evolution of lower to middle Miocene half-graben basins related to an extensional detachment fault (western Crete, Greece). *Terra Nova* 19, 39–47.

Simpson, C., Schmid, S.M., 1983. An evaluation of criteria to deduce the sense of movement in sheared rocks. *Geological Society of America Bulletin*, 94, 1281 – 1288.

Sircombe, K.N., 2000. The usefulness and limitations of binned frequency histograms and probability density distributions for displaying absolute age data. Radiogenic age and isotopic studies, Report 13, Geological Survey of Canada, Current Research 2000-F2, 11pp.

Sircombe, K.N., 2004. AgeDisplay: an EXCEL workbook to evaluate and display univariate geochronological data using binned frequency histograms and probability density distributions. *Computers & Geosciences* 30, 21–31.

Skarpelis, N., 1989. Metamorphosed ultramafic rocks in the blueschist (Arna Unit) of the external metamorphic belt of the Hellenides (Peloponnese and Kythira Island, Greece). *Bull. Geol. Soc. Greece*, XXIII/2, 345 – 358.

Skourtos, Em. Kranis, H., 2009. Structure and evolution of the western Corinth Rift, through new field data from the Northern Peloponnesus. *Geological Society, London, Special Publications* 2009; v. 321; p. 119–138.

Sokoutis, D., Brun, J.-P., Van Den Driessche, J., Pavlides, S.A., 1993. Major Oligo-Miocene detachment in southern Rhodope controlling north Aegean extension. *Journal of Geological Society (London)* 150, 243–246.

Sorel, D., 2000. A Pleistocene and still-active detachment fault and the origin of the Corinth-Patras rift, Greece. *Geology* 28, 83 – 86.

Spear, F., Cheney, J., 1989. A petrogenetic grid for pelitic schists in the system SiO_2 – Al_2O_3 – FeO – MgO – K_2O – H_2O . *Contrib. Mineral. Petrol.* 101, 149 – 164.

Spiess, R., Casera, B., Mazzoli, C., Sassi, R., Sassi, F.P., 2010. The crystalline basement of the Adria microplate in the eastern Alps: a review of the palaeostructural evolution from the Neoproterozoic to the Cenozoic. *Rend. Fis. Acc. Lincei* 21 (Suppl 1) S31–S50.

Stampfli, G.M., Borel, G.D., 2002. A plate tectonic model for the Paleozoic and Mesozoic constrained by dynamic plate boundaries and restored synthetic oceanic isochrones. *Earth and Planetary Science Letters* 196, 17–33.

Stampfli GM, Borel G.D., 2004. The TRANSMED transect in space and time: constraints on the paleotectonic evolution of the Mediterranean domain. In: Cavazza W, Rour F, Spakman W, Stampfli GM, Ziegler PA (eds) *The TRANSMED Atlas—the Mediterranean Region from Crust to Mantle*. Springer, Berlin, pp 53–80.

Surpless, K.D., Graham, S.A., Covault, J.A., Wooden, J., 2006. Does the Great Valley Group contain Jurassic strata? Reevaluation of the age and early evolution of a classic forearc basin. *Geology*, 34, 21–24, doi: 10.1130/G21940.1.

Tataris, A., Christodoulou, G., 1965. The tectonic structure of Lefka Ori (W. Crete). *Bull. Geol. Soc. Greece* VI(2), 319–347.

Tataris, A. and Christodoulou, G., 1967. Geological map of Greece (scale 1:50,000), sheet Alikianou. IGME, Athens.

Taylor, S.R., McLennan, S.M., 1985, *The Continental Crust - Its Composition and Evolution, an Examination of the Geochemical Record Preserved in Sedimentary Rocks*: Oxford, Blackwell Scientific, 312 p.

Teipel, U., Eichhorn, R., Loth, G., Rohrmuller, J., Holl, R., Kennedy, A., 2004. U-Pb SHRIMP and Nd isotopic data from the western Bohemian Massif (Bayerischer Wald, Germany): Implications for Upper Vendian and Lower Ordovician magmatism. *Int J Earth Sci (Geol Rundsch)* 93, 782–801.

Tera, F., Wasserburg, G.J., 1972. U-Th-Pb systematics in Lunar highland samples from the Luna 20 and Apollo 16 missions. *Earth Planet. Sci. Lett.* 17, 36–51.

Theye, T., Seidel, E., 1991. Petrology of low-grade high-pressure metapelites from the External Hellenides (Crete, Peloponnese). A case study with attention to sodic minerals. *European J. Mineral.*, 3, 343–366, Stuttgart (Schweizerbart).

Theye, T., Seidel, E., Vidal, O., 1992. Carpholite, sudoite and chloritoid in low-temperature high-pressure metapelites from Crete and the Peloponnese, Greece. – *European J. Mineral.*, 4, 487–507, Stuttgart (Schweizerbart).

Theye, T., Seidel, E., 1993. Uplift-related retrogression history of aragonite marbles in Western Crete (Greece). *Contrib Mineral Petrol* (1993) 114:349–356.

Thiébault, F., 1982. Evolution géodynamique des Héllénides externes en Péloponnèse méridional (Grèce). Société Géologique du Nord. Publication N° 6.

Thiébault, F., Triboulet, C., 1983. Alpine metamorphism and deformation in the Phyllite nappe (external hellenides, southern Peloponnesus, Greece), geodynamic interpretation. *J. Geol.* 92, 185–199.

Thomson, S., Stoeckhert, B., Brix, M., 1998a. Miocene high-pressure metamorphic rocks of Crete, Greece: rapid exhumation by buoyant escape. In: Ring, U., Brandon, M.T., Lister, G.S., Willett, S.D. (Eds.), *Exhumation Processes: Normal Faulting, Ductile Flow and Erosion*. Geological Society of London, pp. 87–107.

Thomson, S.N., Stöckhert, B., Rauche, H., Brix, M. R., 1998b. Apatite fission-track thermochronology of the uppermost tectonic unit of Crete, Greece: Implications for the post-Eocene tectonic evolution of the Hellenic subduction system, in Van den haute, P., and De Corte, F., eds., *Advances in fission-track geochronology*: Dordrecht, Kluwer Academic Publishers (in press).

Thomson, S., Stockhert, B., Brix, M.R. 1998c. Thermochronology of the high-pressure metamorphic rocks of Crete, Greece: implications for the speed of tectonic processes. *Geology*, 26, 259–262.

Tomaschek, F., Kennedy, A., Keay, S., Ballhaus, C., 2001. Geochronological constraints on Carboniferous and Triassic magmatism in the Cyclades: SHRIMP U/Pb ages of zircons from Syros, Greece. *Journal of Conference Abstracts* 6, 315.

Tomaschek, F., Keiter, M., Kennedy, A.K., Ballhaus, C., 2008. Pre-Alpine basement within the Northern Cycladic Blueschist Unit on Syros Island, Greece. *Z. dt. Ges. Geowiss.*, 159/3, p. 521–532.

Tran, J.T., Ansdell, K., Bethune, K., Watters, B., Ashton, K., 2003. Nd isotope and geochemical constraints on the depositional setting of Paleoproterozoic metasedimentary rocks along the margin of the Archean Hearne craton, Saskatchewan, Canada. *Precamb. Res.* 123, 1–28.

Trotet, F., Goffé, B., Vidal, O., Jolivet, L., 2006. Evidence of retrograde Mg-carniolite in the Phyllite–Quartzite nappe of Peloponnes from thermobarometric modelisation – geodynamic implications. *Geodin. Acta* 19 (5), 323–343.

Varga, A., Szakmány, G., Árgyelán, T., Józsa, S., Raucsik, B., and Máté, Z., 2007, Complex examination of the Upper Paleozoic siliciclastic rocks from southern Transdanubia, SW Hungary Mineralogical, petrographic, and geochemical study, in Arribas, J., Critelli, S., and Johnsson, M.J., eds., *Sedimentary Provenance and Petrogenesis: Perspectives from Petrography and Geochemistry*: Geological Society of America Special Paper 420, 221 – 240.

van Hinsbergen, D.J.J., Langereis, C.G., Meulenkamp, J.E., 2005. Revision of the timing, magnitude and distribution of Neogene rotations in the western Aegean region. *Tectonophysics* 396, 1–34.

van Wyck, N., Williams, I.S., 2002. Age and provenance of basement metasediments from the Kubor and Bena Bena Blocks, central Highlands, Papua New Guinea: constraints on the tectonic evolution of the northern Australian cratonic margin. *Aust. J. Earth Sci.* 49, 565–577.

Vavra, G., Schmid, R., Gebauer, D., 1999. Internal morphology, habit and U-Th-Pb microanalysis of amphibolite-to-granulite facies zircons: geochronology of the Ivrea Zone (Southern Alps). *Contrib. Mineral Petrol* 134, 380–404.

Vermeesch, P., 2004. How many grains are needed for a provenance study? *Earth Planet. Sci. Lett.* 224, 351–441.

von Raumer, J.F., Stampfli, G.M., 2008. The birth of the Rheic Ocean—Early Palaeozoic subsidence patterns and subsequent tectonic plate scenarios. *Tectonophysics* 461, 9–20.

von Raumer, J.F., Bussy, F., Stampfli, G.M., 2009. The Variscan evolution in the external massifs of the Alps and place in the Variscan framework. *C R Geosci* 341, 239–252.

Walcott, C.R., White, S.H., 1998. Constraints on the kinematics of post-orogenic extension imposed by stretching lineations in the Aegean region. *Tectonophysics* 298, 155–175.

White, N.M., Pringle, M., Garzanti, E., Bickle, M., Najman, Y., 2002. Constraints on the exhumation and erosion of the High Himalayan Slab, NW India, from foreland basin deposits: *Earth and Planetary Science Letters*, 195, 29–44, doi: 10.1016/S0012-821X(01)00565-9.

Williams, I.S., Buick, I.S., Cartright, I., 1996. An extended episode of early Mesoproterozoic metamorphic fluid flow in the Reynolds Range, central Australia. *J Metam Geol* 14, 29–47.

Williams, I.S., 2001. Response of detrital zircon and monazite, and their U–Pb isotopic systems, to regional metamorphism and host-rock partial melting, Cooma Complex, southeastern Australia. *Aust. J. Earth Sci.* 48, 557–580.

Xypolias, P., Doutsos, T., 2000. Kinematics of rock flow in a crustal-scale shear zone: implication for the orogenic evolution of the southwestern Hellenides. *Geol. Mag.* 137, 81–96.

Xypolias, P., Koukouvelas, I.K., 2001. Kinematic vorticity and strain rate patterns associated with ductile extrusion in the Chelmos Shear Zone (External Hellenides, Greece). *Tectonophysics* 338, 59 – 77.

Xypolias, P., Dörr, W., Zulauf, G., 2006. Late Carboniferous plutonism within the pre-Alpine basement of the External Hellenides (Kithira, Greece): Evidence from U-Pb zircon dating. - *J. geol. Soc. London*, 163, 539–547.

Yamashita, K., Creaser, R.A., Villeneuve, M.E., 2000. Integrated Nd isotopic and U–Pb detrital zircon systematics of clastic sedimentary rocks from the Slave Province, Canada; evidence for extensive crustal reworking in the early- to mid-Archean. *Earth Planet. Sci. Lett.* 174, 283–299.

Zeh, A., Brätz, H., Millar, I.L., Williams, I.S., 2001. A combined zircon SHRIMP and Sm–Nd isotope study on high-grade paragneisses from the Mid-German Crystalline Rise: evidence for northern Gondwanan and Grenvillian provenance. *Journal of the Geological Society (London)* 158, 983–994.

Appendix A

Four available median values from 24 sandstones (Varga et al. 2007) were used for the calculation of the Rb and Y+Nb swift of the sample Fe1 (**Table 5.1**). The median values are shown in **Table A2**. A relatively immobile element (Yb) was chosen for the normalization of REE and multi-element diagrams (**Fig. A1**). The REE patterns (**Fig. A1a**) are identical between the quartzite studied (Fe1) and the sandstones (SS) with $3.28 < \text{LREE}_{\text{SS}} / \text{LREE}_{\text{Fe1}} < 8.55$ and $2.42 < \text{HREE}_{\text{SS}} / \text{HREE}_{\text{Fe1}} < 3.15$. For the correction of the Rb, Y and Nb contents the multi-element diagrams were used (**Fig. A1b**).

Specifically, for the Rb content of the sandstones the minimum and maximum values obtained after the normalization is 76.46 and 179.6 respectively, resulting in $6.909 < \text{Rb}_{\text{SS}} / \text{Rb}_{\text{Fe1}} < 16.23$ and corrected Rb value for the quartzite between 63 and 148 ppm (**Table A1**). For the Y content of the sandstones the minimum and maximum values obtained after the normalization is 25.49 and 41.26 respectively, resulting in $3.24 < \text{Y}_{\text{SS}} / \text{Y}_{\text{Fe1}} < 5.245$ and corrected Y value for the quartzite between 21 and 34 ppm (**Table A1**). For the Nb content of the sandstones the minimum and maximum values obtained after the normalization is 8.495 and 13.35 respectively, resulting in $1.523 < \text{Nb}_{\text{SS}} / \text{Nb}_{\text{Fe1}} < 2.393$ and corrected Nb value for the quartzite between 7 and 11 ppm (**Table A1**).

The new values for the Rb ($63 < \text{Rb}_{\text{Fe1}} < 148$) and Y+Nb ($28 < (\text{Y} + \text{Nb})_{\text{Fe1}} < 45$) of the quartzite under investigation are shown in **Table A1** and are plotted in **Fig. 5.3c** (grey box).

Table A1. Corrected Rb, Y+Nb values for the quartzite Fe1. Details in the text.

Coef.	Corrected Y Rb Nb values			
	Rb	Y	Nb	Rb
3,24		21		63
5,245		34		148
6,909	63			
16,23	148			
1,523			7	
2,393			11	

Table A2. Median values from 24 sandstone samples from southern Transdanubia, SW Hungary (Varga et al. 2007).

Sample	(6)	(3)	(4)	(8)
SiO₂	73,77	72,51	73,06	72,12
TiO₂	0,38	0,66	0,54	0,59
Al₂O₃	13,06	14,02	15,36	13,56
Fe₂O₃	2,19	4,01	2,97	4,15
MnO	0,07	0,07	0,02	0,04
MgO	1,46	1,95	0,12	1,71
CaO	2,69	2,26	0,76	0,61
Na₂O	4,27	3,49	1,73	3,49
K₂O	1,56	2,12	3,37	3,09
P₂O₅	0,09	0,09	0,14	0,15
Rb	63	87	123	148
Sr	210	196	65	134
Ba	388	428	536	552
Th	9	6,8	7,9	12
U	2,6	1,9	1,9	3,3
Zr	180	157	147	179
Hf	6	5	6	6
Nb	8	9,3	7	11
Y	24	21	28	34
Sc	7,8	9,3	7,8	10,2
V	40	47	37	64
Cr	34	45	30	95
Co	5	9	3	10
Ni	L.D.	L.D.	L.D.	41
La	31	23	30	30
Ce	46	52	58	64
Pr	5,5	6,1	6,7	7,4
Nd	25	24	25	30
Sm	4,5	4,5	5,1	6,3
Eu	0,94	0,94	1,01	1,11
Gd	3,7	3,3	3,9	5,1
Tb	0,62	0,52	0,64	0,86
Dy	3,2	3	3,8	4,9
Ho	0,7	0,6	0,8	1
Er	2,1	1,8	2	2,7
Tm	0,3	0,28	0,33	0,43
Yb	1,9	1,6	2	2,6
Lu	0,3	0,25	0,32	0,39

Trace elements in ppm

Major elements in weight per cent

Total iron measured as Fe₂O₃

L.D. below detection limit

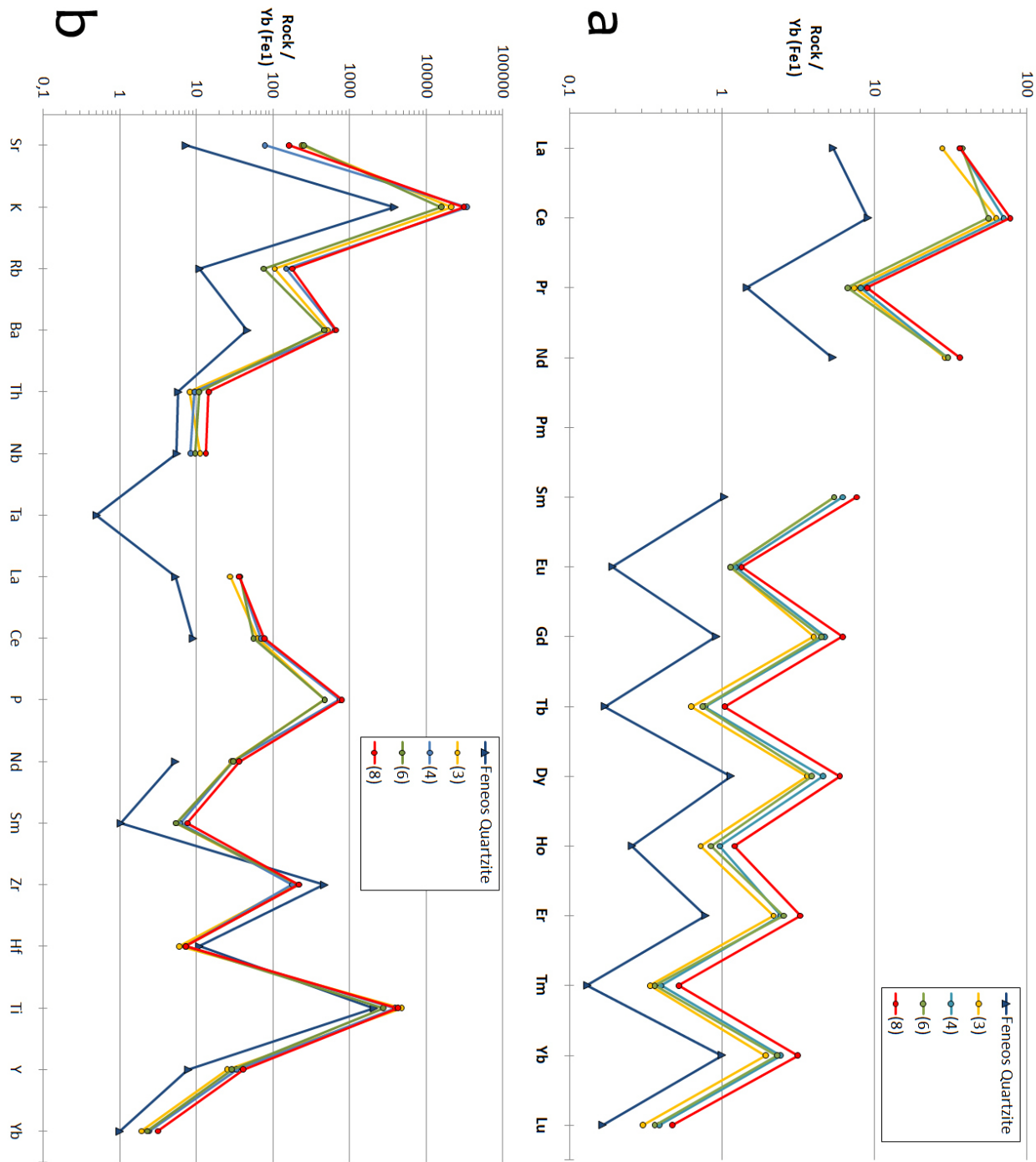


Fig. A1. (a) REE diagram of Feneos quartzite (Fe1; Table 5.1) and the four median values of analyzed sandstones (Table A1; Varga et al. 2007). (b) Multi-element diagram of Feneos quartzite (Fe1; Table 5.1) and the four median values of analyzed sandstones (Table A1; Varga et al. 2007). In both diagrams the normalization is done using the Yb content of Fe1 sample (Table 5.1).

Appendix B

Isotopic dataset of the quartzite analyzed (Fe1).

Grouping	Analysis #	Grain	Comments*	Pb	U	Th/U	$^{207}\text{Pb}/^{206}\text{Pb}$	$\pm 1\sigma$	$^{207}\text{Pb}/^{235}\text{U}$	$\pm 1\sigma$	$^{206}\text{Pb}/^{238}\text{U}$	$\pm 1\sigma$	Br. Cor.	$^{207}\text{Pb}/^{206}\text{Pb}$	$\pm 1\sigma$	$^{206}\text{Pb}/^{238}\text{U}$	$\pm 1\sigma$	$^{207}\text{Pb}/^{235}\text{U}$	$\pm 1\sigma$	Agg.	
Group 1	05240211C	Fe1-ia-001	A	5	46	1.469	0.00037	0.000105	0.81842	0.01506	0.09831	0.00125	0.69	61.7	37	60.5	7	60.7	8	98.0	
	06240211C	Fe1-ia-002	A	24	234	0.515	0.00151	0.000073	0.88584	0.01211	0.10481	0.00129	0.69	65.7	25	64.3	8	64.6	7	97.8	
	07240211C	Fe1-ia-004	B	79	756	0.139	0.00549	0.00007	1.0792	0.01364	0.1195	0.00146	0.97	79.0	22	77.8	8	74.3	7	92.1	
	08240211C	Fe1-ia-005	A	18	179	0.103	0.00813	0.000084	0.73051	0.01151	0.09112	0.00113	0.79	53.4	32	56.2	7	55.7	7	105.2	
	09240211C	Fe1-ia-006	A	7	66	0.902	0.0052	0.000088	0.9049	0.01359	0.09114	0.00117	0.74	57.4	33	58.0	7	60.0	8	96.0	
	10240211C	Fe1-ia-006	A	25	55	1.635	0.12193	0.00138	5.98667	0.07756	0.35426	0.00431	0.93	198.5	20	195.5	21	197.0	11	98.5	
	11240211C	Fe1-ia-006	A	17	44	1.273	0.12028	0.00155	5.59177	0.07789	0.33216	0.00409	0.87	198.7	22	184.9	20	191.5	12	93.1	
	12240211C	Fe1-ia-007	A	14	149	0.370	0.06022	0.00077	0.8209	0.01169	0.09885	0.00112	0.85	61.2	26	60.8	7	69.9	7	99.4	
	15240211C	Fe1-ia-008	B	2	10	0.300	0.00876	0.00181	2.03971	0.04641	0.18316	0.00242	0.58	121.6	44	108.4	13	112.9	16	89.2	
	19240211C	Fe1-ia-009	A	5	48	0.611	0.06172	0.00104	0.87136	0.0153	0.10337	0.00125	0.70	66.5	36	62.8	7	63.6	8	94.5	
	20240211C	Fe1-ib-008	D	10	76	1.337	0.06102	0.00089	0.94942	0.01401	0.10744	0.00126	0.77	64.0	31	65.8	8	65.4	7	102.8	
	21240211C	Fe1-ib-007	A	37	352	0.165	0.006102	0.00059	0.94503	0.01123	0.00131	0.93	64.0	24	68.6	8	67.6	6	105.2		
	22240211C	Fe1-ib-006	D	84	138	0.957	0.17877	0.00188	12.57322	0.14991	0.51002	0.00593	0.98	264.2	17	265.7	25	264.8	11	100.6	
	25240211C	Fe1-ib-006	D	101	177	0.897	0.18006	0.00185	11.67199	0.13636	0.46749	0.00536	0.98	265.3	17	247.3	24	257.3	11	93.2	
	26240211C	Fe1-ib-005	B	110	181	0.865	0.16718	0.00185	12.41197	0.14618	0.51112	0.00587	0.98	261.7	17	266.1	25	263.7	11	101.7	
	27240211C	Fe1-ib-005	C	13	23	0.674	0.17672	0.00206	12.15719	0.15447	0.49888	0.00583	0.92	262.2	19	260.9	25	261.7	12	99.5	
	28240211C	Fe1-ib-004	A	76	721	0.019	0.06263	0.00067	0.99251	0.01189	0.11553	0.00132	0.95	68.4	23	70.5	8	70.0	6	103.0	
	29240211C	Fe1-ib-003	A	52	435	0.406	0.03035	0.00076	1.04547	0.01269	0.11987	0.00136	0.93	71.0	23	72.5	25	72.5	6	102.7	
	30240211C	Fe1-ib-003	A	25	203	0.535	0.06401	0.00064	1.04545	0.01355	0.11945	0.00136	0.98	74.2	25	72.7	8	73.1	7	98.0	
	31240211C	Fe1-ib-002	D	71	228	0.719	0.06804	0.00064	1.07357	0.01682	0.0904	0.00102	0.94	53.1	24	55.8	6	55.3	5	105.1	
	32240211C	Fe1-ib-001	A	3	21	0.651	0.00127	0.00633	0.02185	0.012307	0.00148	0.97	261.7	42	274.8	9	247.7	11	101.8		
	35240211C	Fe1-ic-001	B	32	226	0.363	0.06564	0.00076	1.25082	0.01549	0.13816	0.00155	0.91	79.5	24	83.4	9	82.4	7	105.0	
	36240211C	Fe1-ic-001	C	15	108	0.294	0.05851	0.00069	1.18076	0.01668	0.1301	0.00147	0.80	80.1	26	78.8	8	79.2	6	98.5	
	37240211C	Fe1-ic-002	D	69	408	0.478	0.07138	0.00078	1.59483	0.01653	0.16955	0.00185	0.94	96.8	22	96.8	10	96.8	7	100.0	
	38240211C	Fe1-ic-002	A	34	195	0.365	0.07145	0.00082	1.65302	0.0203	0.16778	0.00187	0.91	97.0	23	100.0	10	99.1	8	103.1	
	39240211C	Fe1-ic-003	A	14	118	0.341	0.06165	0.00083	0.95179	0.01328	0.11222	0.00162	0.80	65.7	29	68.6	7	67.9	7	104.4	
	40240211C	Fe1-ic-004	D	21	187	0.142	0.06276	0.00076	1.01662	0.01298	0.11746	0.00113	0.87	70.7	26	71.6	8	71.2	7	104.2	
	41240211C	Fe1-ic-005	A	145	171	0.180	0.05886	0.00065	0.65747	0.00832	0.08593	0.00094	0.92	56.2	24	53.1	6	53.7	5	94.6	
	42240211C	Fe1-ic-006	D	22	119	0.169	0.05721	0.00099	1.73776	0.02235	0.17326	0.00192	0.86	100.6	25	103.0	11	103.3	8	102.4	
	45240211C	Fe1-ic-007	D	38	80	0.604	0.17631	0.00213	0.84757	0.02329	0.04033	0.00451	0.89	261.8	20	219.2	21	241.1	12	83.7	
	46240211C	Fe1-ic-008	A	168	335	1.574	0.12197	0.000131	6.19363	0.06935	0.36481	0.00194	0.95	198.5	19	200.5	19	199.5	10	101.0	
	47240211C	Fe1-ic-009	A	27	92	1.005	0.10358	0.00122	3.07598	0.03698	0.21992	0.00232	0.89	168.0	22	124.4	12	141.4	9	74.1	
	48240211C	Fe1-ic-010	A	8	51	0.513	0.06347	0.00093	1.03123	0.01553	0.11782	0.0013	0.73	72.4	32	71.8	8	72.0	8	99.2	
	49240211C	Fe1-ic-007	A	31	275	0.345	0.06129	0.00073	1.01108	0.01119	0.11776	0.00117	0.88	64.9	25	65.8	6	65.6	6	101.6	
	50240211C	Fe1-ic-004	D	22	125	0.344	0.07337	0.00089	1.77779	0.02049	0.16995	0.00183	0.87	103.3	24	101.2	10	101.9	8	97.9	
	51240211C	Fe1-ic-003	C	10	120	0.031	0.05766	0.00083	0.67029	0.00799	0.08433	0.0092	0.75	516	31	52.1	52	52.1	52	101.0	
	52240211C	Fe1-ic-002	A	33	271	0.434	0.06407	0.00076	0.97811	0.01186	0.1107	0.00118	0.88	74.4	25	67.7	7	69.3	6	91.0	
	55240211C	Fe1-ic-001	A	36	325	0.061	0.06174	0.00072	0.95628	0.01112	0.11086	0.00117	0.89	64.8	25	67.8	7	67.1	6	104.6	
	56240211C	Fe1-ic-001	A	86	149	0.777	0.06274	0.00071	10.91303	0.01130	0.11219	0.00483	0.94	258.4	18	243.1	21	251.6	10	94.1	
	57240211C	Fe1-ic-002	B	65	186	0.002	0.11494	0.00127	5.45987	0.06127	0.34313	0.00361	0.93	187.9	20	190.2	17	189.1	10	101.2	
	58240211C	Fe1-ic-002	C	42	102	0.754	0.11493	0.00131	5.38078	0.06169	0.33761	0.00355	0.91	187.9	20	187.5	17	187.7	10	99.8	
	59240211C	Fe1-ic-003	D	15	126	0.326	0.0619	0.00083	0.94118	0.01235	0.11026	0.00117	0.80	67.1	28	67.4	7	67.4	7	100.5	
	60240211C	Fe1-ic-005	B	33	54	0.535	0.1904	0.000219	13.20702	0.15226	0.50298	0.00531	0.92	274.6	23	269.5	23	269.5	11	95.7	
	61240211C	Fe1-ic-005	D	147	419	0.037	0.10341	0.00071	0.90189	0.00883	0.14591	0.00074	0.87	249.1	18	243.6	21	246.6	10	97.8	
	62240211C	Fe1-ic-006	A	42	29	1.345	0.05952	0.00071	0.74499	0.00883	0.15622	0.00117	0.88	586	26	560	6	565	5	104.6	
	65240211C	Fe1-ic-007	D	9	65	0.599	0.05946	0.00074	0.80128	0.01267	0.09808	0.00105	0.68	576	35	603	6	598	7	104.7	
	66240211C	Fe1-ic-008	D	17	86	0.034	0.07405	0.00099	0.76578	0.01238	0.09704										

Grouping	Analysis #	Grain	Pb	U	Th/U	$^{207}\text{Pb}/^{206}\text{Pb}$	$\pm 2\sigma$	$^{202}\text{Pb}/^{235}\text{U}$	$\pm 2\sigma$	$^{206}\text{Pb}/^{238}\text{U}$	$\pm 2\sigma$	ρ_{H}	$^{207}\text{Pb}/^{206}\text{Pb}$	$\pm 2\sigma$	$^{206}\text{Pb}/^{238}\text{U}$	$\pm 2\sigma$	$^{207}\text{Pb}/^{235}\text{U}$	$\pm 2\sigma$	Conc	
Group II	05250211a	Fe-I-1a-002	D	140	300	0.297	0.17224	0.00185	9.80382	0.19558	0.41287	0.00798	0.50	2580	18	2228	36	2417	17	86.4
	06250211a	Fe-I-1a-003	A	50	449	0.774	0.06181	0.00089	0.7966	0.01679	0.09347	0.00182	0.92	688	30	576	11	595	9	86.3
	07250211a	Fe-I-1a-004	D	33	300	0.258	0.06255	0.00083	0.93301	0.01904	0.10819	0.0021	0.95	693	28	662	12	669	10	95.6
	08250211a	Fe-I-1a-005	A	9	78	0.900	0.05665	0.00119	0.72065	0.01862	0.09226	0.00183	0.77	477	46	569	11	551	11	119.2
	09250211a	Fe-I-1a-006	B	11	106	0.398	0.05971	0.00108	0.80733	0.01914	0.09807	0.00193	0.83	593	38	603	11	601	11	101.7
	10250211a	Fe-I-1a-007	D	12	110	0.962	0.06289	0.00114	0.76344	0.01813	0.08605	0.00174	0.83	704	38	544	10	576	10	77.2
	11250211a	Fe-I-1b-007	D	64	446	0.222	0.07036	0.00084	1.36035	0.02684	0.14023	0.00273	0.99	939	24	846	15	872	12	90.1
	12250211a	Fe-I-1b-006	B	35	243	0.283	0.0725	0.00107	1.39484	0.02985	0.13945	0.00274	0.92	1001	30	842	15	887	13	84.1
	13250211a	Fe-I-1b-006	C	78	990	0.005	0.06005	0.00071	0.69263	0.01361	0.08366	0.00163	0.99	605	25	518	10	534	8	85.6
	16250211a	Fe-I-1b-002	D	204	351	0.617	0.18179	0.00194	11.87246	0.22666	0.47367	0.00924	0.50	2669	18	2500	40	2594	18	93.6
	17250211a	Fe-I-1b-001	A	127	329	0.705	0.12243	0.00135	5.41288	0.10441	0.32067	0.00626	0.50	1992	20	1793	31	1887	17	90.0
	18250211a	Fe-I-1c-001	A	196	393	0.539	0.16694	0.00118	9.63902	0.18481	0.41877	0.00818	0.50	2527	18	2255	37	2401	18	89.2
	19250211a	Fe-I-1c-002	C	25	137	0.642	0.07459	0.00106	1.662	0.03518	0.1616	0.00319	0.93	1057	29	966	18	994	13	91.3
	20250211a	Fe-I-1c-004	A	22	238	0.128	0.06083	0.0009	0.80316	0.01729	0.09575	0.00189	0.92	633	31	590	11	599	10	93.1
	21250211a	Fe-I-1c-006	D	44	341	0.398	0.07241	0.00093	1.19799	0.02443	0.11999	0.00236	0.96	998	26	731	14	800	11	73.2
	22250211a	Fe-I-1d-006	D	40	333	0.365	0.06601	0.00087	1.02499	0.02107	0.11266	0.00222	0.96	807	27	688	13	716	11	85.3
	25250211a	Fe-I-1d-003	B	8	85	0.313	0.06186	0.00115	0.81334	0.01974	0.09535	0.00191	0.83	669	39	587	11	604	11	87.7
	26250211a	Fe-I-1d-002	A	40	317	0.464	0.05356	0.00081	1.02088	0.02079	0.11642	0.0023	0.97	728	27	710	13	714	10	97.5
	27250211a	Fe-I-1d-001	D	28	238	0.862	0.06128	0.00091	0.85625	0.01855	0.10134	0.00201	0.92	649	31	622	12	628	10	95.9
	28250211a	Fe-I-1e-001	B	132	248	0.650	0.15565	0.00172	9.57515	0.18645	0.44615	0.0088	0.50	2409	19	2372	39	2395	18	98.7
	29250211a	Fe-I-1e-002	B	374	594	0.373	0.09318	0.00089	1.69664	0.0341	0.16814	0.00333	0.99	1019	24	1002	18	1007	13	98.3
	30250211a	Fe-I-1e-005	D	34	407	0.212	0.05961	0.00082	0.68172	0.01436	0.08293	0.00165	0.94	590	30	514	10	528	9	87.1
	31250211a	Fe-I-1e-006	A	42	309	0.175	0.06862	0.00089	1.29518	0.02673	0.13669	0.00272	0.96	887	27	827	15	844	12	93.2
	32250211a	Fe-I-1e-007	D	22	219	0.342	0.06009	0.00088	0.80896	0.01754	0.09758	0.00194	0.92	607	32	600	11	602	10	98.9

Grouping	Analyses #	Grain	Pb	U	Th/U	$^{207}\text{Pb}/^{206}\text{Pb}$	$\pm 2\sigma$	$^{207}\text{Pb}/^{235}\text{U}$	$\pm 2\sigma$	$^{206}\text{Pb}/^{238}\text{U}$	$\pm 2\sigma$	ρ_{Hg}	$^{207}\text{Pb}/^{206}\text{Pb}$	$\pm 2\sigma$	$^{206}\text{Pb}/^{238}\text{U}$	$\pm 2\sigma$	$^{207}\text{Pb}/^{235}\text{U}$	$\pm 2\sigma$	Conc	
Group III	35250211a	Fe1-IIia-001	D	155	239	0.979	0.17747	0.00199	12.38275	0.24363	0.050601	0.001005	0.50	2029	19	2640	43	2634	18	100.4
	36250211a	Fe1-IIia-002	A	204	674	0.349	0.10949	0.00123	4.2986	0.08471	0.28473	0.00566	0.50	1791	20	1615	28	1693	16	90.2
	37250211a	Fe1-IIia-003	D	18	88	0.839	0.07161	0.00152	1.66969	0.04443	0.1691	0.0034	0.76	975	43	1007	19	997	17	103.3
	38250211a	Fe1-IIia-004	B	20	120	0.169	0.07642	0.00115	1.80089	0.03957	0.1709	0.00343	0.91	1106	30	1017	19	1046	14	92.0
	39250211a	Fe1-IIia-005	A	36	321	0.358	0.06162	0.00082	0.91817	0.01922	0.10806	0.00216	0.95	661	28	662	13	661	10	100.1
	40250211a	Fe1-IIia-006	A	79	826	0.174	0.06072	0.00074	0.81446	0.01653	0.09728	0.00194	0.98	629	26	598	11	605	9	95.1
	41250211a	Fe1-IIia-007	C	9	68	1.677	0.06605	0.00114	0.77597	0.02047	0.08052	0.00175	0.78	808	44	527	10	583	12	65.2
	42250211a	Fe1-IIia-008	A	55	527	0.259	0.06195	0.00078	0.88874	0.01829	0.10404	0.00208	0.97	672	27	638	12	646	10	94.9
	43250211a	Fe1-IIia-009	B	92	1008	0.030	0.05774	0.00073	0.79227	0.01637	0.09951	0.002	0.97	520	28	612	12	593	9	117.7
	46250211a	Fe1-IIb-005	B	294	842	0.059	0.12167	0.00114	5.98641	0.11969	0.35679	0.00715	0.60	1981	20	1987	34	1974	17	99.3
	47250211a	Fe1-IIb-004	A	50	74	0.388	0.2143	0.00057	1.74535	0.35259	0.39061	0.0119	0.99	2938	19	2992	48	2960	19	101.8
	48250211a	Fe1-IIb-003	D	26	114	2.465	0.06374	0.000108	1.20255	0.02816	0.1366	0.00278	0.87	733	36	827	16	802	13	112.7
	49250211a	Fe1-IIb-001	B	56	102	0.703	0.15768	0.00196	9.89376	0.02323	0.4536	0.00919	0.98	2431	21	2418	41	2425	19	99.4
	50250211a	Fe1-IIc-002	A	62	642	0.059	0.06028	0.00079	0.87565	0.01835	0.10534	0.00213	0.96	614	28	646	12	639	10	105.2
	51250211a	Fe1-IIc-003	A	69	618	0.065	0.06219	0.00018	1.04441	0.02181	0.12178	0.00246	0.97	681	27	741	14	726	11	108.8
	52250211a	Fe1-IIc-005	D	54	148	0.787	0.10838	0.00114	4.60625	0.06383	0.06626	0.97	1771	23	1734	31	1751	17	97.9	
	55250211a	Fe1-IIc-006	D	122	1344	0.250	0.05878	0.00073	0.74428	0.01542	0.09182	0.00186	0.98	559	27	566	11	565	9	101.3
	56250211a	Fe1-IIc-007	B	126	366	0.475	0.11028	0.00134	4.83999	0.09951	0.31827	0.00645	0.99	1804	22	1781	32	1792	17	98.7
	57250211a	Fe1-IIc-007	D	68	752	0.265	0.06081	0.00086	0.77241	0.01682	0.09211	0.00187	0.93	632	30	568	11	581	10	89.8
	58250211a	Fe1-IIc-008	D	82	242	0.505	0.11056	0.00138	4.69321	0.01742	0.030782	0.0026	0.98	1809	23	1730	31	1766	17	95.7
	59250211a	Fe1-IIc-009	A	126	1240	0.677	0.05719	0.00073	0.71922	0.01508	0.09112	0.00185	0.97	498	28	563	11	550	9	112.9
	60250211a	Fe1-IIc-007	A	291	1203	0.051	0.11187	0.00135	3.90065	0.08028	0.25283	0.00514	0.99	1830	22	1453	26	1614	17	79.4
	61250211a	Fe1-IId-005	A	117	912	0.084	0.06478	0.00082	1.23865	0.02587	0.13866	0.00282	0.97	767	26	837	16	818	12	109.1
	62250211a	Fe1-IId-005	A	93	1090	0.082	0.05846	0.00077	0.74876	0.01859	0.09288	0.00189	0.96	547	28	573	11	568	9	104.7
	65250211a	Fe1-IId-004	D	75	413	0.321	0.07191	0.00094	1.83947	0.03907	0.1855	0.0038	0.96	983	26	1097	21	1060	14	111.6
	66250211a	Fe1-IId-003	B	23	245	0.455	0.05733	0.00096	0.72559	0.01708	0.09183	0.00189	0.87	503	36	566	11	554	10	112.7
	67250211a	Fe1-IId-003	C	10	101	0.566	0.08434	0.00169	1.02812	0.02655	0.08835	0.00185	0.81	1300	39	546	11	718	13	42.0
	68250211a	Fe1-IIe-001	D	98	393	0.289	0.10383	0.00136	3.51862	0.07493	0.24574	0.00505	0.97	1694	24	1417	26	1531	17	83.6
	69250211a	Fe1-IIe-002	D	98	384	0.508	0.05053	0.00113	3.38083	0.07183	0.24365	0.00501	0.97	1634	24	1407	26	1500	17	86.1
	70250211a	Fe1-IIe-003	D	54	309	1.085	0.06402	0.00091	1.2875	0.02828	0.14582	0.003	0.94	742	30	878	17	840	13	118.2
	71250211a	Fe1-IIe-007	D	20	150	0.927	0.05982	0.00108	0.924	0.02268	0.112	0.00233	0.85	597	39	14	665	12	114.6	
	72250211a	Fe1-IIe-007	A	81	205	1.007	0.01918	0.00147	4.88344	0.01551	0.32202	0.00667	0.96	1786	24	1804	32	1796	18	101.0
	75250211a	Fe1-IIe-008	A	92	888	0.157	0.06203	0.00086	0.95113	0.02079	0.1118	0.0023	0.95	675	29	680	13	679	11	100.6
	76250211a	Fe1-IIf-005	C	1	9	0.005	0.06151	0.00338	0.89754	0.05032	0.10581	0.00261	0.44	657	114	648	15	650	27	98.7
	77250211a	Fe1-IIf-005	B	7	7015	0.0926	0.00418	1.3852	0.0645	0.1084	0.00266	0.53	1481	83	664	15	883	27	44.8	
	78250211a	Fe1-IIf-004	D	65	325	0.633	0.07352	0.00103	1.91751	0.04226	0.18919	0.00392	0.94	1029	28	1117	21	1087	15	108.6
	79250211a	Fe1-IIf-003	A	150	1838	0.127	0.0581	0.00079	0.715	0.01563	0.08923	0.00185	0.95	533	30	551	11	548	9	103.4
	80250211a	Fe1-IIf-002	A	625	1137	0.495	0.1625	0.00212	1.1919518	0.244114	0.49995	0.01037	0.96	2482	22	2612	45	2540	20	105.2
	81250211a	Fe1-IIf-001	A	100	905	0.133	0.06138	0.00095	1.01644	0.02235	0.12008	0.00235	0.95	653	29	731	14	712	11	112.0
	82250211a	Fe1-IIg-001	D	285	832	0.348	0.011563	0.00154	5.32386	0.11562	0.23386	0.00694	0.96	1890	24	1857	34	1873	19	98.3

Red data are outside the 90%-110% concordance limit

* A: Homogenous grain, B: Core, C: Rim, D: Growth zoning-overgrowth

